



The University of
Nottingham

UNITED KINGDOM • CHINA • MALAYSIA

**Void growth mitigation in high heating
rate Out-of-Autoclave processing of
composites**

BY

Kishen Rengaraj

MEng (Hons)

Thesis submitted to the University of Nottingham

for the degree of Doctor of Philosophy

February 2016

Abstract

Increased pressure on the transport industry to reduce greenhouse gas emissions has hastened the adoption of high performance composites, particularly in the aerospace industry where the value of weight saving is very high. However, the current method of choice for manufacturing high performance composites (autoclave processing) is not cost effective for processing large (greater than 5m²) structural composite components. Developments in Out-of-Autoclave (OoA) prepreg systems have facilitated the use of vacuum only consolidation pressure to process laminates with autoclave level mechanical properties. However, owing to the low consolidation pressure, the process is heavily dependent on de-bulk quality and low cure temperatures; leading to reduced margin for error as well as long cycle times. In parallel, developments in high heating rate OoA processes have been shown to enable short cure cycle times and autoclave-level mechanical properties; albeit with a high tendency towards porosity. To date, studies on high heating rate OoA processing have been limited and the processes are not well understood.

The main objectives of this self-funded study were to understand the mechanism of void growth mitigation in high heating rate OoA processes and to study the feasibility of achieving further reduction in cycle time and cost, whilst maintaining high mechanical properties.

The primary mechanism of void growth was identified and an analytical model was used to predict the propensity for void growth during a given cure cycle. The model outcome highlighted a window within the cure cycle during which void growth takes place. It was hypothesised that a reduced time to resin gelation in high heating rate processes can reduce the window for void growth, leading to lower laminate porosity. A novel high heating rate pressurised tooling system (the Pressure Tool) was developed to process laminates at 15°C/min combined with the application of up to 7 Bar hydrostatic pressure. The Pressure Tool was used to verify the hypothesis that reduction in size of the window for void growth, facilitated by high heating rate, can lead to lower laminate porosity. Good agreement was observed between the model outcome and the experimental results.

Studies have claimed that the reduction in resin viscosity due to high heating rate can lead to gains in mechanical properties; sometimes even higher than that of autoclave cured laminates. OoA prepregs cured using up to 15°C/min heating combined with up to 3 Bar hydrostatic pressure did not result in the claimed additional gain in mechanical properties. The study confirmed earlier suggestions that additional factors such as void geometry and location within the laminate have to be taken into consideration.

The final part of this thesis addresses the physical limitations to high heating rate processes; such as, the effect of tooling material, process ancillaries, laminate thickness and resin kinematics on reducing cure cycle time. The poor thermal characteristics of commonly used process ancillaries limit the dissipation of energy released by the laminate during cure. Due to which, laminate core temperature can exceed by up to 5°C, even if the laminate is processed on a highly conductive tooling material. The optimum tooling material to achieve reductions in cure cycle time whilst minimising laminate core thermal overshoot was found to have a combination of high thermal conductivity and low thermal mass. However, currently used tooling systems are not optimum for achieving further reductions in cycle time, due to unfavourable combination of thermal mass and thermal conductivity. Furthermore, the high reactivity of current resin systems and the inherently poor thermal conductivity of the polymer matrix limits the gains in cure cycle times that can be achieved.

To mom and dad. No words or tokens can express my joy and gratitude for your eternal unconditional love, support and guidance in every stage of my life.

Acknowledgements

I would like to thank my academic supervisors Prof. Nick Warrior, Dr. Tom Turner and Dr. Lee Harper for the advice and guidance offered throughout this work.

Thanks go to the staff and technicians for sharing their skills, knowledge and wisdom in developing the novel tooling system and for the practical aspects of this study; in particular, to Paul Johns, Ben Jennison and Roger Smith (now retired).

Thanks go to my colleagues, both in the Polymer Composites Research Group and the Division of Materials, Mechanics and Structures at the University of Nottingham, for sharing their vast collective knowledge and experience.

Special thanks to my friends and family; in particular, to my sisters Anusha and Varsha, for patiently listening to my babbles about the difference between prepregs and autoclaves whilst encouraging me to push on.

Finally, to Marisha, my pillar of support.

Contents

Abstract.....	i
Acknowledgements.....	iv
Contents.....	v
1. Introduction	1
1.1. Strengths and limitations of autoclave processing.....	3
1.2. Review of recent developments in Out-of-Autoclave processing of high performance composites.....	6
1.2.1. Conduction.....	6
1.2.1.1. Shell tooling with an on-board heating system for processing prepregs	6
1.2.1.2. The Quickstep process	8
1.2.1.3. Prepreg compression moulding.....	10
1.2.2. Convection based Out-of-Autoclave process – Oven cure	11
1.2.3. Radiation	12
1.2.3.1. Microwave cure of composites.....	12
1.2.3.2. Electron-beam cure.....	13
1.3. Theme of work.....	14
2. Literature review: Causes of void and void growth mitigation strategies.....	16
2.1. Causes of voids.....	16
2.1.1. Entrapped air	16
2.1.1.1. Effect of fibre architecture on air permeability	16
2.1.1.2. Vacuum quality	20
2.1.1.3. Part size.....	21
2.1.1.4. Lay-up ancillaries.....	23
2.1.1.5. Resin rheological characteristics.....	24
2.1.2. Organic volatiles.....	24
2.1.3. Dissolved moisture.....	26
2.1.4. Summary	27
2.2. Void dissolution mechanism	27
2.3. Void growth models.....	30
2.4. Void growth summary	37
2.5. Void growth mitigation strategies	38
3. Experimental methodology	43
3.1. Materials	43

3.1.1. Prepreg.....	43
3.1.2. Resin.....	44
3.1.3. Ancillaries.....	44
3.1.3.1. Breather.....	44
3.1.3.2. Release film.....	44
3.1.3.3. Vacuum bag.....	45
3.1.3.4. Release agent.....	45
3.2. Design and development of the Pressure Tool.....	45
3.3. Study on optimising cure cycle time: Chapter 4 and Chapter 5.....	50
3.3.1. Prepreg lay-up.....	50
3.3.2. Specimen processing.....	51
3.3.2.1. Autoclave.....	51
3.3.2.2. Oven.....	52
3.3.2.3. Pressure tool.....	53
3.3.3. Cure cycles.....	54
3.3.4. Testing methods.....	57
3.3.4.1. Inter-laminar shear strength.....	58
3.3.4.2. Flexural strength.....	59
3.3.4.3. Fibre volume fraction.....	60
3.3.4.4. Void volume fraction.....	60
3.4. Study on limitations to achievable reductions in cure cycle time (Chapter 6).....	63
3.4.1. Process modelling: Characterisation Equipment.....	63
3.4.1.1. Thermal conductivity.....	63
3.4.1.2. Resin rheology.....	64
3.4.1.3. Resin kinematics.....	64
3.4.2. Resin kinematic models.....	65
3.4.2.1. Review of resin kinematic models.....	65
3.4.2.2. Resin kinematics model parameters.....	66
3.4.3. Thermo-kinematic process model.....	72
3.4.3.1. Review of developments in modelling heat transfer in prepreg processing..	73
3.4.4. Thermal conductivity of tooling materials and process ancillaries.....	75
3.4.5. Material choice and material thickness.....	78
3.4.5.1. Normalising tooling thickness for the design of experiment.....	79

3.4.6. Design of Experiment for the study on effect of tooling material and ancillaries on cure cycle time	82
3.4.7. Boundary conditions	85
4. Effect of high heating rate processing on void growth.....	88
4.1. Introduction	88
4.2. Methodology.....	88
4.3. Results and discussion	90
4.3.1. Void volume fraction.....	90
4.3.2. Understanding void mitigation in high heating rate processes	94
4.4. Conclusion.....	101
5. Combined effect of high heating rate and hydrostatic pressure on the physical and mechanical properties of composites.....	103
5.1. Introduction	103
5.2. Methodology.....	103
5.3. Results and discussion	105
5.3.1. Void volume fraction and surface quality.....	105
5.3.2. Fibre volume fraction and laminate thickness.....	115
5.3.3. Inter-laminar Shear Strength and Flexural Strength.....	117
5.4. Conclusions	122
6. Effect of tooling material and process ancillaries on reductions in cure cycle time	124
6.1. Introduction	124
6.2. Methodology.....	125
6.3. Results and discussion	125
6.3.1. Optimum resin system analysis	125
6.3.2. Effect of processing films and heating method	134
6.3.3. Effect of tooling material and process ancillaries.....	137
6.4. Conclusion.....	153
6.5. Recommendations	154
7. Conclusion.....	156
7.1. Void growth mitigation strategy	156
7.2. Predicting and evaluating laminate porosity	157
7.3. Combined effect of high heating rate and consolidation pressure on the physical and mechanical properties of laminates	158
7.4. Effect of resin chemistry	159
7.5. Effect of process ancillaries	160

7.6. Effect of tooling material and laminate thickness	161
7.7. Recommendations for future studies	162
7.8. Processing recommendations.....	163
8. Appendix	164
8.1. Appendix A.....	164
Appendix B: Empirical derivation of optimum burn-off temperature for analysing fibre volume fraction.....	166
Appendix C: Effect of contact agent on measured thermal conductivity.....	167
Appendix D: Rheometer calibration	168
Appendix E: Effect of varying the resin kinematic parameter (D) for conditioned MTM44-1 resin	170
Appendix F: Mesh sensitivity analysis.....	171
Appendix H: References.....	179

1. Introduction

There is growing pressure in the transport industry to develop technologies to reduce greenhouse gas emissions; in particular, the aerospace and automotive industries. Despite the global economic slowdown, between 2007 and 2013 global commercial air travel has been increasing at an average rate of 5% per annum [1], with the current growth rate predicted to continue for the next 20 years [2-4]. In 2011, air travel was responsible for approximately 2% of global emissions of greenhouse gases [5, 6]. Although greenhouse gas emissions by the aviation sector has been decreasing since the 1990s [6], current growth rates can lead to a substantial increase in greenhouse gas emissions. Due to which, the aviation sector is predicted to become a major contributor of global greenhouse gas emissions by 2050, unless considerable increase in fuel efficiency and consequent reduction in greenhouse gas emissions has been achieved.

For airlines, fuel cost can account for up to 30% of operational cost [7]. Naturally, with increasingly volatile fuel prices and uncertainty in supply, there is additional pressure on aircraft manufacturers to increase fuel efficiency. At the 38th session of the International Civil Aviation Organization (ICAO) assembly in 2013, the aviation industry reaffirmed its commitment to increase fuel efficiency by 2% per annum up to 2020 [8]. Furthermore, to minimise the impact of greenhouse gas emissions the aviation sector aims to achieve carbon neutral growth from 2020 onwards. In the long run, the aviation sector aims to continue to increase fuel efficiency by 2% per annum up to 2050 so as to achieve a 50% reduction in greenhouse gas emissions compared to 2005 levels [6].

Of the 50% reduction in greenhouse gas emissions (more specifically CO₂ emissions), 15% - 25% can be achieved through developments in engine technologies; improvements in air traffic management is suggested to yield 5 – 10% reductions; increasing aircraft efficiency yielding 20% - 25% [9]. Increasing aircraft efficiency includes: weight savings achieved by using lightweight metallic and polymer composite materials, increasing aerodynamic efficiency and the use of advanced fly-by-wire systems to name a few [6].

Composite materials are renowned for their directional, high specific mechanical properties. This facilitates the development of components that can be “tailor made” to fulfil specific design requirements, maximising weight savings. Additionally, composites can be fabricated into complex geometry. This enables the consolidation of numerous parts into a single component, reducing assembly time and easing inventory maintenance; ultimately leading to reducing overall manufacturing cost. The ability to fabricate complex geometry also enables the opportunity to create more aerodynamic designs; potentially increasing design flexibility over metallic materials [10].

Since 2000, new generation wide-body aircraft, such as the Boeing 787, the Airbus A380 and A350, make extensive use of composite materials (up to 53% by weight). This has contributed to the acclaimed 20% increase in fuel economy (Boeing) and 25% decrease in fuel burn per passenger seat (Airbus) over competing aircraft [3, 11, 12]. In addition, development of the Bombardier CSeries (greater than 40% composite materials by weight [6]) indicates the beginning of the extensive use of composites in narrow-body aircraft segment as well.

Whilst the increasing use of composite materials in the aviation industry is encouraging, it has been widely acknowledged that weight savings and aerodynamics tweaks alone is insufficient to meet emissions targets. Radical change in all aspects of aviation is needed – unconventional wing designs, new generation propulsion systems, alternative fuels and operational management systems to name a few [6]. However, as it will be evident from the following sections, composites processing technology currently used in the aviation industry, is neither cost effective nor practical for processing excessively large ($> 5\text{m}^2$) primary structural components.

1.1. Strengths and limitations of autoclave processing

Autoclave processing of prepregs has been the method of choice for processing large (up to 5m²) structural components in the aerospace industry. An autoclave is a gas-fired or electrically heated convection oven that can be pressurised up to 7 Bar using an inert gaseous medium; which is usually Nitrogen or Carbon dioxide. Plies of fibres pre-impregnated with a thermoset (or thermoplastic) resin (commonly called prepregs) are hand-laminated – or, more recently, machine-laminated [11, 13, 14] – onto a tool with a predefined fibre orientation of the plies. This maximises directional properties. The lay-up is then sealed with a vacuum bag and de-bulked to consolidate the laminate by removing entrapped air from between plies. A schematic of a typical autoclave lay-up is shown in Figure 1.1. Following lay-up, the laminate is cured in the autoclave using a prescribed pressure and temperature profile to further consolidate the laminate and to achieve sufficient cross-linking of the polymer to create a structural component.

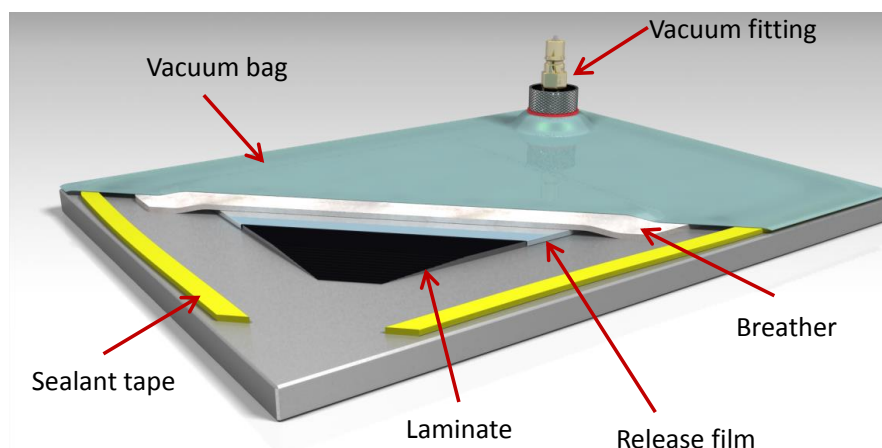


Figure 1.1: Schematic of a typical autoclave prepreg lay-up

Research on optimising the autoclave cure cycle has been on-going since the 1980s and is now well established [15-21]. The extensive research resulted in the development of a process that can consistently and reliably yield laminates with the highest mechanical properties [16, 17, 22]. Indeed, autoclave processed laminates are commonly set as a benchmark when comparing composite processing techniques.

However, the increased production volume and component size demanded by the aerospace industry highlights the limitations of autoclave processing. Based on the most up-to-date (at the time of writing) long-term market forecast published by the major aircraft manufacturers [2-4], it is clear that irrespective of aircraft type (Single Aisle [Narrow-Body], Twin-Aisle [Wide-Body]) there is strong global demand from commercial airlines for new aircraft.

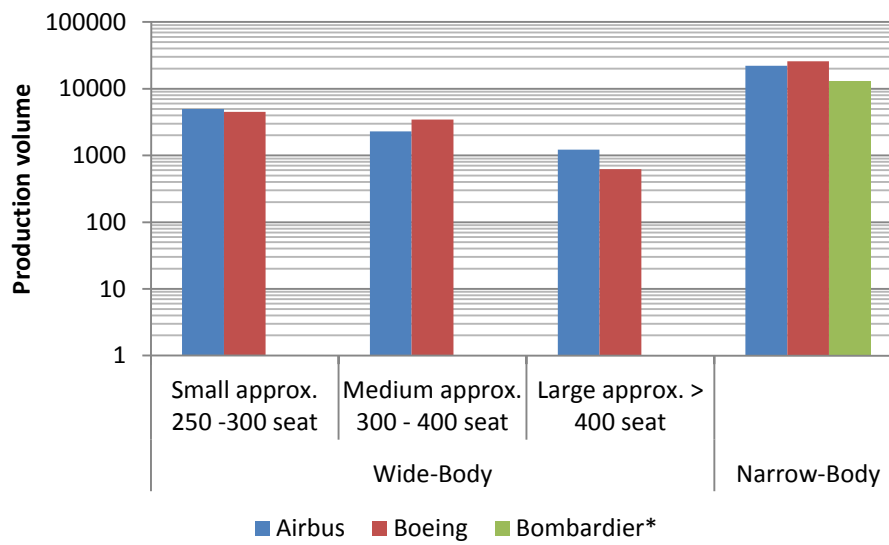


Figure 1.2: Predicted total production volume of “Narrow Body” and “Wide Body” aircraft from 2014 - 2033. *Includes production of 20 – 99 seat regional aircraft with either Turbo-prop and Gas turbine engines [2-4]

Figure 1.2 summarises the predicted sales of new aircraft based on body type from 2014 - 2033. Focusing solely on the predicted number of new wide-body aircraft, both Boeing and Airbus must manufacture an average of 430 and 424 aircraft per annum respectively to meet demand, equating to approximately 36 aircraft per month. Which, using the data by Brosius [23], equates to approximately 144 wing skins, 216 stabiliser, 36 complete fuselages per month – which may not be cost effective using high pressure autoclaves.

Current (as of early 2015) production rate for the Boeing 787 and Airbus A350XWB is 12 aircraft per month and approximately 1 aircraft per month respectively. Boeing has published a target of 14 aircraft per month by 2016 and 16 per month by the end of the decade [24]. Airbus has set a target of 10 aircraft per month by 2018 [25], far less than the 36 aircraft per month needed to meet demand. While the 36 aircraft

per month target includes production of the upgraded versions of current generation Wide-Body aircraft, Boeing 777 (Boeing 777X) and the Airbus A330 (Airbus A330neo), they will inevitably be phased-out and replaced; potentially, introducing models with > 50% composites by weight. Relying on the autoclave for processing large structural components, such as the composite wings on the 777X, forced Boeing to invest more than \$1 billion in upgrading its current facilities and in building a new 'Wing Center' [26]. This highlights the key limitation of the autoclave.

The size of the autoclave is dictated by the size of the component to be processed, an autoclave over 9 metres in diameter and over 50 metres in length is not uncommon in the aerospace industry [27]. Large autoclaves inevitably command higher capital cost and running cost. As shown by Goel [28], the length and diameter of the autoclave are the principal drivers of the capital cost. Also, the autoclave relies on the forced convection of a heated, inert gas (with a high thermal mass) to cure the laminate. The cost of extracting, heating and pressurising the large volume of gas in the autoclave must be taken into account as well; increasing running cost. In addition to the high capital cost and running cost, the combined thermal mass of the gas and the tooling limits the maximum achievable heating rate. This limits the maximum cycle time savings and part turnover that can be achieved. While multiple parts can be cured in an autoclave at the same time, large autoclaves are typically used to cure a single part. The difficulty of predicting the influence of multiple parts on the complex thermo-fluid flow that takes place within the autoclave, and the high value of parts being cured, lead to risk-averse decisions taken by aircraft manufacturers [29, 30].

Owing to the limitations of the autoclave, aircraft manufacturers are hesitant on employing a step increase in the use of large structural composite components in narrow-body aircraft [31] – which accounts for 70% of all new aircraft produced. Manufacturers are now looking at alternatives to autoclave processing that can reliably yield laminates with physical and mechanical properties similar to that processed in an autoclave, but at lower costs and shorter cycle times. Such processes are commonly referred to as Out-of-Autoclave (OoA) and Vacuum Bag Only (VBO) processes.

1.2. Review of recent developments in Out-of-Autoclave processing of high performance composites

Over the last 25 years a variety of Out-of-Autoclave (OoA) processes have been developed, which can be categorised based on the heating method employed: conduction, convection and radiation. This section presents a review of the state-of-the-art OoA processing systems developed for each heating method, with an emphasis on cost, cure cycle time, suitable part size and target production volumes.

1.2.1. Conduction

Processes with a conduction-based heating method employ direct heating of the laminate via either an on-board heating system embedded within the tooling or heating system embedded within cure ancillaries (such as flexible membranes and intensifiers). Compared to convective heating, there is a direct transfer of energy from the heat source to the laminate; increasing efficiency and reducing running cost. In addition, depending on the thermal mass of the tooling and ancillaries, conductive heating methods enable the use of high heating rates to process laminates. In addition to cure cycle time reductions, studies have shown that using high heating rates can increase matrix dominated mechanical properties such as inter-laminar shear strength and flexural strength [32-34]. The following sections highlight the key developments in conductive heating cure methods.

1.2.1.1. Shell tooling with an on-board heating system for processing prepregs

Traditionally, shell tooling consists of a thin tool face, made from metallic or composite materials, supported on an egg crate stiffened or truss stiffened backing structure. Exceptions, such as tooling with a monolithic foam backing structure [35, 36], form a hybrid between shell tooling and monolithic tooling.

Shell tooling is still predominantly used to process composites via convective heating methods. However, examples of shell tooling with on-board heating systems to process large composite components in low volumes have been reported recently. Solent Composite Systems (SCS) process large (>10 m²) wind turbine blades in low volume (< 400 units per annum) using a shell tooling with resistive electric heating elements attached to the back of the tool face [37]. Arney et al [38] and Progoulakis [39] studied the feasibility of using various types of fabric heating elements (also

called “heated fabric”) embedded below the first few surface plies of a composite tooling. Work by Ó Brádaigh et al [40, 41] highlights the advantages of using resistive heating elements embedded in a composite tooling with a ceramic matrix; that is, increased tooling durability, whilst achieving low running cost. Payette et al [42] used a proprietary system where the resistive heating element is applied as a coating on to plies near the surface of a composite tooling. The study highlights the exceptionally low power consumption (when compared to other embedded heating systems) and the high heating rate (50°C/min) that can be achieved. While a reduction in cure cycle time has been achieved when compared to conventional convective heating methods (Oven cure), high void volume fraction has been reported - up to 3.8% compared to 2.9% for oven cured laminates.

Irrespective of the type of electric heating method, all studies highlight the potential to reduce running cost and cure cycle time when compared to convection based heating methods. An additional advantage of electrically heating tooling is the option to configure various heating zones, which facilitate the use of different temperature profiles across the tool face to yield a more optimised cure [37, 43]; though studies on potential gains in mechanical properties by using such a system are limited. Also, in convective heating methods, the size of the heating chamber dictates the maximum size of the part that can be processed. Using tooling with on-board heating systems negates the restriction in part size that can be processed.

However, the disadvantages of shell tooling with on-board heating systems include the limited availability of cost effective cooling options and risk of uneven temperature distribution across the tool face due to the close proximity of the heating element in relation to the tool face. Forced convective cooling using air, whilst relatively inexpensive, increases the risk of a thermal overshoot during cure. This is due to lack of sufficient control over the laminate temperature and limited achievable cooling down rates using this technique. Alternatively, liquid cooling systems can be incorporated into the tool face, but at the expense of increased thickness and complexity – and inevitably cost. In addition, embedded heating systems in composite tooling with a polymer based matrix can accelerate the

degradation of the resin around the heating elements, leading to premature tooling failure.

1.2.1.2. The Quickstep process

The Quickstep process [44] is a well-known, proprietary, high heating rate OoA process. In this process the laminate (on a tool face) is suspended between two flexible membranes filled with an externally heated, temperature controlled heat transfer fluid. A schematic of the system is shown in Figure 1.3. Unlike tooling with an embedded electric heating system, the Quickstep process can achieve high ramp rates during both heating and cooling of the cure cycle. Also, the high heat capacity of the heat transfer fluid facilitates good control over the heat released by the exothermic reaction of the resin.

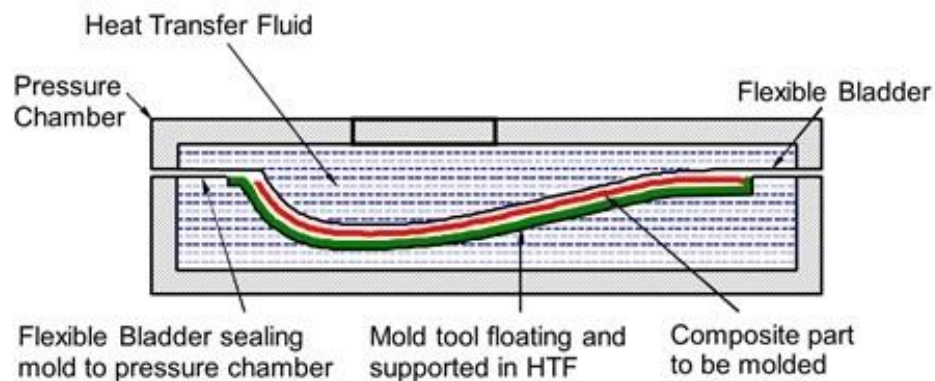


Figure 1.3: Schematic of the Quickstep process [44]

Studies involving the Quickstep process commonly employ a 10°C/min ramp rate [45-47]. However, it has been suggested that up to 40°C/min ramp rates can be achieved [48], combined with between 1.1 to 1.4 Bar absolute hydrostatic pressure [46, 48]. Standard vacuum bagging yields 1 Bar consolidation pressure; while, depending on the Quickstep unit, the flexible membrane applies an additional 0.1 to 0.4 Bar of hydrostatic pressure. The low consolidation pressure relieves the need for expensive, highly stiffened tooling systems, leading to savings in tooling cost [46]. Depending on the system, Quickstep is capable of processing composite components for the aerospace and automotive industry with a maximum part size ranging from 1m² to 20m² [49].

Studies on Quickstep processing highlight the advantages of using high ramp rates – cure cycle time reductions and good laminate properties. Davies et al [32] and Khan et al [33, 34, 47] observed high matrix dominated mechanical properties comparable to or even greater than autoclave cured laminates. Albeit, at the expense of high void volume fraction – up to 1.9%, compared to 0.6% for autoclave cured laminates but less than oven cured laminates (8.9%) by [32]. In addition to reductions in cure cycle time, high heating rates yield a lower minimum resin viscosity (Figure 1.4). The low minimum resin viscosity has been suggested to result in better wet-out; improving matrix adhesion and increasing delamination resistance [32, 50].

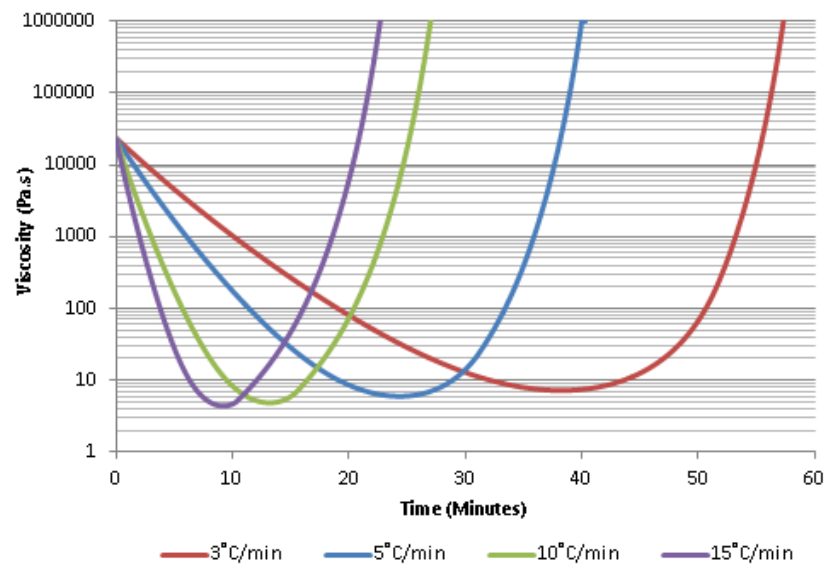


Figure 1.4: Effect of heating rate on resin minimum viscosity of Cytec’s MTM45-1 resin system. Viscosity curves generated using a rheology model presented in [51]

Whilst the advantages of the Quickstep process are clear, as it is a patented process, the cost of royalties per part must be taken into account. The royalty cost is suggested to have led the development of competing high heating rate OoA processes [52]. Also, high heating rate Quickstep cure cycles optimised for low void content (~ 0.5%) are not the shortest cure cycle that can be achieved using the process. Indeed, laminates processed using the shortest cure cycle time have been shown to result in extensive porosity (3 – 9%) [32, 34, 47, 53].

1.2.1.3. Prepreg compression moulding

In prepreg compression moulding the lay-up is performed on a matched, heated tool; following which, both halves of the tool are closed using a platen press, exerting pressure to consolidate the laminate. However, in addition to part geometry limitations that can be processed, it is difficult to apply homogeneous hydrostatic pressure using this process. Attempts have been made to address the hydrostatic pressure limitation via two approaches: The use of a flexible membrane within the tool cavity that can be pressurised using compressed air (such as: bladder moulding and pressure pressing) [54-56]; or the use of a material with a high coefficient of thermal expansion within the tool cavity that is designed to exert hydrostatic pressure when heated (such as the trapped rubber moulding and Thermal Press Cure (TPC) processes) [52, 57-60].

'Pressure pressing' is a patented high heating rate OoA process claimed to process laminates in short cycle time (< 17 minutes) while yielding autoclave level laminate quality [59, 61]. A flexible membrane across a mould cavity replaces the traditional vacuum bag. Vacuum is drawn on the laminate size of the membrane, while up to 24 Bar hydrostatic pressure is applied (using a compressed gas) on the other side of the membrane to consolidate the laminate. Curing of the laminate is performed via the circulation of a heat transfer fluid through cavities within the tool. While a cycle time of 17 minutes has been quoted to process thermoset prepreps, publically available studies on resulting laminate mechanical properties when using this process are limited. Also, a large hydraulic press is required to maintain pressure throughout the cure cycle, limiting the part size that can be processed.

Whilst trapped rubber moulding can yield laminates with good consolidation and high mechanical properties, the low thermal conductivity of the rubber can lead to non-homogeneous thermal expansion when heated, unless a slow heating rate is employed [62, 63]. Walczyk et al [52, 57-59] developed the patented Thermal Press Cure (TPC) to address this limitation while providing an alternative to the Quickstep process. The design of the elastomeric material has been optimised to yield hydrostatic consolidation pressure when heated. A high heating rate (10°C/min) has been achieved while yielding laminates with mechanical properties comparable to

autoclave cure. In addition, capital cost and running cost per part has been shown to be 60% less than that of the Quickstep process [58]. However, current design of the process relies on embedding electric heaters within the tool to reduce cost, limiting the maximum cooling down rate that can be achieved.

1.2.2. Convection based Out-of-Autoclave process – Oven cure

Before the development of the conductive heating systems, oven cure was synonymous with OoA processing. While low consolidation pressure (1 Bar) has been shown to reduce cost when compared to autoclave processing [64, 65], oven cure of first generation OoA prepreg systems yielded laminates with low mechanical properties due to extensive porosity. This limited the uptake of this process in industry to non-structural applications. However, the physical and rheological characteristics of second generation OoA prepreg systems have been optimised to yield low porosity and high mechanical properties when using vacuum only consolidation pressure.

While high mechanical properties can be achieved using oven cured OoA prepreps [42, 66, 67], there is a large variability in reported void volume fraction for oven cured OoA prepreps. Studies have reported void fraction ranging from 0.5% to 6.5% [42, 66, 68, 69] when processing less than 300mm long panels. Nevertheless, processing an autoclave prepreg system using VBO pressure has been shown to yield even higher porosity (8.9%) [32]; but can yield less than 0.5% porosity when processed in an autoclave [32, 68]. Due to the low consolidation pressure, OoA processing is heavily dependent on the efficacy of the removal of entrapped air via the engineered air evacuation channels in the prepreg. Issues such as premature filling of the air evacuation, insufficient edge breathing and insufficient vacuum can lead to high void content; indicating a lower margin of error than autoclave processing. In addition, oven cure of composites suffers from the same limitations of autoclave processing; namely: part size being limited to the size of the oven, the high energy cost due to the high heat capacity of the gas based heat transfer medium and the slow heating rate increasing cure cycle time.

1.2.3. Radiation

Whilst conduction and convection based heating methods are the more established routes of processing composites, continual developments in radiation based processing over the last three decades cannot be ignored. Radiation based processing of composites involves curing the resin system using: X-Rays [70], gamma rays, microwaves [71-73], electron beam [74] or ultraviolet rays [75]. However, most radiation based processing have their unique limitations. The issue of handling and disposal of used radioactive material hinder processing composites on an industrial scale using gamma rays and X-ray processing of composites. Ultraviolet curing of resin is said to be limited to open-moulding processes and transparent composites [74]. Due to which, interest is primarily focused on processing composites using microwaves and electron beam. However, as it will be evident from the following sections further work must be done before such technologies can be considered a viable alternative to conduction and convective processing of composites.

1.2.3.1. Microwave cure of composites

Unlike thermal-based processes, microwave processing relies on the transfer of energy by the interaction of the material with electromagnetic waves at a molecular level. This leads to more efficient use of energy than possible with thermal based heating systems. In addition, instantaneous volumetric heating achieved by microwave processing can potentially eliminate the temperature ramp phase of a typical cure cycle, thus reducing cure cycle time. Studies characterising the mechanical properties of microwave cured composites are well established [71, 72, 76, 77]. In particular, studies highlight the increase in matrix dominated mechanical characteristics, albeit with high void volume fraction – similar to conduction based high heating rate processes.

It has been suggested that the difference in dielectric properties between the fibres and the resin causes selective heating of the fibres, which in turn causes rapid heating of the resin surrounding the fibres [78]. This has been claimed to improve fibre-matrix adhesion and thus mechanical properties. It should be noted however, that characterisation studies on microwave processing focused primarily on composites with glass fibre reinforcement. Due to the high dielectric loss of carbon

fibre, changing the fibre orientation can increase the reflectance of the first few plies, leading to insufficient heating of the laminate [73]. Also, the electrical conductivity of carbon fibre can lead to arching which leads to the formation of localised hot spots within the laminate, in addition to puncturing the vacuum bag. This necessitates the need for microwave grade bagging ancillaries, which is currently limited in supply.

While microwave processing is more efficient than thermal methods, a cost analysis by Witik et al [64] shows that due to the limited availability microwave-grade consumables and the high capital cost is a limiting factor. The study showed that the cost of microwave processing is currently greater than that of autoclave processing.

1.2.3.2. Electron-beam cure

In Electron beam (also called e-beam) cure, high energy electrons emitted by an accelerator initiates crosslinking of the polymer through decomposition of a radiation-sensitive initiator [74]. Current (albeit limited) applications in the aerospace industry include the in-situ cure of automated tape lay-up fabric and repair of composite panels using low energy electron beam. Advantages of e-beam cure include: reduced cure cycle times; use of resin systems with indefinite shelf life (when exposure to UV rays is minimised); the use of low cost tooling such as wood and polystyrene and greatly reduced residual stresses within the laminate. The ability to use low cost tooling is because the tools are not exposed to high temperature. As the processing temperature is not high the issue of mismatch in tool-part temperature is negated; which enables the option of processing large components with low warpage.

While the mechanical properties of e-beam cured laminates are comparable to that of autoclave cured laminates, characterisation studies on laminate properties highlight the reduction in inter-laminar shear strength when compared to autoclave processed laminates [79, 80]. Janke et al [80] suggests that the inter-laminar shear strength can be improved via the addition of e-beam compatible sizing and through surface treatment of the fibres [81]. The low ILSS is due to insufficient resin flow leading to poor wet-out and extensive porosity [74]. In addition, processing thick

laminates (20mm) need high energy electrons (5 - 15MeV) to penetrate the whole thickness of the part. Apart from the increase in capital cost, use of high energy emitters necessitates the need for concrete 'maze' enclosures to shield the emission of x-rays, a by-product of e-beam processes [74]. Finally, while developments in new resin systems with radiation-activated initiators can yield indefinite prepreg shelf-life, gaining approval for the use of new resin formulations in the aerospace industry can be arduously time consuming and expensive.

1.3. Theme of work

Owing to the pressure to reduce green-house gas emissions, the aerospace industry is replacing large structural metallic components with low density, high performance composites. However, there is a need for an alternative OoA processing technique optimised for low production volumes (< 1,000 units per annum), without increasing cycle time or cost and without sacrificing laminate quality. Current OoA processing techniques have been shown to yield high quality laminates, but at the expense of cycle time or cost or restrictions in part design.

Porosity has been shown to be detrimental to matrix dominated mechanical strength and stiffness properties [16, 18, 19]. The aerospace industry commonly uses 2% void volume fraction as the acceptable level of laminate porosity [42]. Studies have shown that porosity above this limit affects laminate properties. Extensive work on optimising the autoclave process resulted in consistently achieving exceptionally low laminate porosity (< 0.5%).

High heating rate processing of prepregs with low consolidation pressure, whilst achieving low cycle time, cannot match the low void volume fraction achieved by the autoclave. Also, the mechanism by which void growth has been mitigated in high heating rate processes is not well understood. Due to which, conservative steps have been employed in improving high heating rate processes. For instance, the use of excessive hydrostatic pressure (10 Bar) combined with high heating rate; reducing cure cycle time at the expense of overall cost.

This work presents the development a novel high heating rate process with low consolidation pressure (up to 3 Bar) to process high performance composites,

without increasing cost or cycle time. Whilst the work is ideally suited for aerospace applications, the findings of this research are applicable to any industry that relies on autoclave processing of composites in low volume – high performance niche automotive and motorsports.

The first stage of this study addresses the limited understanding of how void growth is mitigated in high heating rate processes. A general literature review is performed to understand the dominant mechanism of void growth mitigation (Chapter 2) and to develop optimised high heating rate cure cycles. Chapter 3 summarises the experimental methods used to characterise laminate properties along with the design and development of the novel high heating rate process. Chapter 4 evaluates the effect of the optimised cure cycles on void growth. Chapter 5 addresses the limited studies on the combined effect of high consolidation pressure and high heating rate on mechanical properties of laminates. Chapter 6 defines the bounds of applicability of the novel high heating rate process in terms of applicable laminate thickness, required tooling material and the effect of processing ancillaries on achievable reductions in cure cycle time.

2. Literature review: Causes of void and void growth mitigation strategies

2.1. Causes of voids

Although studies examining the constituent component of voids are limited [45], it is widely accepted that voids are formed either due to the dissolution of dissolved gases within the resin or due to air entrapment during lay-up. However, the dominant source of voids is contested. Some studies argue that voids are formed due to entrapment of air during lay-up [82, 83], while other studies argue that voids are formed due to the dissolution of moisture during the cure cycle [68, 84], still others argue that voids are made up of organic volatiles given off by the resin during cure [37, 45]. So as to develop a void mitigation strategy, the following sections break-down the individual arguments to identify the main source of voids.

2.1.1. Entrapped air

2.1.1.1. Effect of fibre architecture on air permeability

Entrapment of air between plies during lay-up is inevitable. The efficacy of the removal of entrapped air is dependent on the 'breathability' of the prepreg [85, 86]. As stated in a review of OoA processing [67], Thorfinnson and Biermann pioneered the study on the relation between prepreg impregnation and porosity [87, 88]. They defined the quality of prepreg impregnation (degree of impregnation) as the ratio of resin-saturated interstitial volume to total interstitial volume in the prepreg. It was found that high degree of impregnation (92%) resulted in high void content, while a low degree of impregnation (60%) yielded void-free laminates. Dry fibres in prepreps with low degree of impregnation was suggested to create "air escape channels" through which entrapped air, organic volatiles and water vapour released by the resin during cure can be removed (Figure 2.1).

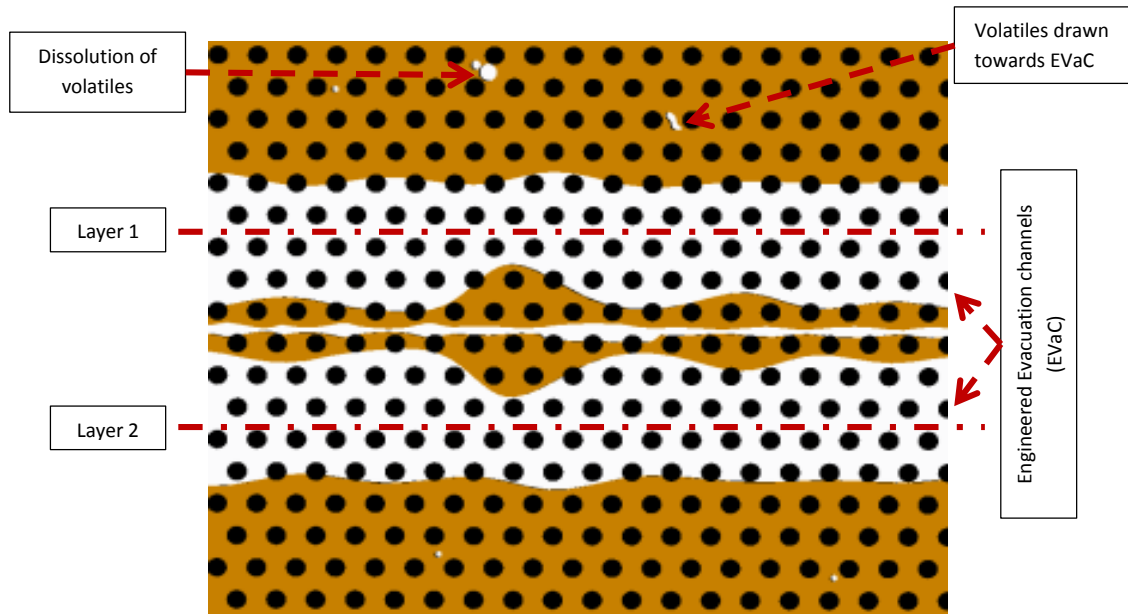


Figure 2.1: Schematic of current generation OoA prepreg during de-bulk. Note the bias in impregnation of current generation OoA prepreps. The bias in impregnation facilitates the removal of entrapped air from between plies.

Over the years various studies attempted to quantify the air-permeability characteristics of prepreps. Nam et al [89] studied the impact of applied pressure and temperature on in-plane gas permeability of a prepreg with a plain weave fibre architecture (Hexcel F593-18/Plain weave T300 carbon fibre fabric). Air permeability was found to decrease with increase in de-bulk duration. In addition, an increase in either temperature or pressure further reduced permeability. This was attributed to fibre nesting and resin flow sealing off the inter-laminar air path formed by the crimp of the woven fibres. From the study, in-plane permeability has been inferred to be $4 \times 10^{-12} \text{ m}^2$ at room temperature with vacuum only consolidation pressure.

A subsequent study [83] isolated the efficacy of in-plane inter-laminar and in-plane intra-laminar air permeability by using selectively impregnated first generation unidirectional prepreg (Fibredux, now Hexcel, 924C/T300-S-34). In-plane inter-laminar air evacuation was found to be more dominant than in-plane intra-laminar extraction. However, even with vacuum only consolidation pressure the air channels were found to collapse due to “cold flow” of resin – a now well-known issue with first generation selectively impregnated prepreps [67]. A combined inter- and intra-

laminar in-plane permeability ranging between $6 - 7 \times 10^{-13} \text{ m}^2$ has been inferred from the study - an order of magnitude lower than woven prepregs.

Hsiao [90] characterised the in-plane and through-thickness permeability of a current generation OoA prepreg (Cytec's CYCOM 5320/T650 3k tow size) with a plain weave fibre architecture. In agreement with Nam et al, in-plane permeability decreased with increase in temperature and de-bulk time. However, the study showed that in-plane permeability increased by an order of magnitude (from 4×10^{-14} to 10^{-13} m^2) when air evacuation channels in the prepreg "opened-up" at approximately 90°C . A combination of low resin viscosity at the elevated temperature and vacuum drawn along the laminate edges was suggested to have 'unblocked' the air evacuation channels, leading to improved permeability. Louis [85] observed a similar trend when characterising the in-plane and through-thickness permeability of Cytec's MTM45-1/CF2426A consisting of 6k carbon fibre in a five-harness satin weave. Rheological analysis of the MTM45-1 resin system confirmed that resin minimum viscosity point occurs just after 100°C for the ramp rate used in the study. This implies that the increase in air permeability could be due to the unblocking of the air evacuation channels. However, this occurrence has not been observed in other studies. Tavares et al [82] reported stabilisation of air permeability after the initial decrease; though, subsequent increase in permeability was observed after the resin underwent gelation. This was attributed to air paths created by micro-cracks formed due to resin shrinkage. However, by this stage the resin viscosity is too high to physically remove any voids. Furthermore, the increase in air permeability was also attributed to experimental artefacts created due to the configuration of the test equipment and the sample size. This suggests that the increase in air permeability may not be observed when processing large components.

Data inferred from the above studies indicate a substantial bias between in-plane and through thickness air permeability. In-plane permeability was found to be up to five orders of magnitude higher than through thickness permeability. Louis reported through thickness permeability from $6.5 \times 10^{-19} \text{ m}^2$ to less than 10^{-20} m^2 (depending on temperature), compared to $8.78 \times 10^{-17} \text{ m}^2$ in the study by Hsiao. The low permeability was attributed to the tortuosity of the path of air flow through the resin

saturated fibres. Attempts at increasing through-thickness permeability have been encouraging. For instance, creating perforations on a unidirectional prepreg, and aligning the perforations to create a continuous air evacuation path, increased through thickness permeability by five orders of magnitude [82]. However, the effect of disturbing the fibre bundles during perforation on the mechanical properties of the laminate is not known.

Grunenfelder and Nutt [91] accounted for the effect of fibre orientation on in-plane air permeability. An intra-laminar in-plane volumetric permeability of $2.24 \times 10^{-17} \text{ m}^3$ was obtained when fibres were longitudinal to the flow (0°) and $1.49 \times 10^{-17} \text{ m}^3$ when fibres were transverse (90°) to the flow. The transverse permeability is comparable to the through thickness permeability obtained by Hsaio. However, further data using different fibre architectures is needed to draw a definitive conclusion.

	Direction	Air permeability (m^2)	Reference
Unidirectional prepreg	in-plane	$7 \times 10^{-13} \text{ (a)} - 2 \times 10^{-14}$	[83, 92]
	through-thickness	5×10^{-18}	[67]
Plain weave woven prepreg	in-plane	$4 \times 10^{-12} \text{ (a)} - 4 \times 10^{-14}$	[89, 90]
	through-thickness	8.8×10^{-17}	[90]
5HS satin weave prepreg	in-plane	$3 \times 10^{-14} - 6 \times 10^{-14}$	[85]
	through-thickness	$1 \times 10^{-18} - 6.5 \times 10^{-19}$	[67]

Table 2.1: Summary of air permeability values for various fibre architectures. In-plane permeability can be up to five orders of magnitude higher than through thickness permeability. Note: (a) signifies data obtained for first generation OoA prepreps.

Table 2.1 summarises the in-plane and through thickness permeability of various fibre architectures. It is clear that through thickness permeability is up to five orders of magnitude less than that of in-plane permeability; hence the emphasis on ensuring effective edge breathing to remove entrapped air [86, 93, 94].

Based on the above data, in-plane permeability of current generation OoA prepreg ranges from 10^{-14} m^2 to 10^{-15} m^2 , compared to 10^{-12} to 10^{-15} m^2 for prepreps

characterised in the 1990s. This appears to indicate that current generation prepregs are not more 'breathable' than previous generation prepregs. The variability indicates that additional factors must be taken into account to understand the likelihood of void formation due to entrapped air; Namely, quality and duration of vacuum application [69, 92, 95, 96], resin flow characteristics [86, 97], effective use of lay-up ancillaries [98, 99] and part size [92].

2.1.1.2. Vacuum quality

Whilst the high consolidation pressure during autoclave processing facilitates void shrinkage and collapse (explained in the subsequent sections), VBO processing relies on a different void removal mechanism. Due to the low consolidation pressure, VBO processing is heavily dependent on the physical removal of entrapped air via the air evacuation channels. It is therefore imperative that a high vacuum level is maintained to achieve low laminate porosity. As highlighted by Ridgard [86, 97], laminate void volume fraction is inversely related to the applied vacuum level. In addition, Ridgard highlighted the issue of altitude on vacuum level, as at high altitude the absolute vacuum that can be applied is reduced, resulting in high voids (Figure 2.2).

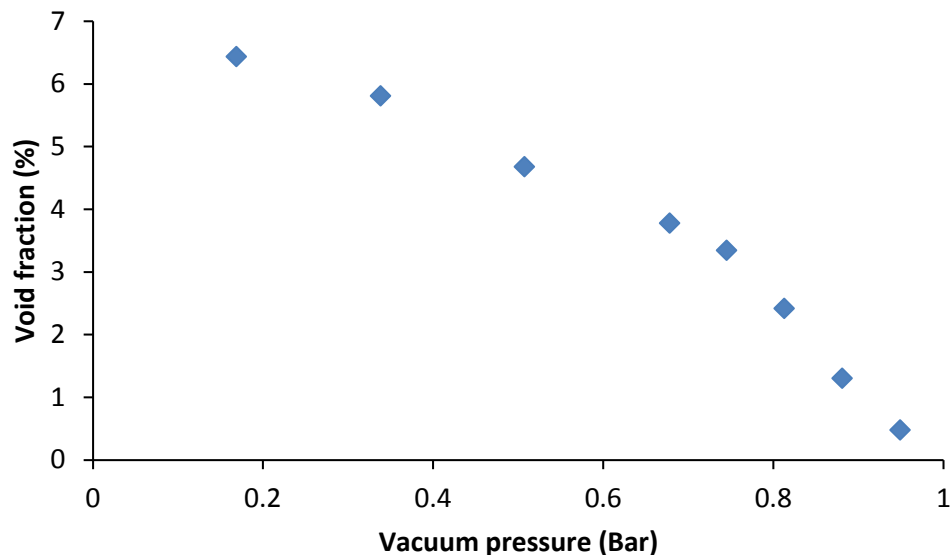


Figure 2.2: Effect of vacuum pressure on laminate porosity. At high altitude the absolute vacuum that can be applied is reduced. Data inferred from [86]

Kay et al [69, 95] characterised the impact of vacuum level, moisture content and de-bulk time on laminate porosity. In-line with the findings by Ridgard, reduced vacuum resulted in higher void content. However, the increase in void content was found to be marginal, 2% compared to up to a 7% increase as per Ridgard. However, it was found that prepregs with higher dissolved moisture content was more sensitive to the level of vacuum applied. As per Ridgard, the OoA prepreg system is designed to remove both entrapped air and dissolved volatiles from the resin through the air evacuation channel, although the science behind the physical removal of dissolved volatiles via the air evacuation channels was not explicitly stated.

2.1.1.3. Part size

In a later study, Kay et al [69] found that in addition to vacuum level the duration of vacuum application is critical to laminate quality. Increasing the duration from 0.5 hours to 24 hours decreased void volume fraction from 12% to < 1% for a 1m long laminates conditioned at 75% relative humidity. Arafath et al [92] developed an analytical model which considers the entrapped gas as a compressible fluid that flows through a permeable, porous medium. The model is based on Darcy's law for gas flow in a porous media combined with the ideal gas law to account for the compressibility of the gas. The following expression predicts the time required to reach a given residual mass fraction of entrapped air within the laminate [92]:

$$t = \frac{\mu L^2}{P_0 K} \left[-\frac{1}{0.9} \ln \left(\frac{m}{m_0} \right) \right]^{\frac{1}{0.6}} \quad \text{Equation 2.1}$$

Where

μ is the viscosity of the gas

P_0 is the initial pressure

L is the laminate length

K is the permeability of the fibre bed

$\frac{m}{m_0}$ is a ratio indicating the residual mass fraction air in the laminate

Using Equation 2.1 and the air permeability data from Table 2.1, a comparison of the required de-bulk time between different fibre architectures and part size can be performed (Figure 2.3 and Figure 2.4).

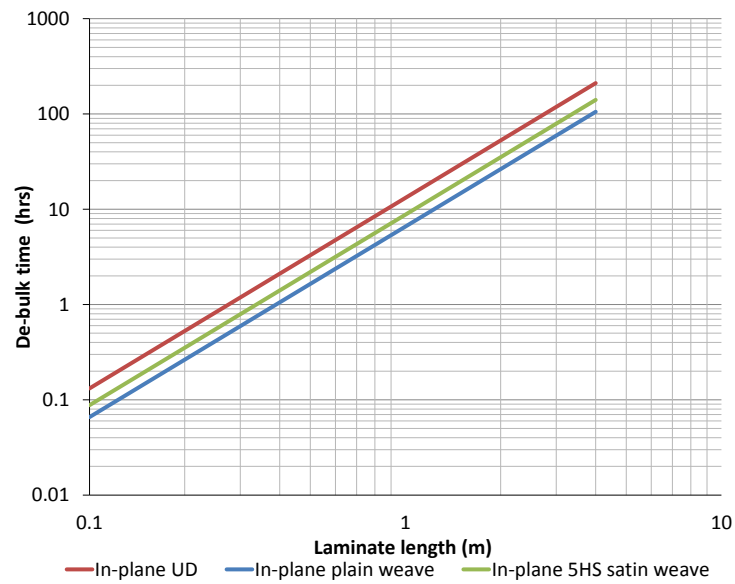


Figure 2.3: Effect of fibre architecture and part size on de-bulk time

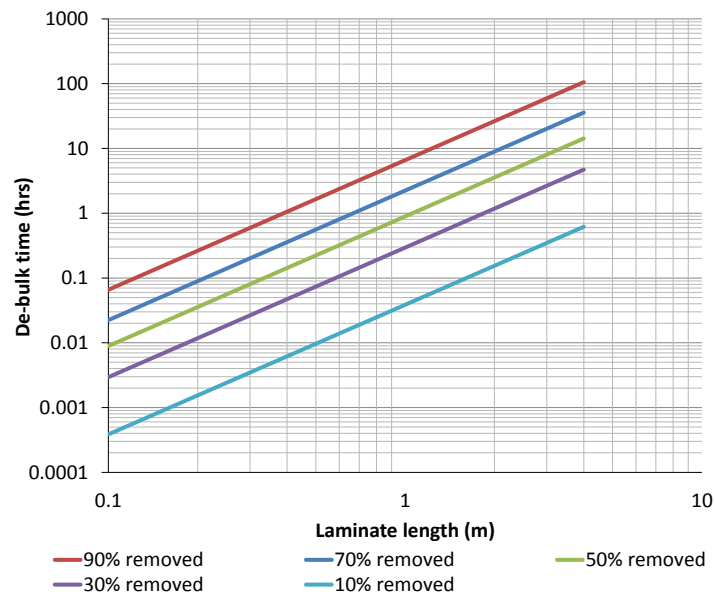


Figure 2.4: De-bulk time required to reach a given residual mass fraction of air in the laminate for a plain twill weave laminate.

Prepregs with low gas permeability (UD prepregs) fare worse than prepregs with relatively higher gas permeability (woven prepregs). For instance, the time required to remove 90% of entrapped air from a 1-metre-long UD prepreg is calculated to be 13.2 hours, compared to 29 minutes for a woven prepreg (Figure 2.3). In addition, as shown in Figure 2.4, the time required to remove entrapped air increases

exponentially with reduction in residual mass fraction of air in the laminate for a given fibre architecture.

While a correlation between the quantity of residual entrapped air and void volume fraction cannot be ascertained (due to lack of sufficient data), assuming an equal residual mass fraction of entrapped gases, a comparison of the findings by Kay et al and Arafath indicate that to physically draw out dissolved volatiles (and moisture) from the prepreg necessitates a longer de-bulk time – 24 hours or greater compared to 13 hours. In addition, the time required to remove entrapped air can be longer what the model suggests. The model fails to account for the decrease in air-permeability with de-bulk time due to “cold flow” of resin sealing the evacuation channels.

2.1.1.4. Lay-up ancillaries

Brilliant [99] studied the impact of lay-up ancillaries (breather, pressure intensifiers and pressure strip) on cured laminate thickness and porosity in parts with 90° corners. Caubergh [98] studied the impact of ply drop-offs and effect of closely spaced, tight corner radii on corner thickness and porosity. In both studies laminates were processed using VBO consolidation pressure, with edge breathing used as the sole means of air evacuation from between plies. Although a pressure intensifier is generally used to achieve good consolidation in sharp corners, both studies reported high porosity; however, at different regions below the intensifier. In the study by Brilliant, voids were observed in the first 2-3 plies under the intensifier; while Caubergh detected voids between plies near the tool side of the laminate, especially when using a concave tool. Brilliant speculated that the high localised pressure resulted in collapse of the air evacuation channels, leading to air entrapment. Caubergh observed signs of resin migration from regions of high pressure (convex corners) to regions of low pressure (concave) corners, potentially sealing off the air evacuation channels due to excessive resin flow. In addition, Caubergh noted that the ply drop-offs did not increase the quantity of entrapped air voids in the laminate, as long as the ply-drop off was in contact with a neighbouring air evacuation channel. However, as shown by Hughes and Hubert [100], the risk of void formation due to ply-drop off is still high.

Both studies reported that optimising the use of process ancillaries – such as sandwiching a layer of breather between the intensifier and release film to prevent localised collapse of the channels – can alleviate void formation in sharp corners and aid in consolidation. However, the low degree of impregnation of OoA prepregs (leading to high bulk factor) has been shown aggravate the formation of secondary defects such as fibre wrinkling in convex (male) corners and corner thickening in concave (female) corners. The findings up to this stage highlight the sensitivity of OoA processing to handling, design and operator experience.

2.1.1.5. Resin rheological characteristics

As is evident from the previous sections, rheological characteristics of the resin during de-bulk and during the cure cycle affect the final void volume fraction within the laminate. The ideal resin system for an OoA prepreg maintains a high resin viscosity during de-bulk to mitigate “cold flow”. During the early part of the cure cycle, the resin maintains a high enough viscosity to prevent the premature infiltration of the evacuation channels. However, the resin must flow sufficiently before gelation to fully infiltrate the evacuation channels to prevent the formation of flow induced voids as seen in first generation OoA prepregs. Current OoA prepregs are designed to have a relatively high viscosity early in the cure cycle to prevent the inadvertent sealing of air evacuation channels [86]. However, further increase in initial resin viscosity, whilst minimising cold flow, could potentially lead to the formation of voids due to insufficient resin flow during cure. In addition, as highlighted by Centea et al [67], the resin’s rheological characteristics is a compromise based on: the temperature profile used during cure, cost, resin life (out-time and shelf life) and the viability of formulating a resin chemistry that can meet all the requirements. The limitation of the resin cure characteristics on cure cycle time reduction is discussion in detail in Chapter 6.

2.1.2. Organic volatiles

The formation of organic-volatile voids is dependent on both the resin impregnation methodology used when manufacturing the prepreg and on the resin chemistry. During manufacture, resin is infused into the reinforcement fabric using either a hot-melt process or a solvent dip process. In the hot-melt process a thin layer of heated

resin is applied onto a backing paper; the reinforcement fabric is then laid onto the resin coated backing paper and consolidation using rollers. The combination of heat and pressure impregnates the fibres with resin, forming the prepreg. The degree of impregnation can be controlled by varying the temperature and pressure. In the solvent dip process, the viscosity of the resin is reduced to aid impregnation by dissolving the resin in an organic solvent (eg. acetone). The reinforcement fabric is then dipped into the solution and then dried in an oven to remove the solvent from the resin.

The solvent dip process is currently being superseded by the hot-melt process owing to stringent regulations on minimising the release of volatile organic compounds (VOCs) – a limitation of the solvent dip process. Also, the degree of resin impregnation cannot be controlled effectively using the solvent dip process. In addition, prepregs processed using the solvent dip process can have high residual solvent in the resin system (ranging from 1 – 2 % [67]), leading to the formation of voids during cure. Owing to the above limitations, current generation OoA epoxy prepregs are manufactured using a hot-melt process.

Some resin systems are inherently more prone to release organic volatiles during cure than others [101]. Phenolic resin systems, such as Novolacs and Resols, are well documented to release organic volatiles and moisture during cure [101, 102]. However, Phenolics have excellent flame resistant properties making it ideal for processing non-structural and semi-structural components – such as aircraft interiors. Epoxy resin systems inherently release very low volatiles during cure ($\ll 0.01\%$ [94]). Studies on combining Phenolics with Epoxy resin based systems are on-going to minimise the release of organic compounds during cure while enhancing thermal properties [101]. Unlike Phenolics, Bismaleimides (BMI) resin systems are renowned for retaining high mechanical properties at elevated temperatures and release negligible volatiles during cure [42], however, is more difficult to process (chemically aggressive, can react with bagging material leading to vacuum loss) and is more expensive than epoxy resin systems.

Strategies to mitigate void formation due to organic volatiles are similar to that employed in minimising entrapped air voids: physical removal via air evacuation channels and preventing dissolution of organic volatiles via the application of hydrostatic pressure. However, as shown in the previous section, physical removal of organic volatiles may not be feasible when processing long structural components due to poor in-plane permeability. In addition, as shown in the study by Agius et al [45], the pressure required to prevent the dissolution of organic volatiles has been shown to increase exponentially with temperature. Inferring from the data presented by Agius et al, the resin pressure required to prevent the dissolution of acetone is 1 Bar at approximately 55°C rising to 5 Bar at approximately 105°C. The temperature at which dissolution of volatiles takes place is less than the minimum cure temperature of current generation OoA resin systems, indicating that dissolution of volatiles leading to void formation is inevitable. Agius et al suggest that owing to the low amount of dissolved volatiles in hot-melt processed epoxy and BMI based prepregs, although more potent than dissolved moisture to form voids, organic volatiles are not a key source of void growth in current generation OoA prepregs.

2.1.3. Dissolved moisture

Owing to the hygroscopic nature of epoxy resins, the quantity of dissolved moisture in the resin increases with time. As-received prepreg can contain up to 0.25 - 0.4% dissolved moisture by weight [68, 103], which without sufficient consolidation pressure have been shown to form voids via a dissolution mechanism. In addition, studies characterising void growth in prepregs have shown that exposure of prepregs to high ambient humidity (> 50% relative humidity) for long duration of time (>24 hours) increases the concentration of dissolved moisture in the resin, increasing the propensity for void formation [35, 68, 103]. While the lay-up of laminates is generally performed in a temperature and humidity controlled clean room, the long lay-up time leads to an inevitable increase in dissolved moisture content.

The high consolidation pressure used in the autoclave has been shown to be capable of processing laminates with low porosity even after exposing the prepreg to 90% relative humidity for 24 hours [68]. On the other hand, VBO processing of prepregs

exposed to 90% relative humidity resulted in high porosity (> 3%). In addition, work by Kardos et al [84] and Brand et al [104] have shown that moisture can diffuse into existing entrapped air voids, increasing the partial pressure of the void, preventing void collapse. Ridgard [86] suggests that dissolved moisture can be drawn out of the prepreg via the air evacuation channels. However, as stated in Section 2.1.1.3, physical removal of moisture may not be feasible for long components.

2.1.4. Summary

Air entrapment during lay-up is inevitable. Owing to the low permeability of the fibre bed, the complete removal of entrapped air and dissolved volatiles (including moisture) by physically drawing out the gases is not feasible. Especially when processing large (> 1m long) components. In addition, the long lay-up time combined with the hygroscopic nature of the resin system leads to an increase in moisture concentration within the resin. The dissolved moisture can diffuse into existing entrapped voids, preventing void collapse by increasing partial pressure, or can create water-vapour voids via a dissolution mechanism. Owing to the OoA prepreg manufacturing process and predominant use of epoxy based prepreps for manufacturing structural components in the aerospace industry, dissolution of volatiles is not considered to be a primary source of voids. While the physical removal of voids is not feasible, strategies on void growth mitigation must focus on optimising conditions to prevent the dissolution of dissolved volatiles and to encourage the shrinkage and collapse of existing voids.

2.2. Void dissolution mechanism

Mathematical models predicting bubble formation and growth using the classical bubble nucleation theory and Fickian diffusion based mechanisms are well established [105-108] and have been adapted to predict void growth in composites.

As per the classical nucleation theory, formation of voids in the bulk resin (homogenous nucleation) will only take place if the driving force for the formation of a new phase within the resin is greater than the interfacial energy (also called surface energy) at the void-resin interface. Assuming that the void is spherical the

expression to define the energy required for the formation of a new phase is given as follows:

$$N = -\frac{4}{3}\pi r^3 \Delta F_v + 4\pi r^2 \sigma$$

Equation 2.2

$-\frac{4}{3}\pi r^3 \Delta F_v$

$+ 4\pi r^2 \sigma$

Driving energy

Interfacial energy

Where,

r is the radius of the void

ΔF_v is the free energy change per unit volume for the phase transformation

σ is the surface energy

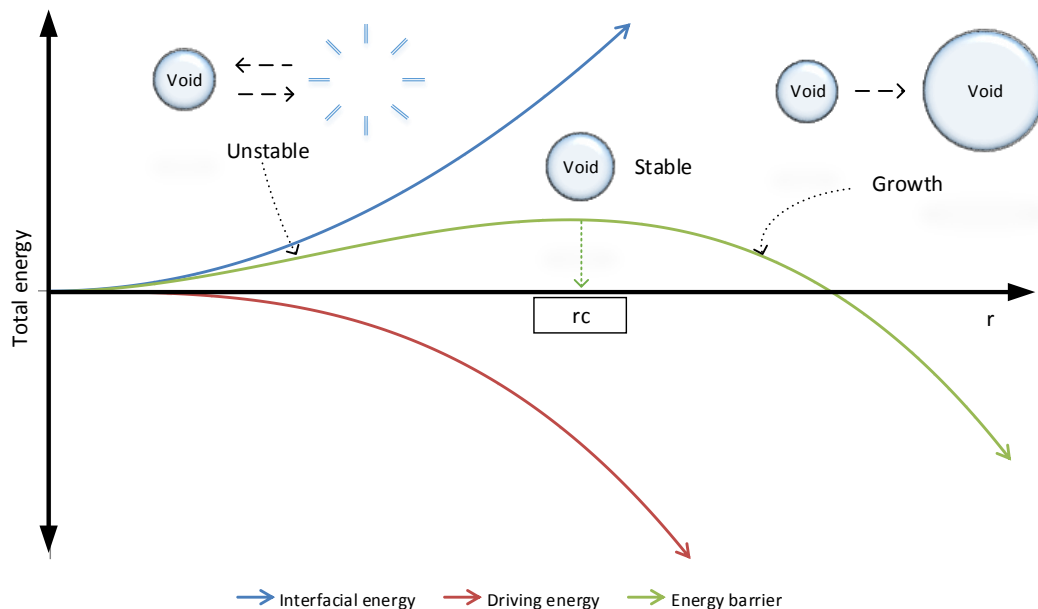


Figure 2.5: Generic plot of bubble radius (r) against the total energy (N) with annotations to indicate the critical bubble radius (r_c) needed for the formation of stable voids.

A generic plot of the driving energy, interfacial energy and the energy barrier (N) is given in Figure 2.5. There exists a critical value of r where the sum of the driving energy and interfacial energy is equal to zero (r_c). Stable void formation can only take place when the radius of the nucleating void is greater than the critical radius. However, the surface tension force (identical to the interfacial energy) acting on the void surface is inversely proportional to the void diameter; implying that, due to the surface tension force, the probability of homogeneous (any point in the bulk medium

devoid of an interface) void nucleation is low. Other studies also noticed a large discrepancy between the bubble nucleation rates determined by the classical homogeneous nucleation theory and experimental observations [43, 106]. Interfaces and impurities within the resin domain, such as: dust particles, contaminations (release agent, skin oil from improper handling) and fibres, reduce the energy required for void nucleation – heterogeneous nucleation. While attempts have been made to account for this limitation, studies using the alternate models to predict void nucleation in composites are limited [106, 109]. In addition, the accuracy of the alternative models has been found to be lacking [106].

Jones et al [106] highlighted the discrepancy between the predicted nucleation rate (as per the classical nucleation theory) and observed results. The classical nucleation theory assumes that nucleation takes place either in the homogeneous fluid domain or at interfaces within the domain. However, Jones et al showed that nucleation preferentially occurs at the interface of pre-existing voids within the fluid domain. This significantly reduced or negated the energy required for void nucleation to take place. Dean [44] studied the effect of adding broken glass to a saturated fluid on bubble nucleation. The study showed that entrapped air in cavities (scratches on the glass surface) ranging from 8 – 75 μm could act as nucleation points. In composites processing, work by Chambers et al [29] highlights the presence of ‘micro-voids’ in uncured hot-melt processed resin films, which can act as a potential nucleation point. Work by Jones et al explains the science behind Ridgard’s [86] suggestion of removing moisture and dissolved volatiles via the air evacuation channels: dissolution at the interface potentially leads to physical removal via the air evacuation channels.

Owing to the size and random distribution of the micro-voids and impurities within the resin, the assumption of instantaneous nucleation of voids, as done in several prominent studies on modelling void growth in composites [68, 84, 104, 110], is therefore a reasonable and valid approximation when modelling void growth.

2.3. Void growth models

From the review so far it has been established that physical removal of voids via the air evacuation channels is not feasible for reductions in production cycle time. The high pressure used in the autoclave has been shown to yield laminates with low porosity, but increases running cost. Identifying the minimum pressure to prevent void growth for a given cure temperature can maximise reductions in cure cycle time. The required pressure to prevent void growth can be predicted using void growth models. Void growth takes place due to the expansion of the gases within a void and via the diffusion of dissolved moisture (and organic volatiles) into existing voids. Models developed by Brand et al [104] and Kardos et al [84] to predict the growth of a water-vapour void via diffusion are well established. Both models have been shown to be effective at predicting the minimum pressure required to prevent void growth in prepregs during an autoclave cure cycle. Several assumptions have been made to simplify the complex behaviour of void growth [84, 104, 111]. The key assumptions made are listed below –

1. Void growth takes place in an infinite isotropic medium – Effect of fibres ignored
2. Void coalescence and void transport are neglected – No net movement of resin
3. Temperature and moisture concentration in the bulk resin are uniform – Thin laminates with high through thickness thermal conductivity
4. Moisture concentration in the resin system is assumed to be constant – concentration of moisture in the resin does not decrease as moisture diffuses into voids
5. Surface tension effects, viscous effects and inertial effects are neglected
6. Resin pressure is assumed to be equal to the applied pressure – no excessive resin bleed

7. By neglecting surface tension effects void, nucleation is assumed to be instantaneous
8. As the critical void nucleation diameter is only a few molecules across [84], initial void diameter is taken as zero.

Due to the above assumptions (particularly 1, 4 and 5) the model developed by Kardos et al (referred to as the Kardos model) overestimates the minimum pressure required to prevent void growth and significantly overestimates the final diameter of any voids formed – For instance, formation of 20mm voids in 2mm thick laminates. The model developed by Wood and Bader [112] improved the accuracy of the void model by accounting for the effect of surface tension forces on void growth. However, as stated by Kardos et al [84], the effect of surface tension is only significant for small void diameters ($< 100\mu\text{m}$). This implies that for large voids, such as those formed due to the collapse of the air evacuation channels, surface tension effects can be ignored.

Gu et al [113] used the Kardos model to predict the growth of an air-water vapour mixture void in both an epoxy and bismaleimide resin system, while ignoring surface tension and viscous effects. Similar to the Kardos model, using the above method provides an upper bound for the minimum pressure that must be applied to prevent void growth. Using the governing void growth equation from the two models, a comparison between the minimum pressure required to prevent the growth of a pure water-vapour void and an air-water vapour mixture void is made (Figure 2.6).

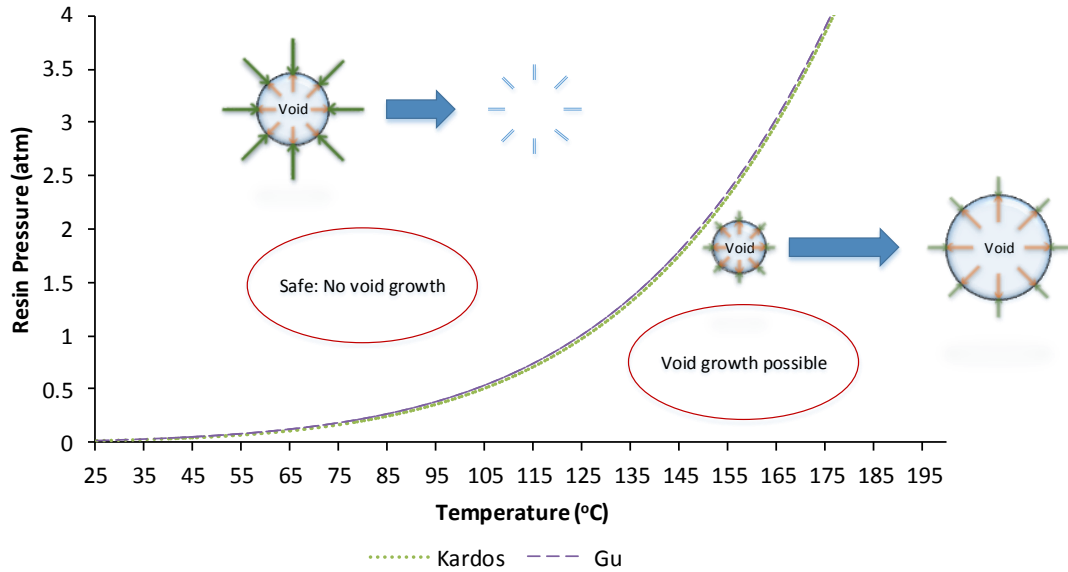


Figure 2.6: Comparison between the void growth model developed by Kardos et al [4] for a pure water-vapour void and Gu et al [43] for an entrapped air – water vapour mixture void. Note the negligible difference in required resin pressure for void collapse.

The difference between the two models is almost negligible. For instance, at 130°C the required consolidation pressure to prevent the growth of voids in a prepreg with 50% dissolved moisture by weight is 1.32 Bar as per the Kardos model, compared to 1.36 Bar as per Gu’s model. This indicates that the vapour pressure of moisture is more dominant than the pressure exerted by entrapped air, in-line with findings from other studies [68, 103]. Crucially, using the Kardos model to predict the growth of a pure water-vapour void can therefore provide an approximation of the pressure required to collapse entrapped air voids as well; simplifying the analytical expression and reducing computational cost.

Ledru et al [110] further developed the void growth model by accounting for the combined effect of expansion of the gases due to temperature, diffusion of moisture, surface tension and resin viscosity. The study highlights a 30% reduction in initial void growth when compared to diffusion-only void growth models. Furthermore, the study confirmed that void growth post gelation is minimal. This has been attributed to the exponential increase in surface viscosity preventing the expansion of voids. However, similar to previous models, at various points in the cure cycle the model predicted void diameters that were not possible in a typical lay-up (> 50 mm diameter voids when using thin laminates). This has been attributed to

the assumption that concentration of moisture within the bulk resin remains constant and assuming that void growth takes place in an infinite isotropic medium.

The work by Ledru et al shows that to be able to accurately predict changes in void diameter in a physical laminate it is necessary to account the secondary parameters - such as, variation in concentration of moisture during the cure cycle, changes in moisture concentration gradient due to the presence of fibres and neighbouring voids, effect of void coalescence, void and resin transport. This indicates a need for a paradigm shift from analytical models to a combined micro-scale and macro-scale finite element models. However, solving the governing equations of a void model that takes all the above parameters into account will be computationally costly; potentially limiting the uptake of the void model in industry. An ideal void model must be capable of being employed during the production process so as to optimise the cure cycle based on prepreg lay-up and storage conditions.

Also, quantitative studies verifying the validity of the void model are few and far between. Subsequent development in void growth modelling since the Kardos model focused predominantly on predicting void growth in neat resin. The use of void growth models in predicting and verifying void diameter in prepregs is limited to a few studies [21, 68, 103]. Grunenfelder et al [68] studied the impact of ambient humidity during lay-up or storage on void growth during an OoA cure cycle. The parameters of the Kardos model were updated for a current generation OoA prepreg system (Cytec's MTM44-1) to predict the void diameter. To account for the assumption that void growth takes place in an infinite isotropic medium, void volume fraction was predicted by scaling the predicted void diameter to a constant unit matrix volume, similar to the method described by Boey and Lye [21]. Anderson et al [103] expanded on the work by Grunenfelder et al by accounting for additional cure pressures. Both studies reported good agreement between the predicted void volume fraction and the actual measured void volume fraction. However, it should be noted that the measured void volume fraction is relatively low (< 6%). There is a possibility that this technique may not be applicable for laminates with high void content (> 10%) due to extensive void coalescence.

As per the Kardos model, void diameter at any given point in the cure cycle is given as [84]:

$$\phi_{void} = 4\beta\sqrt{Dt} \quad \text{Equation 2.3}$$

Where,

D is the diffusivity of the given resin system (mm²/hr) which is given as

$$D = 10.5 \exp\left(-\frac{2817}{T}\right) \quad \text{Equation 2.4}$$

T as the resin temperature (K)

t as time (hrs).

$$\beta = \frac{C_{bulk} - C_{sat}}{\rho} \quad \text{Equation 2.5}$$

ρ is the density of the gas within the void (g/mm³), which for a void consisting of pure water vapour is given as

$$\rho = \frac{M_{H_2O} P_g}{RT} \quad \text{Equation 2.6}$$

Where;

M_{H_2O} is the molecular weight of water (g/mol)

ρ_g is the density of the gas within the void (atm)

R is the gas constant (mm³/molK)

C_{bulk} is defined as the bulk concentration of dissolved moisture in the resin (g/mm³)

Which is given as;

$$C_{bulk} = C_{rm}(RH_o)^2 \quad \text{Equation 2.7}$$

Where;

RH_o is the relative ambient humidity during lay-up

C_{rm} is the resin moisture content coefficient - Which is given as:

$$C_{rm} = \frac{S}{100} \rho_r \quad \text{Equation 2.8}$$

With;

S is the resin solubility coefficient

ρ_r is the resin density at conditioning temperature

C_{sat} is the moisture concentration on the surface of the void (g/mm^3) - Which is given as:

$$C_{sat} = 8.651 \times 10^{-14} \exp\left(\frac{9784}{T}\right) P_{H_2O}^2 \quad \text{Equation 2.9}$$

Where;

P_{H_2O} is the partial pressure of vapour in the void.

As per Dalton's law, water vapour partial pressure is given as:

$$P_{H_2O} = x_{H_2O} P_g \quad \text{Equation 2.10}$$

Where;

P_g is the resin pressure

x_{H_2O} is mole fraction of water in the gaseous mixture

However, studies using the Kardos model assume that the void is composed entirely out of pure water vapour. Therefore;

$$P_{H_2O} = P_{resin} \quad \text{Equation 2.11}$$

Also, the following conditions are used:

$$t = 0 \text{ when } C_{sat} = C_{bulk}$$

$$\text{At } t = 0 \phi_{void} = 0$$

Based on Equation 2.3 and Equation 2.5, if C_{bulk} is greater than C_{sat} moisture will diffuse into the void causing it to grow. Also, if the concentration of moisture at the void-resin interface is greater than the concentration of moisture in the bulk resin then moisture can diffuse out of the void, which ultimately leads to void collapse.

Equating $C_{sat} \geq C_{bulk}$ yields the following equation which gives the minimum pressure required to prevent void growth from taking place at any point in the cure cycle for a current generation OoA prepreg (MTM44-1) [68]:

$$P \geq 4.233 \times 10^3 \exp\left(-\frac{4892}{T}\right) RH_o \quad \text{Equation 2.12}$$

Where;

P is the resin pressure required to keep dissolved moisture in solution (atm)

Equation 2.3 - Equation 2.12 can be used to predict the timeframe during which void growth takes place during the cure cycle and the resulting void diameter. As evident from previous studies on void growth [68, 84, 110], void growth does not take place once resin gelation has occurred. The time at which resin gelation occurs is used to define the end point of the model. As the Kardos model does not take resin viscosity into account, the point of resin gelation is to be determined experimentally using a rheometer.

2.4. Void growth summary

This section presents a summary of the complex physics behind void growth mitigation in OoA processing of prepregs.

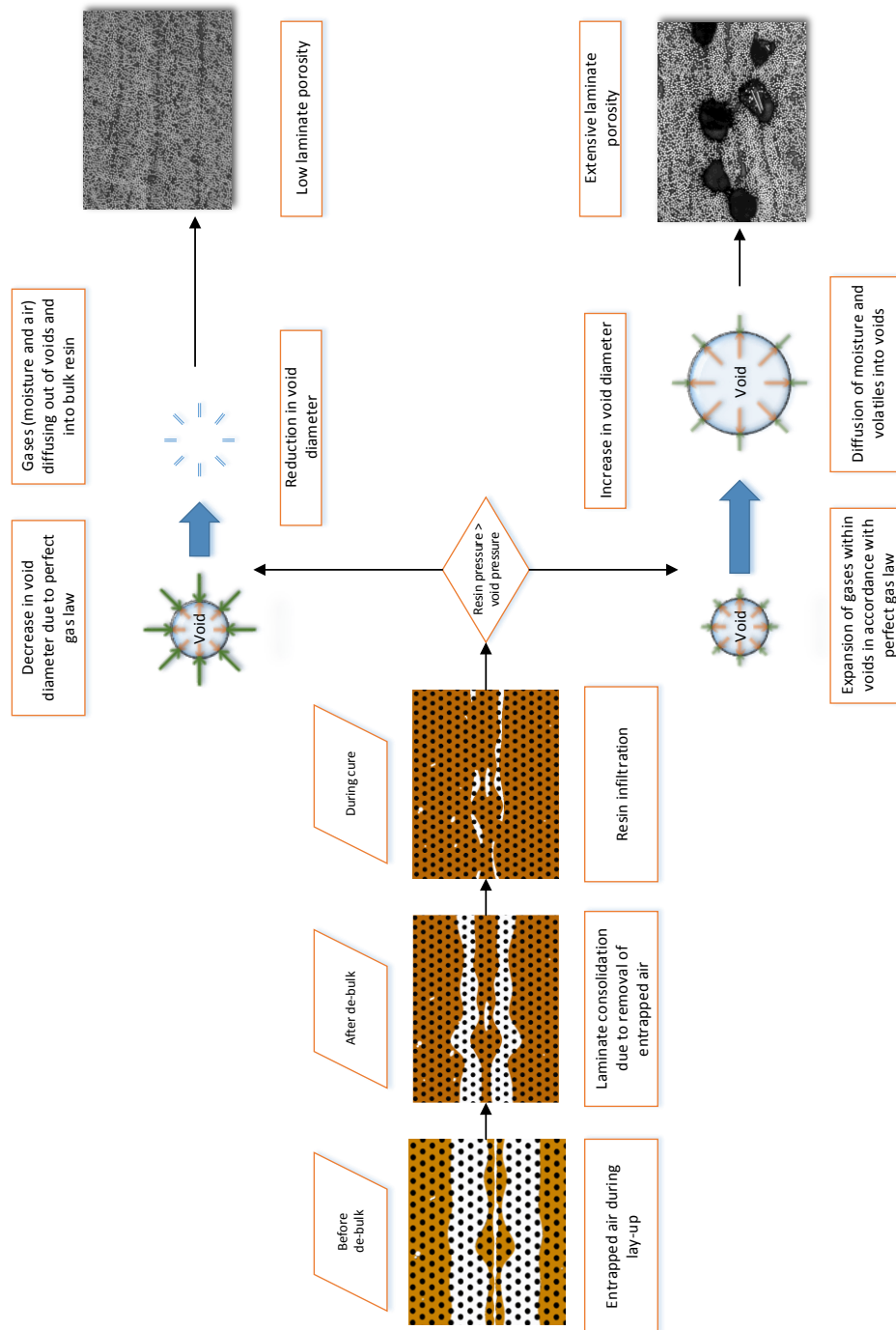


Figure 2.7: Schematic summarising the process of void removal during processing of OoA prepreg.

Figure 2.7 summarises the mechanism of void removal across various stages of the processing of OoA prepregs. Entrapment of air during lay-up is inevitable. The engineered air evacuation channels facilitate the removal of entrapped air during de-bulk. However, the low permeability of the fibre bed hinders complete evacuation of entrapped air. Nevertheless, the removal of entrapped air results in partial consolidation of the laminate. Also, depending on the resin system cold-flow can take place during de-bulk, leading to partial filling of the evacuation channels. At worst, this can lead to premature collapse of the air evacuation channels. During cure the combination of applied consolidation pressure, low resin viscosity and vacuum drawn causes the resin to infiltrate and fill the evacuation channels. Complete infiltration of the channels is unlikely, leading to the formation of entrapped air voids. If resin pressure is sufficient to prevent void growth, then two mechanisms take place: The void shrinks in accordance to perfect gas law and the gases within the void diffuse in to the bulk resin (the more dominant mechanism of the two). If the resin pressure is insufficient, then moisture diffuses into the voids causing void growth.

2.5. Void growth mitigation strategies

The key to mitigating void growth is to inhibit the diffusion of moisture into voids. Using Equation 2.12 a plot of minimum pressure required to prevent the diffusion of moisture is calculated for an OoA prepreg (MTM44-1) conditioned at varying ambient humidity levels (Figure 2.8). As expected, the consolidation pressure achieved during a standard autoclave cure cycle is sufficient to prevent the dissolution of moisture even when lay-up is performed in a highly humid environment.

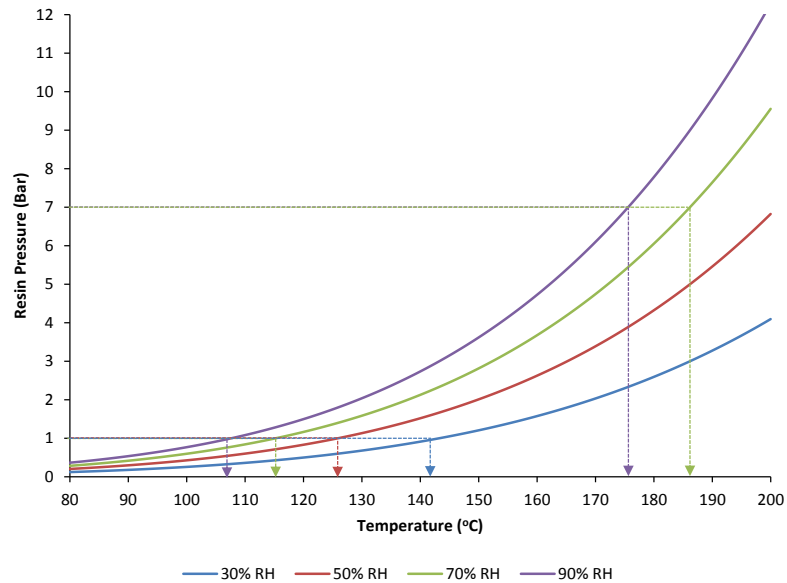


Figure 2.8: Minimum pressure required to prevent void growth in laminates conditioned at various humidity.

However, depending on the resin chemistry, the minimum resin cure temperature can be less than the maximum temperature to prevent void growth. In addition, processing at low cure temperature necessitates a longer dwell time to ensure sufficient cross-linking of the polymer network, increasing cure time. For instance, curing Cytec’s MTM45-1 at 80°C requires a 20-hour dwell time. While efforts are generally made to prevent prepreg exposure to high ambient humidity, accidental exposure to moisture due to improper storage or laminating errors is not uncommon. Owing to the low consolidation pressure, when compared to autoclave processing, the margin for error is lower for VBO processing of composites.

It must be highlighted that processing composites with a resin pressure less than the safe pressure for a given temperature does not necessarily imply extensive porosity. Figure 2.9 shows the standard OoA processing temperature profile for Cytec’s MTM44-1. Assuming a 24-hour lay-up at 50% RH, diffusion of moisture into voids can take place during cure. However, in the early phase of the cure void growth will not take place as the applied pressure is greater than the required resin pressure. Indeed, moisture can diffuse out of existing voids leading to void shrinkage and collapse. During the intermediate dwell, moisture diffuses into existing voids leading to void growth, as the required resin pressure is greater than what can be achieved

with VBO processing. Potentially, moisture can diffuse into the air evacuation channels and can be drawn out of the prepreg to yield laminates with autoclave-level porosity [68]. However, as stated in Section 2.1.1.3, this is only valid for small parts. Instead the void growth rate will be reduced - as the drive for diffusion is reduced due to the reduced pressure differential between the applied pressure and the required pressure. However, the long duration before gelation can potentially lead to extensive porosity. In contrast, Figure 2.10 shows a temperature profile used for a standard autoclave cure but with VBO consolidation pressure. Owing to the high drive for diffusion – due to the greater difference between the required pressure and the applied pressure - the final void size (and thus void volume) will be greater.

Therefore, reducing the size of the window for void growth can potentially result in lower laminate porosity. This can be achieved by reducing the time to gelation through (1) high heating rate to reduce time to gelation (2) by using a more reactive resin system. Alternatively, void growth can be mitigated by reducing the void growth rate by increasing pressure (sacrificing cost) or reducing temperature (sacrificing cycle time).

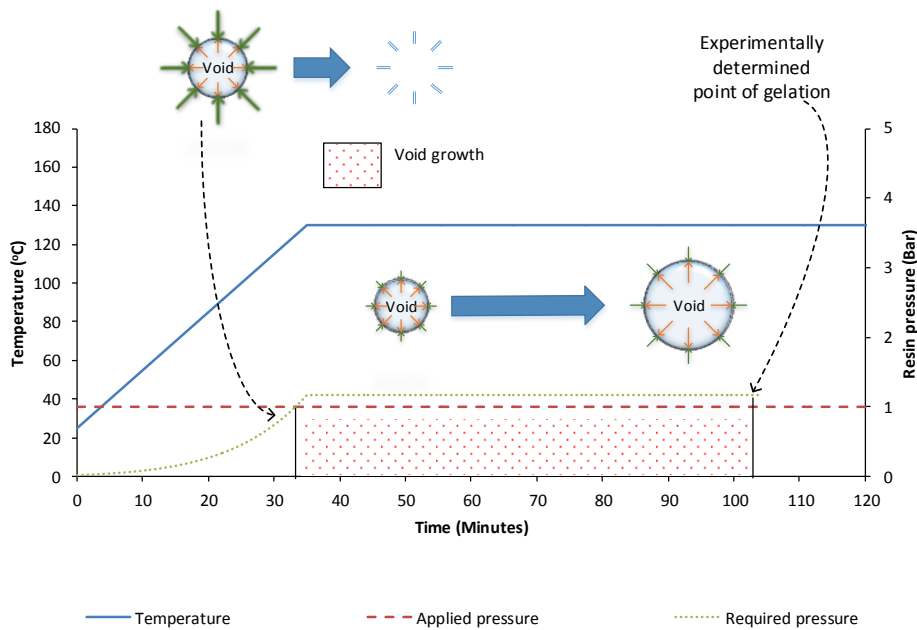


Figure 2.9: Size of window for void growth for a conditioned laminate (at 50% RH) processed using the manufacturer recommended VBO cure cycle. Note the low drive for void growth due to the differential pressure.

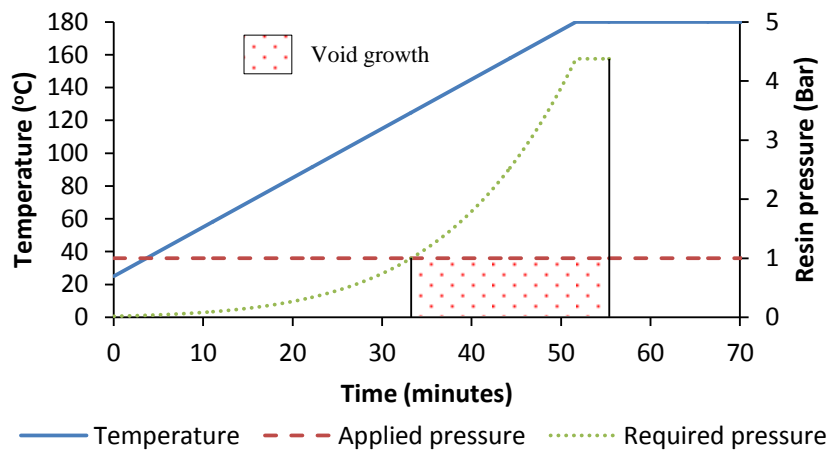


Figure 2.10: Size of window for void growth for a conditioned laminate (at 50% RH) processed using a standard autoclave temperature profile but with VBO consolidation pressure. Note the high drive for void growth due to the differential pressure.

While high heating rate processes have been shown to reduce void growth, Davies et al [32] has shown that it is not possible to achieve autoclave-level void volume fraction when using high heating rate with low consolidation (1.1 Bar). Using high heating rate combined with low hydrostatic pressure (up to 3 Bar) can potentially lead to void growth mitigation, whilst maintaining low running cost. However, the

drop in resin viscosity can potentially lead to excessive resin flow, leading to a drop in resin pressure [113-115]. When excessive resin flow takes place, the applied load is partially taken up by the fibre bed, resulting in a net drop in resin pressure. The drop in resin pressure can enable void growth. Chapter 4 experimentally tests the hypothesis of reducing void growth by reducing the size of the window for void growth. Meanwhile, the following chapter summarises the experimental setup used in this study.

3. Experimental methodology

The work in this thesis can be divided into three studies. The first study addresses the hypothesis that void growth mitigation in high heating rate processes is due to reduction in time to gelation (Chapter 4). The second study addresses the implication of high heating rate combined with hydrostatic pressure on the physical and mechanical properties (Chapter 5). The third study addresses the limitations in achievable reductions in cure cycle time; namely in terms of effect of resin kinematics, process ancillaries and tooling material (Chapter 6). The present chapter outlines the materials, cure cycles and characterisation studies used in Chapter 4 and Chapter 5. Also, this chapter presents model parameters and boundary conditions used in Chapter 6. Furthermore, this chapter also summarises the design and development of a novel high heating rate processing system.

3.1. Materials

3.1.1. Prepreg

The material used was Cytec's MTM44-1/HTS5631 non-crimp Unidirectional (UD) prepreg with an uncured resin mass fraction of 32%. The MTM44-1 series has gained certification for use in the aerospace industry and is currently used to make wing secondary structure on the Airbus A350 [48].

As per the manufacturer's recommendations, before the plies were cut from the roll, the prepreg was allowed to thaw to room temperature in a clean room. Following which, 160mm x 160mm samples were cut manually. As stated in *Chapter 2*, lay-up of large components can increase the moisture concentration within the resin due to exposure of the resin to ambient humidity, leading to void growth. To simulate long lay-up times in relatively high ambient humidity in a consistent manner, the cut plies were conditioned in an environmental chamber at 50% \pm 5% Relative Humidity (RH) for 24 hours at 25°C \pm 0.5°C. During conditioning the backing paper from the resin rich side was removed so as to aid in moisture absorption. After conditioning, the backing paper was re-applied before the plies were sealed in a labelled envelope bag – with 14 samples in each bag - and stored in a walk-in freezer at -18°C. Before lay-up, the plies were removed from the freezer and allowed to thaw to room

temperature before the envelope bag was reopened. A process flow diagram of the prepreg preparation process is shown in Figure 3.1.

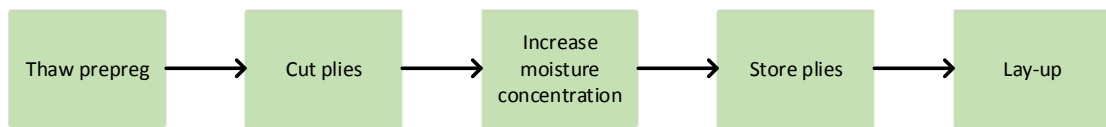


Figure 3.1: Steps involved in preparing the prepreg for lay-up this study

3.1.2. Resin

Cytec’s MTM44-1 resin film was used to obtain process modelling parameters used in Chapter 6. In addition, experimentally verified kinematic and rheological model data for Hexcel’s 8552 and Cytec’s MTM45-1 is obtained from the literature [51, 116] and used in Chapter 6 to highlight the impact of the kinematic and rheological characteristics of a resin system on the maximum achievable reductions in cure cycle time. Historically, Hexcel’s 8552 (a toughened epoxy resin system) has been commonly used as a benchmark autoclave resin system during process modelling [116, 117]. The MTM45-1 is a toughened, alternative current generation resin system with lower minimum cure temperature than the MTM44-1 series.

3.1.3. Ancillaries

3.1.3.1. Breather

The breather used was Richmond Aerovac’s AB1060UHA non-woven breather fabric. The AB1060UHA is made from a polyester blend with an areal weight of 330g/m². This was chosen to minimise the risk of vacuum ‘lock-off’ – where the consolidation pressure against the vacuum bag seals off sections of the tool surface, creating an uneven pressure distribution across the tool face and laminate.

3.1.3.2. Release film

The release film used during de-bulk was Cytec’s A6000 20µm thick film with a P3 perforation pattern. After de-bulk the perforated release film was replaced with Cytec’s A6000 20µm thick non-perforated release film to prevent resin from bleeding into the breather during cure. The A6000 series is made from a Fluoropolymer (ETFE) with a maximum service temperature of 232°C [49, 52].

3.1.3.3. Vacuum bag

The vacuum bag used was Aerovac's Capran 518, a blown Nylon 6 film with a maximum service temperature of 199°C. After the final de-bulk, the vacuum bag was replaced to minimise the risk of leakage during cure [61].

3.1.3.4. Release agent

The release agent used was Chemtrend's Chemlease® PMR-90 EZ, a widely used semi-permanent release agent with a maximum rated temperature of 400°C. For the initial application, the tool surface was cleaned with acetone following which the release agent was applied by hand using a lint-free cotton cloth in a circular, overlapping motion. A total of 5 coats of the release agent were applied with a 10-minute cure time between each application. Although the PMR-90 EZ is classed as a semi-permanent release agent capable of withstanding multiple laminate releases from the tool, two coats of release agent were applied to the tool surface in a similar fashion before each run, to minimise the risk of the laminate bonding to the tool surface.

3.2. Design and development of the Pressure Tool

Isolating the effect of high heating rate and pressure on void mitigation necessitated the development of a system capable of achieving 15°C/min combined with up to 7 Bar hydrostatic pressure. This novel system is called the Pressure Tool in this study. The design requirements of the Pressure Tool are as follows:

1. Achieve controlled heating at 15°C/min from ambient temperature up to 180°C
2. Achieve controlled cooling at 8°C/min from 180°C to 100°C
3. Provide a uniform temperature distribution across the tool surface so to reduce the build-up of residual stress within the laminate
4. Achieve up to 7 Bar consolidation pressure within the lay-up cavity
5. Facility to draw vacuum throughout the cure cycle – provided via built-in the vacuum channels

The size of the lay-up area within the tool was dictated by the size of the plaques required for the characterisation studies in Chapter 4 and Chapter 5. This in turn

dictated the size of the tool and the maximum dimensions of the heater bank. Based on the above dimensional limitations, the minimum required power density of the heater bank was analytically calculated (See Appendix A). The Pressure Tool was then designed using a commercial CAD package (Catia V5R20) and optimised using Ansys Fluent (V14.5).

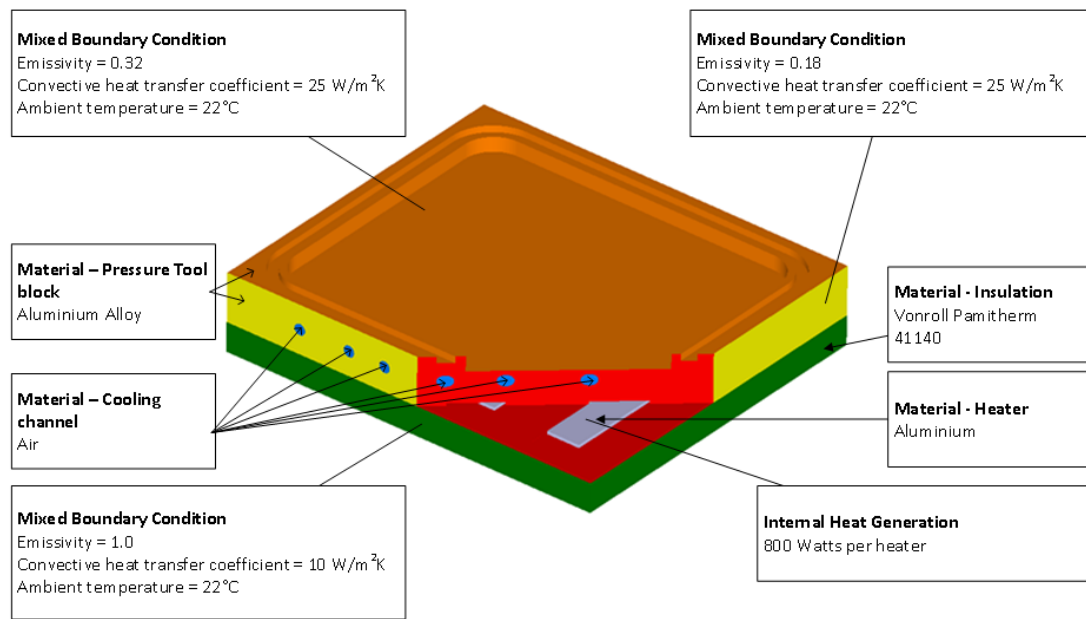


Figure 3.2: Summary of boundary conditions applied for the optimisation study in Ansys Fluent

Figure 3.2 summarises the thermal boundary condition set during the optimisation study. The material properties of the insulation material and the main body of the pressure tool used for the optimisation study is summarised in Table 3.1. The emissivity of the surfaces of the tool was determined empirically using a thermal imaging camera (FLIR T400 Series). In the interest of safety, the Pressure Tool was designed to be operated within a gated up-stroke press. Advantageously, this would reduce heat loss via forced convection of air. Therefore, a low convective heat transfer coefficient was approximated to simulate convective losses in the model. The maximum power density of the heater was derived using data from the manufacturer supplied datasheet [118]. It was assumed that no air flow takes place through the cooling channel. A reasonable approximation, considering that the PID controlled air flow regulator for the cooling channels would be in the closed position during a temperature ramp.

Aluminium – 6061	
Density (kg/m ³)	2719
Heat capacity (<i>C</i>) (J/KgK)	871
Thermal conductivity (W/mK)	202.4
Insulation material – VonRoll Pamitherm® 41140	
Density (kg/m ³)	2200
Heat capacity (<i>C</i>) (J/KgK)	979.9*
Thermal conductivity (W/mK)	0.18 [#] , 0.2*
Air	
Density (kg/m ³)	1225
Heat capacity (<i>C</i>) (J/KgK)	1006.43
Thermal conductivity (W/mK)	0.0242

Table 3.1: Summary of the material properties used for thermal analysis of the Pressure Tool. # Data obtained from the manufacturer’s datasheet [119]. * Experimentally derived data.

The distance between the heater bank and the tool face along with the spacing between the heaters were optimised so as to obtain a uniform temperature distribution across the tool face, whilst also achieving the required heating rate. The proprietary heated composite tooling system highlighted in Chapter 1.2.1.1 would have facilitated the development of a leaner, more optimised tooling system. However, strip heaters embedded within an aluminium tool was chosen for this study on the account of: low cost, ease of availability and safety when operating at 7 Bar pressure at 180°C. However, there is a performance penalty in using this approach.

As evident from the optimisation study in Fluent (summarised in Figure 3.3), the design of the tool is a compromise between meeting the required heating rate and achieving a uniform temperature distribution across the lay-up cavity. Increasing the spacing between the tool face and the heaters (by increasing the thickness of the

aluminium block) yields a uniform temperature distribution across the tool face; but, at the expense of the maximum achievable heating rate. As per the optimisation study, the maximum achievable heating rate, while minimising the temperature gradient across the tool face, is only 9.6°C/min. Figure 3.4, presents a plot of the experimentally determined surface temperature from the centre of the lay-up cavity. Temperature was measured using a K-type thermocouple attached to the tool surface using a flash tape. The mismatch between the experimental and the model results is to be expected due to the assumption that convective heat transfer film coefficient is constant. The film coefficient changes due to an increase in temperature of the air surrounding the tool.

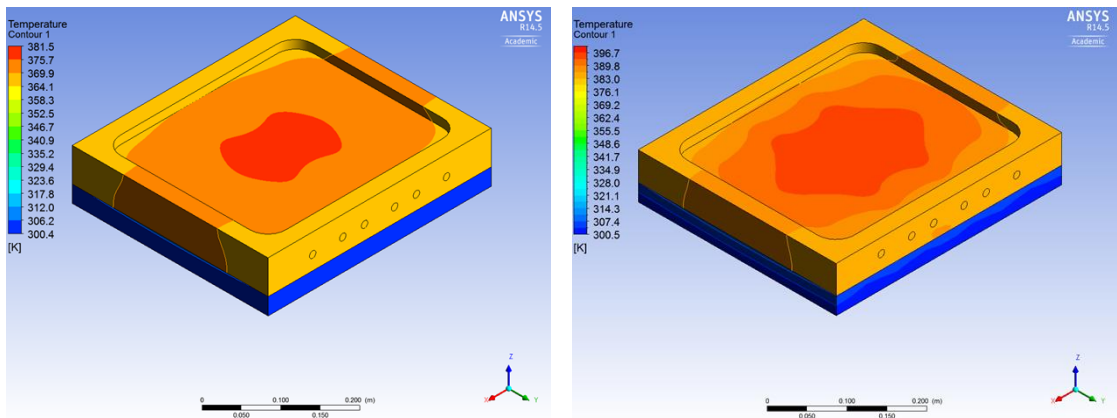


Figure 3.3 (Left): Temperature distribution across the lay-up cavity for the preliminary design (60mm Aluminium block), with a total power input of 3.2kW in 10 minutes. Figure 3.3 (Right): Temperature distribution across the lay-up cavity when using a 45mm thick Aluminium block.

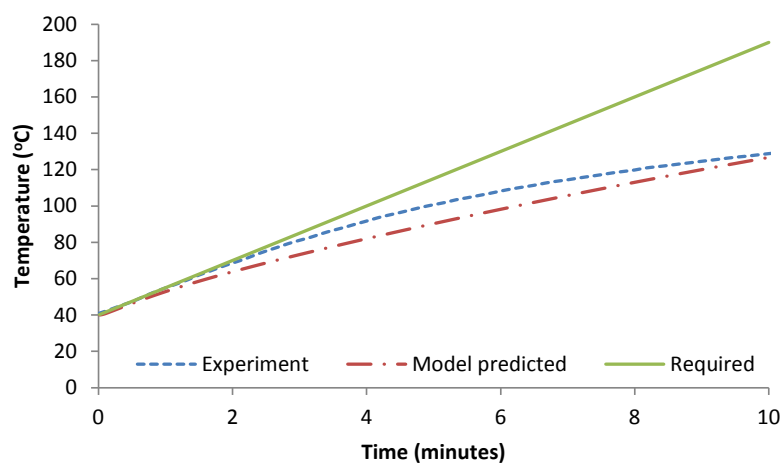


Figure 3.4: Comparison between the model predicted maximum heating rate of the optimum Pressure Tool design and experimentally measured maximum heating rate of the Pressure Tool.

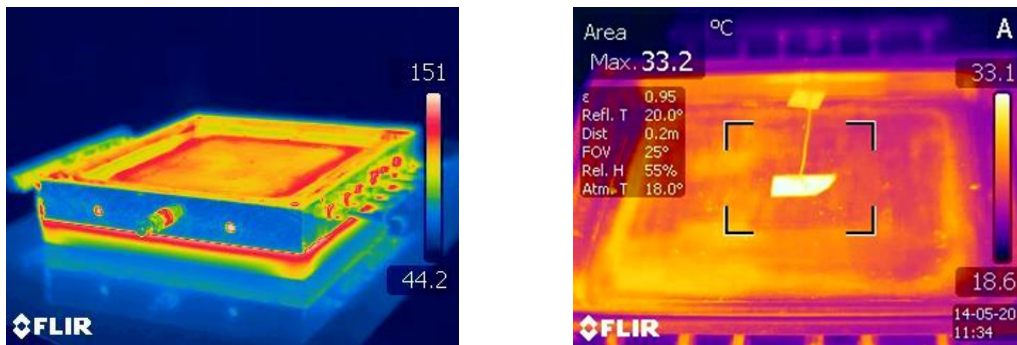


Figure 3.5 (Left): Thermal image of the lay-up cavity of the Pressure Tool. Image was taken during a temperature ramp from 50°C to 160°C. **Figure 3.5 (Right):** Calibration of the emissivity of the cavity surface using a flash tape and a K-type thermocouple.

Figure 3.5 (Left) highlights the surface temperature distribution of the lay-up cavity of the physical tool taken using a thermal imaging camera. The accuracy of the temperature distribution recorded by the thermal imaging camera is dependent on the material emissivity data defined by the operator. In-line with the recommendations by the camera manufacturer, emissivity of the tool surface was determined by comparing the temperature reading taken from the surface of a material with high emissivity - for instance, a flash tape stuck to the tool - against the bulk tool material (Figure 3.5 (Right)). Emissivity data was then empirically adjusted to minimise the difference in temperature between the surface of the flash tape and the bulk surface of the tool. In addition, temperature data obtained using the thermal imaging camera was also compared to data obtained using a K-Type thermocouple. The variation in emissivity between the cavity surface and the sides of the pressure tool is due to the difference in surface finish – The sides of the tool have a machined surface finish while the cavity was hand polished. As the camera was calibrated using the emissivity of the cavity surface, the magnitude of temperature shown along the sides of the Pressure Tool shown in Figure 3.5 (Left) is not valid.

Despite optimising the design of the Pressure Tool, it was not possible to meet the required heating rate. Owing to the lack of commercial availability of strip heaters with a high enough power density whilst meeting the dimensional requirements, the Pressure Tool was operated with the platens of the press pre-heated. The optimum temperature of the platens was empirically derived so as to achieve a heating rate of 15°C/min up to 180°C. The top and bottom platens of the press were pre-heated to

230°C and 180°C respectively before the Pressure Tool was loaded into the press, commencing the cure cycle. Figure 3.6 summarises the experimentally obtained heating and cooling down rate of the Pressure Tool when used in the pre-heated platen press. As the Pressure Tool relies on air cooling in combination with the cooling system of the platen press, thermal overshoot during the temperature ramp is inevitable.

As void growth takes place during the early phase of the cure cycle, optimisation of the Pressure Tool was predominantly focused on meeting the heating rate and surface temperature distribution rather than on the cooling abilities of the tool. Nevertheless, the maximum cooling down rate achievable was experimentally verified to ensure that design requires were met (Figure 3.6).

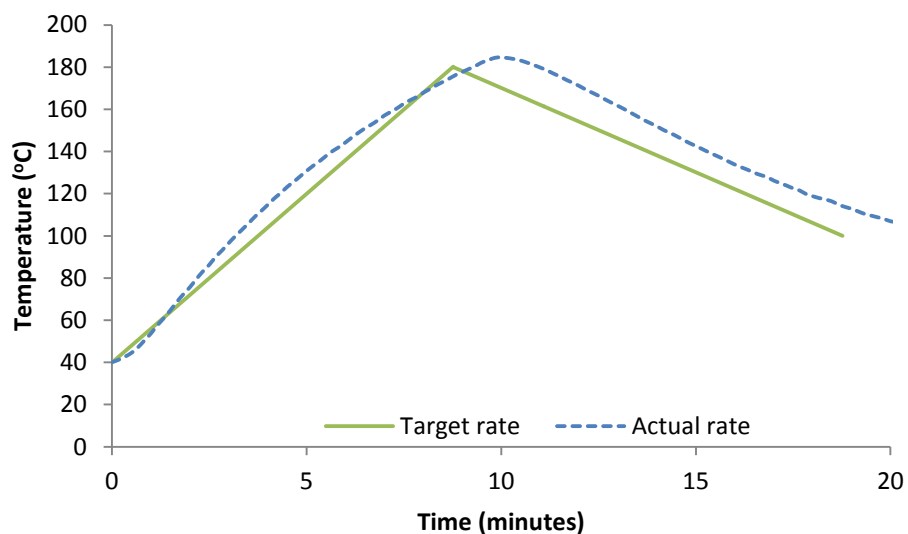


Figure 3.6: Maximum achievable heating rate and cooling down rate of the Pressure Tool when used in conjunction with a pre-heated platen press

3.3. Study on optimising cure cycle time: Chapter 4 and Chapter 5

The following sections present the experimental setup, cure cycles and characterisation studies presented in Chapter 4 and Chapter 5

3.3.1. Prepreg lay-up

For autoclave and oven cured laminates, lay-up was performed on a 6mm thick aluminium plate. The surface of the plate was hand polished using progressively

finer wet and dry sandpaper – 500 grit, 1,500 grit and 2,500 grit – to reduce surface roughness. Bags containing conditioned plies were removed from the freezer and allowed to thaw to room temperature in a clean room at 18°C with a relative ambient humidity of less than 40%. Once the plies reached ambient temperature - after approximately 1 hour - the seal on the envelope bag was broken and lay-up commenced. The lay-up consisted of 14 plies with a stacking sequence of $[0]_{7S}$. De-bulks were performed after the lay-up of ply 1, 5, 9, 13 and 14, with de-bulk duration set at 6 minutes; which, as per the model presented in *Chapter 2.1.1.3*, would be sufficient to remove up to 80% of entrapped air from between plies.

Edge dams were not used during de-bulks or cure so as to increase the quantity of residual entrapped air in the laminate - to simulate the scenario of residual air left in the laminate when processing large components. Also, the omission of the edge dam during cure was to facilitate resin bleed, with the consequential drop in resin pressure leading to void growth – albeit resin flow would be minimal due to the non-perforated release film. Nevertheless, glass tows were placed at the laminate corners to aid air evacuation during de-bulk.

After lay-up, the plaques were processed using the following processing routes depending on the temperature and pressure profile: Convection oven (VBO cure cycles with slow heating rate), Autoclave (High pressure, slow heating rate), Pressure tool (High heating various pressures – from VBO to 7 Bar).

3.3.2. Specimen processing

3.3.2.1. Autoclave

Plaques were processed in an electrically heated LBBC T1000 autoclave. The autoclave was pressurised using an Atlas Copco GA-11 air compressor with a compressor motor power of 11kW resulting in a Free Air Displacement (FAD) of 30.7 l/s at 7.5 Bar (the working pressure). PID controlled proportional valves connected to a control PC regulated the pressure within the autoclave to within ± 0.1 Bar. The required cure cycle was programmed into the control PC, which also recorded and controlled the laminate temperature using the temperature feedback signal from a K-Type thermocouple attached to the top of the laminate (outside the vacuum bag).

Laminate temperature was controlled to within $\pm 0.5^{\circ}\text{C}$ of the prescribed temperature profile. The vacuum fitting (on the vacuum bag) was connected to one of the three vacuum lines within the autoclave to draw vacuum. A second vacuum fitting was connected to a vacuum gauge so as to record vacuum levels throughout the cure cycle using the control PC. A schematic of the setup is shown in Figure 3.2. Before commencing the cure cycle, the vacuum bag was leak tested using an “accelerated leak-test” sequence programmed into the control PC. The vacuum bag passed the leak-test if the drop in pressure is less than 7 mBar over 2 minutes, in comparison to the manufacturer recommended maximum vacuum loss of 35 mBar over 10 minutes.

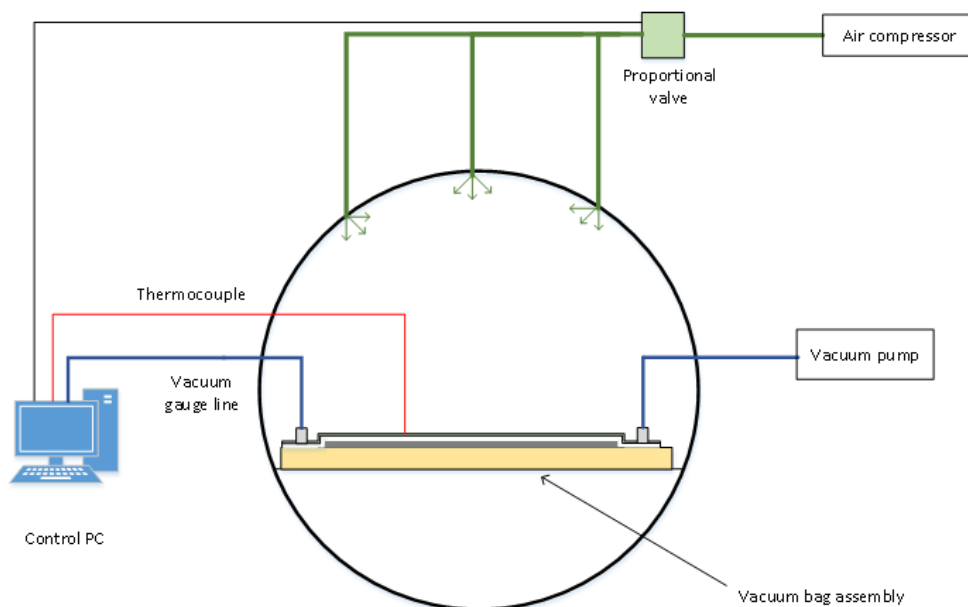


Figure 3.7: Schematic of the autoclave

3.3.2.2. Oven

For VBO processing, plaques were processed in the LBBC T1000 but with the compressor switched off - ambient pressure within the heating chamber matched atmospheric pressure. Similar to the above setup, the cure profile was programmed into the control PC, with a K-type thermocouple attached to the top of the laminate providing the required feedback signal to regulate the laminate temperature. Laminate temperature was controlled to within $\pm 0.5^{\circ}\text{C}$ of the prescribed cure cycle. Similar to the autoclave cure cycle, the second vacuum line was connected to a

vacuum gauge so as to record vacuum levels throughout the cure cycle using the control PC. An “accelerated leak-test” was performed before commencing the cure cycle.

3.3.2.3. Pressure tool

A cut-away of the Pressure Tool is in Figure 3.8. Lay-up was performed within the cavity of the tool, which, similar to the 6mm aluminium plate, was hand polished using progressively finer grit sandpapers. A K-Type thermocouple was attached to the laminate (outside the vacuum bag) to provide the required temperature feedback signal to the PID controller. Once the top half of the tool was assembled and loaded into an upstroke press, the cavity was pressurised using compressed air.

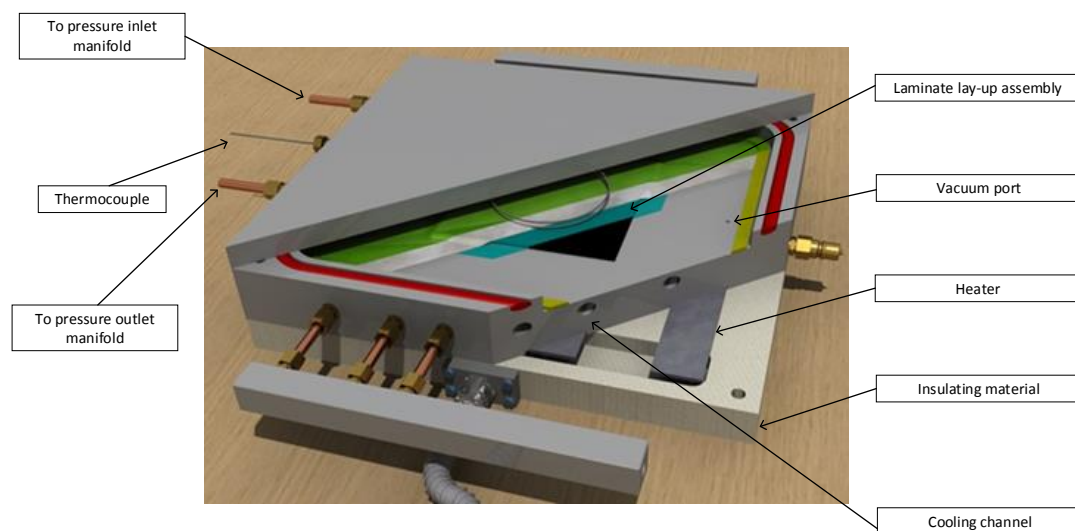


Figure 3.8: Cut-away of the Pressure Tool showing the laminate lay-up in the cavity, cooling channels and heater bank

The cavity pressure was set and regulated manually throughout the cure cycle using an in-line pressure regulator. Cooling was achieved by passing pressurised air through the cooling channels built into the tool. A PID controlled flow regulator controlled the flow rate so as to achieve the required cooling down rate. The cooling system of the press (water cooled with an external chiller unit) and that of the Pressure Tool were used simultaneously to achieve high cooling rates - up to 8°C/min from 180°C to 100°C. Vacuum channels leading from the tool face to the vacuum fittings at the sides of the tool facilitate vacuum to be drawn throughout the

cure cycle to aid in laminate consolidation. During cure, pressure, temperature and time were logged manually and then processed using Microsoft Excel 2013.

3.3.3. Cure cycles

The cure cycles used in Chapter 4 and Chapter 5 is presented in this section along with the convention used to name the specimens. Figure 3.9 outlines the temperature profiles of the four cure cycles used for this work.

In Type 1, the laminate is heated at 15°C/min heating rate up to 180°C. The laminate is allowed to dwell at 180°C for 2 hours before cooling down at 3°C/min. This temperature profile is analogous to the manufacturer recommended autoclave temperature profile except in the use of 15°C/min heating rate.

Type 2 is the manufacturer recommended autoclave temperature profile for the material, where a 3°C/min heating rate is employed.

Type 3 is the manufacturer recommended OoA temperature profile. A maximum ramp rate (both during heating and cooling) of 3°C/min is employed.

Type 4 is called a 'Spike' cure, a cure cycle commonly used in the Quickstep process [32, 33]. Unlike in the Quickstep process, a higher heating rate (15°C/min) is employed in the present study to further reduce the size of the window for void growth.

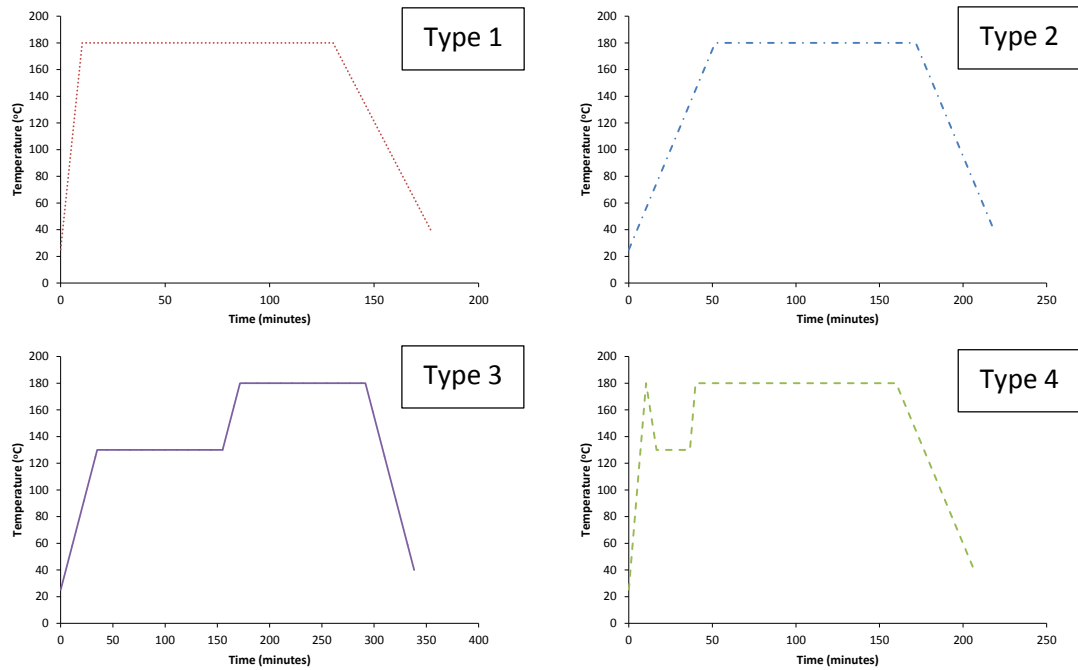


Figure 3.9: Cure cycle temperature profiles used in this study.

The applied resin pressure varies for Chapter 4 and Chapter 5. One of the aims of Chapter 4 is to identify the minimum consolidation pressure that can be applied to achieve cure cycle time reductions, whilst maintaining low laminate porosity. In Chapter 5 the study focuses on the implications of processing laminates with high heating rate combined with high hydrostatic pressure.

In Chapter 4 a maximum consolidation pressure of 1 Bar (vacuum only consolidation pressure) is applied for temperature profile Type 1 - 3. For laminates processed using the spike cure (Type 4), an additional hydrostatic consolidation pressure of 1 Bar was applied using compressed air along with the vacuum consolidation pressure, yielding a total consolidation pressure of 2 Bar. Published data indicates that 2 Bar is not sufficient to prevent void growth in a spike cure with 10°C/min heating rate. The higher heating rate combined with 2 Bar consolidation pressure could potentially minimise void growth.

Table 3.2 summarises the cure cycles and consolidation pressure applied in both studies.

Sample name	Temperature profile	Consolidation pressure (Bar)	Heating method
E-1-P-T1-C	Type 1	1	Pressure Tool
E-2-P-T1-C		2	
E-3-P-T1-C		3	
E-4-P-T2-C	Type 2	4	
E-2-P-T4-C	Type 4	2	
<hr/>			
E-4-A-T2-C	Type 2	4	Autoclave
B-7-A-T2-C		7	
<hr/>			
E-1-O-T2-C	Type 2	1	Oven
B-1-O-T3-C	Type 3		
B-1-O-T3-UC			

Table 3.2: Summary of experimental parameters used in this study. Sample names in bold are processed in Chapter 5.

Figure 3.10 summarises the sample naming system used.

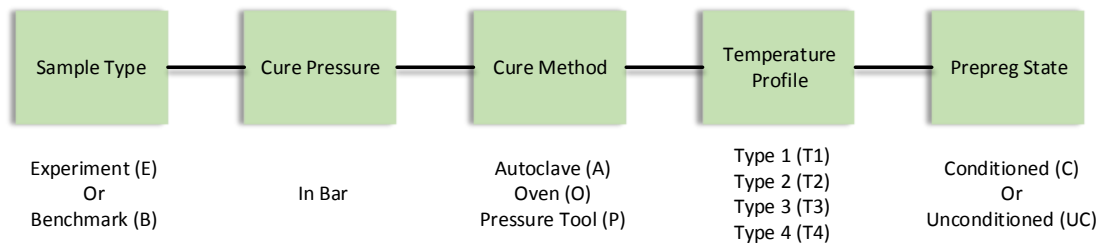


Figure 3.10: Schematic of the coupon naming convention

For instance, B-7-A-T2-C signifies: Benchmark laminate cured at 7 Bar in the Autoclave with a Type 2 (T2) temperature profile (Figure 3.9) using conditioned prepregs. Laminate names that are greyed out in Table 3.2 indicate the plaques processed for the void characterisation study in Chapter 4, which is now used for the mechanical characterisation tests in the present chapter.

The benchmark laminates are processed using the manufacturer recommended autoclave and VBO cure cycles. Laminate B-7-A-T2-C is processed using the

manufacturer recommended autoclave cure cycle (Type 2 temperature profile with 7 Bar pressure); Laminate B-1-O-T3-C and B-1-O-T3-UC are based on the recommended VBO cure cycle (Type 3 temperature profile with 1 Bar vacuum only consolidation pressure), but with conditioned and unconditioned prepregs respectively. This is to highlight the impact of increased resin moisture content on laminate quality.

For laminates E-1-P-T1-C and E-1-O-T2-C, the consolidation pressure is maintained at 1 Bar to isolate the effect of high heating rate on the physical and mechanical properties. The 15°C/min heating rate of the Type 1 (T1) cure cycle is achieved using the Pressure Tool, while the 3°C/min heating rate of the Type 2 (T2) cure cycle is achieved using the oven.

For laminates E-2-P-T1-C and E-3-P-T1-C, the high heating rate temperature profile is maintained (Type 1) while increasing consolidation pressure to isolate the effect of consolidation pressure on laminate properties.

Laminate E-2-P-T4-C is processed using the spike cure (Type 4) with 2 Bar consolidation pressure.

Laminates E-4-A-T2-C and E-4-P-T2-C (Type 2) are based on the manufacturer recommended autoclave cure cycle but with a reduced consolidation pressure; a comparison of the two laminates isolates the effect of heating method (convection versus conduction) on laminate properties.

3.3.4. Testing methods

Specimens for physical and mechanical characterisation tests were cut from the cured plaques, as shown in the cutting plan (Figure 3.11), using a diamond wheel. The dimensions were chosen in accordance with the testing standards as stated in the following sections. Cut specimens were dried in an oven for 6 hours at 40°C. Edges of the specimens were lightly sanded using a 500 grit sandpaper to remove stands of broken fibres. The specimens were then stored at 25°C with <40% ambient RH for 24 hours before testing.

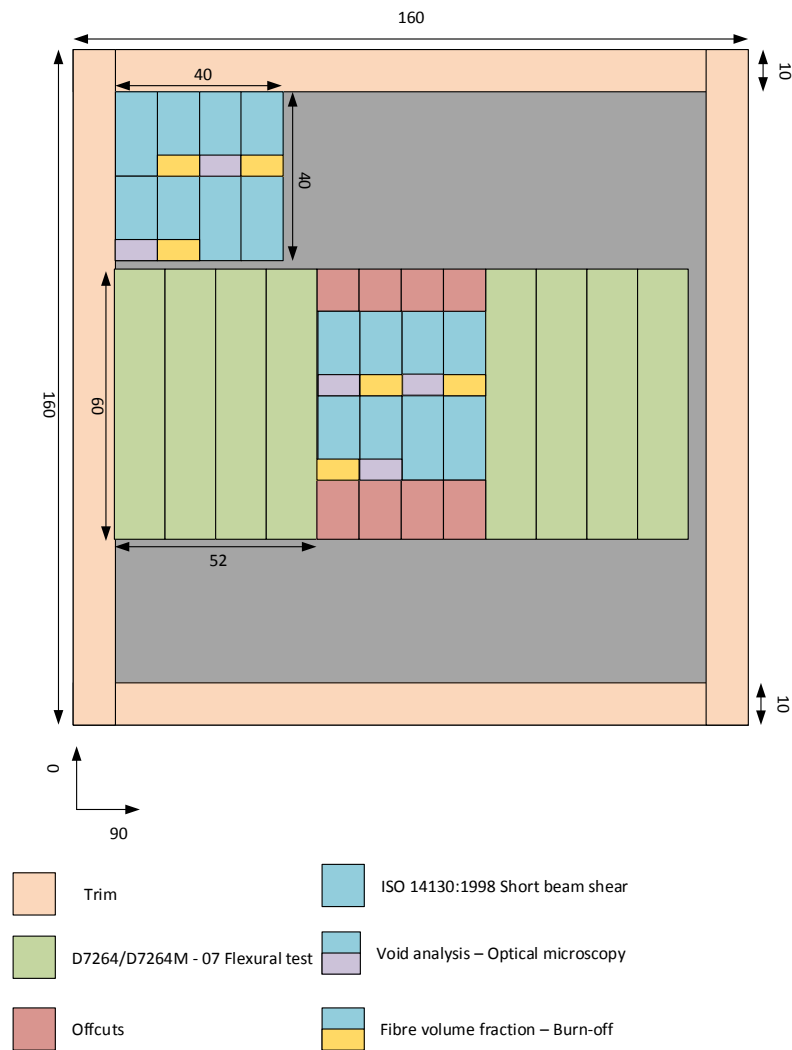


Figure 3.11: Schematic of coupon cutting plan for the characterisation studies in Chapters 4 – 6. Note: samples used for the short beam shear test are reused for physical characterisation tests

3.3.4.1. Inter-laminar shear strength

Inter-laminar shear strength tests were conducted in accordance to BS EN ISO 14130:1998. Testing was performed using a 50kN Instron 5969 electro-mechanical testing machine with a feed rate of 5mm/min. A total of 16 samples were tested from each plaque – as shown from the locations in Figure 3.11 – to obtain a representation of the plaque average mechanical properties. Load and displacement data were logged using the control PC attached to the testing machine. A four point bend test could have been used to characterise inter-laminar shear strength [120]. Nevertheless, testing was performed using a three-point bend jig so as to make a direct comparison with data available in the literature for laminates processed using high heating rates [32, 34, 53]. Specimens from the inter-laminar shear strength

tests were later used in the physical characterisation tests – void volume fraction and fibre volume fraction.

ILSS (MPa) of the specimen was determined using the following expression:

$$\tau_M = \frac{3F_M}{4bh} \quad \text{Equation 3.1}$$

Where,

F_M is the peak load (failure load) in Newton

b is the specimen width in millimetres

h is the specimen thickness in millimetres

3.3.4.2. Flexural strength

Flexural strength tests were conducted in accordance to ASTM D7264/7264M – 07. Specimens with a span to thickness ratio of 20:1 were cut from each cured plaque. A total of 8 samples were tested from each plaque – spanning the width of the cured plaque (Figure 3.11) - providing a representation of the average property of the plaque. Testing was performed using an Instron 5969 with a feed rate of 1mm/min setup with a 3 point bend test jig. Load and displacement data were logged using the control PC.

Flexural strength (MPa) of the panel was determined using the following expression:

$$\sigma_f = \frac{3FL}{2bh^2} \quad \text{Equation 3.2}$$

Where,

F is the failure load in Newton

L is the span length in millimetres

b is the same width in millimetres

h is the sample thickness in millimetres

3.3.4.3. Fibre volume fraction

Fibre volume fraction was determined by burning off the resin from the specimens using an ashing furnace set at 500°C. Specimens were placed in pre-weighed steel trays and left in the furnace for 1 hour. Five specimens – previously used in the Inter-laminar shear strength tests - were used from each plaque to obtain a representative volume fraction across the panel. The burn-off temperature was determined empirically to minimise fibre oxidation (See Appendix B for details).

The following equation was used to determine the fibre mass fraction [58]:

$$W_f = \frac{m_i - m_f + m_t}{m_i} \quad \text{Equation 3.3}$$

Where,

m_i is the initial mass of the specimen (mg)

m_f is the final mass of the specimen after the burn off test (mg)

m_t is the mass of the steel tray used to hold the specimen during the test (mg)

3.3.4.4. Void volume fraction

Void volume fraction was determined by using image analysis – a commonly used technique [68, 121, 122]. Images were recorded using a camera attached to an optical microscope (Zeiss laboratory microscope). The specimen stage was motorised so as to move the sample. The camera, the microscope and the motorised stage were controlled using a PC. Following the mechanical characterisation tests, 5 specimens were cast in high clarity polyester resin, mixed with 1% Butanox M50 catalyst and 0.5% NL49-P accelerator. The cast specimens were placed in an oven at 40°C for 3 hours to accelerate the cure of the polyester resin. Following cure, the specimens were polished on a Struers DAP-7 polishing machine with a Pedemin-S specimen holder. The DAP-7 was set to rotate at 120RPM in an anti-clockwise direction while the Pedemin-S provided complimentary rotation in a clock-wise direction. The grit size of the polishing paper used and the duration of polishing is summarised in Table 3.3. For 1µm grit size, the abrasive paper was replaced with a polishing cloth with 1 µm alumina particles applied as slurry every 30 seconds. Whilst polishing using 1 µm was found to be effective at removing broken fibres, excessive

polishing was found to increase the amount of fibre artefacts picked up during image analysis due to rounding off the edges of the fibres.

Grit size	200	800	1500	2500	4000	1μ
Duration (min.)	2	5	10	15	20	As Needed

Table 3.3: Summary of specimen polishing routine

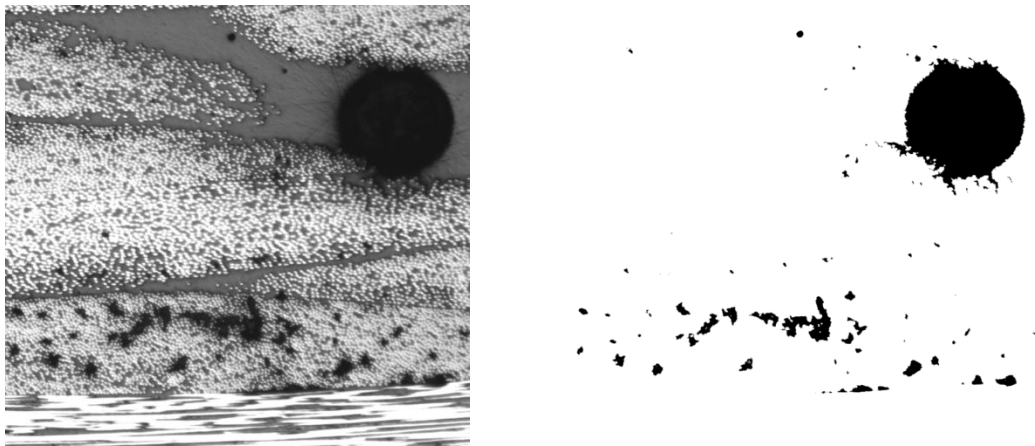


Figure 3.12: (Left): Inter-laminar and Intra-laminar voids in a twill weave composite. Figure 3.12 (Right): Thresholding mask applied to the original image. The software calculates void area by calculating the area of the dark regions in the thresholded image.

The microscope and the motorised specimen stage were programmed so as to take 80 images at x10 magnification across the sample cross section (13mmx2mm) while minimising overlap. Void volume fraction was measuring using greyscale thresholding image analysis technique [123] – See Figure 3.12 for an example. Images were processed using the open-source image analysis software ImageJ. A macro was created which applied a thresholding mask so as to isolate the voids in the image. The software calculated the area of the void (as number of pixels) in the given image and saved the result in an Excel file. Total void volume fraction for a specimen is calculated as:

$$V_f = \frac{\sum_{i=1}^{i=80} V_a}{\sum_{i=1}^{i=80} T_a} \quad \text{Equation 3.4}$$

Where,

V_a is the void area in an individual image (in number of pixels)

T_a is the total area of an individual image (in number of pixels)

i is the number of images

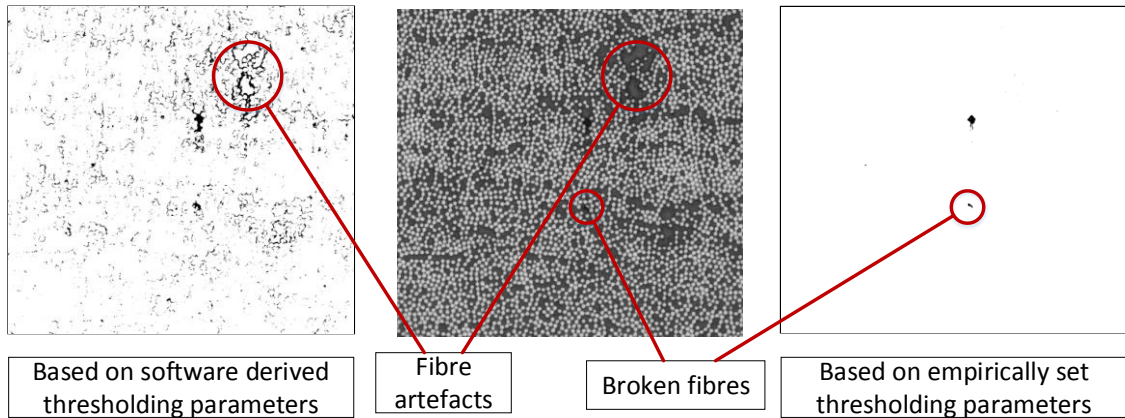


Figure 3.13 (Left): Processed image with thresholding parameters analysed and set by the software. Note the increase in false void detection due to fibre artefacts. **Figure 3.13 (Centre):** Original image. **Figure 3.13 (Right):** Processed image with empirically set thresholding parameters. While an improvement over the parameters set by the software, it was not possible to completely avoid false detections.

During thresholding, the software automatically controls the thresholding input parameters so as to not to mask voids, but at the expense of increased false detection – picking up fibre artefacts as voids (Figure 3.13). Due to which, the optimum parameters were empirically determined and coded into the macro which minimises, if not negates, false reading due to fibre artefacts and other defects. Nevertheless, processed images were examined and poorly masked images were corrected and re-analysed manually.

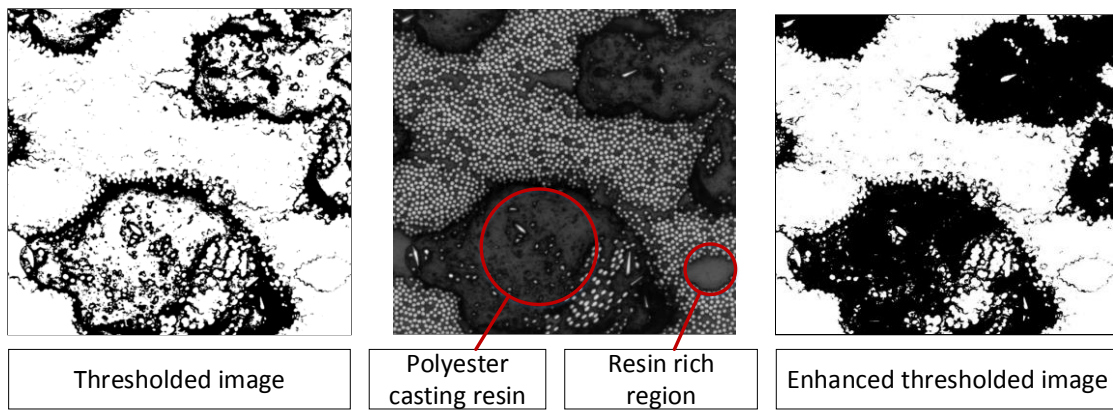


Figure 3.14: Poorly thresholded image due to casting resin filling existing voids. Figure 3.14 (Centre): Original image. Note the resin rich region with a different colour and texture to the surrounding matrix. Figure 3.14 (Right): Digitally enhanced thresholded image to aid in void analysis.

In samples with extensive porosity, such as shown in Figure 3.14, the casting resin flowed into the voids, which appear as resin rich regions with a different colour and texture to the surrounding matrix when examined under the microscope. In such samples the thresholded images were digitally enhanced so as to obtain a true representation of the level of porosity (Figure 3.14 (Right)).

3.4. Study on limitations to achievable reductions in cure cycle time (Chapter 6)

Chapter 6 highlights the physical limitations to cure cycle time reductions; Limitations such as resin characteristics, tooling material, process ancillaries and laminate thickness. The effects of the above parameters are studied using a thermo-kinematic model. The following sections derive and outline the model parameters.

3.4.1. Process modelling: Characterisation Equipment

3.4.1.1. Thermal conductivity

Thermal conductivity was measured using a C-THERM TCi thermal conductivity analyser. The TCi thermal conductivity analyser uses a modified transient plane source technique to measure thermal conductivity - a known current is applied via the heating element built into the sensor, raising the temperature of the sample at the sample-sensor interface, leading to a drop in voltage across the sensor element due to the increase in temperature of the sample [124]. The rate of change of sensor voltage is inversely proportional to the material's thermal characteristics – thus

thermal properties such as effusivity, heat capacity and thermal conductivity can be determined by analysing the voltage signal using the TCi analyser and the accompanying proprietary software. A contact agent was used to improve contact between the sensor and the sample. Two types of contact agent were available: Distilled water and Wakefield Type 120 silicone paste. The effect of contact agent type on thermal conductivity is presented in Appendix C.

3.4.1.2. Resin rheology

Rheological characterisation of the MTM44-1 resin system was performed using a Bohlin Instruments C-VOR 200 rheometer with 40mm diameter parallel plates. An external temperature control unit (ETC) blows heated air into the test chamber to increase resin temperature. A K-type thermocouple mounted below the specimen stage provides the required temperature feedback signal to the control PC to control the ETC. However, as the system relies on forced convection of heated air, thermal overshoot during high ramp rates or high temperature is inevitable. Nevertheless, calibration was verified before each run (Appendix D).

3.4.1.3. Resin kinematics

Kinematic analysis of the MTM44-1 resin system was performed using a Differential Scanning Calorimeter (DSC) – TA Instruments Q10. Resin samples were cut from the resin film and weighed using an Ohaus Analytical mass balance with a resolution of 0.1mg. The weighed resin film was placed in a hermetically sealed aluminium pan and then placed on the sample platform within the DSC cell. An empty aluminium pan was placed on the reference platform to act as a reference material. The accompanying software in the control PC used data from the embedded area thermocouples within the platforms along with the cell thermocouple to log the heat flow into (or out of) the resin.

A baseline run was performed for each run of the characterisation study to account for the presence of contaminants on the platform surface. Heat flow from the baseline was subtracted from the raw data of the experimental run.

3.4.2. Resin kinematic models

The following section presents a review of the various resin kinematic models available in the literature. Following which the parameters of the resin kinematic model for the conditioned MTM44-1 resin system is presented.

3.4.2.1. Review of resin kinematic models

Models predicting the cure kinematics of a resin system can be divided into two types: Mechanistic models and phenomenological models. Mechanistic models account for the reactions of the individual species in the resin system and can be considered to be more accurate than phenomenological models. However, the accuracy of the mechanistic model is dependent on the in-depth knowledge of the constituent reactants utilised of the resin system; which is not possible due to the proprietary nature of commercial resin systems. Phenomenological models are based on empirically and semi-empirically derived cure rate equations. Whist considered to be less accurate for dynamic temperature profiles [125], is more commonly used for characterising the cure kinetics of commercial resin systems [117, 126-132].

Kamal and Sourour [133] used an n-th order autocatalytic reaction cure model to describe the cure reaction of thermoset resin systems. The study reported good agreement observed between experimental data and model results for isothermal temperature profiles. However, as stated by Yousefi et al [125], an n-th order autocatalytic reaction cure model cannot capture the multiple, simultaneous reactions that take place in many commercial resin systems. In addition, it has been widely acknowledged that the model cannot capture the sharp decrease in reaction that takes place after vitrification of the resin [51, 116, 125]. Cure rate is dependent on a diffusion controlled mechanism after vitrification. This mechanism is slower due to the reduction in molecular mobility brought about by the increase in cross-linking density of the resin.

Various studies attempted to capture the multiple cure reaction rates that take place in a resin system using more complex phenomenological models. Lee et al [126] introduced a secondary rate equation to account for the activation of the secondary reaction in the Hercules 3501 resin system. However, the method resulted in a step

change in reactivity after the resin crosses a critical degree of cure. Despite the limitation, the model has been widely used in several cure process models to predict laminate consolidation [130, 132, 134]. Both Cole et al [135] and Khanna and Chanda [136] developed analytical expressions to account for the sharp decrease in cure rate. The model developed by Cole has been used extensively by Hubert and other researchers to characterise both autoclave (Hexcel 8552) and OoA (MTM45-1) resin systems [51, 116, 137]. Dimopoulous [131] used the expression developed by Kanna and Chanda to account for transition to the diffusion based reaction for the MTM44-1 resin system. While studies comparing the two models are limited, both systems have been shown to yield good agreement with experimental data.

In this study, the method adopted by Kratz et al [51], which incorporates the diffusion-transition analytical expression by Cole et al, is employed. The governing equations of the kinematic model are given below:

$$\frac{d\alpha}{dt} = K_1\alpha^{m_1}(1-\alpha)^{n_1} + \frac{K_2\alpha^{m_2}(1-\alpha)^{n_2}}{1 + \exp(D(\alpha - (\alpha_{CO} + \alpha_{CT})))}$$
Equation 3.5

With,

$$K_{1,2} = A_{1,2} \exp\left(\frac{-E_{A1,2}}{RT}\right)$$
Equation 3.6

Where,

E_A is the activation energy of the resin

α_{CO} is the critical degree of cure at absolute zero

α_{CT} accounts for the increase in critical degree of cure with temperature

A, m, n and D are model constants

3.4.2.2. Resin kinematics model parameters

A resin kinematic model for the conditioned MTM44-1 resin used in this study is not available in the public domain. This section outlines the methodology employed to obtain the parameters of the resin kinematics model for the above resin system. Table 3.4 summaries the experimental condition used to obtain the parameters for the kinematic model of the conditioned MTM44-1 resin. A TA Instruments DSC (Q10)

has been used to analyse the resin. Dynamic scans yield the total heat of reaction while the isothermal scans measure the heat flow into the sample.

	Temperature (°C)				
Isothermal scan	120	140	160	180	200
	Ramp rate (°C/min)				
Dynamic scan	1	2	5	12	

Table 3.4: Summary of experimental runs used to obtain the parameters for the kinematic model of conditioned MTM44-1 resin film

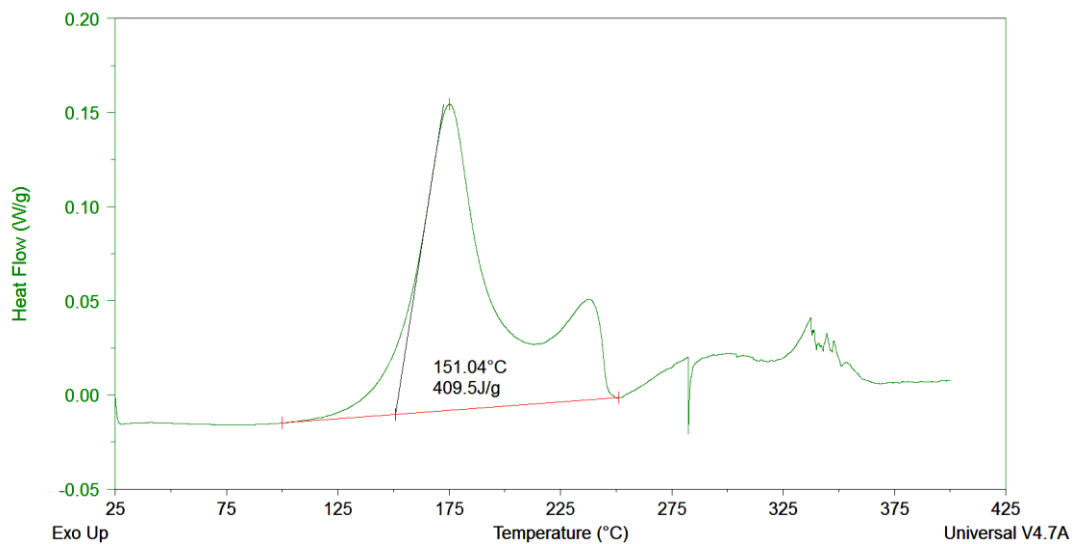


Figure 3.15: Representative dynamic scan at 1°C/min. The area under the curve is used to determine the total heat of reaction. The measured heat release beyond 250°C is due to decomposition of the resin.

Figure 3.15 presents a representation of a dynamic scan performed at 1°C/min. The total heat of reaction (H_{Total}) is obtained by performing a linear integration of the area under the curve. This method is in-line with the technique used in earlier studies [131, 137]. The average total heat of reaction for the conditioned resin system was found to be 392 ± 15 J/g. As per data in the literature [131], unconditioned, fresh MTM44-1 resin has a total heat of reaction of 470 J/g. This indicates that the resin (and prepreg) used in this study had already undergone up to 19.8% cure before the start of experimental studies used in Chapter 4 and in Chapter 5. As will be evident later in Chapter 6, the high degree of cure offers additional benefits (with inevitable additional limitations).

In accordance with earlier studies [51, 137], the rate of reaction of the resin is assumed to be proportional the rate of heat flow into the resin.

$$\frac{d\alpha}{dt} = \frac{1}{H_T} \frac{dH}{dt} \quad \text{Equation 3.7}$$

Integrating Equation 3.7 yields the degree of cure of the resin, which is given as:

$$\alpha = \frac{1}{H_T} \int_0^t \left(\frac{dH}{dt} \right) dt \quad \text{Equation 3.8}$$

The activation energy (E_A) is obtained by calculating the gradient of a plot of $\ln\left(\frac{d\alpha}{dt}\right)$ against $\frac{1}{T}$. E_{A1} is obtained by plotting $\ln\left(\frac{d\alpha}{dt}\right)$ against $\frac{1}{T}$ for low degree of cure ($\alpha = 0.01$) - Figure 3.16.

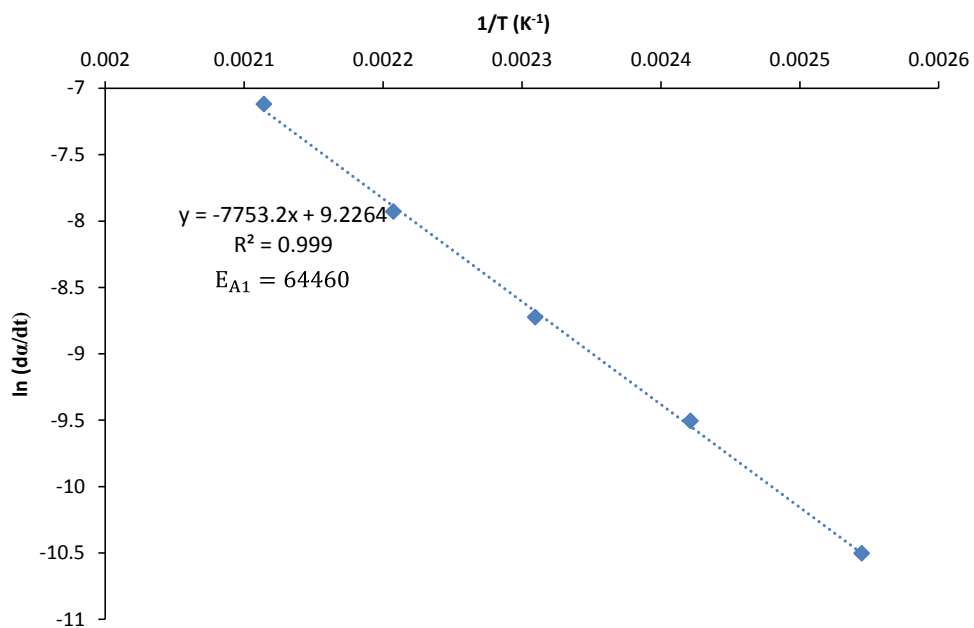


Figure 3.16: Plot of (1/T) against $\ln(d\alpha/dt)$ for $\alpha = 0.01$ to obtain E_{A1}

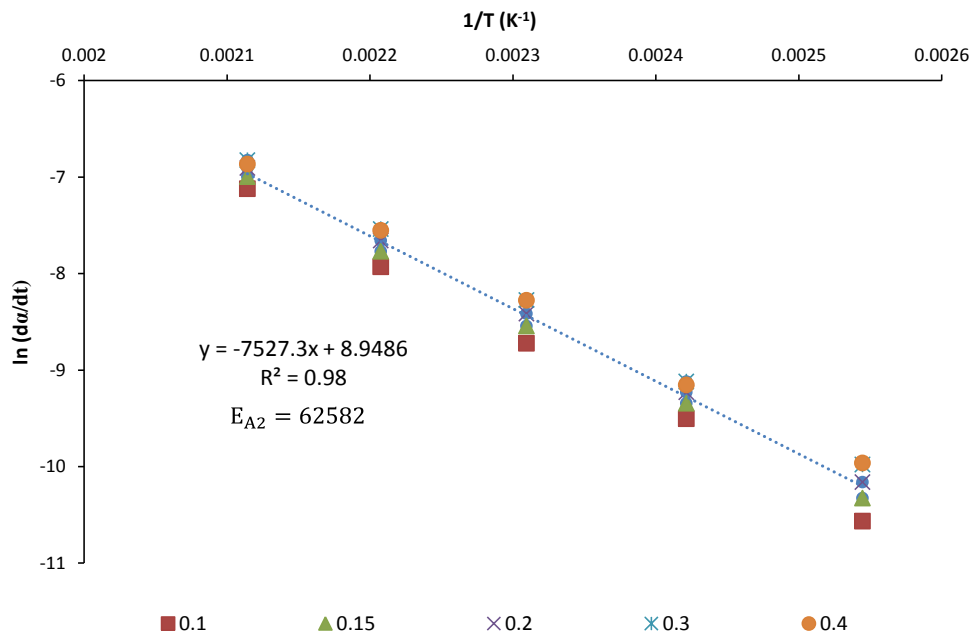


Figure 3.17: Plot of 1/T against $\ln(d\alpha/dt)$ for various degree of cure to obtain E_{A2}

E_{A2} is obtained by plotting $\ln\left(\frac{d\alpha}{dt}\right)$ against $\frac{1}{T}$ for additional degree of cure ($\alpha = 0.1, 0.2, 0.3, 0.4$) for the isothermal temperatures used in the study (Figure 3.17).

The constants α_{CO} and α_{CT} are obtained by plotting glass transition temperature against the ultimate degree of cure for each isothermal temperature. After the isothermal run, the samples are allowed to dwell at 25°C for 10 minutes within the DSC test chamber. Following which a dynamic scan is performed to measure the residual heat of reaction of the resin. Glass transition temperature is determined using the data from the DSC in accordance to BS EN ISO 11357-2:2014. Figure 3.18 presents a plot of the glass transition temperature obtained for each isothermal cycle and the corresponding maximum degree of cure.

Using the above parameters and initial values for A1, A2, m, n and D, a plot of degree of cure against cure rate is performed. The model constants, A1, A2, m, n and D are refined using non-linear least square regression in Microsoft Excel 2013. Figure 3.19 compares the experimental data against the model results.

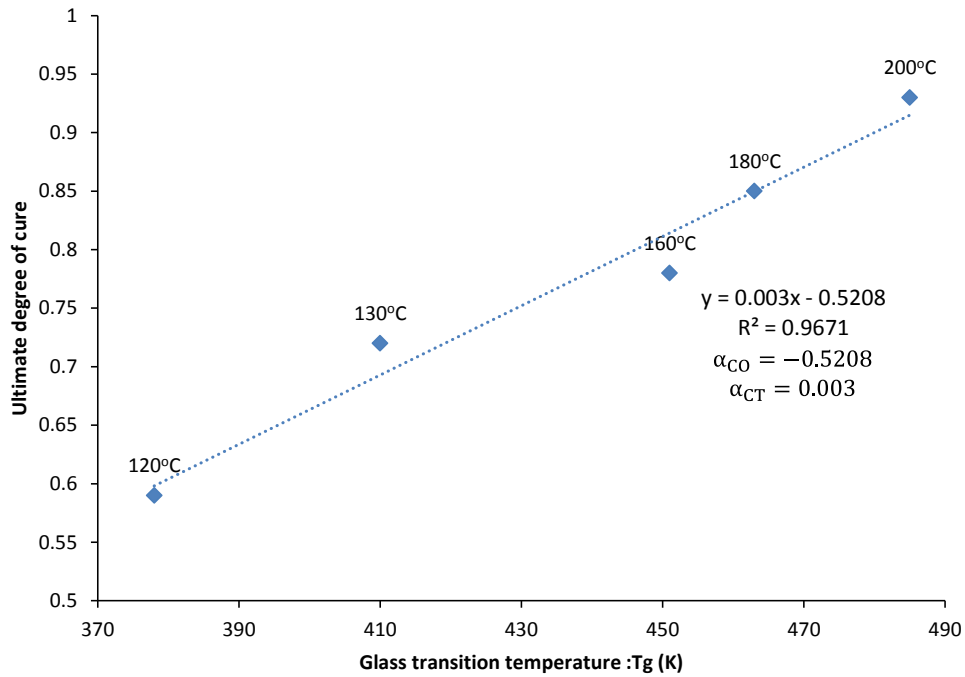


Figure 3.18: Plot of glass transition temperature against the ultimate degree of cure for each isothermal cure temperature. Isothermal cure temperature is shown above the data points.

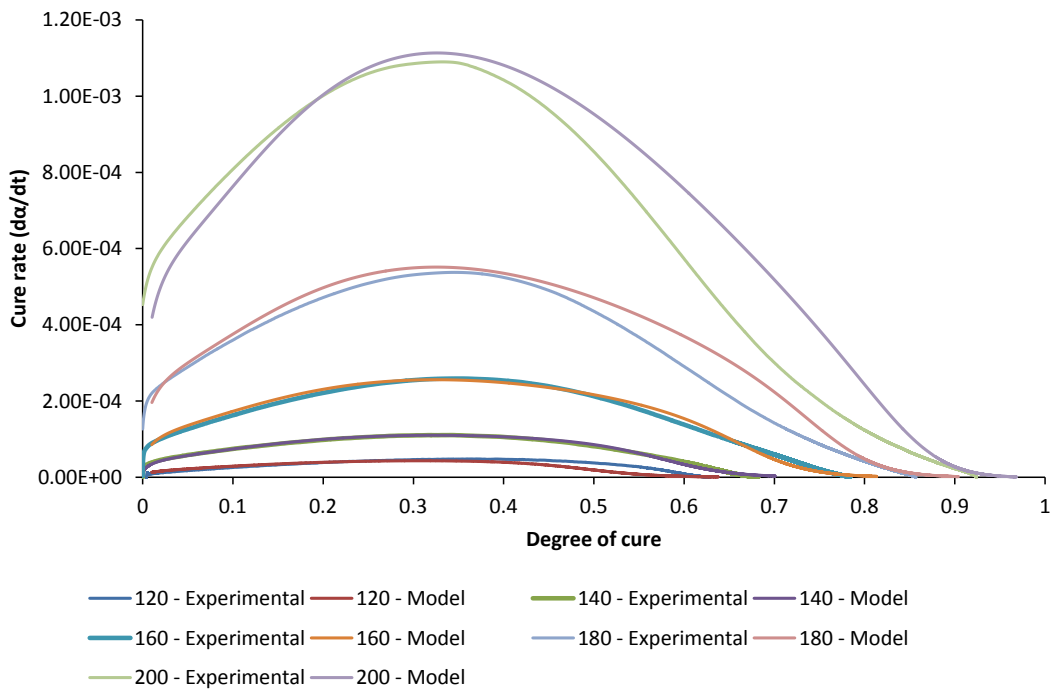


Figure 3.19: Comparison between experimental data and model outcome

There is good agreement between the experimental data and the model outcome. However, the accuracy of the model decreases when cure temperature is greater than 180°C or less than 140°C (Figure 3.20). Beyond 180°C the model fails to capture the sharp decrease in resin reactivity at a high degree of cure (> 0.5). When cure

temperature is less than 120°C, the model underestimates the diffusion controlled cure reaction. Altering the model constants can improve the degree of fit at the two extremes, but at the expense of accuracy between 130°C and 180°C (See Appendix D). Furthermore, as the temperature range of interest in the present study is between 130°C – 180°C, the parameters were optimised by centring on 160°C to maximise accuracy within the required range.

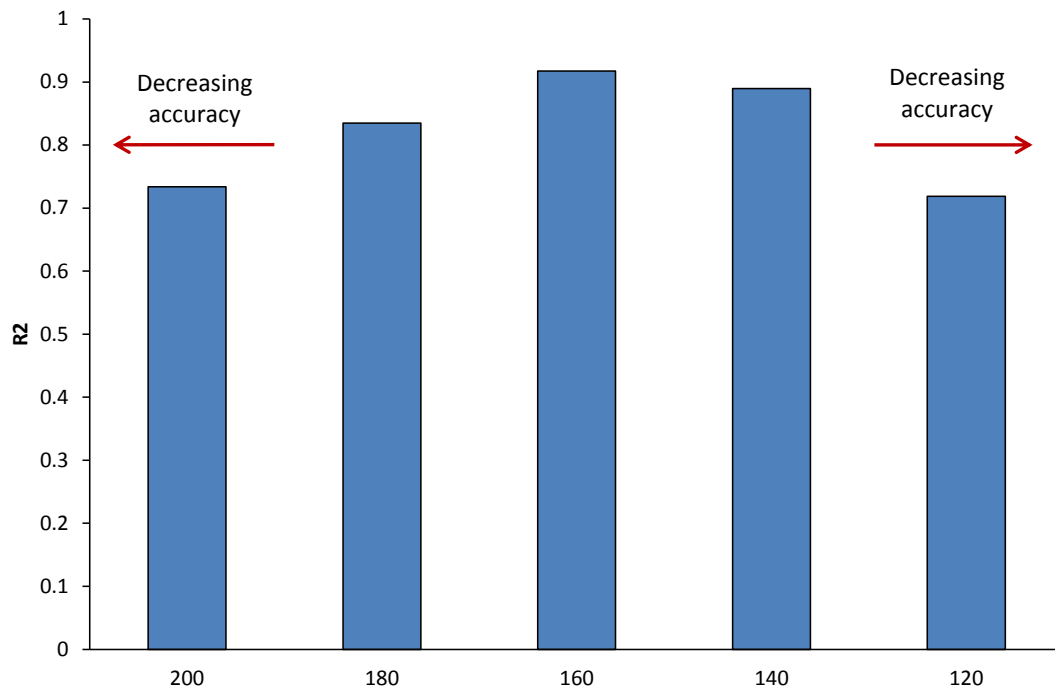


Figure 3.20: Decrease in R² values at high isothermal cure temperature and low isothermal cure temperature.

Table 3.5 summarises all the parameters of the resin kinematics model for the conditioned MTM44-1 resin. In addition, Table 3.5 summarises the model parameters for several other resin systems available in the public domain [51, 116, 137]. The effect of the processing parameters on the achievable cure cycle time reduction is presented in Chapter 6.3.1.

Parameter	Conditioned MTM44-1	MTM45 -1 [51]	Cycom 890RTM [137]	Hexcel 8552 [116]
H_{Total} (J/g)	390	368.9	430	556
A_1 (s ⁻¹)	70,000	25,300	N/A	N/A
E_{A1} (J/mol)	64,460	60,628	N/A	N/A
m_1	0.275	0.55	N/A	N/A
n_1	21.1	21.1	N/A	N/A
A_2 (s ⁻¹)	44,500	48,400	58,528	153,000
E_{A2} (J/mol)	62,582	61,752	68,976	66,500
m_2	0.82	0.80	0.63	0.813
n_2	1.7	1.18	0.6	2.74
D	25	44.3	15.66	43.1
α_{CO}	-0.5208	-1.4	-0.90	-1.684
α_{CT} (K ⁻¹)	3.0×10^{-3}	5.33×10^{-3}	3.9×10^{-3}	5.475×10^{-3}

Table 3.5: Summary of model parameters for conditioned MTM44-1. Model parameters for addition resin systems obtained from the literature.

The following section presents the governing equations of the process model and a summary of the thermal parameters of the materials used in the study.

3.4.3. Thermo-kinematic process model

The full process model is an amalgamation of a series of phenomenological and mechanistic sub-models (Figure 3.21). However, as the aim of the study in Chapter 6 is based exclusively on the thermal characteristics of the resin system and ancillary materials, only the following sub modules are used in the design of experiment: The heat transfer model and the resin kinematics model. Nevertheless, a qualitative assessment of the impact of resin rheology on cure cycle time is performed.

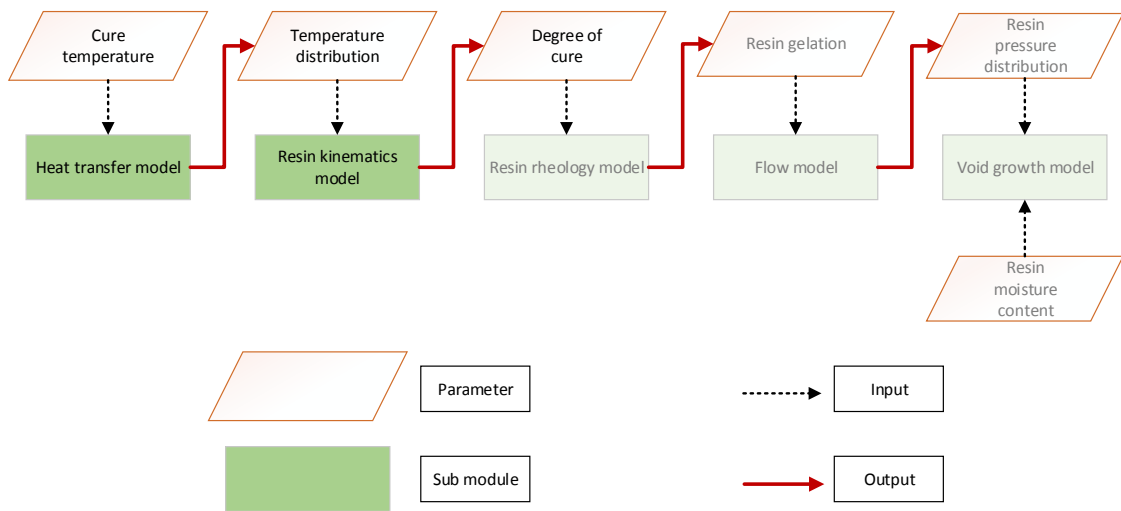


Figure 3.21: Schematic of full-scale process model. Greyed out sub-models are not used in the current study

The following section presents a review of the developments in heat transfer modelling in prepreg processing.

3.4.3.1. Review of developments in modelling heat transfer in prepreg processing

Thermal models predicting the temperature distribution within the laminate are well established. Early models [128, 138, 139] only accounted for through-thickness conduction and internal heat generation by the chemical reaction. Loos and Springer [139] pioneered the development of the full process model incorporated laminate compaction. Later studies incorporated the effect of anisotropic thermal conduction into the heat transfer model. The governing equations were solved using a finite difference scheme [127, 140-142]. Parallel studies attempted to solve the governing equations using a finite element scheme [134, 143]. In particular, Joshi et al [134] presented a method of using a commercial finite element package to solve the governing heat transfer, resin kinematics and viscosity equations. Costa et al [130] expanded on the work by Joshi et al by solving the governing 3D heat transfer and consolidation equations. Ganapathi et al [132] accounted for the use of a thick (13mm) aluminium tooling and ancillary materials (bleeder and vacuum bag) on resin flow and temperature distribution. However, the study did not explore the effect of using alternate tooling materials and laminate thickness on the degree of exotherm.

The general heat transfer model is based on Fourier's heat conduction equation for three-dimensional, transient, orthotropic heat transfer with an internal heat generation term; given as:

$$\frac{\partial}{\partial t}(\rho CT) + \rho_R C_R \left[\frac{\partial}{\partial x}(uT) + \frac{\partial}{\partial y}(vT) + \frac{\partial}{\partial z}(wT) \right] = \frac{\partial}{\partial x} \left(k_{xx} \frac{\partial T}{\partial x} \right) + \frac{\partial}{\partial y} \left(k_{yy} \frac{\partial T}{\partial y} \right) + \frac{\partial}{\partial z} \left(k_{zz} \frac{\partial T}{\partial z} \right) + \dot{m}''' \frac{e}{1+e} \Delta H$$

Convection term Conduction term Heat generation

Equation 3.9

Where,

ρ is the density of the composite

ρ_R is the resin density

C is the specific heat capacity of the composite

T is Temperature

k_{ii} (with $i = x, y, z$) is the thermal conductivity of the composite. For thermal conductivity in the fibre direction of a unidirectional prepreg is determined using the rule of mixtures [130]:

$$k_{xx} = V_f k_f + V_r k_r \tag{Equation 3.10}$$

For in-plane transverse and through-thickness thermal conductivity, Costa et al proposed the following expression [130]:

$$\frac{k_{yy}}{k_r} = \frac{k_{zz}}{k_r} = 1 - 2 \sqrt{\frac{V_f}{\pi}} + \frac{1}{B} \left[\pi - \frac{4}{\sqrt{1-c}} \tan^{-1} \left(\frac{\sqrt{1-c}}{1 + B \sqrt{\frac{V_f}{\pi}}} \right) \right] \tag{Equation 3.11}$$

Where,

$$B = 2 \left(\frac{k_r}{k_f} - 1 \right) \tag{Equation 3.12}$$

$$c = B^2 \frac{V_f}{\pi} \tag{Equation 3.13}$$

Where,

V_f is the fibre volume fraction which = $1 - V_r$

k_r is the thermal conductivity of the resin

k_f is the thermal conductivity of the fibre

e is the ratio between the volume of resin and volume of fibres

ΔH is the heat of reaction per unit mass of the resin

\dot{m}''' is the mass conversion rate which is given as:

$$\dot{m}''' = \rho_R \frac{\partial \alpha}{\partial t} \quad \text{Equation 3.14}$$

With,

$\frac{\partial \alpha}{\partial t}$ as the rate of degree of cure

While Fourier's heat transfer equation does account for conductive and convective heat transfer, studies commonly ignore the effect of convective heat transfer within the resin [130, 132, 134]. It has been suggested that the resin flow within the prepreg stack is not sufficient for convective heat transfer to be a significant. Experimental verification confirms that ignoring convective heat transfer is not detrimental to model accuracy [126]. The accuracy of the model is ultimately dependent on the accuracy of the thermal conductivity data for the constituent materials and in accurately predicting the heat released during the chemical reaction.

The following section summarises the experimentally determined thermal conductivity, heat capacity and density data for the tooling materials and process ancillaries used in this study.

3.4.4. Thermal conductivity of tooling materials and process ancillaries

Using the methodology summarised in Chapter 3.4.1.1, the thermal conductivity of the process materials was quantified. In-line with the instructions for the C-THERM TCi thermal conductivity analyser, heat capacity was derived using the following equation:

$$C_p = \frac{ef^2}{k\rho} \quad \text{Equation 3.15}$$

Where,

ef is the material effusivity; determined using the thermal conductivity analyser

k is the thermal conductivity

Thermal properties of tooling materials were obtained from the literature and manufacturer supplied datasheets. Composite tooling typically use a 1-8-1 quasi-isotropic lay-up, with “light” woven plies for the surfaces of the tool (~250gsm) and “heavy” woven plies (~600gsm) for the inner layers. Density and heat capacity of the composite tooling were approximated using the rule of mixtures technique; keeping fibre volume fraction constant at 55%. In-plane thermal conductivity was determined using the rule of mixtures with an efficiency factor to account for the ply orientation. Through-thickness thermal conductivity was approximated using Equation 3.11. Table 3.6 summarises the thermal conductivity and heat capacity of the materials used in this study. Table 3.7 presents the properties of the constituent materials of the composite.

Studies have shown that the density and heat capacity of epoxy resin to vary with degree of cure [132]. However, other studies on process modelling have used constant density and heat capacity to good effect [130, 134]. The thermal properties of the HTS 5631 fibres in the prepreg could not be experimentally verified. Therefore, the properties of an equivalent PAN based fibre were used. Table 3.7 presents a comparison between the properties of uncured resin (Hercules 3501-6) and cured resin (MTM44-1). While the comparison is not valid per se due to the difference in resin generation and potentially composition, the properties of both epoxy resins are similar. The changes in thermal conductivity of the MTM44-1 resin between $\alpha = 0$ to the point of gelation could not be verified without risk of damage to the sensor; due to resin bonding to the sensor. Therefore, to avoid ambiguity, density and heat capacity of the resin were kept constant in this study.

	Material	Density (kg/m ³)	Heat Capacity (J/Kg.K)	Thermal conductivity (W/m.K)	Reference/Note
Process materials	Breather	97	1220	0.06	Experimentally derived
	Release film	1683	1038	0.14	Experimentally derived
	Vacuum bag	1078	1409	0.35	Experimentally derived
Tooling materials	Composite tooling (55% fvf)	1578	887	Kx 15.7 Ky, Kz 0.687	Table 3.7
	Aluminium	2700	896	167	[144]
	Invar	8000	515	10.4	[144]
	Syntactic foam (Epoxy)	680	2090*	0.127	[145]. * Experimentally derived
	Carbon foam	480	710	0.3	[146]
	Ceramic tooling	1600	0.4	0.308	[41]
	Graphite	1780	1046	56	[147]
	Polystyrene	33	1400	0.028	[148]
	Diamond (Aspirational material)	3500	520	1000	[149]

Table 3.6: Summary of thermal properties of tooling materials and process ancillaries

Material		Density (kg/m ³)	Heat Capacity (J/Kg.K)	Thermal conductivity (W/m.K)	Reference/Note
Carbon Fibre	(AS4)	1790	712	26	[130, 146]
Hercules 3501-6 epoxy resin for Autoclave cure	Uncured resin	1260	1260	0.167	[130, 146]
Cytec MTM44-1 Epoxy resin for OoA cure (conditioned)	Cured resin	1180	1831	0.208	Experimentally derived

Table 3.7: Summary of thermal properties of epoxy resin and carbon fibre

The materials listed in Table 3.6 commonly used tooling materials in composites processing; naturally, with the exception of diamond. However, additional factors such as part size and production volume dictate the choice of tooling material employed. Also, the tooling material choice varies, where potentially a “rule-of-thumb” approach is used so as to increase tooling life. The following section outlines the materials selection methodology and presents a method of normalising tooling thickness. The data is then used to isolate the effect of material parameters on achievable reduction in cure cycle time.

3.4.5. Material choice and material thickness

From a mechanical point of view, the ideal tooling material would have high specific stiffness to resist deflection during pressurisation/vacuum bagging. Also, crucially, maintains high mechanical properties at cure temperature. From a thermal point of view, the ideal tooling material matches the thermal expansion of the composite. Studies have shown that a mismatch in thermal expansion between the tool and the part lead to the build-up of residual stresses within the laminate [150, 151]. The

build-up of residual stresses has been shown to result in part distortion and dimensional inaccuracies, leading to part scrappage (increasing cost). In addition to thermal expansion the effect of both thermal conductivity and thermal mass must be taken into account as well. Low thermal conductivity reduces the rate at which energy can be transferred to/from the laminate. Processing reactive resin systems on tooling with low thermal conductivity can exacerbate the risk of an uncontrolled exothermic reaction. For processes (such as RTM) which utilise an isothermal cure cycles a high thermal mass is desirable; owing to the reduction in energy required to maintain the set tool temperature. However, for dynamic cure cycles used in prepreg processing, high thermal mass potentially hinders the maximum ramp rates that can be achieved.

3.4.5.1. Normalising tooling thickness for the design of experiment

The thermal mass of the material is dependent on the heat capacity and the volume of the material. If the length and width of the tooling is kept constant, then the mass of the tooling is dependent on the tooling thickness and material density. Therefore, a direct comparison of the thermal mass of various tooling materials can be made by normalising the thickness of the material to tool deflection. The deflection of a standard prepreg tooling is used as benchmark. Based on experimental observation, the cured laminate thickness of a composite tooling with 1-8-1 quasi-isotropic lay-up comes to 6mm. The elastic modulus of the laminate is estimated using the rule of mixtures technique with an efficiency factor to account for fibre orientation. To simplify calculations, the composite tooling is approximated as a simply supported beam with a span length of 300mm and width of 30mm. The composite material is approximated as a “black metal” so as to make a direct comparison with other materials [152]. A point load of 500N is applied to the centre of the span. Using standard beam bending equations the maximum deflection of the composite material is calculated. The thickness of the other tooling materials is scaled so as to match the deflection of the composite tooling. The relative thickness (wrt. Tooling prepreg) and the resulting thermal mass have been summarised in Table 3.8.

Tooling material	Density (kg/m ³)	Relative tool thickness	Tooling weight (Kg)	Thermal conductivity (W/mK)	Heat capacity (J/KgK)	Thermal mass (J/m ³)	Thermal mass (J)#
Aluminium	2700	0.98	0.07	167	896	2.4E+06	127.8
Invar	8050	0.77	0.16	10.4	515	4.1E+06	171.8
Syntactic foam (Epoxy)	680	3.85	0.07	0.127	2090	1.4E+06	295.5
Carbon foam	560	2.63	0.04	0.3	710	4.0E+05	56.5
Polystyrene	33	17.45	0.01	0.028	1400	4.6E+04	43.6
Tooling prepreg	1578	1.00	0.04	0.687	887	1.4E+06	56.5
Ceramic	1800	0.89	0.04	0.4	0.375	6.7E+02	0.03
Gold*	19300	0.93	0.47	318	129	2.5E+06	125.7
Silver*	10490	0.92	0.25	235	230	2.4E+06	119.3
Diamond*	3520	0.39	0.04	1000	510	1.8E+06	37.7
Graphite	1790	2.04	0.09	73	1047	1.9E+06	206.5

Table 3.8: Summary of the material properties of both commonly used tooling materials and aspirational materials (*). # indicates thermal mass per unit volume of the normalised tooling material – Energy required to raise the temperature of the normalised tooling by 1°C.

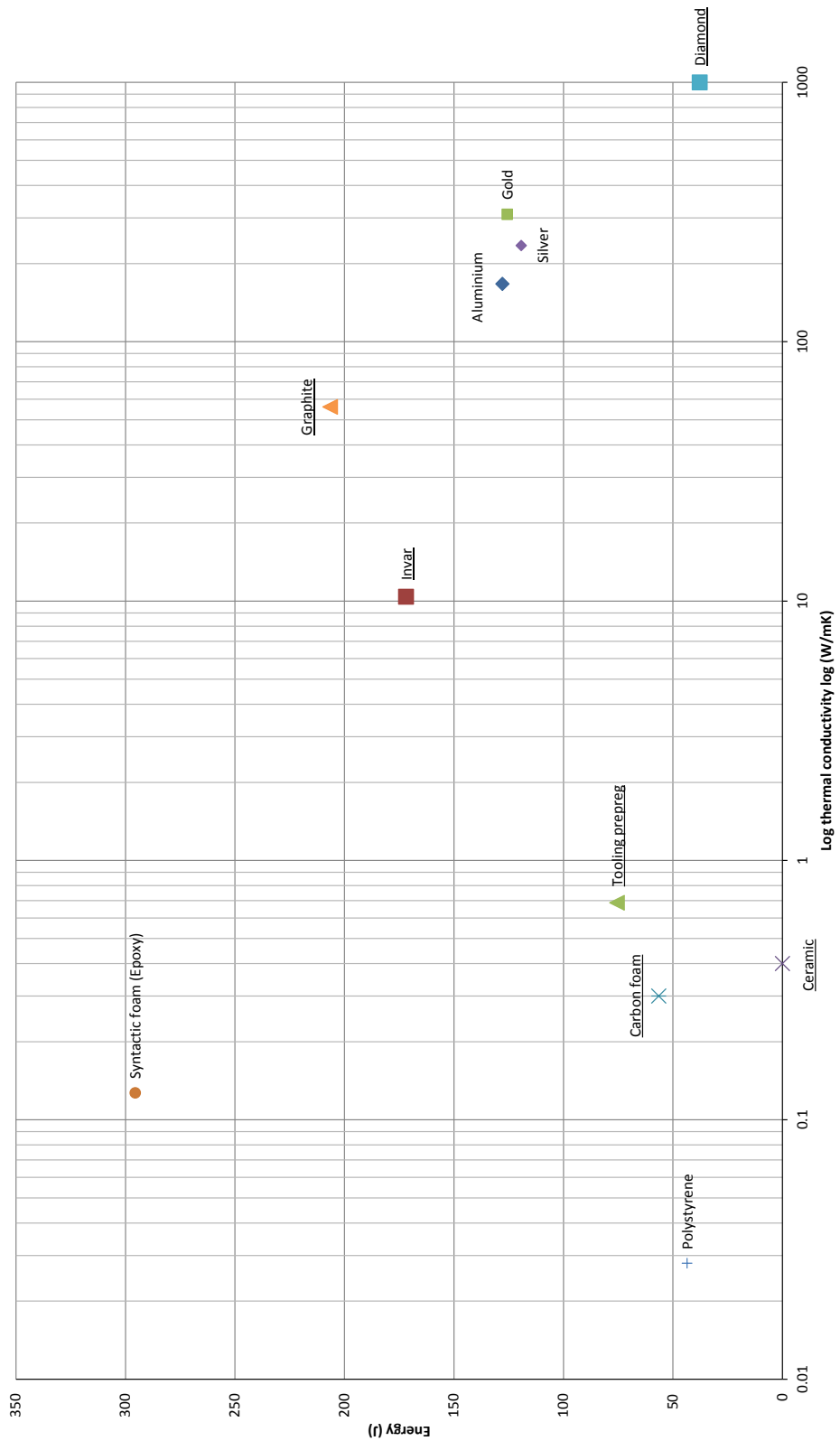


Figure 3.22: Plot of thermal conductivity of materials against energy required to raise the temperature of the normalised tooling by 1°C. Materials with the optimum coefficient of thermal expansion for processing carbon fibre composites are underlined.

Figure 3.22 presents a plot of the thermal conductivity of the materials against the energy required to raise the material temperature by 1°C. In addition, the coefficient of thermal expansion of the material is taken into account as well.

Whilst the above technique does facilitate the comparison of different materials on a level platform, the limitations of this method must be acknowledged. The method fails to account for failure of the beam due to the applied load. For instance, the maximum bending stress experienced by the Aluminium beam is 290MPa; greater than the yield strength of the material. For both syntactic foam and the carbon foam the high span to thickness ratio invalidates conditions of the standard beam bending equations (Span to thickness ratio of less than 10). Furthermore, this method does not truly reflect practises used in industry. For instance, low material thickness can lead to distortion and warpage of Invar when welding, necessitating greater thickness. Owing to the poor mechanical properties, both syntactic foam and carbon foam are generally used as monolithic tooling. Similarly, due to the ease of machining, monolithic aluminium tooling have been used to process small components ($< 1\text{m}^2$). To account for the limitations of the approach, a study is performed to isolate the effect of thermal mass and thermal conductivity on increasing laminate core temperature.

3.4.6. Design of Experiment for the study on effect of tooling material and ancillaries on cure cycle time

The following section presents the design of experiment used to isolate the effect of tooling materials and process ancillaries on cure cycle time reduction. The study is divided into five consecutive stages.

The first stage verifies the setup of the analysis in Ansys Fluent (V14.5). Also, a sensitivity analysis is performed to identify the effect of mesh size on model output. The results of this stage are presented in Appendix E. The second stage experimentally verifies the resin kinematic model using model parameters obtained for the conditioned MTM44-1 prepreg. This results of stage are presented in Appendix F. The third stage studies the effect of resin chemistry on cure cycle time. The fourth stage identifies the effect of processing films (vacuum bag and release film), which are part of process ancillaries. The three scenarios are studied in this

stage (Figure 3.23). Scenario 1 and Scenario 2 represent the commonly used vacuum bagging arrangement. Scenario 1 is used when envelope bagging is not feasible; such as, when bagging tooling with an egg-crate bagging structure. Scenario 2 (envelope bagging) is commonly used when processing components using monolithic tooling (with low mass) or shell face. Scenario 3 is a simplified case which ignores the effect of processing films on ancillaries. It can be postulated that owing to the low thickness ($\sim 0.06\text{mm}$), excluding both materials from the meshed domain may not have a significant impact on the model outcome.

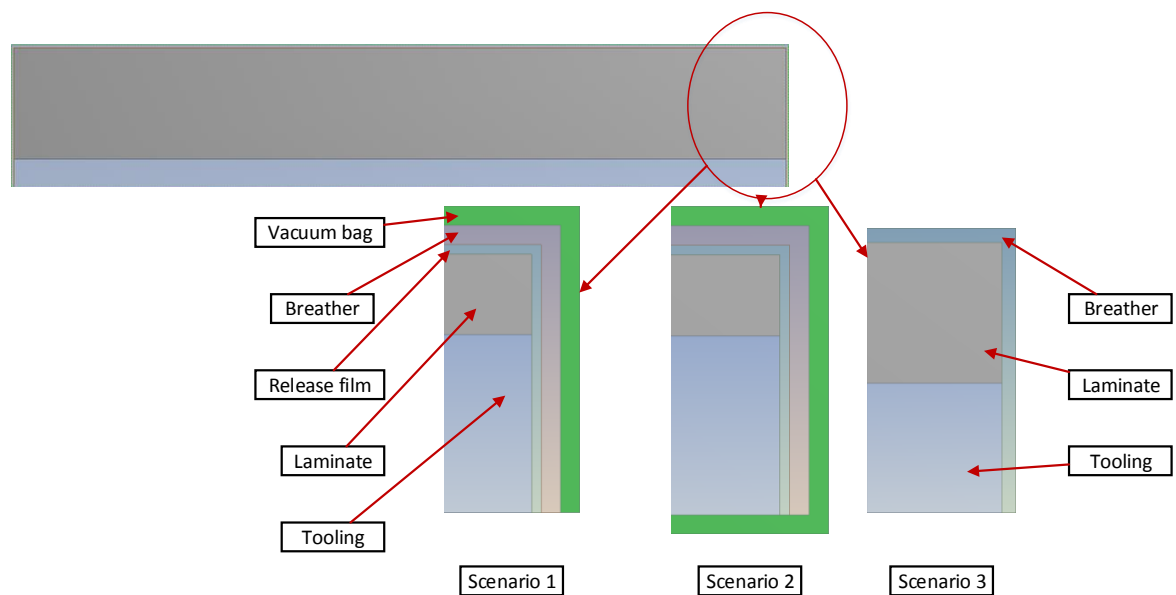


Figure 3.23: Schematic of study on the effect of vacuum bag and release film on laminate core temperature. Note: Thickness of both vacuum bag and release film has been increased to improve clarity

Stage five studies the effect of tooling materials and process ancillaries on achievable reductions in cure cycle time. Table 3.9 presents the parameters studied in stage five. The results obtained from Run 1 – 8 ignore the effect of tooling and process ancillaries, setting a benchmark. Runs 9 – 56 isolates the effect of tooling material and laminate thickness on cure cycle time. Runs 57 – 84 highlight the effect of process ancillaries on cycle time. More specifically, runs 57 – 68 isolate the effect of breather thickness and breather configuration (single sided and envelope); Runs 69 – 76 isolate the effect of using a foam core; Runs 77 – 84 isolate the effect of using a pressure intensifier. The temperature profiles indicated is summarised in Figure 3.9.

Benchmark							
Run No.	Tooling material	Laminate thickness	Breather thickness	Foam core thickness	Intensifier thickness	Cure cycle	Note
01 - 04.		5				T1 - T4	
05 - 08.		15				T1 - T4	
Effect of tooling material							
Run No.	Tooling material	Laminate thickness	Breather thickness	Foam core thickness	Intensifier thickness	Cure cycle	Note
09 - 12.	Aluminium	5				T1 - T4	
13 - 16.	Aluminium	15				T1 - T4	
17 - 20.	Invar	5				T1 - T4	
21 - 24.	Invar	15				T1 - T4	
25 - 28.	Graphite	5				T1 - T4	
29 - 32.	Graphite	15				T1 - T4	
33 - 36.	Composite tooling	5				T1 - T4	
37 - 40.	Composite tooling	15				T1 - T4	
41 - 44.	Ceramic	5				T1 - T4	
45 - 48.	Ceramic	15				T1 - T4	
49 - 52.	Carbon foam	5				T1 - T4	
53 - 56.	Carbon foam	15				T1 - T4	
Effect of process ancillaries							
Run No.	Tooling material	Laminate thickness	Breather thickness	Foam core thickness	Intensifier thickness	Cure cycle	Note
57 - 60.			1.2			T1 - T4	
61 - 64.			4.8			T1 - T4	
65 - 68.			1.2			T1 - T4	Enveloped
69 - 72.				5		T1 - T4	
73 - 76.				10		T1 - T4	
77 - 80.					5	T1 - T4	
81 - 84.					10	T1 - T4	

Constant Breather thickness (0.6mm)
Constant tooling material (Aluminium)
Constant laminate thickness (5mm)
Not used

Table 3.9: Summary of the parameters used in design of experiment stage five

The boundary conditions used in the design of experiment are summarised in the following section.

3.4.7. Boundary conditions

The temperature boundary conditions in the design of experiment is summarised in Figure 3.9. In stage one and stage three (setup verification study and resin kinematics model comparison study), the laminate is represented as a hexahedral mesh, with the temperature profile to the walls of the meshed domain as a User-Defined-Function (UDF). The boundary condition for stage two (model verification study) is presented in Appendix F. The boundary conditions used in stage four are summarised in Table 3.10; Figure 3.24 indicating the location of Boundary A and Boundary B.

	Boundary A	Boundary B
Condition 1 (C1)	Conduction	Zero Heat flux
Condition 2 (C2)	Conduction	Conduction
Condition 3 (C3)	Conduction	Convection – Film coefficient of 20 W/m ² K, ambient temperature
Condition 4 (C4)	Forced convection – Film coefficient of 70 W/m ² K	Forced convection – Film coefficient of 70 W/m ² K

Table 3.10: Summary of the study on effect of heating method on laminate core temperature

In Table 3.10, Condition 1 (C1) simulates a perfectly insulated system with no heat flux through the vacuum bag. Condition 2 (C2) simulates the use of a closed conduction based cure process; such as, Quickstep, Thermal Press Cure and matched tooling with on-board heating. Condition 3 (C3) represents a single free standing tooling with on-board heating system. A low heat transfer coefficient has been

arbitrarily chosen to simulate free convection. Condition 4 (C4) simulates forced convective heating, such as in an autoclave.

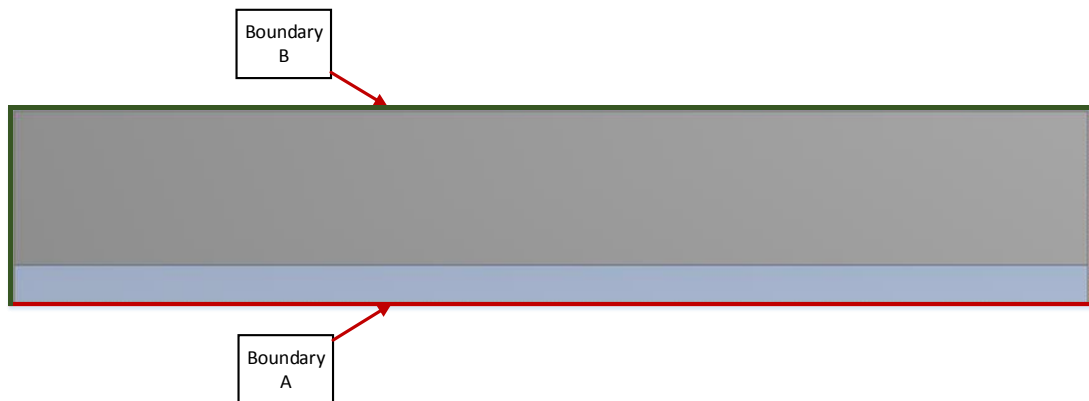


Figure 3.24: Boundary conditions for stage three and stage four of the design of experiment

It should be noted that the forced convective heat transfer coefficient is dependent on ambient pressure, surface geometry and Reynolds number of the flow of the heat transfer medium. However, studies on process modelling have commonly employed a fixed coefficient of ranging between 10 – 85 W/m²K when simulating the processing of flat plaques [132, 134]. Whilst the heat transfer coefficient varies with cure cycle and location of the tooling within the autoclave, it has been suggested that there is little variation in convective coefficient along the centre-line of the heating chamber of an autoclave [153, 154]. Similar to the work by Ganapathi et al [132], convective heat transfer coefficient is kept fixed at 70W/m²K in the present study. The high coefficient is chosen to simulate effective heat transfer due to the pressurised environment within the autoclave.

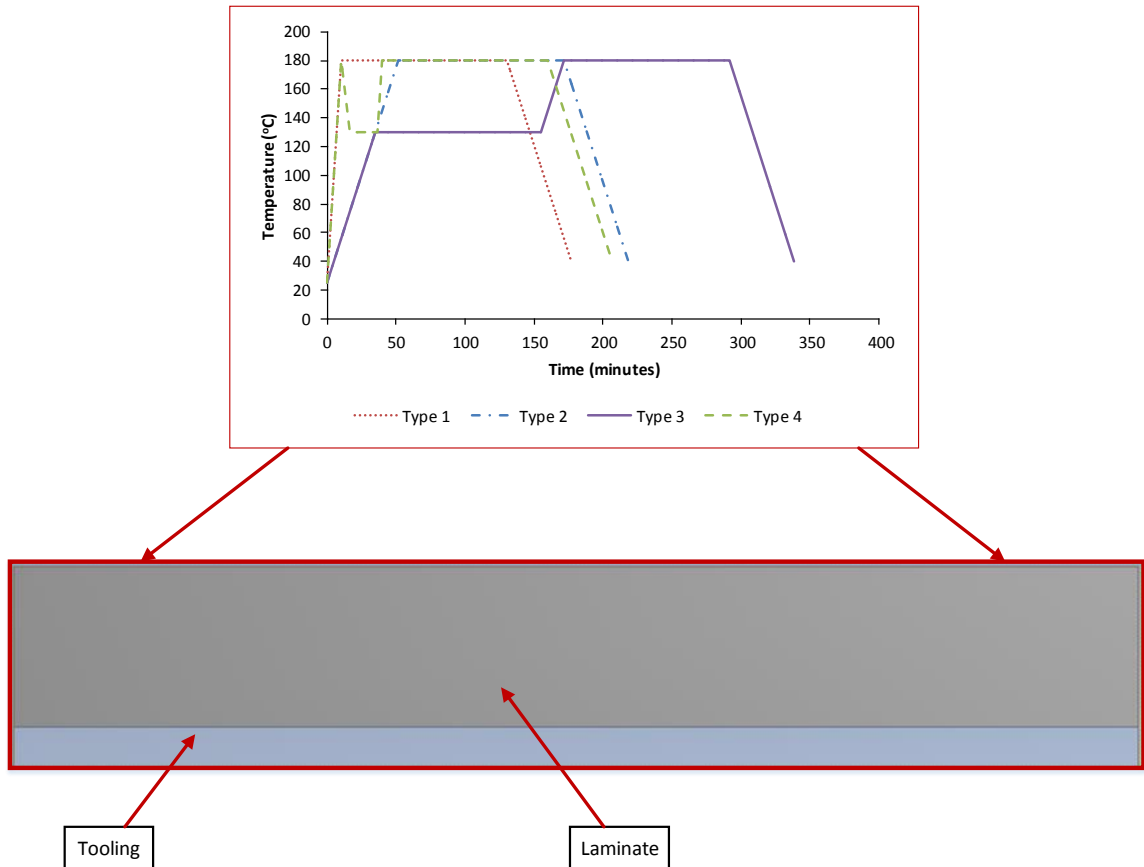


Figure 3.25: Temperature boundary condition applied to the edges using a User-Defined-Function (UDF).

Figure 3.25 presents a schematic of the boundary condition for stage 5 (effect of tooling material and process ancillaries). High heating rate cure cycles (Type 1 and Type 4) have been limited to conduction only boundary conditions. Slow heating rate cure cycles (Type 2 and Type 3) have been limited to convection only boundary condition, with a convective heat transfer film coefficient of $70\text{W}/\text{m}^2\text{K}$.

4. Effect of high heating rate processing on void growth

4.1. Introduction

It has been hypothesised in Chapter 2 that void growth mitigation in high heating rate processes is achieved via the reduction in time for resin gelation. This reduces the quantity of dissolved moisture diffusing into voids, leading to reduced void volume and porosity levels, when compared to standard cure cycles. The present chapter aims to verify this hypothesis by processing laminates using high heating rate (15°C/min) combined with low consolidation pressure (up to 2 Bar) and comparing the level of porosity against standard OoA processing techniques.

4.2. Methodology

The material used in this study is Cytec's MTM44-1 unidirectional prepreg. However, to simulate the effect of long lay-up time on prepreg moisture content, the prepreg has been conditioned in high ambient humidity as outlined in Chapter 3.1.1. The size of the void growth window for the cure cycles used and the resulting void diameter is analytically determined using the governing equations summarised in Chapter 2.3. The point of resin gelation, required to define the endpoint of the void growth window, has been experimentally determined by running the temperature profiles outlined in Chapter 3.4.1.2 in a rheometer and monitoring the changes in viscosity of MTM44-1 resin film samples. In-line with other studies [68, 113], the point of gelation is taken as the cross-over point of the storage modulus and the loss modulus. Void volume fraction is determined by using greyscale thresholding image analysis technique – summarised in Chapter 3.3.4.4. The temperature profiles used in this study and the convention used for the sample names have been summarised in Chapter 3.3.3. Figure 4.1 and Table 4.1 recaps the temperature profiles and pressure used in this study. Sample names ending with "UC" indicate unconditioned prepreps.

Sample name	Temperature profile	Consolidation pressure (Bar)	Heating method
E-1-P-T1-C	Type 1	1	Pressure Tool
E-1-O-T2-C	Type 2		Oven
B-1-O-T3-C	Type 3		
B-1-O-T3-UC			
E-2-P-T4-C	Type 4	2	Pressure Tool
B-7-A-T2-C	Type 2	7	Autoclave

Table 4.1: Summary of cure profiles, consolidation pressure and heating method used in this study.

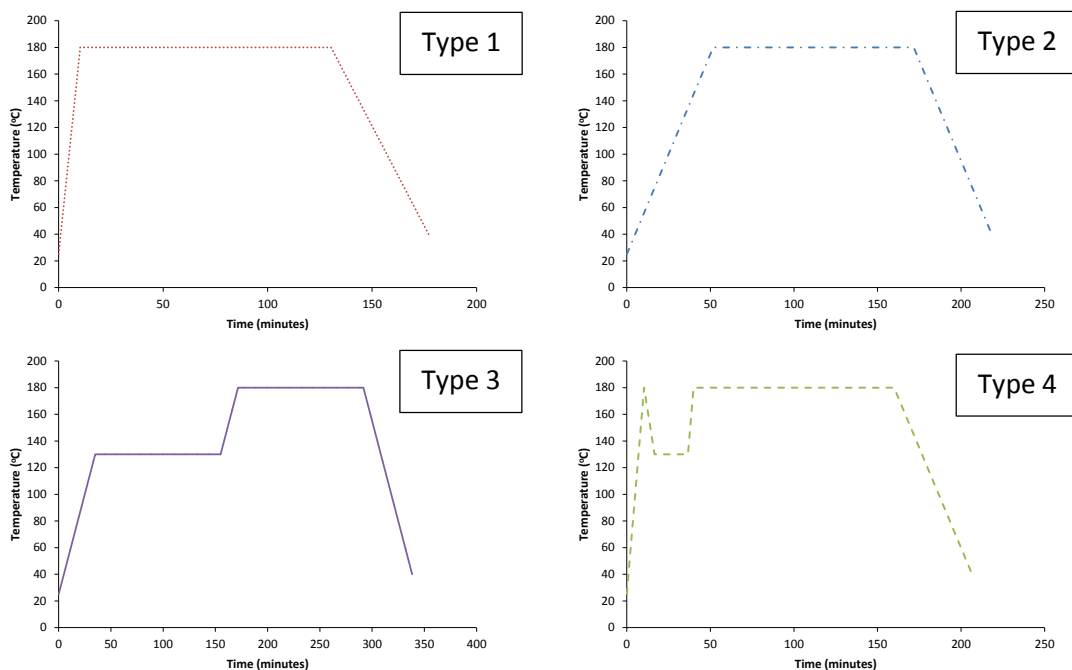


Figure 4.1: Temperature profiles used in this study.

In Type 1, the laminate is heated at a 15°C/min heating rate up to 180°C. The laminate is allowed to dwell at 180°C for 2 hours before cooling down at 3°C/min. This temperature profile is analogous to the manufacturer recommended autoclave temperature profile except in the use of 15°C/min heating rate.

Type 2 is the manufacturer recommended autoclave temperature profile for the material, where a 3°C/min heating rate is employed.

Type 3 is the manufacturer recommended OoA temperature profile. A maximum ramp rate (both during heating and cooling) of 3°C/min is employed.

Type 4 is called a 'Spike' cure, a cure cycle commonly used in the Quickstep process [32, 33]. Unlike in the Quickstep process, a higher heating rate (15°C/min) is employed in the present study to further reduce the size of the window for void growth.

4.3. Results and discussion

4.3.1. Void volume fraction

Representative optical micrographs for each cure cycle are shown in Figure 4.2 - Figure 4.7 with the measured void volume fraction summarised in Table 4.2. Individual images have been taken at x5 magnification and stitched to create the sample cross-section shown in Figure 4.2 – Figure 4.7. Top side of the image represents the bag side while the bottom side of the image is the tool side.

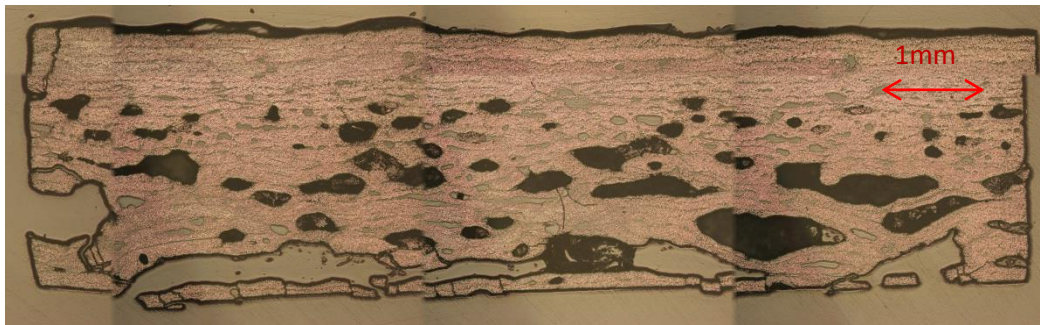


Figure 4.2: Representative stitched optical micrograph of a laminate processed at 15°C/min to 180°C with 1 Bar consolidation pressure (E-1-P-T1-C).

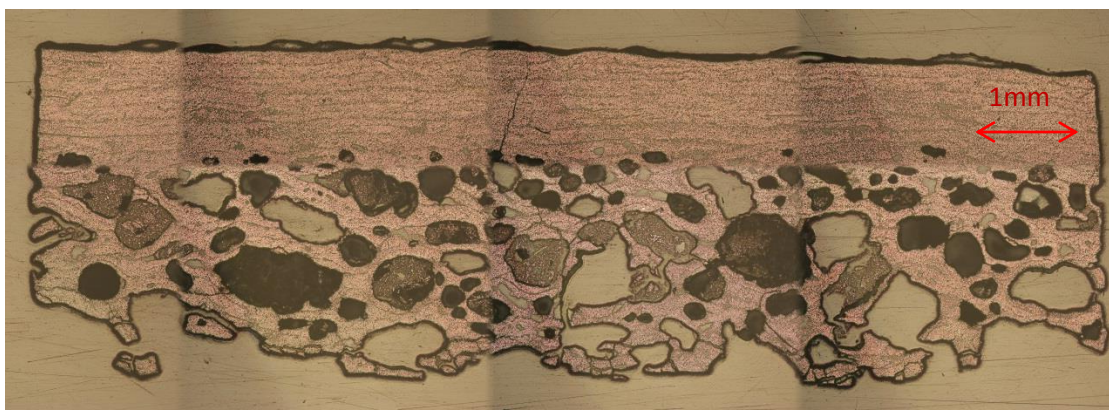


Figure 4.3: Representative stitched optical micrograph of a laminate processed at 3°C/min to 180°C with 1 Bar consolidation pressure (E-1-O-T2-C).

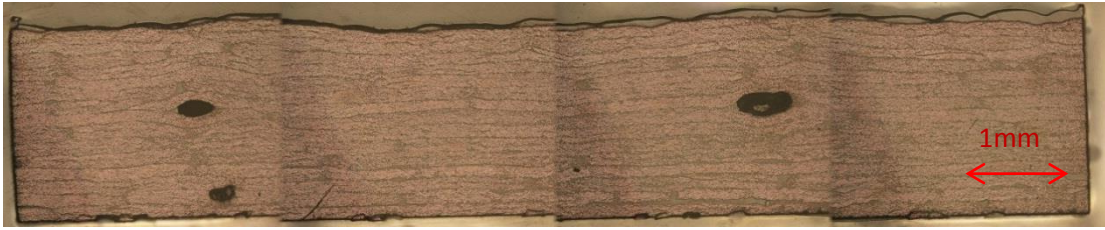


Figure 4.4: Representative stitched optical micrograph of a laminate processed using the benchmark VBO cure cycle with conditioned prepreg (B-1-O-T3-C).

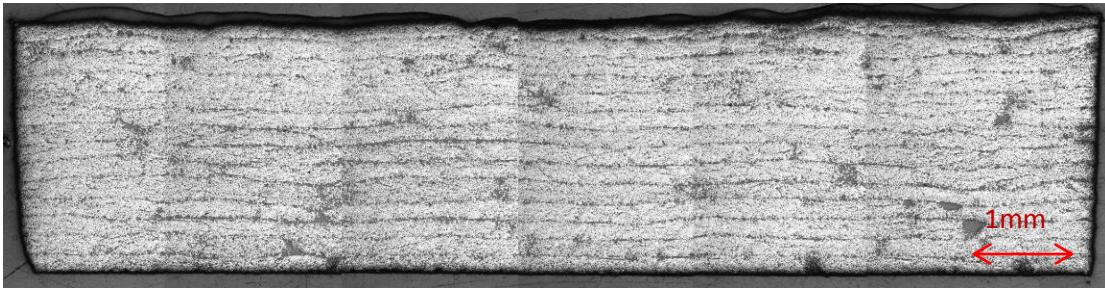


Figure 4.5: Representative stitched optical micrograph of a laminate processed using the benchmark VBO cycle with unconditioned prepreps (B-1-O-T3-UC). Note: unconditioned prepreps were used to process the above sample.

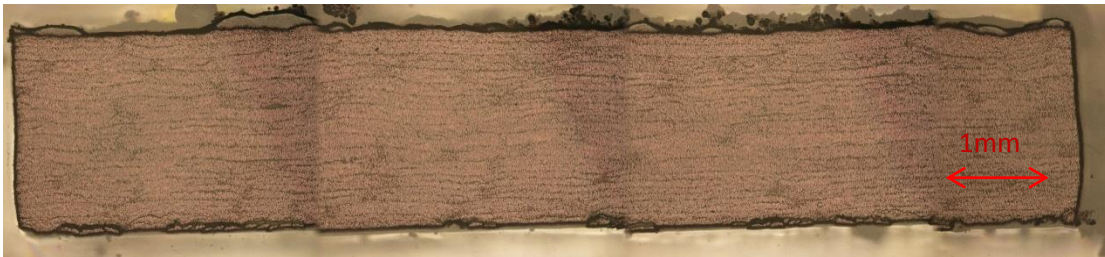


Figure 4.6: Representative stitched optical micrograph of the laminate processed with the 15°C/min spike cure and 2 Bar consolidation pressure (E-2-P-T4-C).

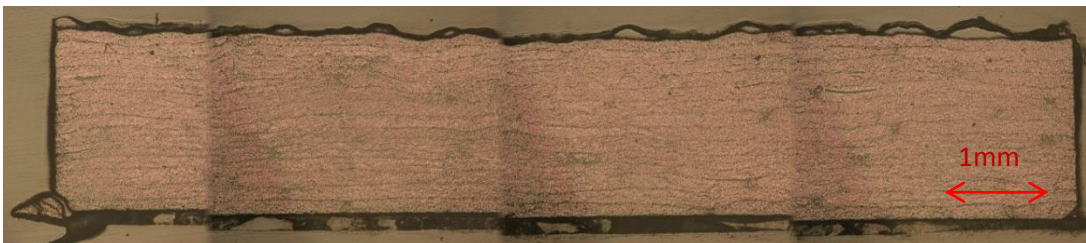


Figure 4.7: Representative stitched optical micrograph of a laminate processed using the benchmark autoclave cycle (B-7-A-T2-C).

Both the benchmark autoclave laminate (B-7-A-T2-C) and the benchmark OoA laminate with unconditioned prepreg (B-1-O-T3-UC) exhibit excellent consolidation and negligible porosity, in-line with published data [68, 93]. Manual examination of the laminates under the microscope did not reveal the presence of voids. Therefore, the non-zero recorded void volume fraction (Table 4.2) can be attributed to fibre artefacts picked up during image analysis, a known drawback of using image analysis techniques [155].

Alternative void analysis techniques, such as ultrasound and acid digestion, whilst capable of increasing accuracy, cannot show the location and distribution of the voids within the laminate, which studies have shown to be critical to mechanical properties [16, 50]. Furthermore, small void diameters ($< 7\mu\text{m}$) observed in the laminates, cannot be detected effectively when using the ultrasound attenuation technique [156]. While X-Ray tomography, has been used effectively in other studies [50, 155, 157] to study 3D void distribution and dimension, owing to the combination of sample size and small void diameters, the resulting machine time and cost would be prohibitive for this study.

	Benchmark 1	Benchmark 2	Cycle 1	Cycle 2	Cycle 3	Cycle 4
Measured void volume fraction (%)	0.2	0.4	0.53	12.78	24.80	2.25

Table 4.2: Summary of measured void volume fraction.

The laminate cured using the 15°C/min spike cure (E-2-P-T4-C) exhibits low void volume fraction (0.53%). The measured void volume fraction is significantly less than published data for laminates cured with a 10°C/min ‘Spike’ cure and 1.1 Bar consolidation pressure (1.7% - 4.3%) [32, 34, 47]. Moreover, the measured void volume fraction in the present study is less than laminates processed with a 10°C/min ‘Spike’ cure combined with 2 Bar consolidation pressure applied throughout the cycle, 0.53% against 1.1% [50]. This indicates that pressure is not solely responsible for the low porosity observed in the present study. However, unlike the benchmark laminates, during manual examination micro-voids have been observed in resin rich bands running the length of the laminate (Figure 4.8).

Although the high heating rate during the 'spike' phase of the cure cycle yielded low minimum resin viscosity, the 12°C thermal overshoot and subsequent slow cooling down rate reduced the duration at which minimum resin viscosity was maintained. The exponential increase in resin viscosity and the short duration at minimum viscosity limited resin flow leading to the formation of resin rich bands at ply interfaces. Although an edge dam has not been used during cure (Chapter 3.3.1), excessive resin bleed did not take place. This has been confirmed by the lack of excessive resin in the breather material post-cure. This implies that void dissolution is the primary void mitigation mechanism during cure.

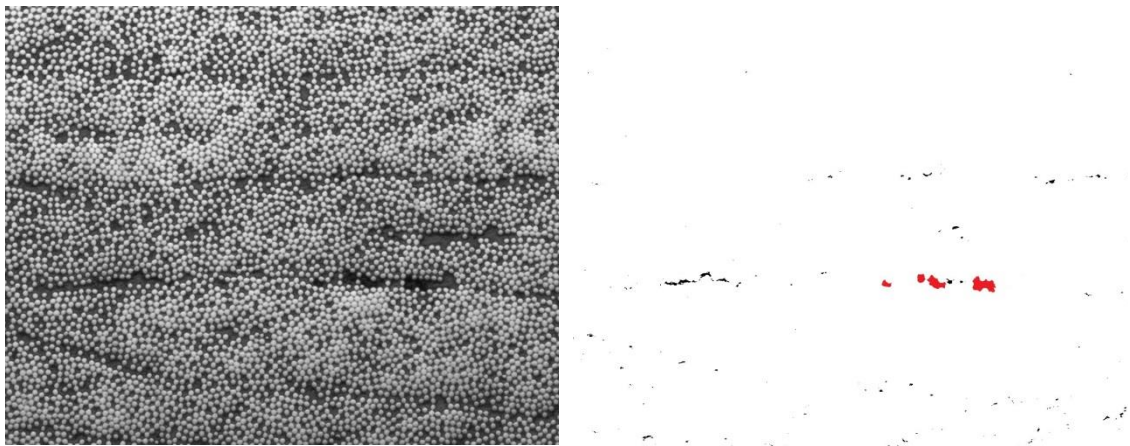


Figure 4.8 (Left): Representative optical micrograph from a specimen at x10 magnification. **Figure 8 (Right)** Manually thresholded image. Note: Voids have been highlighted as red for illustration. Black regions represent fibre artefacts.

In both E-1-P-T1-C (15°C/min to 180°C cycle) and E-1-O-T2-C (3°C/min to 180°C cycle) extensive porosity and evidence of void coalescence have been detected, with void volume fraction lower in E-1-P-T1-C (12.78%) than in E-1-O-T2-C (24.8%). Also, in both cure cycles there is a distinctive distribution of voids through the laminate thickness, with a greater concentration of voids detected in plies closer to the tool surface (Figure 4.3 and Figure 4.4). This type of distribution of voids has not been observed in the other laminates. Studies characterising through thickness distribution of voids in a laminate are limited. Olivier et al [16] observed a non-homogeneous distribution of voids through the laminate thickness. However, in this study voids were predominantly detected in plies near the tool surface. In the work by Olivier et al voids were detected in plies near the bag side. Hernandez et al [50] observed voids predominantly in the middle of the laminate when using hot pressing

to process laminates with low (2 Bar) consolidation pressure. Comparing E-1-P-T1-C and E-1-O-T2-C, it is clear that the method of heating – conduction against convective heating – did not have an impact on void distribution through the laminate thickness in the present study. As stated in Chapter 2.2, moisture preferentially nucleates at interfaces within the resin system, including with the laminate tool-interface. As the surfaces of both the Pressure Tool and the Aluminium plate have undergone similar preparation, it could be that the combination of surface texture on the tool surface and the release agent used reduced the energy required for heterogeneous nucleation to take place at the tool surface. However, substantiating this hypothesis requires an in-depth analysis of the transport of the diffusive species through the resin system and a greater understanding of void nucleation – which is currently an intensely researched area.

Isolated instances of voids have been detected in the centre of laminates cured using the manufacturer recommended temperature profile with conditioned prepregs (B-1-O-T3-C) (2.25%). Due to the low consolidation pressure, the quality of laminates processed using B-1-O-T3-C is heavily dependent on the effectiveness of the air evacuation channels at removing entrapped air. The absence of edge dams during lay-up lead to the incomplete removal of entrapped air – which along with the high moisture content in the resin due to conditioning and low consolidation pressure, facilitated void growth via diffusion of moisture. In addition, studies have shown that high resin moisture content increases resin viscosity. This leads to the formation of porosity due to insufficient resin flow [67]. The findings of this study concur with earlier studies highlighting the sensitivity of OoA processing to lay-up and storage conditions as well as laminating technique.

4.3.2. Understanding void mitigation in high heating rate processes

Using Equation 2.12 from Chapter 2.3 and the data on ‘time to resin gelation’ from the rheological study, a window for void growth is generated for each cure cycle. (Figure 4.9 - Figure 4.12). Also, the change in void diameter up to the point of gelation has been predicted for each cure cycle (Figure 4.13 and summarised in Table 4.2)

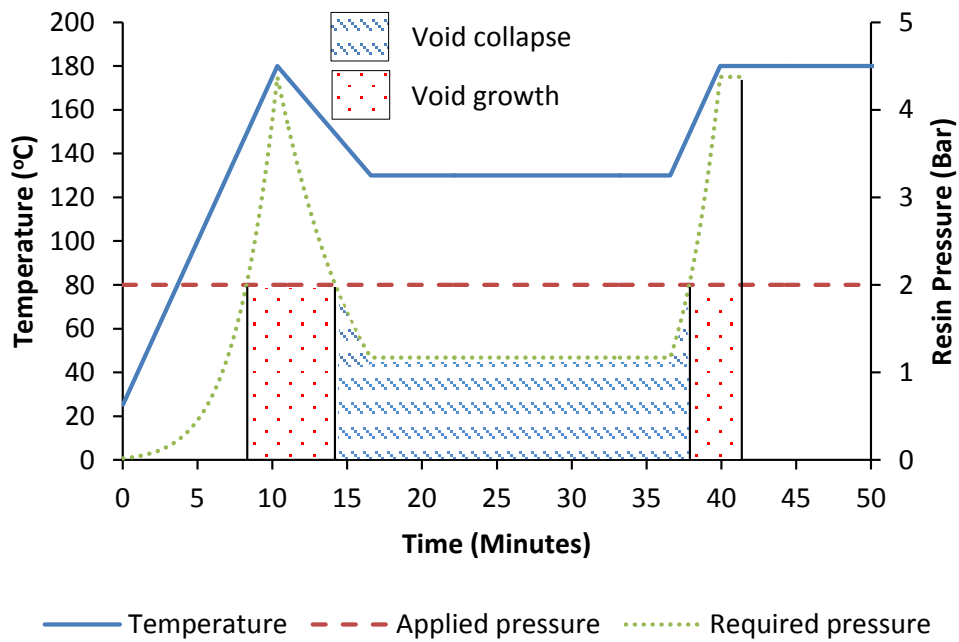


Figure 4.9: Section of the 15°C/min spike cure cycle with 2 Bar pressure (E-2-P-T4-C). Voids formed in the spike phase collapses in the dissolution phase. The predicted size of the final window for void growth is 3.0 minutes.

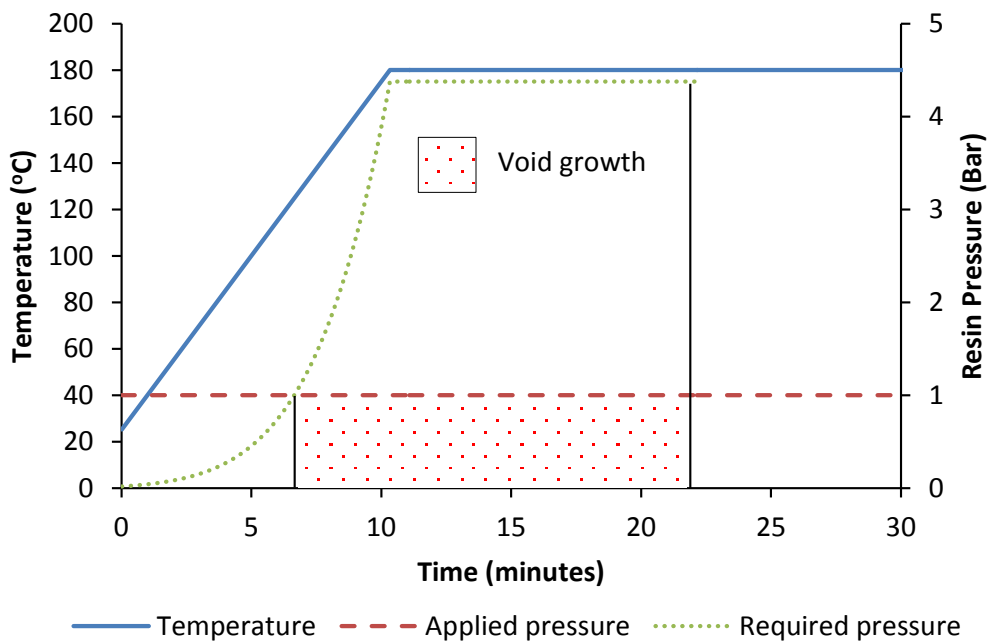


Figure 4.10: Section of 15°C/min to 180°C cure cycle with 1 Bar pressure (E-1-P-T1-C). Size of window for void growth is 15.3 minutes.

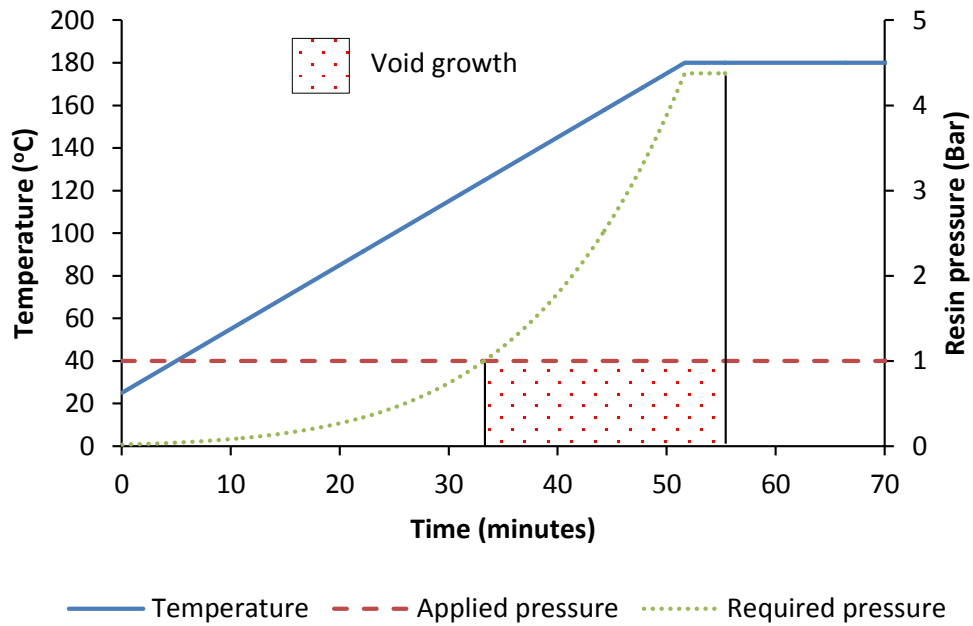


Figure 4.11: Section of the 3°C/min to 180°C cure cycle with 1 Bar pressure (E-1-O-T2-C). Size of window for void growth is 23.3 minutes.

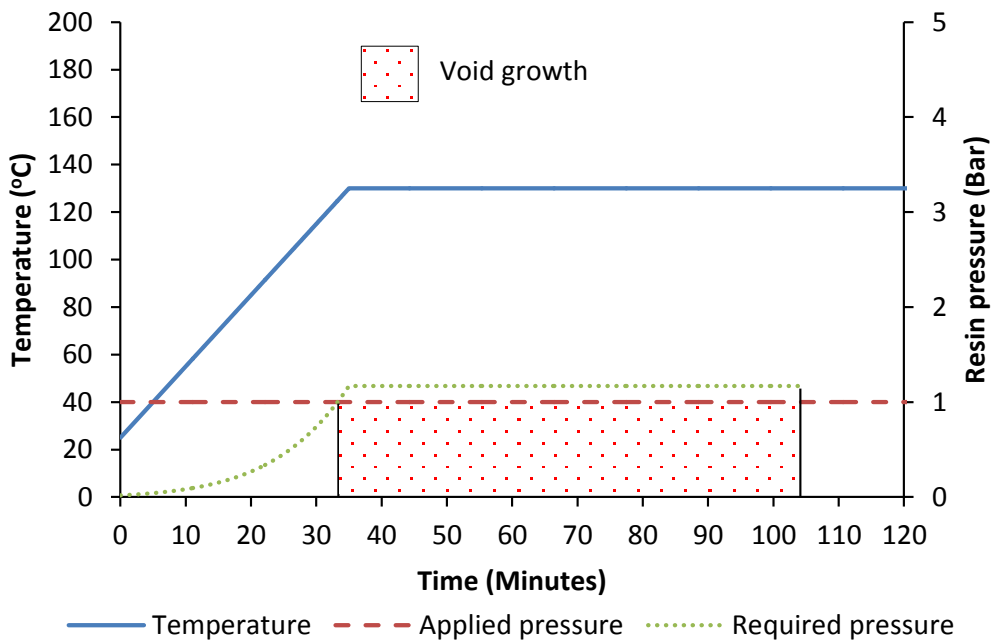


Figure 4.12: Section of the benchmark VBO cure cycle using conditioned prepreps (B-1-O-T3-C). Size of window for void growth is 70.8 minutes.

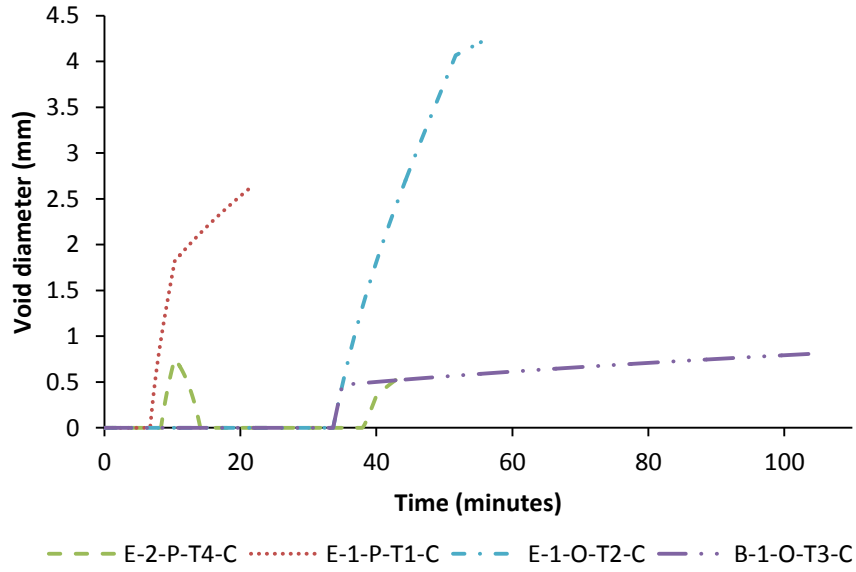


Figure 4.13: Calculated change in void diameter up to point of gelation.

	B-7-A-T2-C	B-1-O-T3-UC	B-1-O-T3-C	E-2-P-T4-C	E-1-P-T1-C	E-1-O-T2-C
Predicted void diameter (mm)	0	0	0.84	0.57	2.65	4.21

Table 4.3: Summary of predicted void diameter. Due to the assumption of void growth taking place in an infinite isotropic medium, final predicted void diameter can be larger than the actual laminate thickness (2mm).

As shown in Figure 4.9 and Figure 4.13, any voids formed during the initial temperature ramp of the spike phase will collapse during the dwell at 130°C. As the applied pressure is greater than the required pressure for void growth during the dwell, moisture diffuses out of the void leading to void shrinkage and ultimately collapse. Due to the advancement of cure of the resin, the time to resin gelation in the 180°C dwell is reduced. This minimises the window for void growth, leading to low void fraction.

A comparison of Figure 4.10 and Figure 4.11 highlights the impact of heating rate on void growth. In the 15°C/min cure cycle, the high heating rate reduces the time to resin gelation. This leads to a decrease in time for diffusion of moisture to take place, leading to a decrease in final void diameter. While in the 3°C/min cure cycle, due to

the slow heating rate resin gelation occurs later in the cure cycle. This increases the size of the window for void growth. The window for void growth is 58.9% longer than in the 15°C/min cycle, leading to an increase in final void diameter and ultimately observed void fraction.

In the benchmark VBO cycle with conditioned prepreg, although the window for void growth is the longest (Figure 4.12), the drive for diffusion is minimised as the applied pressure closely matches that of the required consolidation pressure. This results in a smaller final void diameter that is comparable to that of predicted for the 15°C/min spike cure (Figure 4.13). This implies that in a conventional OoA cure cycle the mechanisms of minimising void growth are twofold: low initial dwell temperature reducing the drive for void growth; and by the physical removal of any voids formed via the air evacuation channels. While in high heating rate, low consolidation pressure processes void growth mitigation is achieved by a reduction in time for the diffusion of moisture to take place. Davies et al [32] suggests that the low minimum viscosity combined with the sufficient flow time facilitates the physical removal of voids via void transport; leaving ellipsoid resin rich regions and disturbed fibre bundles within the bundle. However, based on the image analysis of samples in the present study, there has been no evidence of void transport taking place in the high heating rate cure cycles.

Similar to previous models, void growth is assumed to take place in an infinite isotropic medium without any fibre influence, due to which the predicted void diameter is far larger than the actual laminate thickness. However, due to extensive void coalescence and high void volume fraction in E-1-P-T1-C and E-1-O-T2-C, it has not been possible to make a comparison between the predicted void diameter and the measured void volume fraction using scaling factor used in earlier studies [21, 68]. In this study the predicted void diameters are normalised to that of E-1-O-T2-C and compared with normalised measured void volume fraction (Figure 4.14).

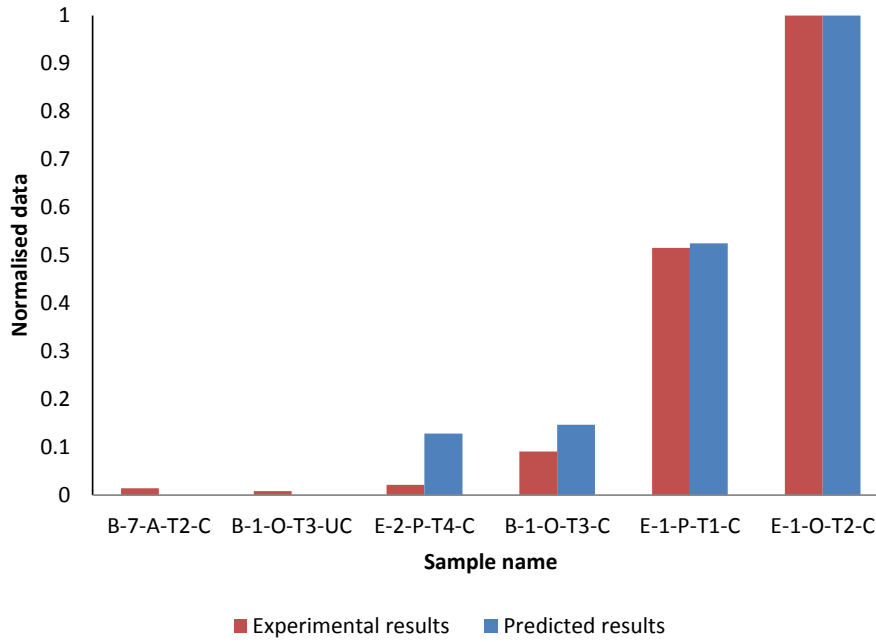


Figure 4.14: Comparison between normalised predicted void diameter and normalised measured void volume fraction.

Even with additional factors, such as void coalescence and void gas composition (air-water vapour mixture), it can be seen that there is a good correlation (correlation coefficient: 0.92) between the normalised, predicted void diameter and the normalised measured void volume fraction, except for the 15°C/min spike cure. The accuracy of the size of the predicted void diameter is dependent on the accuracy of the experimentally determined point of resin gelation during the cure cycle. Based on the prescribed temperature profile for the 15°C/min spike cure, gelation occurs at 43 minutes in. However, due to the thermal overshoot resin gelation occurs earlier in the experimental cure cycle (Figure 4.15).

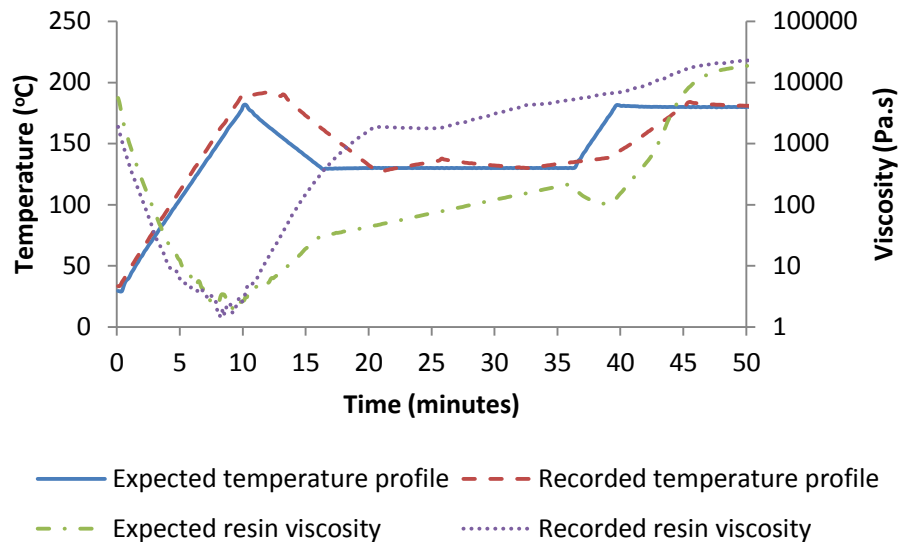


Figure 4.15: Comparison between resin viscosity for prescribed temperature profile of Cycle 1 and actual resin viscosity due to thermal overshoot

In addition, both the plasticisation of the resin and long out-time due to conditioning further reduced the time to resin gelation. Based on the results of the image analysis, it is clear that resin gelation occurs during the void dissolution phase of the cure cycle, leading to the collapse of any voids formed during the 'spike' phase, and crucially, preventing the regrowth of voids during the subsequent temperature ramp - hence the low observable final void volume fraction. However, this study highlights the drawback of the spike cure – low margin of error. A 12°C increase in temperature of the spike phase and the 'blunting' of the spike results in a large shift in point of resin gelation. This increases the risk of gelation occurring before the start of the void dissolution phase, resulting in extensive porosity and poor laminate consolidation.

Current generation tooling with on-board electric heaters cannot achieve the high cooling down rate required to reliably control the point of gelation. Further work is needed to optimise the tooling design and tooling material selection; in addition to understanding the feasibility of this cure cycle for curing thick (>10mm) laminates. Nevertheless, it is clear that in high heating rate processes void growth is minimised due to the reduction in time for diffusion to take place. In addition, it may be possible to further reduce void content by using a resin system optimised for high heating rate processes. For example, a resin system with a short time to gelation

would minimise the size of the void growth window, whilst crucially increasing the time at minimum viscosity to maintain sufficient time for resin flow.

4.4. Conclusion

There is a strong trend between the predicted void diameter and the measured void volume fraction, with a good degree of fit (correlation factor of 0.92) after normalising the two data. Compared to previously used methods, this technique has been found to be suitable even for extreme cases; such as high void volume fraction (>10%), extensive void coalescence and mixture void gas composition (air-water vapour).

It can be concluded from this work that void growth in high heating rate processes is minimised due to a reduction in time for void growth via diffusion to take place. High heating rate processes reduce the time to gelation, which in turn reduces the time for resin diffusion to take place. A 'spiked' temperature profile with 2 Bar consolidation pressure has been shown to yield low void content (0.52%). The 2 Bar consolidation pressure and the low dwell temperature after the initial spike creates a window for void dissolution. Equally, with the right temperature during the spike phase it is possible to ensure that resin gelation occurs during the dwell phase, preventing void growth during the subsequent temperature ramp, yielding low void content.

The OoA resin system used in this study has been found to be suitable for high heating rate cure cycles. However, preconditioning the prepreg and withholding the use of edge dams resulted in porosity even when after using the manufacturer recommended oven cure cycle - Indicating that high void content can occur if the lay-up conditions, storage conditions or lay-up technique (e.g. lack of edge dams) is less than ideal.

Although using 2 Bar consolidation pressure in combination with the spiked temperature profile yielded laminates with the lowest void content, further studies are needed to further assess the limitations of this type of cure cycle. These include, ensuring sufficient wet-out before gelation and achieving suitably high cooling rates with electrically heated tooling. In addition, further study is needed in understanding

the limitations of high heating rate processes for composites manufacturing, such as the maximum laminate thickness that can be processed, impact of the cure cycle on the build-up of residual stress and component cost. Finally, there is a need to understand the impact of using high heating rate combined with hydrostatic pressure greater than that used in typical OoA processes on mechanical properties – which will be addressed in the following chapter.

5. Combined effect of high heating rate and hydrostatic pressure on the physical and mechanical properties of composites

5.1. Introduction

High heating rate processes that can process laminates with greater than 2 Bar consolidation pressure have in development for over the last decade. It has been claimed that high heating rate combined with high consolidation pressure yields high laminate quality. However, quantitative data on the impact such cure cycles on the physical and mechanical properties of laminates is limited. The current chapter expands on the findings from Chapter 4 by using the Pressure Tool to process hygrothermally conditioned prepregs with high heating rate combined with consolidation pressure ranging from 1 Bar to 3 Bar.

5.2. Methodology

The methodology of prepreg conditioning and lay-up is outlined in Chapter 3.1.1 and Chapter 3.3.1 respectively. A summary of the coupon preparation technique for the characterization study methodology is presented in Chapter 3.3.4; the physical and mechanical characterisation tests performed is outlined in Chapter 3.3.4.1 to Chapter 3.3.4.4. Chapter 3.3.3 summarises the cure profiles and convention of sample names used in this study. Table 5.1 and Figure 5.1 recap the temperature profiles and pressure used in this study. Sample name ending with “UC” indicate unconditioned prepregs.

Sample name	Temperature profile	Consolidation pressure (Bar)	Heating method
E-1-P-T1-C	Type 1	1	Pressure Tool
E-2-P-T1-C		2	
E-3-P-T1-C		3	
E-4-P-T2-C	Type 2	4	
E-2-P-T4-C	Type 4	2	
E-4-A-T2-C	Type 2	4	Autoclave
B-7-A-T2-C		7	
E-1-O-T2-C	Type 2	1	Oven
B-1-O-T3-C	Type 3		
B-1-O-T3-UC			

Table 5.1: Summary of cure profiles, consolidation pressure and heating method used in this study.

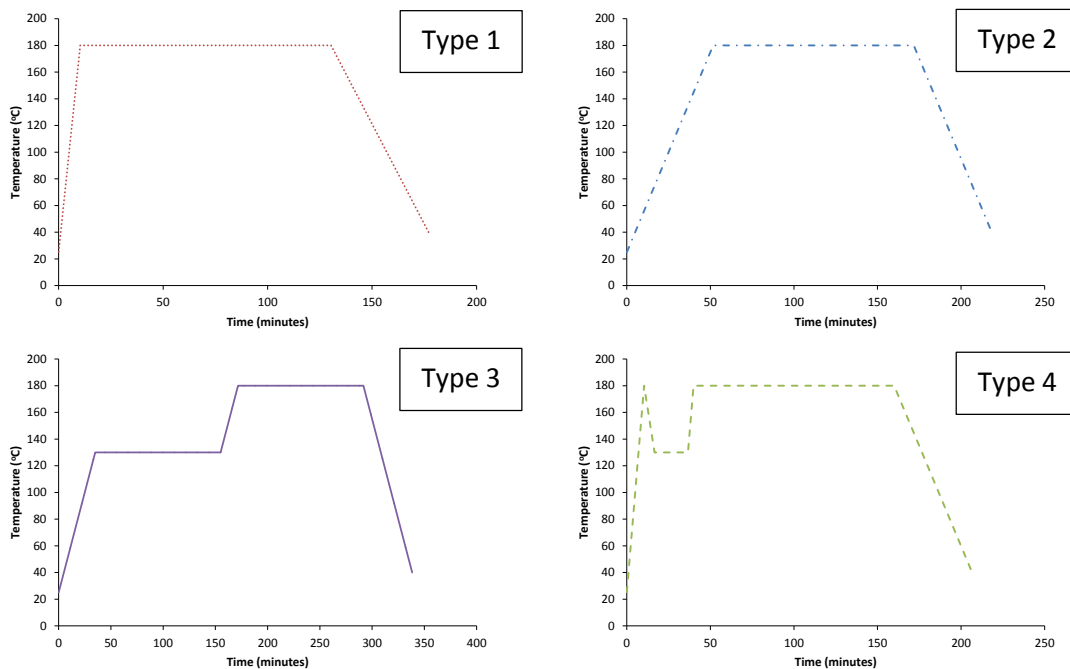


Figure 5.1: Temperature profiles used in this study.

In Type 1, the laminate is heated at a 15°C/min heating rate up to 180°C. The laminate is allowed to dwell at 180°C for 2 hours before cooling down at 3°C/min. This temperature profile is analogous to the manufacturer recommended autoclave temperature profile except in the use of 15°C/min heating rate.

Type 2 is the manufacturer recommended autoclave temperature profile for the material, where a 3°C/min heating rate is employed.

Type 3 is the manufacturer recommended OoA temperature profile. A maximum ramp rate (both during heating and cooling) of 3°C/min is employed.

Type 4 is called a 'Spike' cure, a cure cycle commonly used in the Quickstep process [32, 33]. Unlike in the Quickstep process, a higher heating rate (15°C/min) is employed in the present study to further reduce the size of the window for void growth.

5.3. Results and discussion

5.3.1. Void volume fraction and surface quality

The results of the void volume fraction characterisation study are summarised in Table 5.2 to Table 5.7. In Table 5.2, B-7-A-T2-C represents conditioned prepregs cured using the standard autoclave cure cycle (Type 2) with 7 Bar consolidation pressure. E-2-P-T4-C represents conditioned laminates processed using 2 Bar consolidation pressure and 15°C/min spike cure (Type 4). B-1-O-T3-C represents conditioned prepregs processed using the benchmark VBO cure cycle (Type 3). B-1-O-T3-UC represents unconditioned prepregs processed using the benchmark VBO cure cycle.

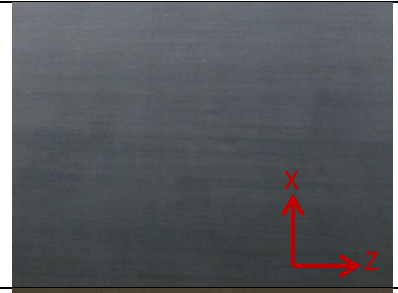
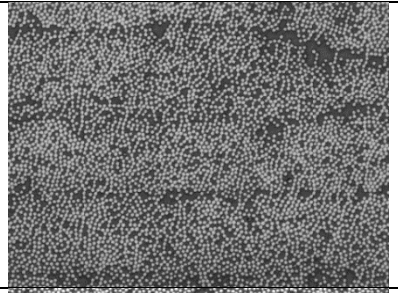



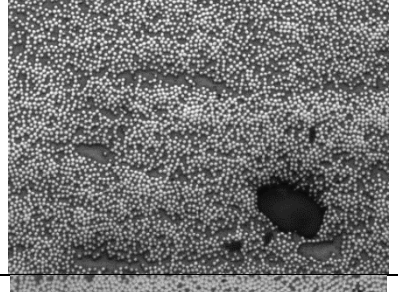
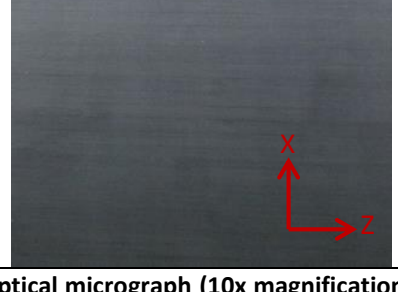
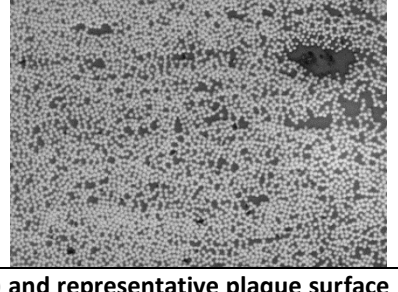
Sample name	Void fraction	Surface quality	Optical microscopy
B-7-A-T2-C	0.14*		
E-2-P-T4-C	0.53*		
B-1-O-T3-C	2.24*		
B-1-O-T3-UC	0.4*		

Table 5.2: Representative optical micrograph (10x magnification) and representative plaque surface finish of benchmark samples. Note: * implies data inferred from the results of Chapter 4

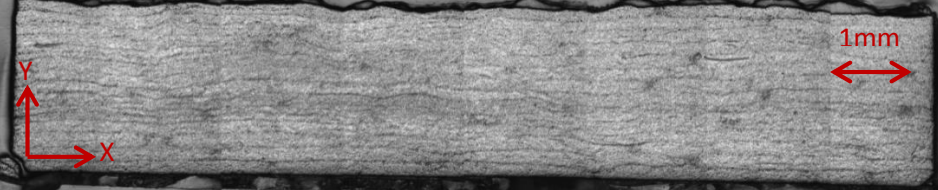

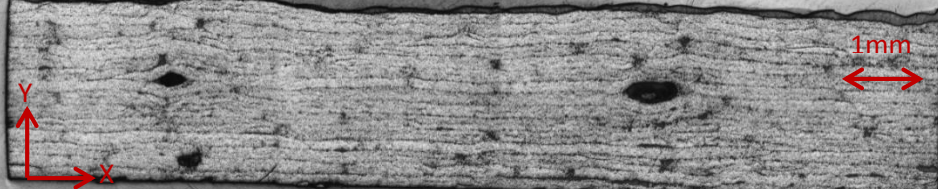
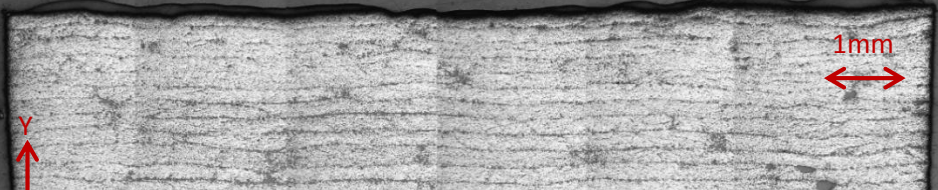
Sample name	Sample cross section
B-7-A-T2-C	
E-2-P-T4-C	
B-1-O-T3-C	
B-1-O-T3-UC	

Table 5.3: Representative cross section of benchmark samples. Note: Cross sectional area is approximately $2 \times 10 \text{mm}^2$ for all samples. Bottom surface of the specimens is the tool side.

Note the presence of resin rich bands running the entire length of the specimen, particularly in samples cured with 1 Bar consolidation pressure and $3^\circ\text{C}/\text{min}$ heating rate (B-1-O-T3-C, B-1-O-T3-UC).


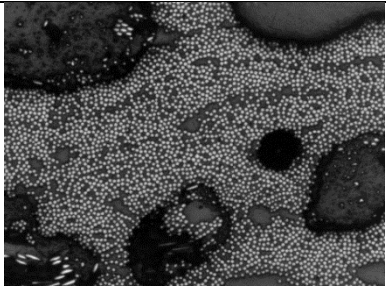

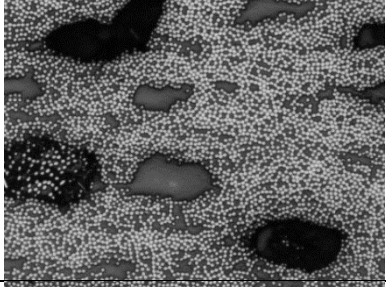

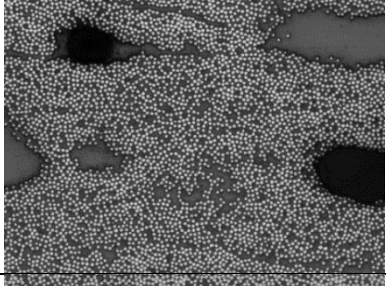
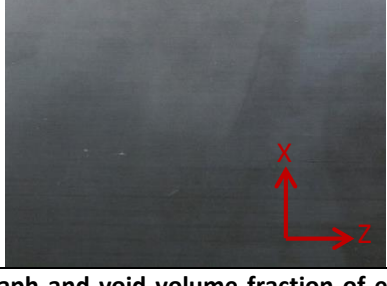
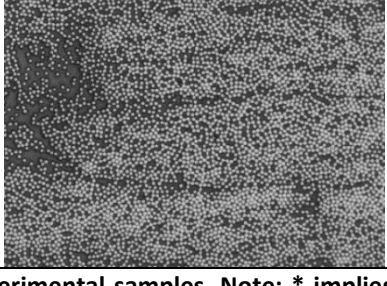
Sample name	Void fraction	Surface quality	Optical microscopy
E-1-O-T2-C	24.80*		
E-1-P-T1-C	12.78*		
E-2-P-T1-C	5.87		
E-3-P-T1-C	0.31		

Table 5.4: Optical micrograph and void volume fraction of experimental samples. Note: * implies data inferred from the results of Chapter 4.

E-1-O-T2-C represents conditioned laminates processed using 1Bar consolidation pressure, with 3°C/min to 180°C. E-1-P-T1-C represents conditioned laminates processed using 1 Bar consolidation, with 15°C/min to 180°C temperature profile. E-2-P-T1-C and E-3-P-T1-C represent conditioned laminates processed using 15°C/min and 180°C temperature profile with 2 and 3 Bar consolidation pressure respectively.

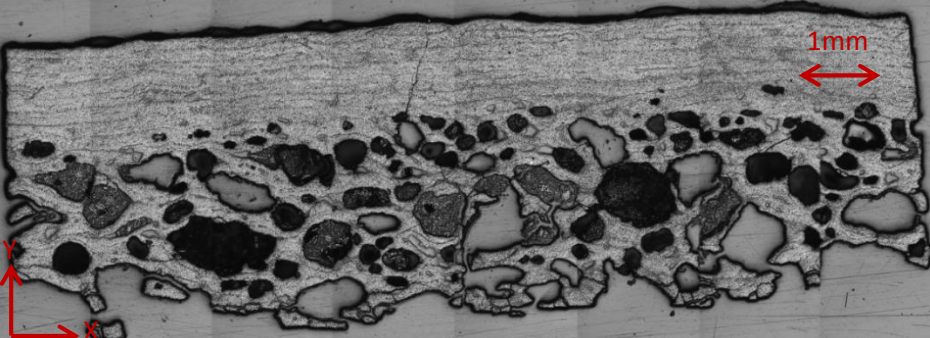
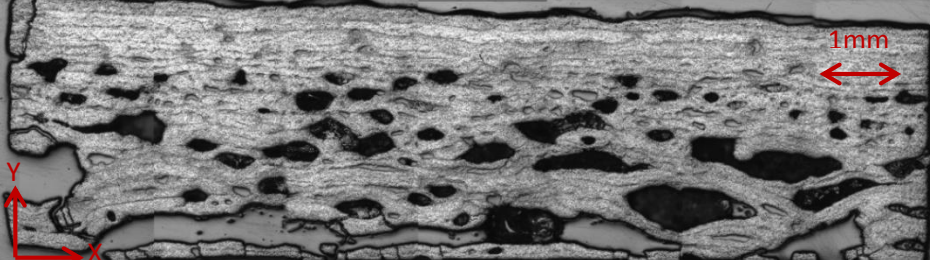
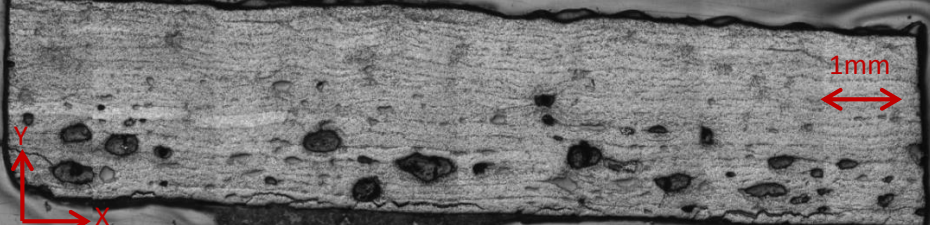
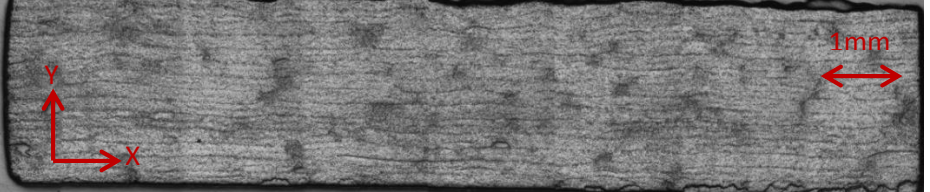
Sample name	Sample cross section
E-1-O-T2-C	
E-1-P-T1-C	
E-2-P-T1-C	
E-3-P-T1-C	

Table 5.5: Representative cross section of experimental samples. Note the distinctive distribution of voids.

Voids have been detected predominantly in plies near the tool side. Due to extensive porosity, the polyester resin used to cast the samples flowed into channels formed by the void network, appearing as resin rich regions within the laminate.

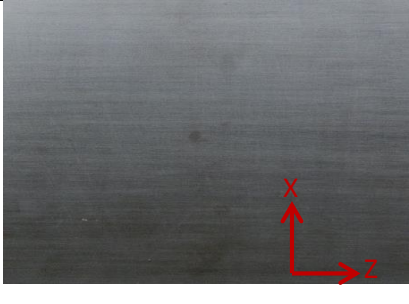
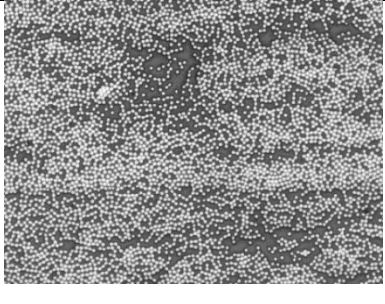
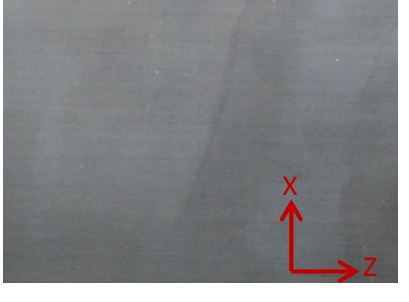
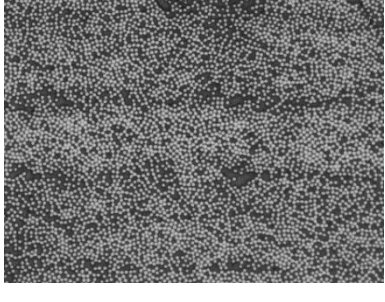
Sample name	Void fraction	Surface quality	Optical microscopy
E-4-A-T2-C	0.08		
E-4-P-T2-C	0.2		

Table 5.6: Representative optical micrograph and representative plaque surface finish – Comparison of the effect of heating method on laminate quality.

E-4-A-T2-C and E-4-P-T2-C represents conditioned laminates processed using 4 Bar consolidation pressure, with 3°C/min to 180°C temperature profile on the autoclave and the pressure tool respectively.

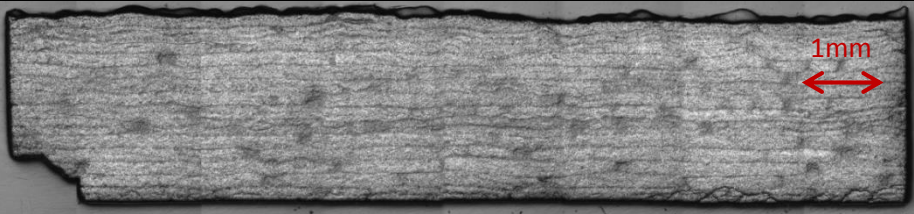
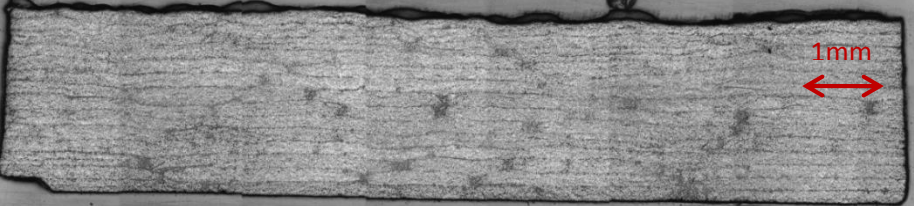
Sample name	Sample cross section
E-4-A-T2-C	
E-4-P-T2-C	

Table 5.7: Representative cross section of experimental samples. Note the regions of disturbed fibre bundles in both samples.

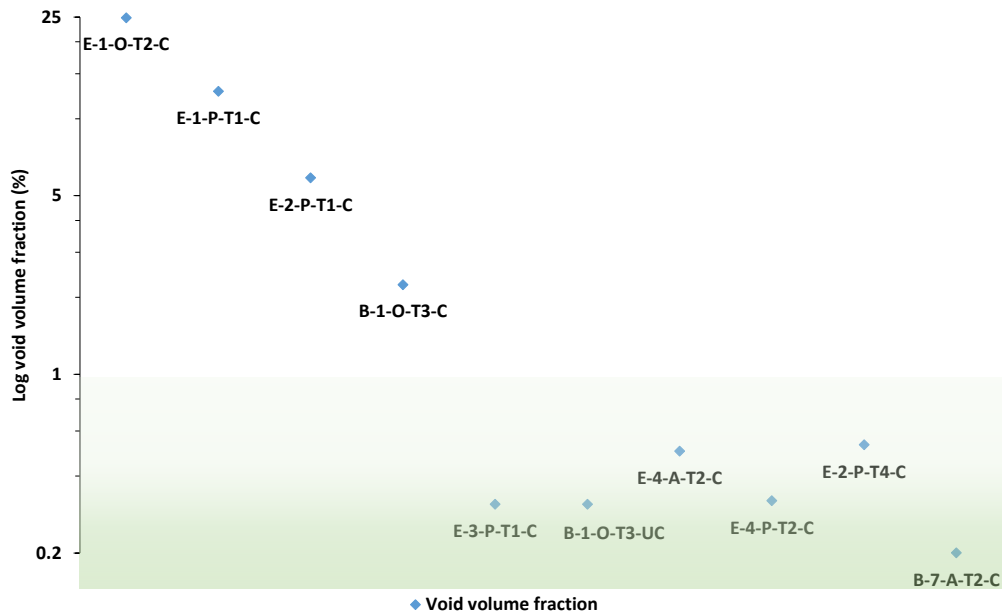


Figure 5.2: Measured void volume fraction for different cure cycles. Shaded area represents increasing random error due to fibre artefacts.

Both the benchmark autoclave cured laminate (B-7-A-T2-C) and the 15°C/min spike cured laminate (E-2-P-T4-C) have low internal porosity and no observable surface defects. However, while voids have not been detected in the autoclave cured laminates, voids (both micro-scale and macro-scale) have been detected in the resin rich bands running the entire length of E-2-P-T4-C (Chapter 4.3.1). As shown in the comparison between the two benchmark VBO cycles, (B-1-O-T3-C, and B-1-O-T3-UC, conditioned and unconditioned prepreg respectively), VBO processing can yield laminates with low porosity if the moisture content is low.

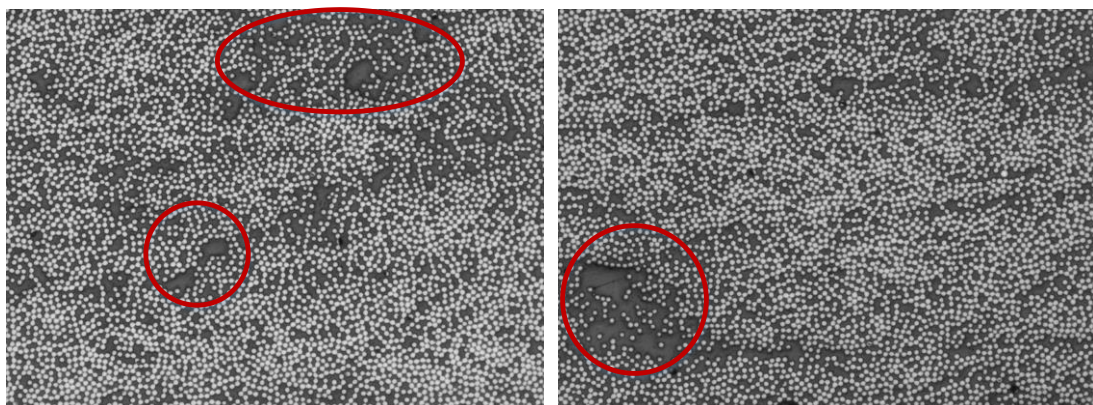


Figure 5.3: Example of disturbed fibre bundles with resin rich regions. (Circled in red) These indicate regions within a laminate that used to be voids [32].

Table 5.4 to Table 5.7 catalogues the impact of: heating rate on void mitigation (E-1-O-T2-C and E-1-P-T1-C, 3°C/min and 15°C/min respectively), combined effect of high heating rate and consolidation pressure on void volume fraction (E-1-P-T1-C, E-2-P-T1-C, E-3-P-T1-C; 1, 2 and 3 Bar respectively with 15°C/min ramp rate) and the effect of heating method and reduced consolidation pressure on laminate quality (convective heating in E-4-A-T2-C against conductive heating in E-4-P-T2-C).

The reduction in void fraction when using 15°C/min heating rate when compared to 3°C/min has been attributed to the reduction in time to gelation in Chapter 4. In addition, while the distribution of voids through the laminate thickness is consistent across the two laminates, the average diameter of voids detected in laminates processed with 15°C/min is less than in laminates processed with 3°C/min, which is as the void model predicts.

Similar to B-7-A-T2-C, inspection of the optical micrographs of E-4-A-T2-C and E-4-P-T2-C did not reveal the presence of voids, implying that the indicated void volume fraction is due to fibre artefacts. However, the decrease in consolidation pressure when compared to B-7-A-T2-C, has resulted in the formation of more resin rich regions within both laminates.

Comparison between E-1-P-T1-C, E-2-P-T1-C and E-3-P-T1-C indicates that high heating rate combined with the consolidation pressure further reduces the size of the void growth window. This results in reduced laminate porosity. However, the measured void volume fraction for the laminate processed with 15°C/min and 3 Bar consolidation pressure result is not as expected (Figure 5.4).

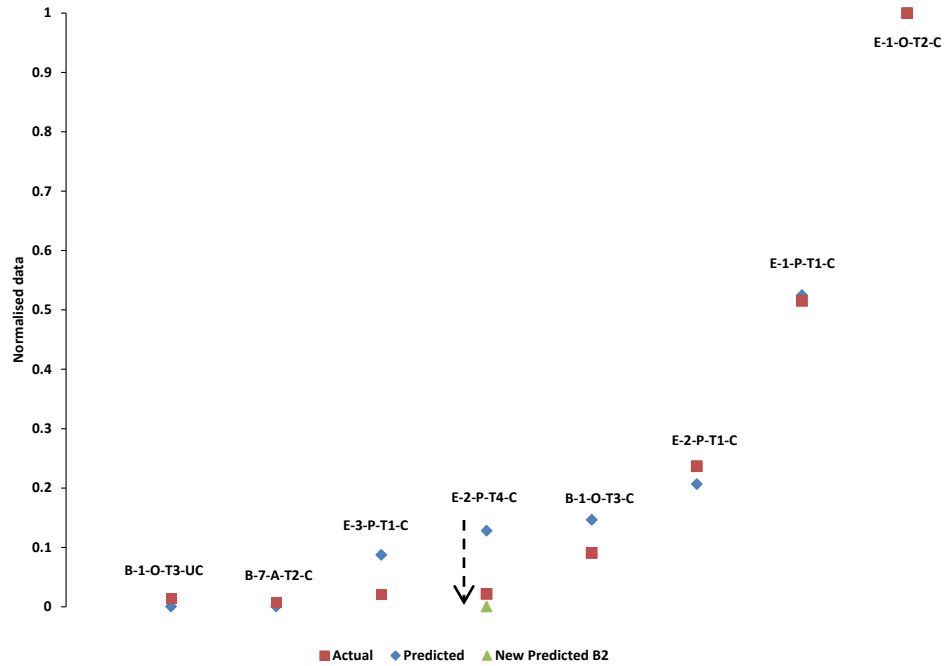


Figure 5.4: Comparison between normalised predicted void diameter and normalized measured void volume fraction taking into account the additional laminates processed in the present chapter. Note: the predicted void diameter for the 15°C/min spike cure has been updated by taking into account the 12°C thermal overshoot observed during the experiment.

As per the void growth model, the applied consolidation pressure is not sufficient to prevent void growth when the dwell temperature is 180°C (Figure 5.5). The presence of disturbed fibre bundles (Figure 5.3) indicate that a different mechanism is at play in removing voids – potentially void transport. Kardos et al [84] stated that due to poor permeability, void removal by physically transporting voids through a resin filled fibre bundle – and out of the laminate - is not feasible. To compound the problem, other studies have shown that the inevitable drop in resin hydrostatic pressure due to resin flow can result in extensive porosity [104, 114]. It could be that the low minimum resin viscosity along with the relatively high consolidation pressure in E-3-P-T1-C (3 Bar) and small sample size (160mmx160mm) was sufficient for void transport to take place via the collapsing air evacuation channels. However, this mechanism may not be possible when processing large parts (> 1m²), indicating that the low observed voids could potentially be due to the experimental setup.

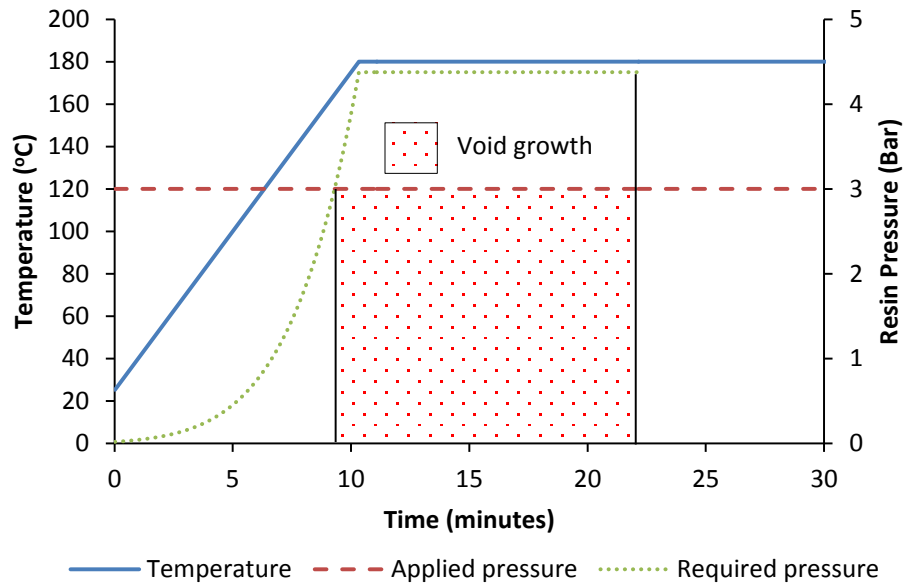


Figure 5.5: Plot highlighting the size of the window for void growth for E-3-P-T1-C. Void growth duration is 12.7 minutes

As shown in the optical micrographs, voids have predominantly been detected in the resin rich bands running the length of the laminate. The resin rich bands could potentially have been the air evacuation channels. It has been suggested that bubble transport through the resin and into the intra-laminar air evacuation channels takes place via a combination of resin advection and pressure gradient in the resin [158]. It is reasonable to expect that dissolution of moisture takes place along an air/resin interface, either at the intra-laminar air evacuation channels or at inter-laminar entrapped air voids. Should the channels not be sealed, such voids can be drawn out of the laminate using vacuum. It is possible that the long out-time combined with the inevitable plasticisation of the resin due to conditioning, sufficient resin flow, and laminate consolidation did not take place, resulting in the formation of the bands. The reduced resin potentially limited “cold flow” or premature collapse of the air channels, leading to extraction of entrapped gases.

Similar to the findings of Olivier et al [16], applying consolidation pressure from the start of the cure cycle yielded a non-homogenous void distribution through the laminate thickness for all cure cycle, with a greater concentration of voids in plies near the breather. However, voids were predominantly detected in plies near the tool surface. Current findings suggest that the degree of surface defects can be used

as a means of providing a qualitative indication of the amount of voids within the laminate. It is possible that surface roughness and release agent used encouraged void formation along the tooling surface by reducing the energy required to form a new phase within the resin [104]. However, the impact of surface roughness on surface porosity has been found to be inconclusive [159]. Work by Wells et al [158] suggest that the formation of surface porosity is predominantly due to insufficient pressure, which reduces the driving force for resin infiltration. However, the findings of the present study suggest that in addition to pressure resin viscosity must be taken into account as well. For instance, the lower minimum viscosity achieved in E-1-P-T1-C when compared to E-1-O-T2-C resulted in significantly reduced surface defects, even though pressure was maintained constant. Whilst both, the work by Wells et al and the present work, reports a correlation between inner laminate porosity and surface porosity, the exact cause of the non-homogenous distribution of voids is still not clear and requires further investigation.

5.3.2. Fibre volume fraction and laminate thickness

Figure 5.6 and Figure 5.7 summarises the variation in fibre volume fraction and laminate thickness between samples. Based on the material datasheet for the MTM44-1 prepreg system used in this study, the expected fibre fraction for this prepreg system is 68% by weight; which, using the resin density and fibre density data, corresponds to 58.7% fibre volume fraction. Typical autoclave cured unidirectional prepreps have fibre volume fractions of 60% [66]. While the expected fibre volume fraction for the prepreg used in this study appears to be low, data for OoA UD prepreps from other manufacturers report similar fibre volume fractions [66, 160].

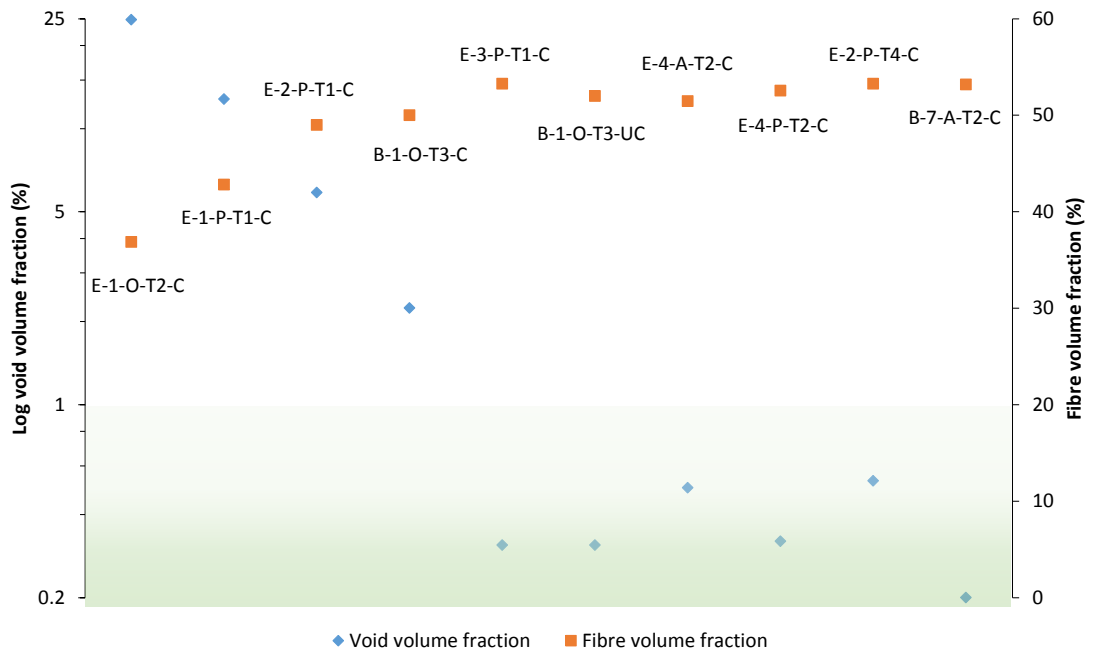


Figure 5.6: Effect of void volume fraction and cure cycle on fibre volume fraction. Shaded area represents increasing random error in measured void volume fraction due to fibre artefacts

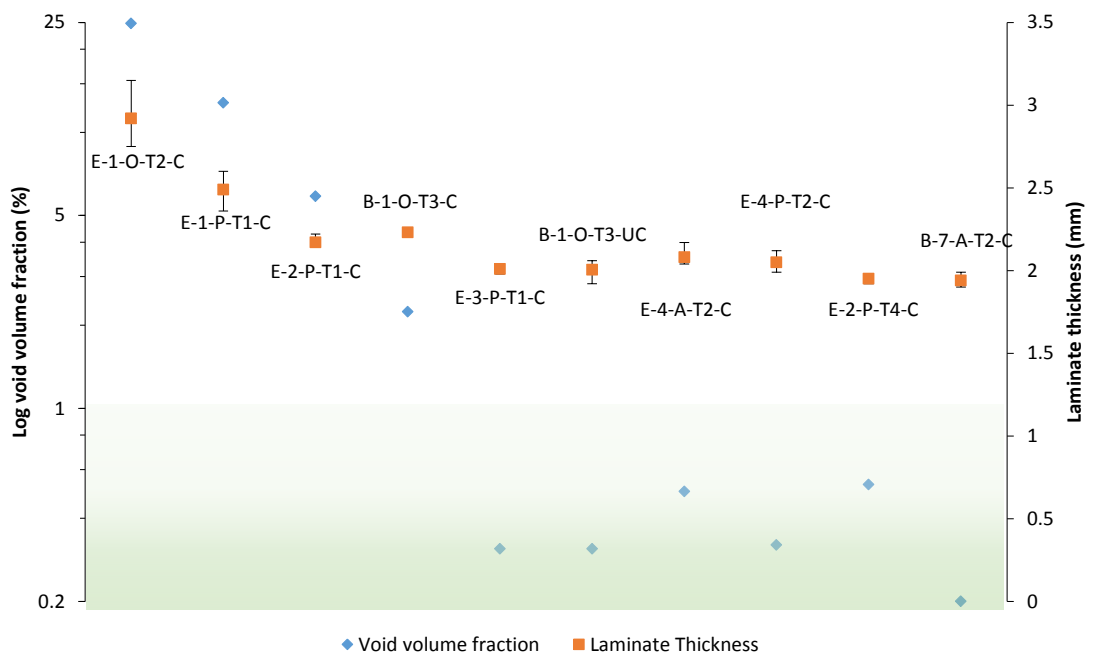


Figure 5.7: Effect of void volume fraction and cure cycle on laminate thickness. Shaded area represents increasing random error in measured void volume fraction due to fibre artefacts. Error bars represent the range of measured laminate thickness. B-1-O-T3-UC is the only unconditioned laminate in this study.

Even with 7 Bar consolidation pressure, the measured fibre volume fraction is less than the expected fibre volume fraction. Plasticisation of the resin due to conditioning and the low residual out-life of the material limited resin flow during cure; leading to insufficient wet-out and reduced fibre volume fraction. High heating rate did indeed facilitate an improvement in fibre wet-out, leading to a better laminate when compared to slow heating rate, low consolidation pressure cure cycles. However, due to the advanced cure of the resin the full potential of the material could not be realised.

In general, fully consolidated laminates exhibit low porosity (less than 1%) with a laminate thickness of 2 ± 0.05 mm and fibre volume fraction greater than 50%. Laminates processed with less than 3 Bar consolidation pressure exhibit poor consolidation, primarily due to extensive porosity. Whilst laminates processed with high consolidation pressure (greater than 3Bar) yield low porosity, Figure 5.6 and Figure 5.7 show that, good properties can be achieved using low consolidation pressure; when using an optimised high heating rate cure cycle (2 Bar spike cure) or prepreg with low moisture content (unconditioned laminate B-1-O-T3-UC).

5.3.3. Inter-laminar Shear Strength and Flexural Strength

Although it has been well established that voids are a volumetric property and that location of voids can have an impact on ILSS [16, 50, 161], various studies [16, 19, 20] have used a comparison between normalised ILSS and laminate void fraction – which does not take void location into account - to assess impact of voids on ILSS. Nevertheless, to be able to make a direct comparison with published data, ILSS is normalised in the present study. Figure 5.8 presents the normalised ILSS (wrt. the highest value) from the current study. Figure 5.9 compares the results from the current study against published data for laminates processed using slow heating rates. Figure 5.10 compares the results from the current study against published data for high heating rate processes.

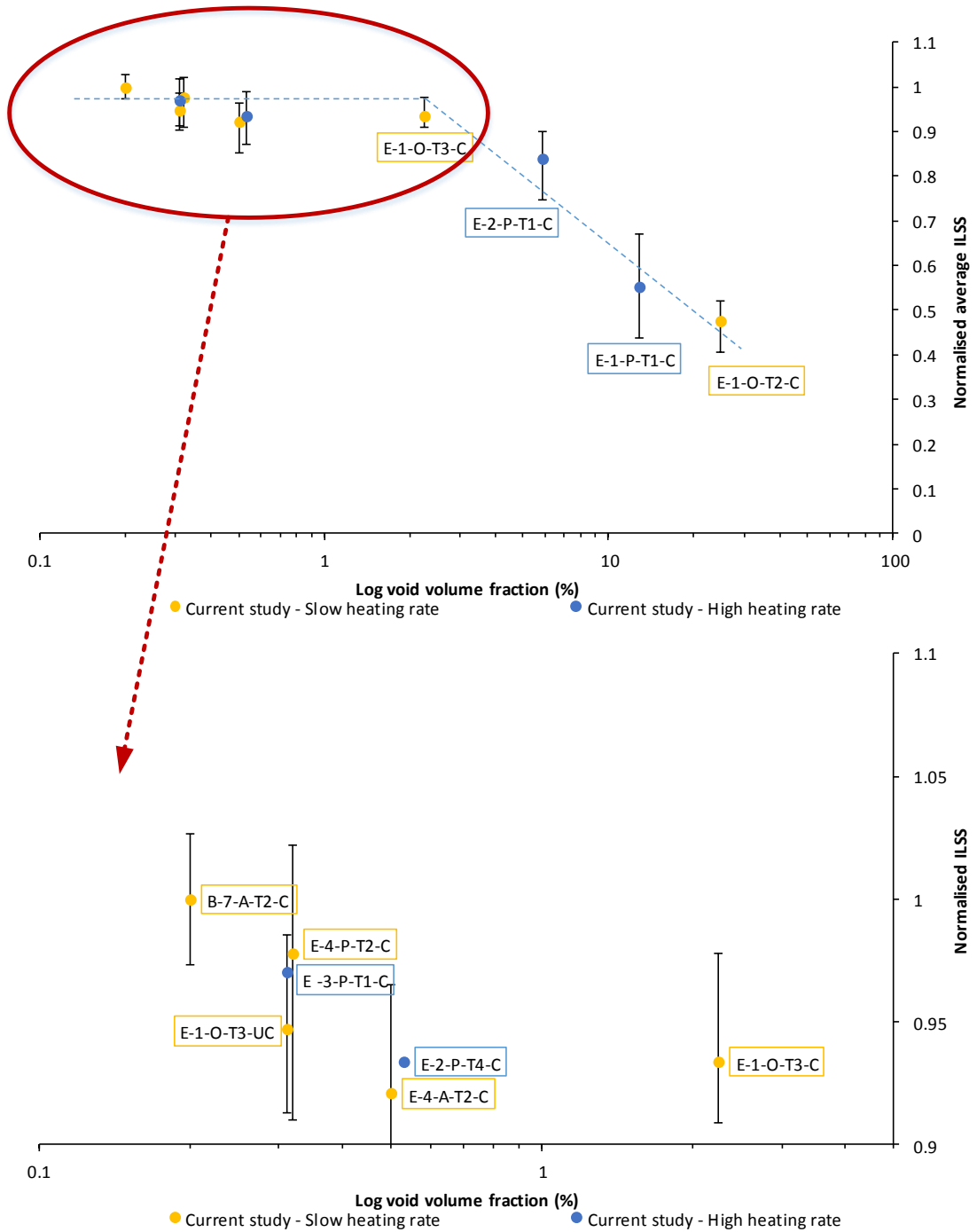


Figure 5.8: Effect of void volume fraction and cure cycle on Inter-laminar Shear Strength. The image on bottom presents an enhanced view of the data for laminates with void fraction of less than 1%. Error bars represents the range of measured values

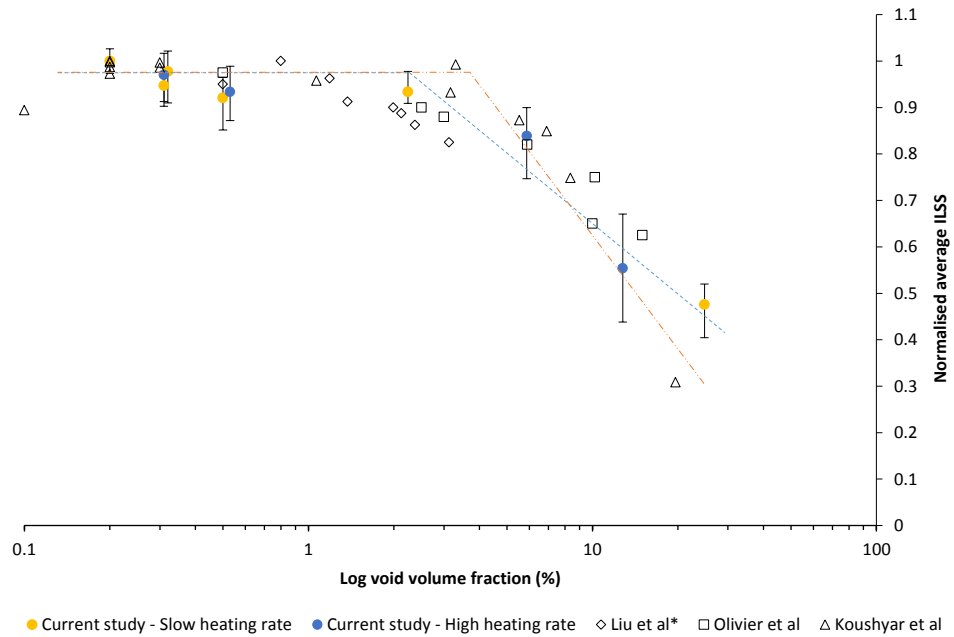


Figure 5.9: Comparison of normalised Inter-laminar Shear strength results from the present study against published data for slow heating rate processes. Note * indicates data inferred from graphs [16, 18-20].

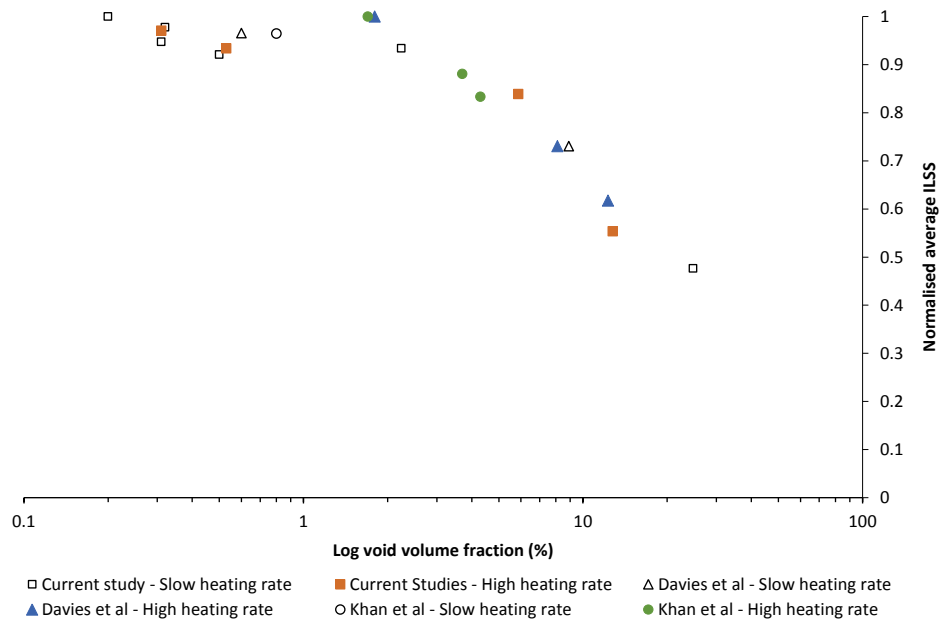


Figure 5.10: Comparison of normalised Inter-laminar Shear Strength results from the present study against published data for high heating rate processes [32-34].

An increase in laminate porosity leads to a decrease in ILSS. However, the rate of decrease is not uniform. Laminates with less than 2% void fraction retain greater than 90% of the maximum strength. Void fraction greater than 2% results in a linear

decrease in strength. Whilst the point of decrease in strength varies, other studies have reported a similar trend [16, 18-20, 22]. The variability in point of decrease in strength is dependent on additional factors such as: the composition of the resin system, void geometry [162], void distribution [50], cross-linking density [32, 50] and the fibre matrix-adhesion[32, 50].

Other studies have reported ILSS greater than that of autoclave cured laminates when using a 'spike' cure cycle [32, 34, 50]. The increase in strength has been attributed to the increase in cross-linking density and the lower minimum viscosity yielding better fibre-matrix adhesion. Although the void fraction of E-2-P-T4-C (15°C/min Spike cure) is less than published data, ILSS is 8% less than that of autoclave cured laminate. Furthermore, for a given void volume fraction, the decrease in ILSS in the present study is higher than that of the autoclave grade prepregs used in the Quickstep process. No discernible increase in mechanical properties has been observed in the present study when using a high heating rate cure cycle combined with high hydrostatic pressure. According to the datasheet [94], MTM44-1 has an ILSS of 94MPa. The average ILSS of E-7-A-T2-C is comparable to that of the published data, indicating that the excess moisture within the resin did not have an impact on ILSS. However, the advanced cure of the resin due to low residual shelf-life and the plasticisation of the resin due to the pre conditioning may have reduced the achievable gains in cross-link density of the resin, minimising the achievable gain in properties when using a high heating rate.

Figure 5.11 presents a plot of the normalised average flexural strength measured in this study. Figure 5.12 presents a comparison between the normalised flexural strength measured in this study against data published in the literature for similar high heating rate processes.

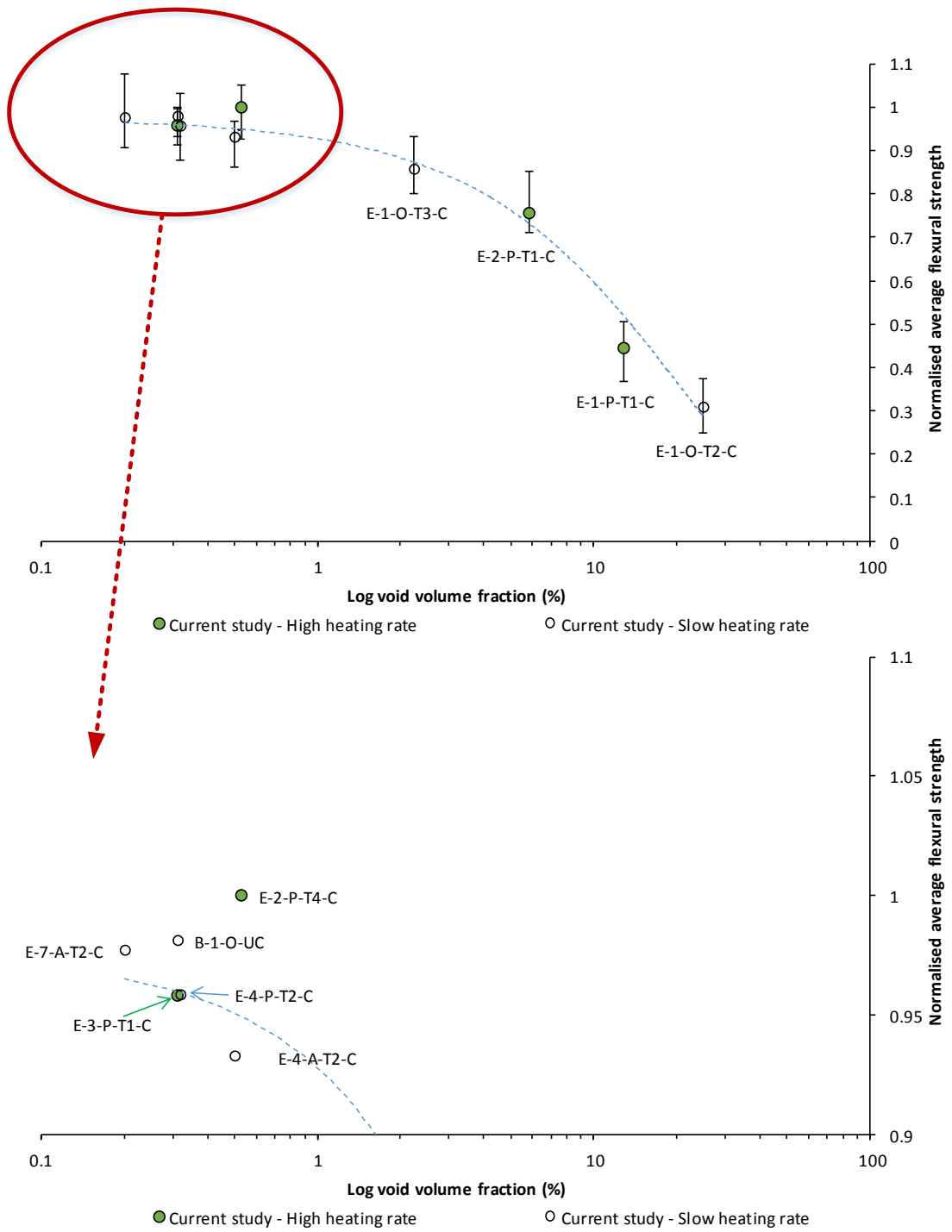


Figure 5.11: Effect of void volume fraction and cure cycle on flexural strength. The image on bottom presents an enhanced view of the data for laminates with void fraction of less than 1%. Error bars present the range of measured values.

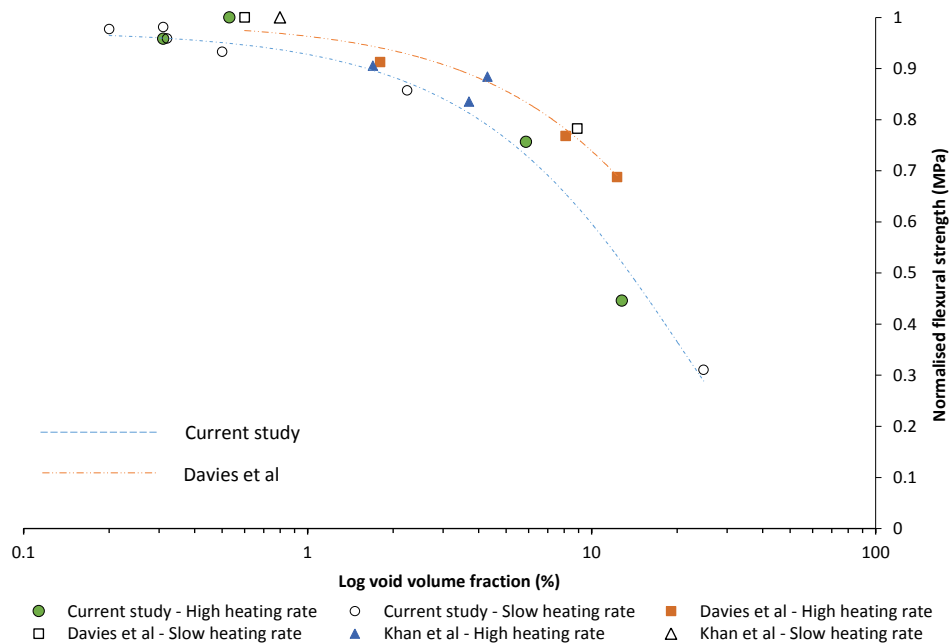


Figure 5.12: Comparison of flexural strength in the current study against data in the literature for high heating rate processes

Similar to ILSS, flexural strength is a matrix dependent property that is sensitive to void volume fraction. However, unlike with ILSS, there is no definite point of decrease in strength. Laminates with up to 1% void fraction retain 90% of the maximum flexural strength. A similar trend can be observed in data published in the literature. Similar to the ILSS data, using high heating rate did not yield additional gains in mechanical properties. However, for laminates the less than 1% void fraction, the decrease in strength is less than 5% of the maximum. For laminates with high void volume fraction the decrease in flexural strength is greater than that of published data. However, this is again due to additional factors such as void geometry, resin composition and cross-linking density.

5.4. Conclusions

The findings show that up to 39% reduction in cure cycle time over autoclave cure, whilst retaining 95% of the mechanical properties. It should be noted that the high heating rate cycles in this study used the same dwell time as per the datasheet. Optimising the duration of the dwell could lead to further reduction in cycle time.

However, the present study could not replicate the published greater than autoclave mechanical properties obtained using a spike cure. The reason behind the lack of increase in strength is inconclusive. It has been speculated that factors such as void

geometry, void location, cross-linking density of the matrix and fibre-matrix adhesion could be responsible for the lack of increase in strength. Furthermore, the findings suggest that resin flow characteristics could be a limiting factor to the maximising the gains in achievable physical and mechanical properties.

High mechanical properties can be achieved with a high heating rate, but require up to 3 Bar hydrostatic pressure. Based on the findings in the review in Chapter 1, this leaves two potential solutions to reduce processing cost: The proposed Pressure Tool system or an Autoclave with a heated tooling. In the latter system the purpose of the autoclave is to provide the hydrostatic consolidation pressure, while the tooling with on-board heating system heats the laminate. This can potentially lead to considerable savings in running cost, though further studies are needed to understand the bounds of applicability of such a system.

From Chapter 4 it has been found that void growth reduction in high heating rate processes is achieved by reducing the time for void growth to take place. Chapter 5 shows that mechanical properties similar to that of autoclaved laminates can be achieved using shorter cure cycle times. The following chapter defines the bounds of applicability of high heating rate processes.

6. Effect of tooling material and process ancillaries on reductions in cure cycle time

6.1. Introduction

As shown in Chapter 4 and Chapter 5, processing laminates with high heating rate combined with up to 3 Bar consolidation pressure can yield laminates with properties comparable to that of autoclaved laminates. However, work up to this point assumed that the high heating rate can employed be irrespective of secondary processing parameters; namely, laminate thickness, tooling material and process ancillaries. Owing to the inherently poor thermal conductivity of the resin (~ 0.2 W/mK), the maximum heating rate and dwell temperature are limited to prevent an uncontrolled exothermic reaction. This is especially true when processing thick laminates (Figure 6.1 (a) and Figure 6.1 (b)). However, low initial dwell temperature and reduced heating rate increase cycle time.

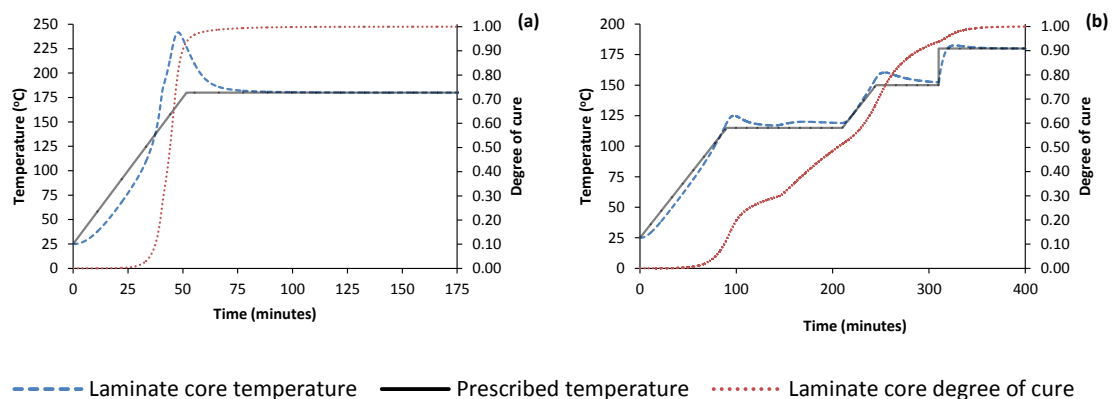


Figure 6.1: (a) Thermal overshoot at the core of a 20mm thick laminate processed with 3°C/min heating rate to 180°C. (b) Thermal over-shoot when processing the same laminate with 1°C/min and intermediate dwell at 120°C. Graphs generated using a process model for the Hercules 3501-6 resin system developed by [130].

Defining the maximum heating rate and dwell temperature by experimental investigation is arduous and expensive. Process modelling can offer a more cost effective alternative, without potentially sacrificing accuracy. In addition, a numerical approach facilitates the comparison of the cure characteristics of various commercial resin systems; which can then be used to define the key characteristics of a hypothetical resin system fully optimised for high heating rate processes. Building on the findings of the previous chapter, this study aims to define the limiting factors to cure cycle time reduction; in particular: the limiting laminate thickness, optimum

resin characteristics, optimum tooling material and effect of process ancillaries. The study is divided into two parts. The first part identifies and presents the kinematic and rheological characteristics of a highly optimised, high heating rate resin system. The second part characterises the impact of tooling materials and process ancillaries on the maximum laminate thickness that can be processed.

6.2. Methodology

This section outlines the methodology used in this study. Chapter 3.4.6 presents the methodology used to analyse and compare the different resin systems in terms of resin kinematics. The setup of the meshed domain and boundary conditions for Chapter 6.3.2 and Chapter 6.3.3 is presented in Chapter 3.4.7. The design of experiment used to characterise the effect of tooling material and process ancillaries is summarised in Chapter 3.4.6.

6.3. Results and discussion

6.3.1. Optimum resin system analysis

The following section presents a comparison between different resin systems in terms of resin kinematics and rheology. The MTM44-1 resin system was primarily chosen for this study due to its availability and current use in industry. However, this may not necessarily be the most optimum resin system for high heating rate processes. Analytical models for various types of resins – autoclave system, RTM and OoA – have been obtained and solved using Microsoft Excel 2013. The output of each model was verified using inferred results from published data to check the model setup; example shown in Figure 6.2.

Based on the findings on the void growth mitigation studies in Chapter 4 and Chapter 5, an optimum resin system for high heating rate processes would have the following kinematic characteristics:

- Low initial dwell temperature (less than 130°C) to minimise void growth
- Attain high degree of cure at low processing temperatures – High reactivity at low temperature

- Low total heat of reaction (H_{Total}) to minimise the heat released during an exothermic reaction

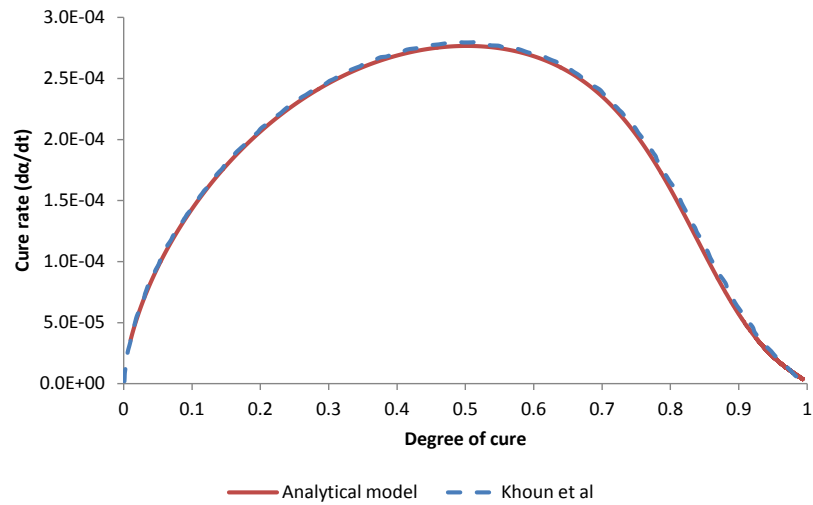


Figure 6.2: Comparison between analytical model output and inferred data. Good agreement between the model output and published data confirming setup fidelity.

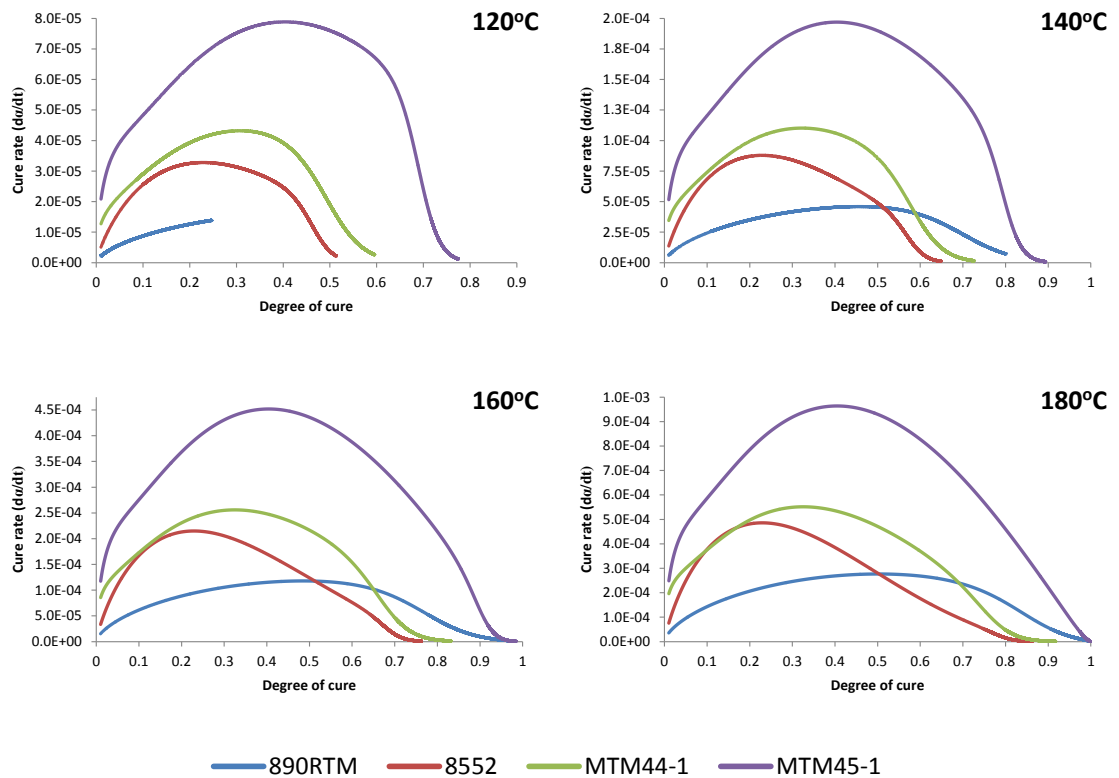


Figure 6.3: Comparison between different resin systems in terms of cure rate and degree of cure.

Figure 6.3 presents a comparison between the various resin systems cured at isothermal temperatures. Whilst definitive conclusions cannot be drawn due to the small range of resin systems tested, the findings indicate that OoA prepreg appear to be more reactive than autoclave prepreg system and RTM resin system. As shown in Figure 6.3, MTM45-1 is the most reactive resin system in the group followed by the conditioned MTM44-1. OoA prepreg resin systems are optimised for low cure temperature. To ensure sufficient cross-linking of the polymer chain takes place in a reasonable dwell time, the OoA resin systems are designed to be more reactive. However, the high reactivity inevitably increases the propensity for thermal overshoot, especially when processing thick laminates (Figure 6.4, Figure 6.5).

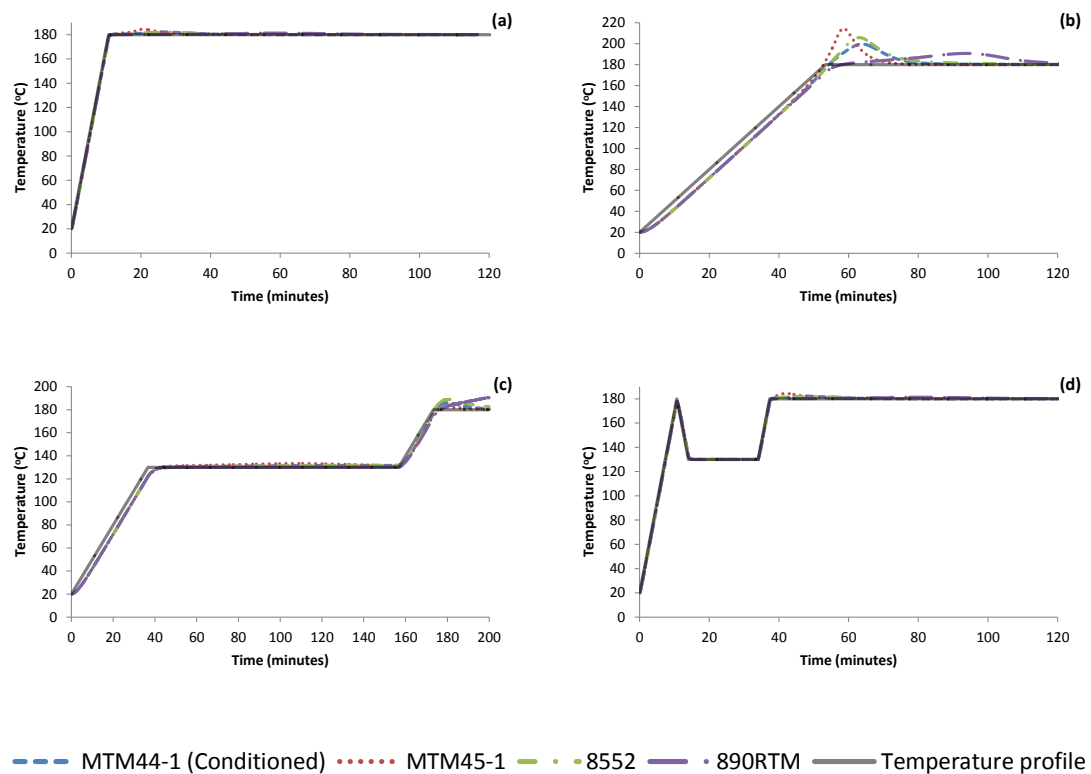


Figure 6.4: Effect of resin system on laminate core temperature.

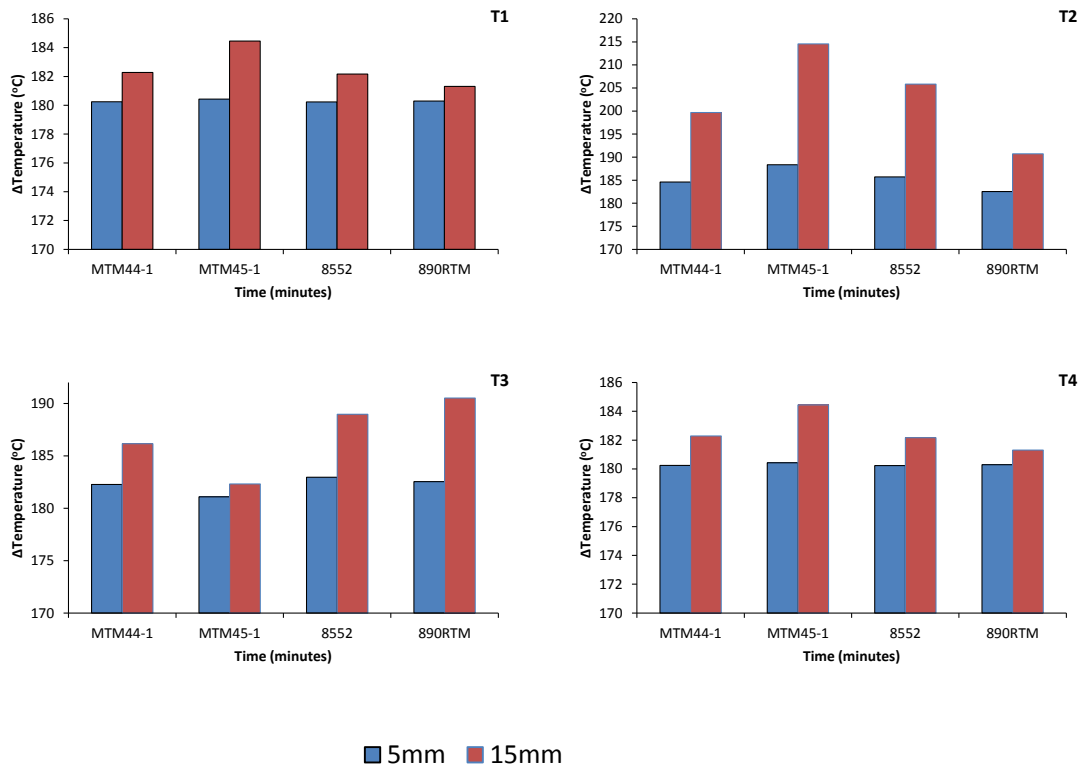


Figure 6.5: Comparison of between resin systems in terms of magnitude of thermal overshoot at the laminate core

CYCOM 890RTM is the least reactive resin system (in the present study) at low temperature. This is to be expected owing to the nature of the process in which the resin is used. The resin system is designed to have a long pot-life at high temperature (80°C) to maximise the injection window. During processing, the pre-heated resin is injected into an isothermal mould (at 180°C), during which peak reactivity occurs. The low reactivity combined with the “plateau” in reactivity across the range of degree of cure yields a more gradual thermal overshoot when compared to other resin systems Figure 6.4 (b). However, the exceptionally low reactivity (wrt. to other resins in the present study) at low temperatures is not ideal for dynamic cure cycles employed in prepreg processing. As shown in Figure 6.6, the degree of cure of the 890RTM resin systems lags behind other prepreg resin system when processed using a dynamic temperature profile. Also, the high cure temperature required to initiate the cross-linking of the polymer chain increases the propensity for void growth when using low consolidation pressures.

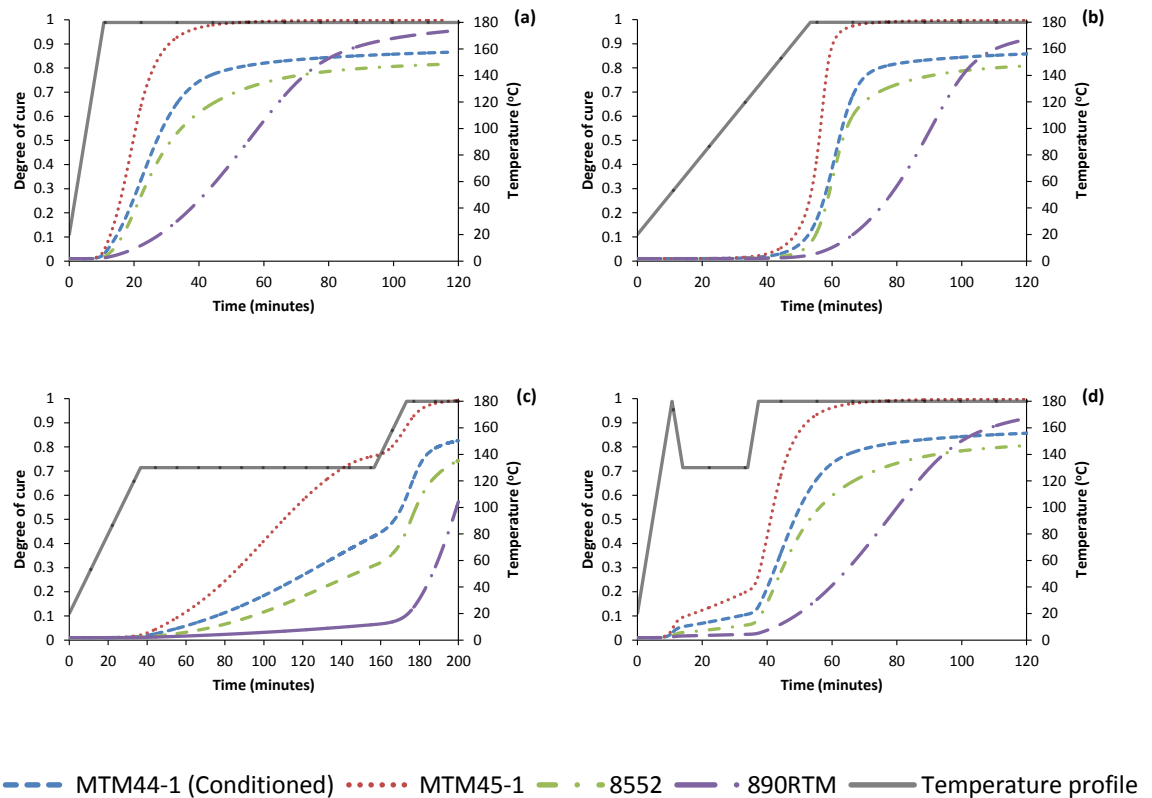


Figure 6.6: Comparison of resin systems in terms on degree of cure.

A comparison between Figure 6.3 and Figure 6.5 shows that the magnitude of thermal overshoot is in-line with the reactivity of the resin system. As shown, MTM45-1 laminates result in the highest level of thermal overshoot; except when processed using the manufacturer recommended OoA cure cycle (T3). Owing to the high reactivity at low temperature, the material achieved a high degree of cure by the end of the first dwell (Figure 6.6), minimising the level of thermal overshoot in the subsequent ramp. A similar trend can be observed in the Spike cure (T4) where the advancement of cure at the low dwell is much higher than the other resins. This indicates that window for void growth in the subsequent ramp would be the lowest for MTM45-1. However, owing to high reactivity, “blunting” of the spike cure (as seen in Chapter 4) increases the risk for premature resin gelation; leading to extensive porosity.

A comparison on the effect of heating method on laminate core temperature shows that laminates processed using convective heating has a higher core temperature than laminates processed using conductive heating. In convective heating the rate of

transfer of energy across the laminate boundary is limited by the convective heat transfer film coefficient. This limitation is not present in conductive heating. As shown in the results, in the idealised scenario (no tooling and no process ancillaries), up to 15mm thick laminates can be processed using conductive heating and high heating rate, without the risk of a substantial thermal overshoot at the laminate core. Isothermal compression moulding of prepreg closely replicates the idealised scenario; except that the laminate core experiences a much higher heating rate. Due to the higher heating rate the laminate experiences, the maximum laminate thickness that can be processed using compression moulding is further limited, especially when processed using the resin systems used in the present study. OoA processes with dynamic cure cycles use process ancillaries and various tooling solutions. Therefore, the effect of tooling materials and process ancillaries must be taken into account; which is shown later in the chapter.

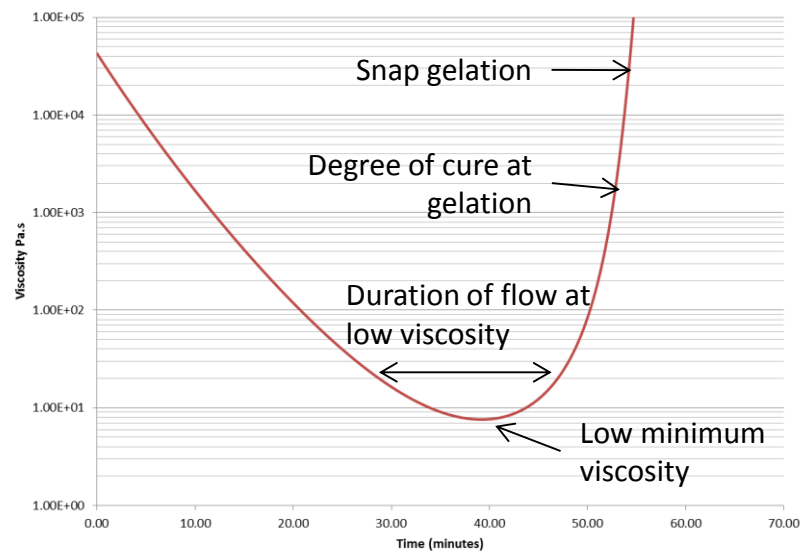


Figure 6.7: Key factors of interest in the present study on optimum rheological characteristics for high heating rate processing

Building on from the study on optimum resin kinematics, the following section explores the optimum rheological characteristics for a hypothetical high heating rate OoA resin system. Figure 6.7 summarises the key factors of interest in this study. Studies on modelling resin rheology (in particular studies employing the gel model [51, 163, 164]) correlate the point of gelation to degree of cure. Using this method, the degree of cure at gelation can be used to compare the different resin systems.

The point of gelation of the MTM45-1 resin system is reported to coincide with peak cure rate (0.4 degree of cure) [51]. However, as summarised in Table 6.1, peak cure rate does not coincide with the point of resin gelation for all resin systems.

	Conditioned MTM44-1	MTM45-1	8552	890RTM
DoC at gelation	0.18	0.4/0.6*	0.47/0.545*	0.7
DoC at peak cure rate	~0.33	~0.41	~0.229	~0.456

Table 6.1: Comparison of degree of cure (DoC) at gelation and DoC at peak cure rate for different resin systems. DoC at peak cure rate varies by 0.05 depending on temperature. * indicates data from [163, 164]

Furthermore, the reported point of resin gelation for a given resin system can vary by up to 0.2 degree of cure. For instance, Shahkarami et al[163] have reported that the point of gelation for the MTM45-1 resin system occurs at 0.6 degree of cure. As suggested by Dykeman, characterisation of resin systems between studies can have up to 50% variability due to uncertainty in external conditions; such as instrument quality, material consistency, measurement quality and modelling practices [117].

The low degree of cure at gelation (when compared to the other resin systems in Table 6.1) for the conditioned MTM44-1 resin could potentially be due to resin plasticisation and limited residual shelf-life. Both of which have been shown to reduce the time to gelation [67, 68]. This minimises the window for resin flow to take place, potentially increasing the propensity for flow induced voids. In contrast, the high degree of cure at gelation for the 890RTM maximises the window for resin flow; however, as shown later in this section, this can lead to processing limitations.

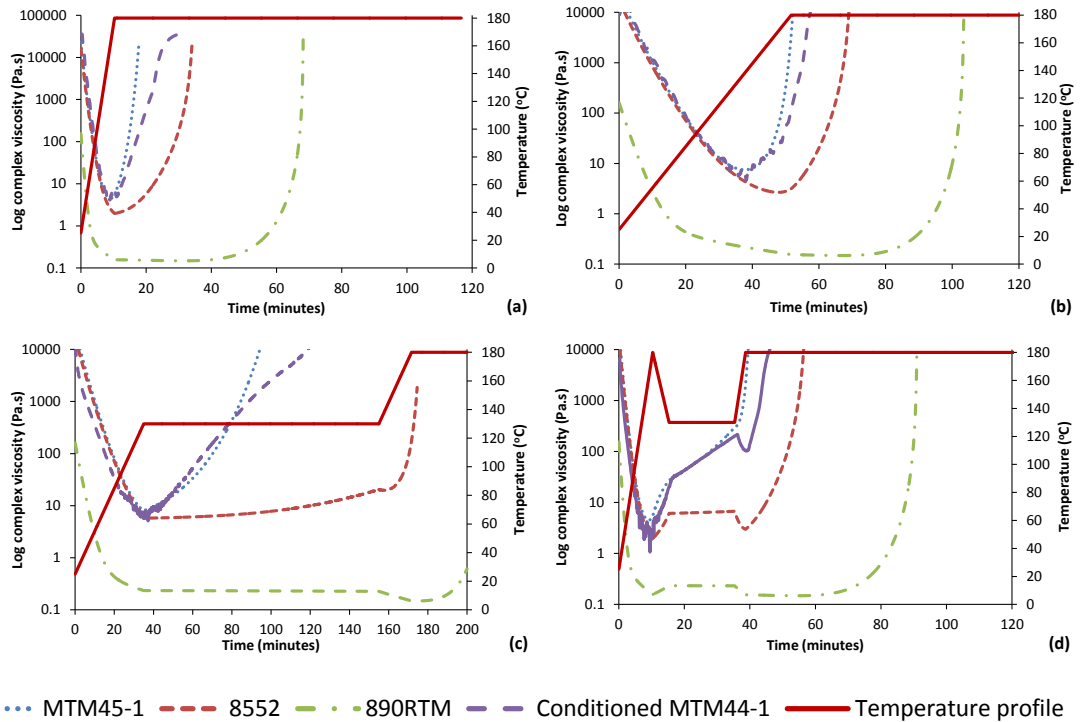


Figure 6.8: Comparison between resin systems in terms of viscosity profile. Ramp rate in (a) and (d) is 15°C/min. Ramp rate in (b) and (c) is 3°C/min. In (c) cycle time was not sufficient for gelation of the 890RTM resin.

Figure 6.8 compares the complex resin viscosity profile of the resin systems used in this study. The viscosity profile for the conditioned MTM44-1 is from experimental data. The data for the other resin systems have been generated using rheological models available in the literature. Despite the plasticisation of the MTM44-1 resin, the rheological profiles of both OoA resin systems are similar. As plasticisation has been shown to reduce the window for resin flow and time to gelation (example illustrated in Figure 6.9), unconditioned MTM44-1 could achieve even lower viscosity and longer flow duration. Due to the high reactivity at low temperature for both OoA resins, resin viscosity continues to increase during the low temperature dwell of the spike cure. This trait can potentially reduce laminate porosity as the window for void growth is reduced during the subsequent temperature ramp. However, as shown in Chapter 4, this also reduces margin of error. A thermal overshoot during the spike phase can cause premature gelation of the resin, “locking-in” voids formed during the spike phase.

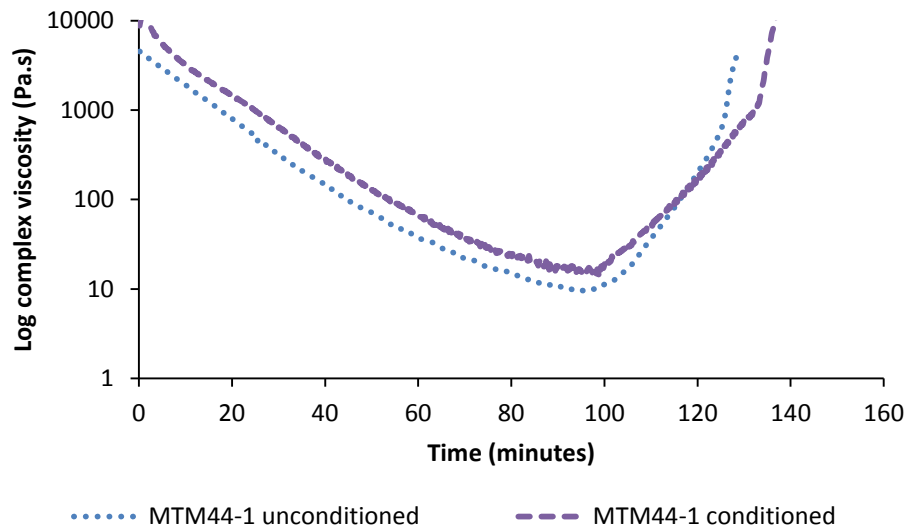


Figure 6.9: Example highlighting effect of increased moisture content on resin minimum viscosity and duration of flow. Ramp rate of 1°C/min. Data for unconditioned resin provided by the resin manufacturer (Cytac)

The autoclave resin system (8552) has a lower minimum viscosity and longer flow duration than the OoA resin systems. Processing 8552 using the OoA cure cycle (T3) offers a long window for resin flow, whereas the OoA resin systems undergo gelation during the low dwell temperature. However, extensively long window for resin flow at low temperature is not ideal for VBO processing. As the resin has not undergone gelation at the end of the initial dwell, void growth can take place during the subsequent ramp with VBO consolidation pressure.

The 890RTM resin offers the lowest resin minimum viscosity and the longest duration for flow. The low reactivity combined with the resin chemistry makes this characteristic ideal for RTM, but not for processing prepregs with low consolidation pressure. The high required cure temperature combined with the long window for resin flow increases the size of the window for void growth.

In terms of rheological characteristics, the optimum high heating rate resin system would have traits similar to the 8552 resin system; but with a shorter time to gelation at low temperature (akin to the OoA resin systems) and higher initial viscosity to aid in de-bulk. However, the feasibility (cost and compatibility of reactive species) of creating such a resin system is currently not known. For instance, low resin reactivity indicates long resin flow time, but requires a high cure temperature

to initiate the cross-linking of the polymer chain. Furthermore, achieving the listed characteristics potentially necessitates compromises in part design flexibility. For instance, sufficient wet-out can be achieved even with high initial viscosity by using a high heating rate cure cycle. However, as highlighted in Chapter 2.1.1.5, this can lead to the formation of secondary defects parts with sharp changes in geometry. Namely, due to the high degree of compaction that takes place during cure. The critical resin temperature beyond which void growth takes place has been shown to be approximately 125°C for epoxy based resin systems (Chapter 2.3). To achieve gelation at a low temperature whilst achieving low cycle times requires high resin reactivity. However, this limits the laminate thickness that can be safely processed.

6.3.2. Effect of processing films and heating method

As shown in Chapter 6.3.1 conductive heating of the idealised scenario (excluding tooling materials and process ancillaries from the meshed domain) results in the lowest amount of thermal overshoot. But, convective heating has been shown to increase the amount of thermal overshoot at the laminate core by up to 35°C. Also, excluding process ancillaries and tooling material is not applicable for processes with dynamic cure cycles.

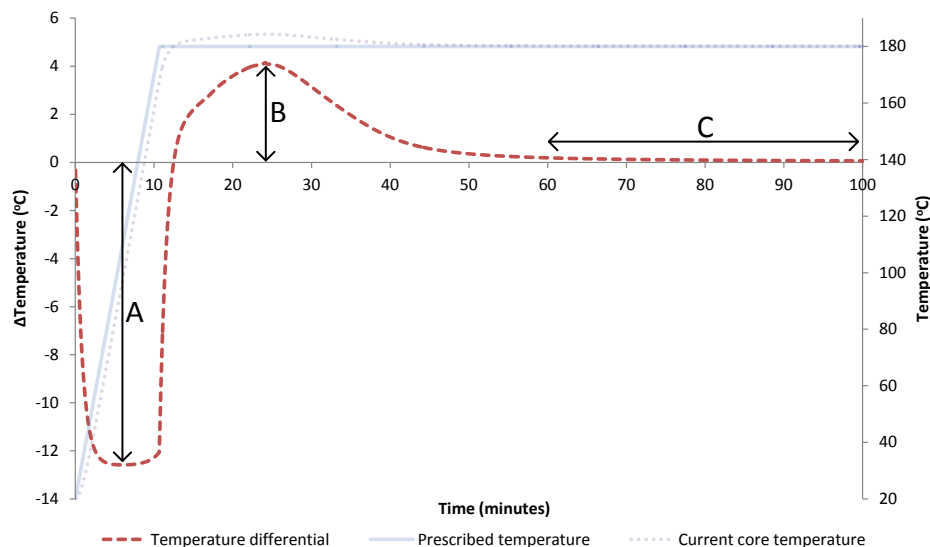


Figure 6.10: Illustration summarising the analysis of the results.

This section summarises the results of the boundary condition optimisation study using the cure kinetics model for the conditioned MTM44-1 resin system. Figure 6.11

presents the effect of boundary conditions on the laminate core temperature for three scenarios: Tooling material and laminate, but with no vacuum bag or release film (Scenario 3), single-sided vacuum bagging (Scenario 1) and envelope bagging (Scenario 2). The results are presented as a temperature differential in relation to Scenario 3. For instance, negative Δ Temperature indicates that the laminate core temperature is less than that of Scenario 3 at the given point in time. High negative Δ Temperature indicates high thermal lag. Conversely, a positive Δ Temperature indicates that the laminate core temperature is higher than that experienced in Scenario 3. High positive Δ Temperature indicates low efficacy of removal of energy released by the laminate during cure. Figure 6.10 summarises the interpretation of the analysis. Magnitude of (A) indicates the level of thermal lag during a temperature ramp. Magnitude of (B) indicates the level of thermal overshoot due to exotherm. High level of (B) indicates low efficacy at removing thermal energy from the laminate core. (C) indicates the steady-state laminate core temperature. Δ Temperature in Chapter 6.3.3 is in relation to (Scenario 3); 5mm laminate with 0.6mm thick single sided breather on Aluminium tooling excluding the effect of vacuum bag and release film.

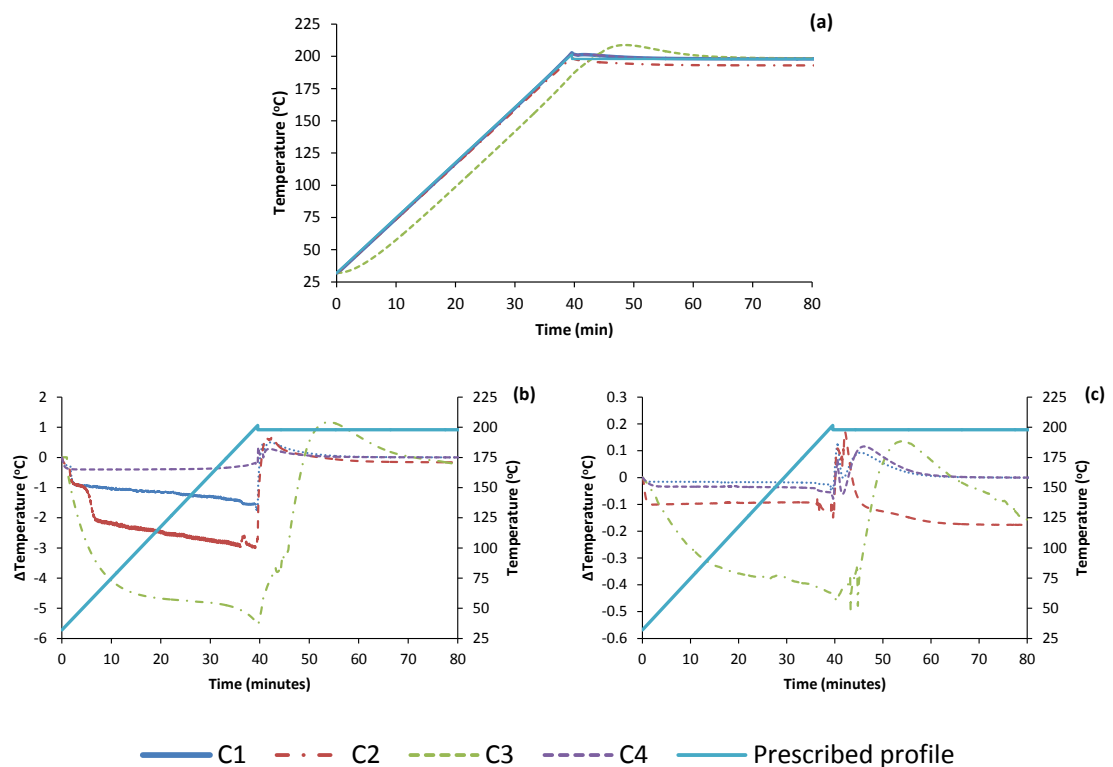


Figure 6.11: Effect of bagging arrangement on the magnitude of thermal overshoot and thermal lag.

To recap the boundary conditions presented in Chapter 3.4.7, C1 represents conductive heating from all sides of the meshed domain, simulating closed mould conductive heating. C2 represents conductive heating from the bottom boundary with $20 \text{ W/m}^2\text{K}$ heat loss to ambient via free convection, simulating free-standing tooling with on-board heating. C3 represents forced convective heating from all sides with a convective film coefficient of $70 \text{ W/m}^2\text{K}$, simulating autoclave cure. C4 represents conductive heating from the bottom boundary with zero heat flux along with top and sides, simulating free-standing heating with a highly insulating material on the laminate. Using no bagging assemblies (vacuum bag and release film) yields the lowest lag in temperature (Scenario 3). Due to conduction heating from all sides (Boundary A and Boundary B) in C1, the laminate core temperature closely matches the applied temperature.

Figure 6.11 summarises the effect of bagging arrangement on core thermal overshoot and thermal lag. (a) Scenario with 5mm thick laminate with single sided breather on aluminium tooling, but without vacuum bag or release film (Scenario 3). (b) Tooling material, laminate thickness and breather configuration kept similar to Scenario 3 but includes single sided release film and envelope vacuum bagging. (c) Tooling material, laminate thickness and breather configuration kept similar to Scenario 3 but includes single sided release film and single sided vacuum bagging (Scenario 1). Δ Temperature in relation to Scenario 3. As evident from Figure 6.11 (b) envelope bagging resulted in an increase in the magnitude of thermal overshoot at the laminate core. However, the increase in core temperature is only up to 1.3°C over Scenario 3 (no bagging assemblies). Whilst envelope bagging does not have a significant impact on laminate core temperature, it did induce up to 5.5°C lag in laminate core temperature. Also, the lag is most prominent in laminates processed using convective heating (C3) than when conduction heating is applied to the tooling surface (Boundary A). Although the film thickness is only $60\mu\text{m}$, the rate of transfer of energy across the film is greatly diminished due to the low thermal conductivity of the material (relative to that of the aluminium tooling). This leads to high thermal lag in all conditions, except C4. By insulating the top and sides of the assembly (zero heat flux) the rate of loss of energy is minimised, hence the low thermal lag.

Furthermore, Figure 6.11 it can be seen that both the magnitude of thermal overshoot and the lag in temperature due to single-sided bagging is less than that of the envelop bagging. This indicates that irrespective of heating method, heat transfer through the tooling material is more dominant than through the breather material and bagging assembly. This is potentially due to the low thermal conductivity of the breather material; the effect of which is analysed in the following section.

To summarise, bagging configuration affects the responsiveness of the laminate to changes in temperature. The low thermal conductivity of the bagging material can induce up to 5.5°C thermal lag in the laminate core when envelope bagging, leading to poor temperature control. The thermal lag can be compensated by reducing the heating rate, which consequently increases cycle time and potentially increases the window for void growth. Envelope bagging is commonly used when processing small components (< 1m²) on easy to manoeuvre tooling. Large structural components are typically processed on tooling with egg-crate stiffened backing structures, where envelope bagging is not possible. Nevertheless, the findings of this study indicate that restricting heat transfer through the bottom of the tooling material can result in poor temperature control, increasing cycle time; such as, restricted air-flow below the tool face due to design of the egg-crate structure.

6.3.3. Effect of tooling material and process ancillaries

As shown in Chapter 6.3.3, limiting the heat transfer rate through the tooling increases thermal lag in the laminate core. This indicates that the thermal properties (thermal conductivity and thermal mass) of the tooling material can have a profound effect on the laminate core temperature. Furthermore, the study focused only on the effect of two process ancillaries: release film and vacuum bag. The present chapter expands on the findings of Chapter 6.3.3 by identifying the effect of other process ancillaries on laminate core temperature; namely: breather, foam core and pressure intensifiers. In addition, the present study explores the effect of tooling material choice on the limiting laminate thickness that can be processed whilst achieving low cycle times.

Similar to Chapter 6.3.2, a comparison between materials is performed as a temperature differential. In this chapter the temperature differential is performed in relation to the idealised scenario; that is, a scenario where only the laminate is present in the meshed domain. Figure 6.12, recaps the data interpretation method using the spike cure as an example. Magnitude of (A) indicates the level of thermal lag in the laminate core. Magnitude of (A*) indicates the level of thermal lag during the cooling down phase (present only in the spike cure). Magnitude of (B) indicates the level of thermal overshoot due to exotherm. (C) indicates the steady state temperature of the laminate core. (C) during the first dwell is higher due to the exothermic cure reaction taking place.

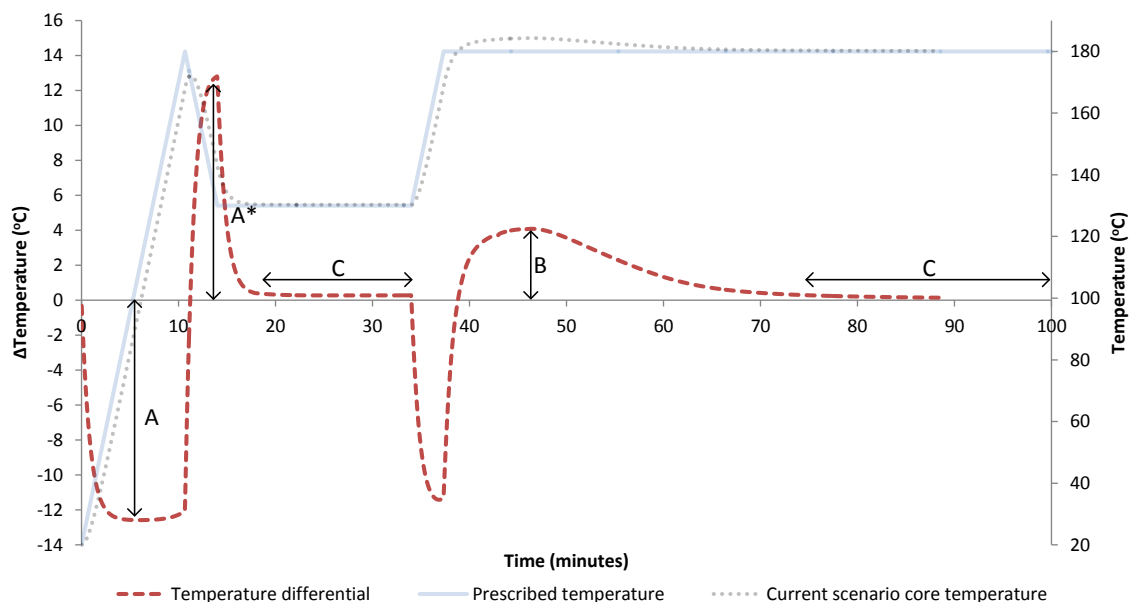


Figure 6.12: Temperature differential in the core of a laminate processed on a ceramic tooling with a 0.6mm thick single-sided breather.

Four temperature cycles have been applied to the boundaries; two conduction based high heating rate cycle and two convective heating cycles (Figure 6.13). For convective heating cycles a convective film coefficient of $70\text{W}/\text{m}^2\text{K}$ has been used. T1 is based on the recommended autoclave cure cycle but with $15^\circ\text{C}/\text{min}$ heating rate. T2 is the recommended autoclave cure cycle for the material (MTM44-1 resin) with a $3^\circ\text{C}/\text{min}$ heating rate. T3 is the recommended OoA cure cycle for the material. T4 is a spike cure with $15^\circ\text{C}/\text{min}$ ramp rates. Both the vacuum bagging material and the release film have been excluded from the meshed domain. As peak cure rate

occurs early in the dwell phase, the cure cycles have been truncated during the dwell phase to reduce analysis time.

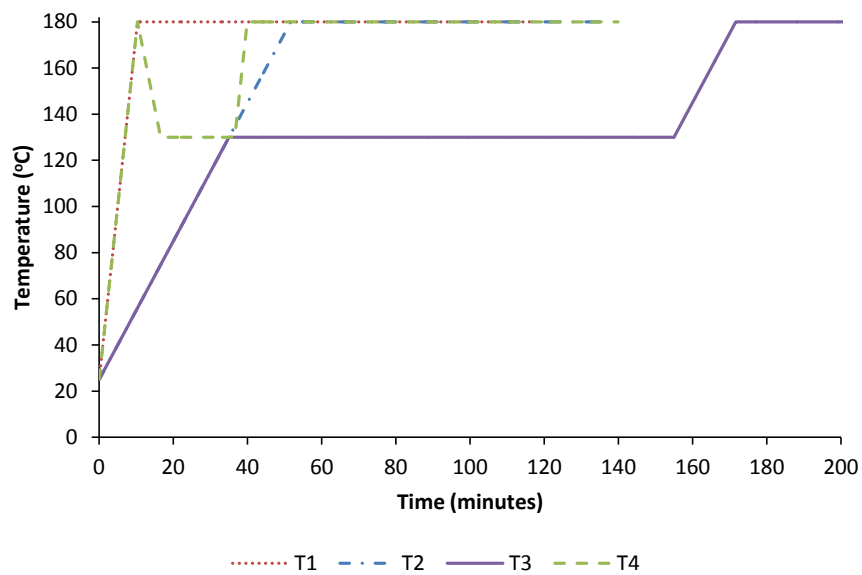


Figure 6.13: Temperature profile used in this study. T1 and T4 are applied as a thermal boundary condition (conduction). T2 and T3 and applied as a convective boundary conditioned with a convective film coefficient of $70W/m^2K$.

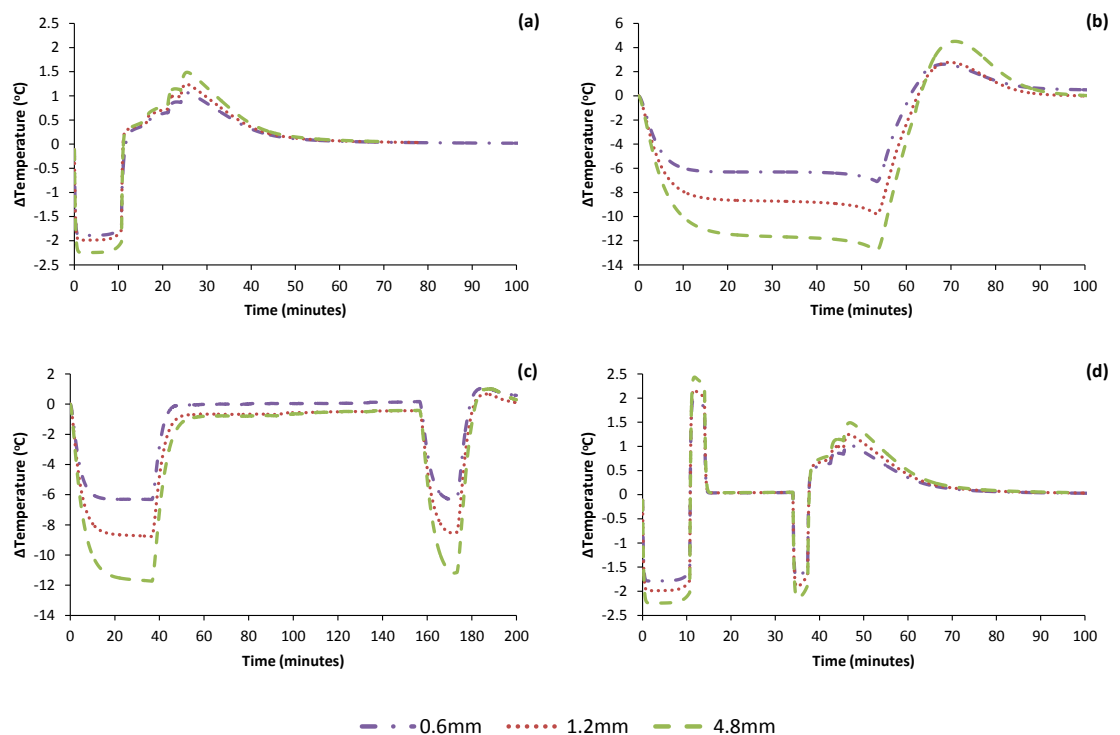


Figure 6.14: Effect of breather thickness on laminate core temperature. (a) – (d) corresponds to Cycle T1 – T4.

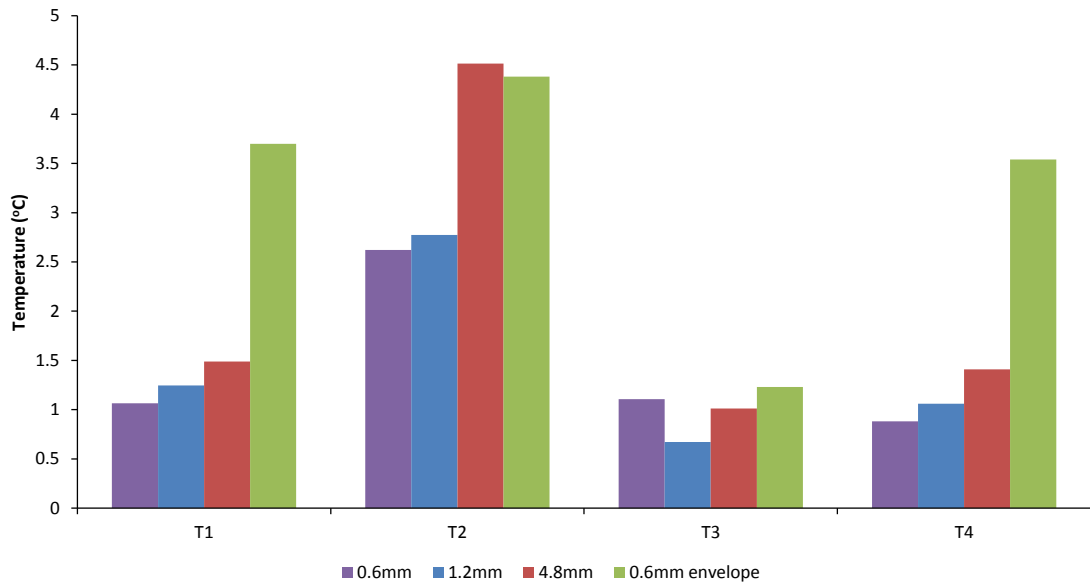


Figure 6.15: Comparison between cure cycles and breather thickness on the magnitude of thermal overshoot. Note the effect of wrapping the breather around the tooling and laminate on laminate core temperature.

Figure 6.14(a – d) presents the effect of breather thickness on the temperature lag at the laminate core. The temperature differential is presented wrt. the idealised scenario (no tooling and no process ancillaries). The observed staggered increase in temperature during exotherm is due to step changes in resin thermal conductivity (Detailed in Appendix F) incorporated as a sub-routine. Figure 6.15 presents the magnitude of thermal overshoot at the laminate core. As shown in Figure 6.14, a single layer of breather (0.6mm) results in reduced thermal lag and thermal overshoot than when using two layers (1.2mm) or eight layers (4.8mm). It must be noted that adding multiple layers of breather material during vacuum bagging is not a commonly used practise during prepreg lay-up. However, the breather material has been known to be used to ‘even out’ regions with sharp changes in geometry to minimise the risk of vacuum bag failure during cure. As evident from the findings of this study, this can lead to poor temperature control and increase the magnitude of a thermal overshoot. The increase in temperature can potentially be sufficient to initiate the diffusion of moisture in the resin, leading to void growth. Furthermore, the gain in temperature can lead to localised, premature gelation of the resin. This can lead to the build-up of residual stresses within the laminate, leading to dimensional errors and ultimately scrappage of the part.

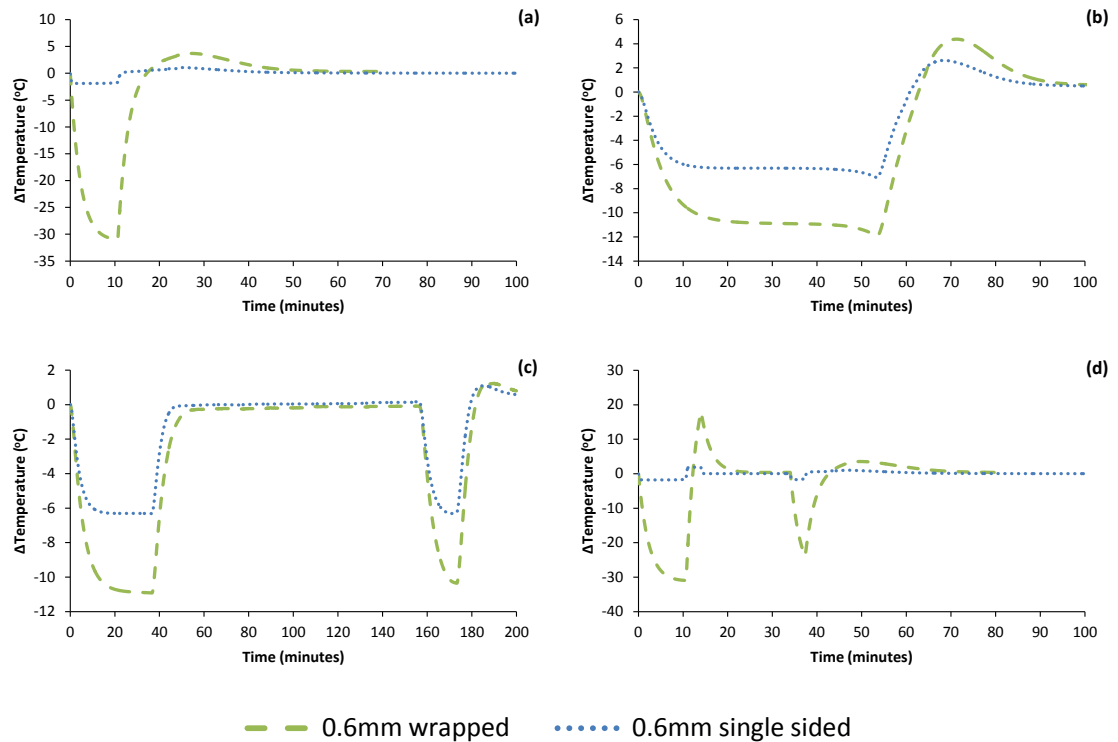


Figure 6.16: Effect of breather configuration on laminate core temperature and thermal lag. Despite using an aluminium tooling, the low thermal properties of the breather material limited the rate of heat transfer.

It is common practice to warp breather material around the tooling when envelope bagging. This is to minimise the risk of the sharp corners in the tooling puncturing. However, as shown in Figure 6.16, due to the low thermal conductivity of the material, the breather acts as an insulating material. This leads to poor temperature control and reduces the rate of transfer of thermal energy across the tooling material, even if a material with high thermal conductivity (Aluminium) is used. This method of vacuum bagging necessitates the need for reduced heating rate to minimise temperature lag, leading to increased cycle time.

Similar boundary conditions have been applied to the studies on the effect of a pressure intensifier and foam core on laminate core temperature. Figure 6.17 and Figure 6.18 summarises the effect of the pressure intensifier on temperature lag and laminate core temperature, respectively. Due to the high thermal conductivity of the aluminium tooling and the low laminate thickness (2.5mm), the effect of increase in foam core thickness is limited. However, similar to the other process ancillaries, the level of thermal lag is dependent on the heating method. Figure 6.19 to Figure 6.20

presents the effect of foam core thickness on temperature lag and laminate core temperature.

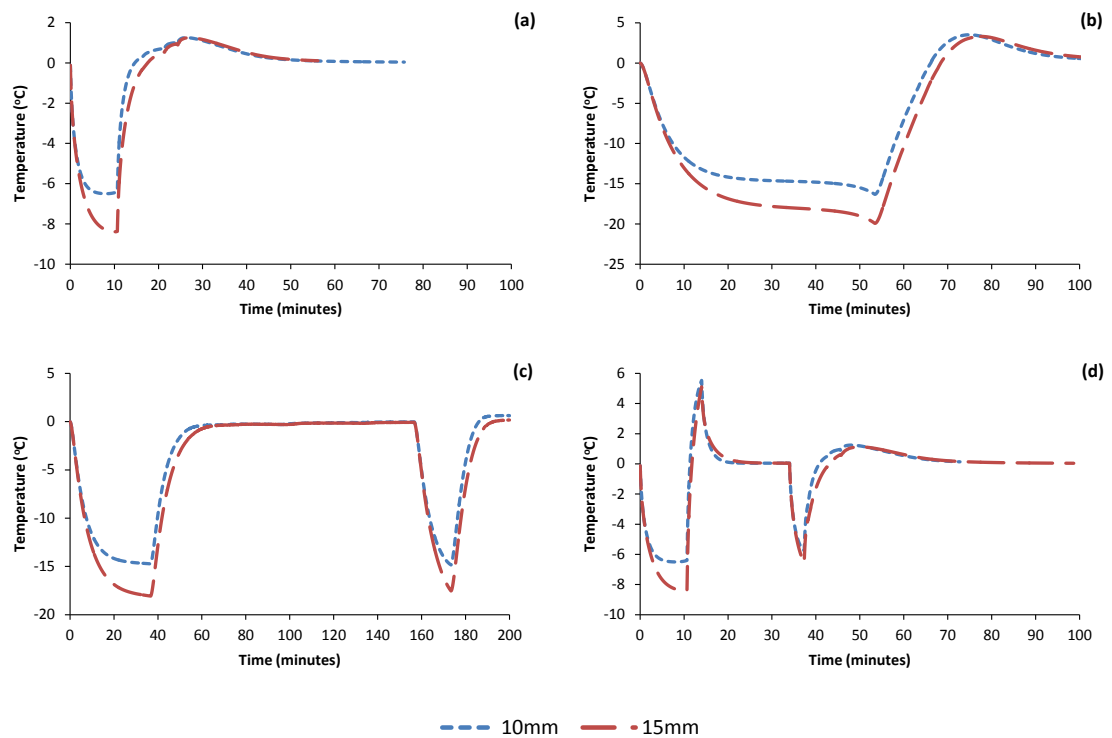


Figure 6.17: Effect of pressure intensifier thickness on laminate core temperature and temperature lag. Temperature is presented as a differential to the idealised scenario

The intensifier is commonly used to aid in localised laminate consolidation; such as in sharp corners. However, owing to poor thermal conductivity of the material, laminate temperature directly below the intensifier can be lower (or higher depending on point in cure cycle) than the bulk laminate. This can lead to the build-up of residual stresses below the intensifier, worsening spring-back. The findings of this study echo the effect of breather material on laminate temperature. Although the pressure intensifier used in this study is 5mm and 10mm thick, they can be moulded to be much thicker. Whilst the order of magnitude increase in thermal conductivity (0.5 against 0.05) could have resulted in reduced thermal lag, the thickness of the intensifier negates potential gains due to the increase in thermal mass. As show in Figure 6.17, this leads to a temperature lag of up to 20°C and up to 3.5°C thermal overshoot, depending on the heating method; necessitating a slower heating rate, resulting in longer cycle time.

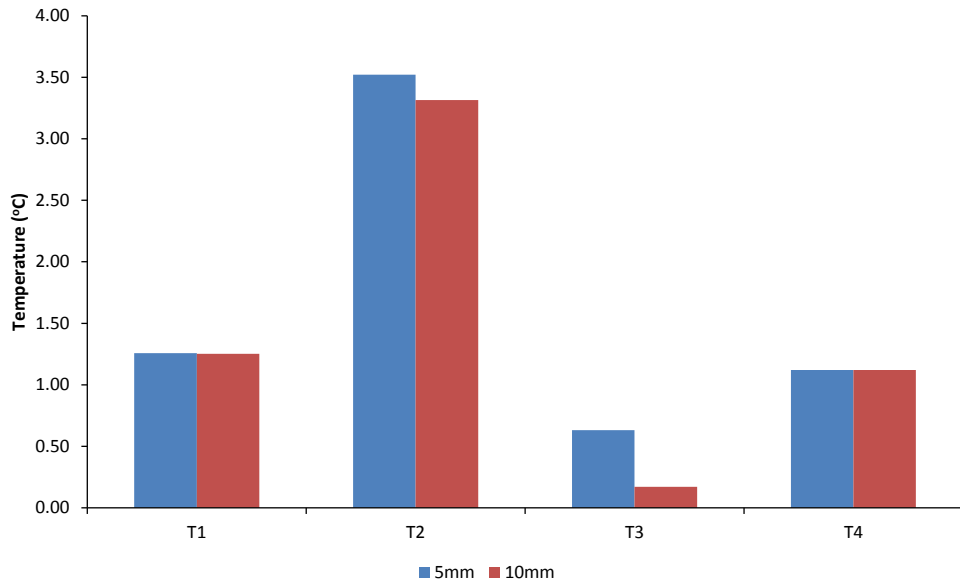


Figure 6.18: Plot presenting effect of intensifier thickness on the magnitude of thermal overshoot.

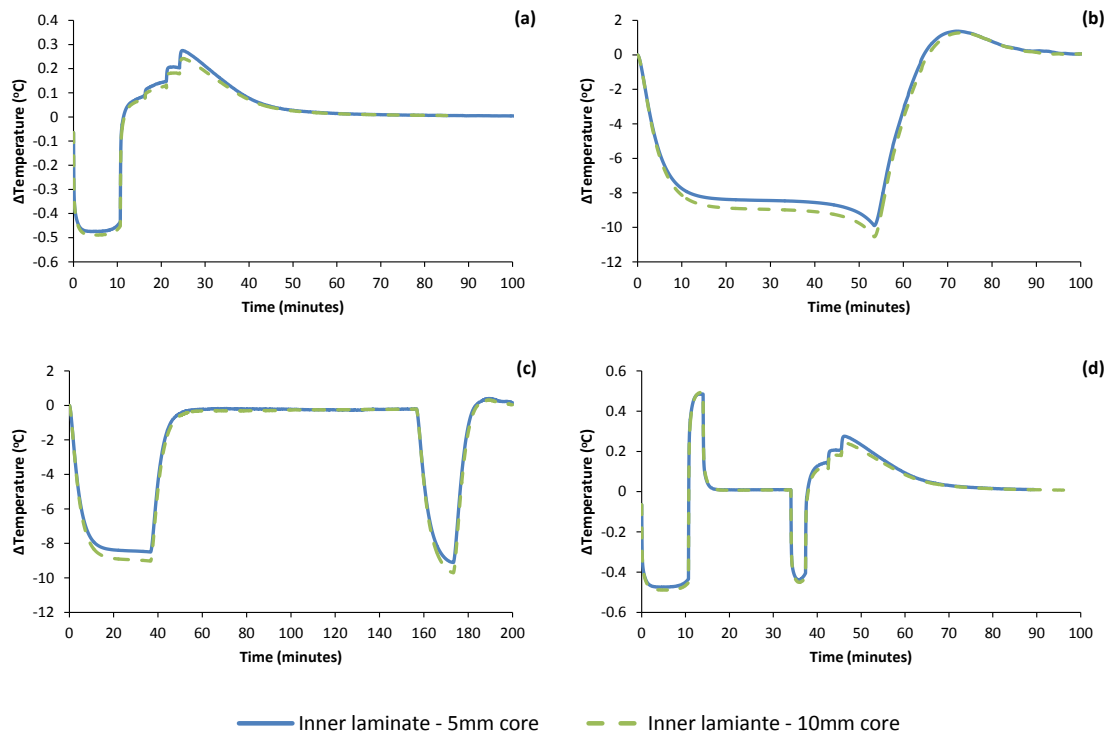


Figure 6.19: Effect of foam core thickness on the inner laminate (laminate on the tooling surface).

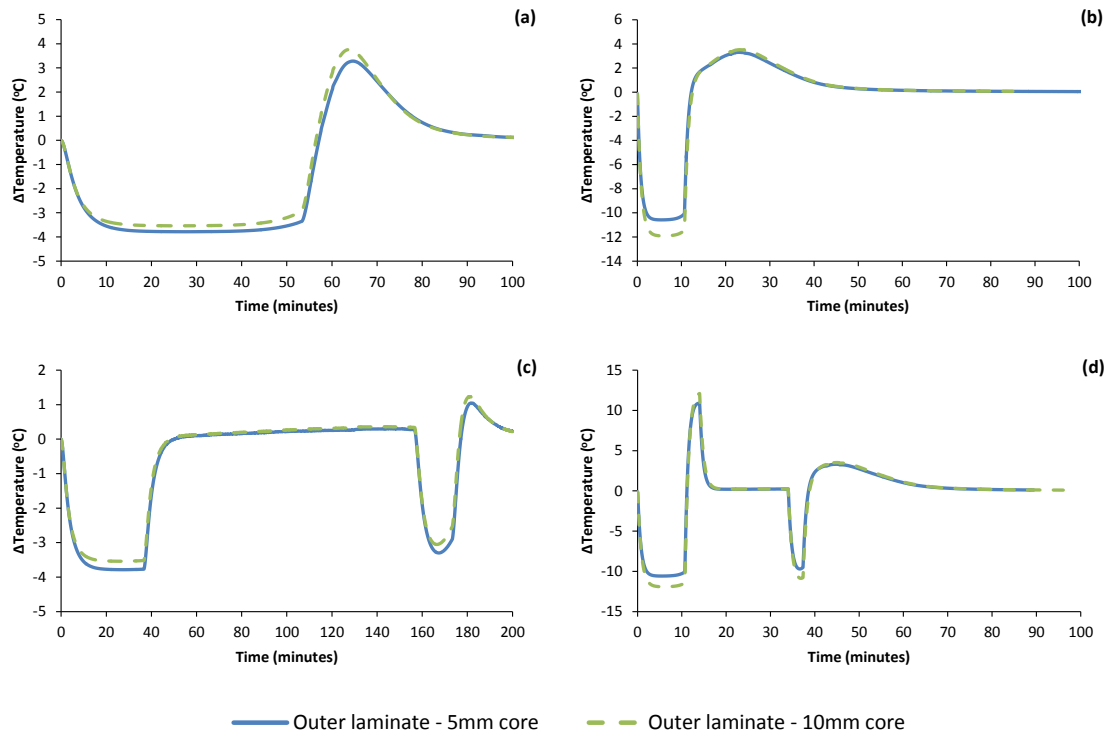


Figure 6.20: Effect of foam core thickness on the outer laminate (laminate adjacent to the breather).

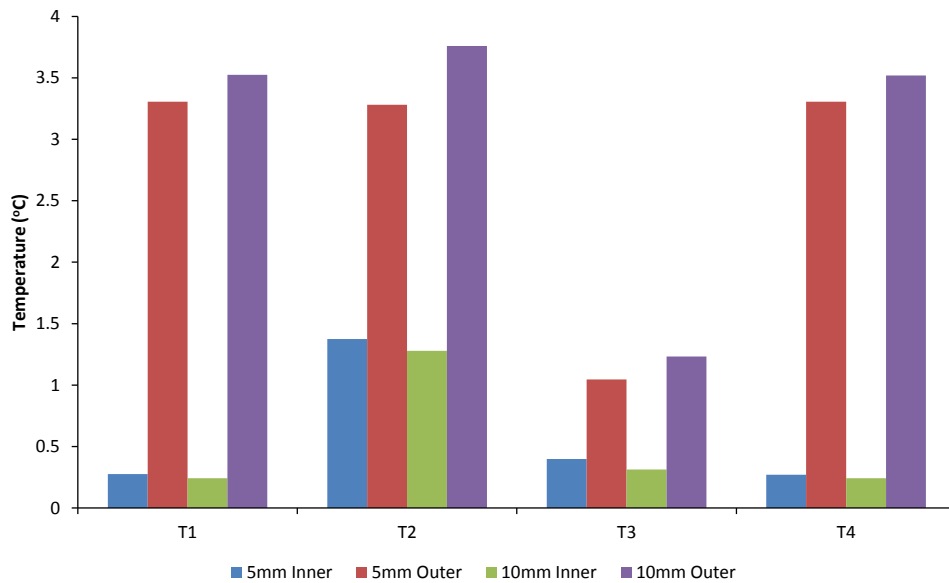


Figure 6.21: Comparison between inner and outer laminate layers on the foam core in terms of magnitude in thermal overshoot.

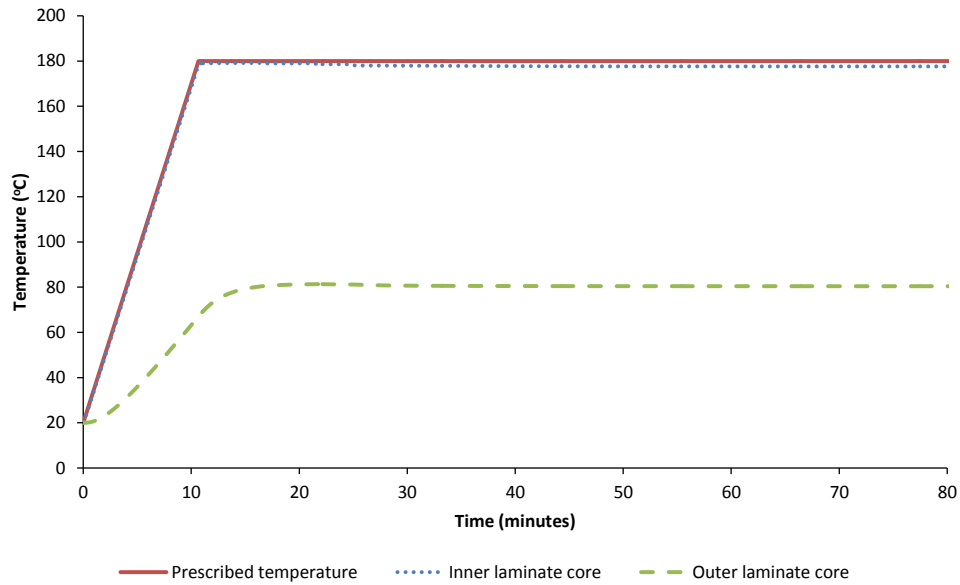


Figure 6.22: Effect of processing a foam cored sandwich panel on a free-standing heated tooling.

The thermal properties of the foam core are comparable to that of the breather material. Processing a foam cored sandwich panel using a free-standing tooling with on-board heating system can lead to a mismatch in laminate temperature. As shown in Figure 6.22, the laminate close to the heated tooling follows the prescribed cure temperature. However, the laminate near the bag side is up to 100°C less than the prescribed cure temperature, leading to grossly insufficient cure. This indicates that free-standing heated tooling is not suitable for processing laminates with a foam core, unless a matched heated tooling is used on the bag side.

In-line with the findings of Chapter 6.3.2, the poor thermal properties of the process ancillaries can limit the maximum heating rate that can be safely employed. Whilst the findings indicate that the thermal overshoot in the laminate core is up to 5°C, it should be noted that a tooling material with a relatively high thermal conductivity (aluminium) and a thin laminate (5mm) has been used. Increase in laminate thickness or tooling materials with poor thermal properties can worsen the thermal overshoot in the laminate core.

Figure 6.23 presents the effect of tooling material choice on laminate core temperature. Figure 6.24 and Figure 6.25 summarises the thermal overshoot and thermal lag expected at the laminate core respectively.

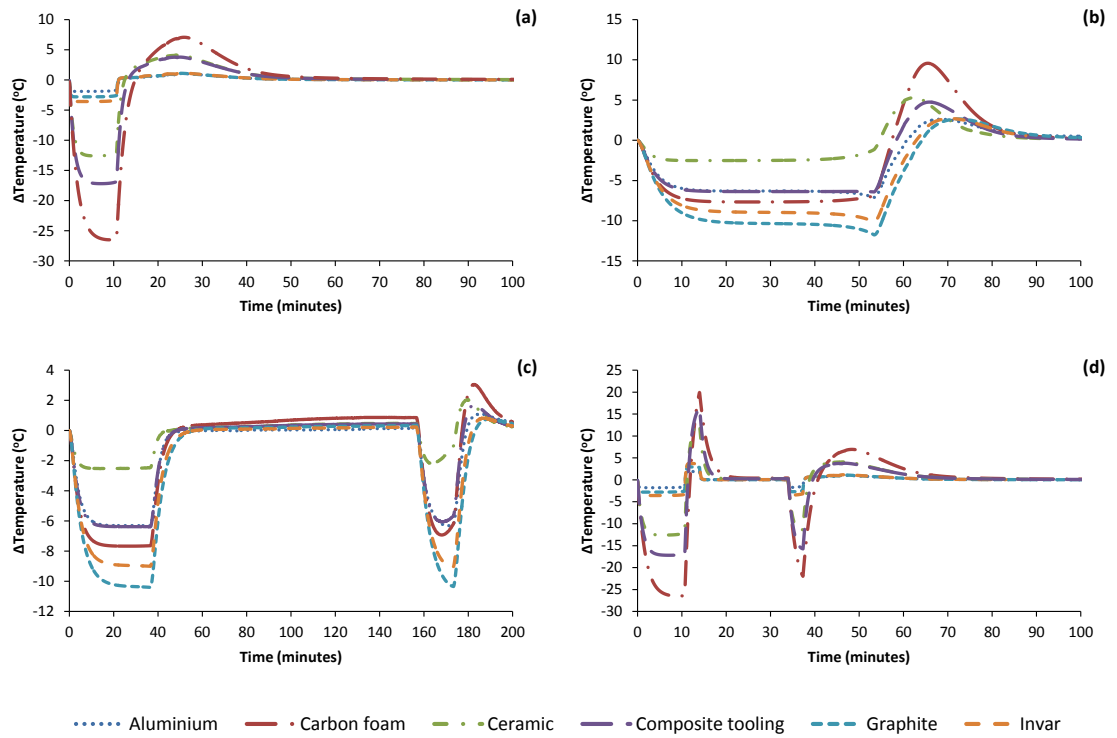


Figure 6.23: Summary of study on the effect of tooling material choice on laminate core temperature. Figure 6.13 presents the prescribed cure cycles that correspond with the alphabet.

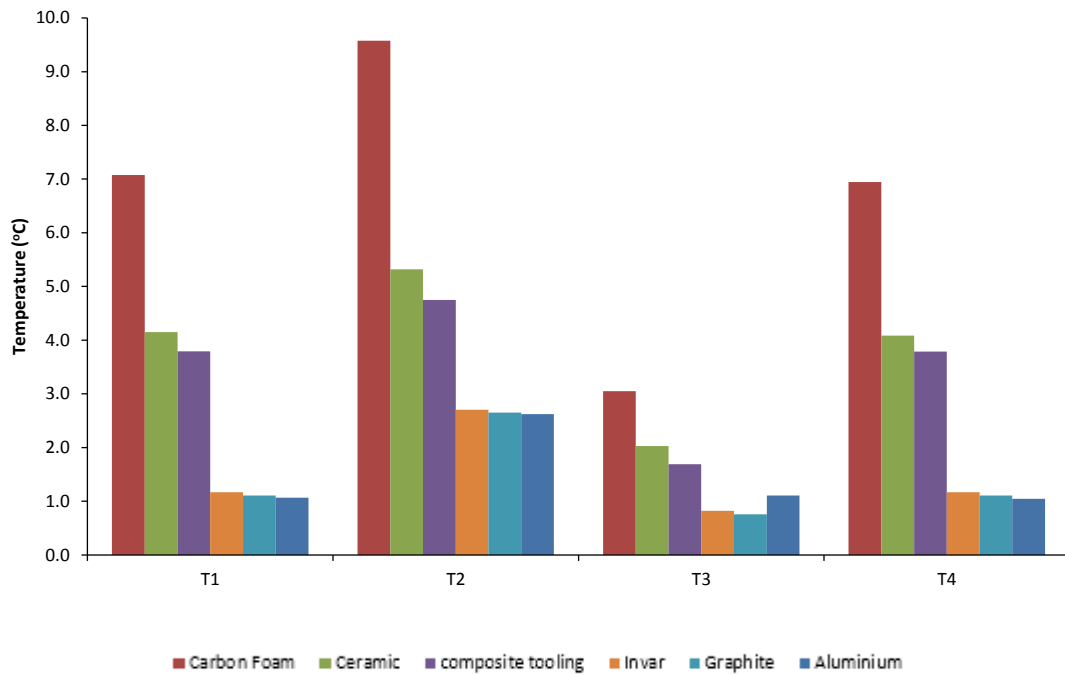


Figure 6.24: Effect of heating method and tooling material choice on laminate core thermal overshoot. T1 – T4 corresponds to (a) – (d) in Figure 6.23.

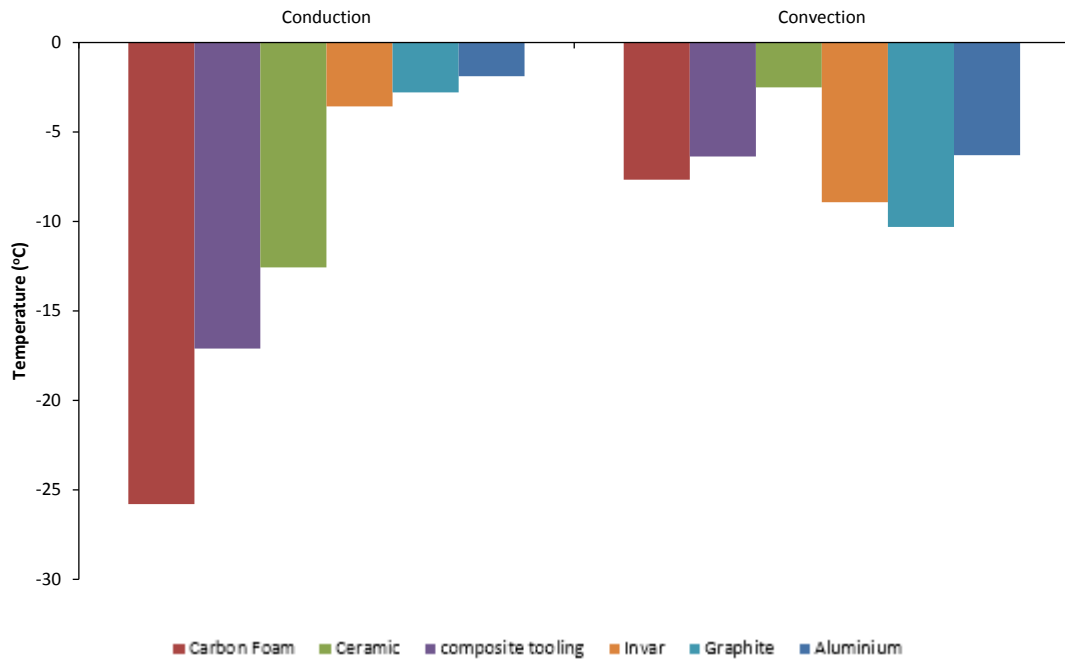


Figure 6.25: Effect of heating method and tooling material choice on laminate core thermal lag. Conduction corresponds and convection to the temperature profile used in (a) and (b) in Figure 6.23

Irrespective of heating method, processing laminates on tooling materials with high thermal conductivity result in low ($< 3^{\circ}\text{C}$) thermal overshoot at the laminate core (Figure 6.23). However, it must be remembered that tooling thickness has been normalised to deflection; the thickness varies depending on the material properties. Although the thickness of the tooling varies, the order of magnitude increase in thermal conductivity from Invar (10.4W/mK) to Aluminium (167 W/mK) did not appear to have a significant impact on laminate thermal overshoot. On the other hand, materials with low thermal conductivity ($< 1\text{ W/mK}$) appear to be more sensitive to changes in tooling thickness and can result in high thermal overshoot (up to 9.6°C) at the laminate core

In terms of heating method, laminates heated via convective heating appear to have a higher thermal overshoot than conductively heated (Figure 6.24). This is to be expected as the rate of transfer of energy across the boundary of the mesh domain is dictated by the convective film coefficient. In conductive heating, there is no restriction to the rate of transfer of energy across the boundary. Figure 6.25 presents the lag in temperature between the laminate core in the idealised scenario and the present study based on heating method. For convective heating the effect of thermal

mass appears to be more dominant. For instance, the lag recorded by the laminate core processed on the ceramic tooling is the lowest (2.5°C), while the laminate processed on the graphite tooling has the highest (10.3°C). Similar trend can be observed in conductive heating, except that materials with high thermal conductivity have lower lag, irrespective of thermal mass.

Furthermore, there appears to be an interactive effect between thermal conductivity and thermal mass on laminate core temperature and thermal lag. For instance, despite the high thermal conductivity of Aluminium and the low tooling thickness, the laminate core temperature is higher than that of graphite in T3. To isolate the contribution of each of the factors on laminate core temperature, an ANOVA has been performed using statistical analysis software (Minitab). Current selection of tooling materials used up to this point have a combination of high thermal conductivity - high thermal mass or low thermal conductivity - low thermal mass. To perform the analysis, two hypothetical materials have been created. Material M has the thermal mass of ceramic tooling but the thermal conductivity of Invar (High thermal conductivity – Low thermal mass). Material A has the thermal mass of an invar tooling but with the thermal conductivity of a ceramic tooling Figure 6.26 presents the location of the new materials in relation to currently available tooling materials. Figure 6.27 and Figure 6.28 presents an interaction plot highlighting the effect of thermal conductivity, thermal mass and heating method on laminate core temperature and temperature lag at the laminate core (both wrt. to the idealised scenario).

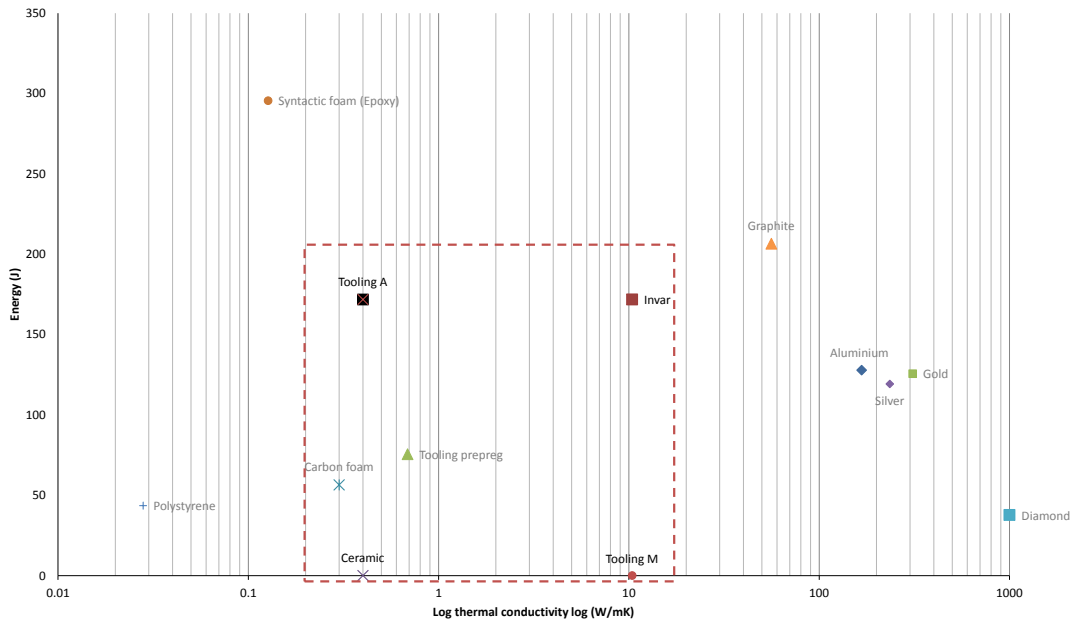


Figure 6.26: Comparison of tooling materials in terms of thermal mass and thermal conductivity.

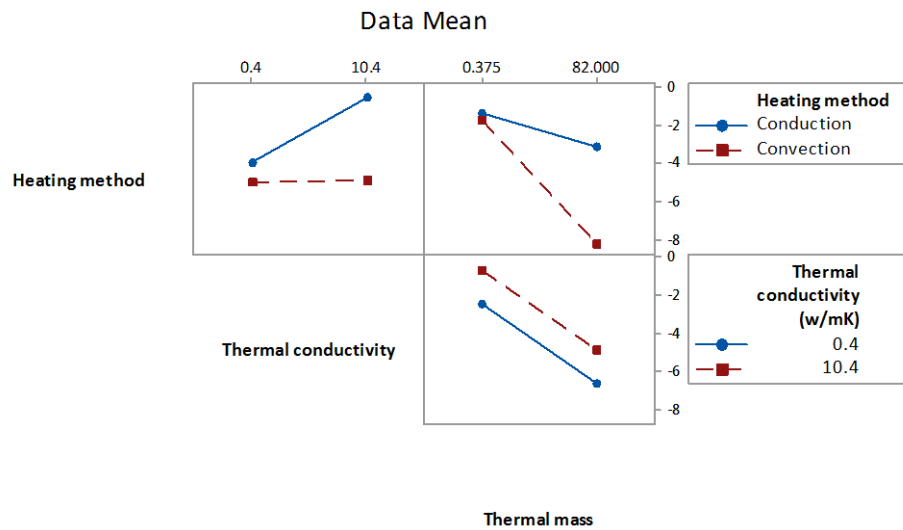


Figure 6.27: Interaction plot presenting the effect of thermal conductivity, thermal mass and heating method on temperature lag at the laminate core.

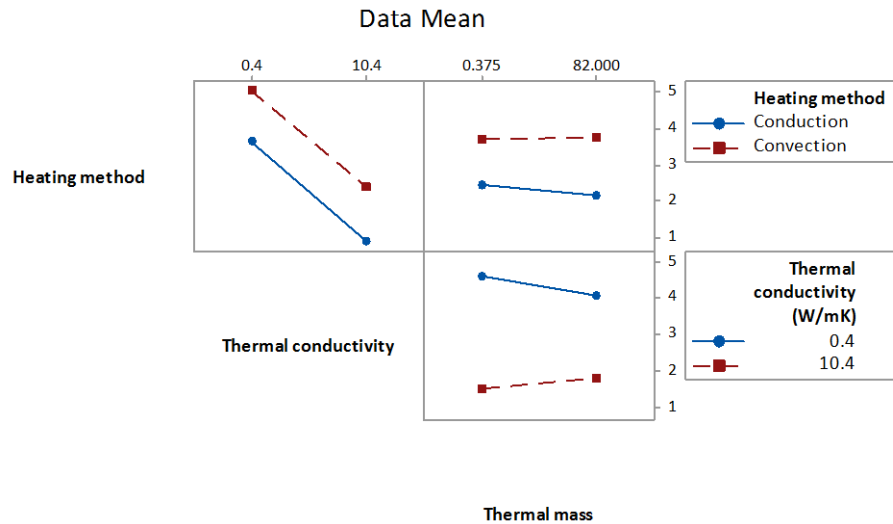


Figure 6.28: Interaction plot presenting the effect of thermal conductivity, thermal mass and heating method on thermal overshoot at the laminate core.

As shown in Figure 6.27, thermal conductivity has a greater impact on laminate core temperature than thermal mass for a given heating method; with convective heating resulting in higher laminate core temperature. The study highlights an interaction between thermal conductivity and thermal mass. A combination of high thermal mass and low thermal conductivity appears to result in a decrease in laminate core temperature. This combination results in a greater thermal lag at the laminate core, which minimises the resulting thermal overshoot.

In terms of thermal lag, the thermal mass of the material is more dominant than thermal conductivity (Figure 6.28). However, this effect is more dominant for convective heating than for conductive heating. This effect can be seen in Figure 6.25 particularly when a comparison is made between graphite and composite tooling. Although the thermal conductivity of graphite tooling is two orders of magnitude higher than that of composite tooling, the thermal lag experienced is higher than that of composite tooling for convective heating.

The findings indicate that to achieve cure cycle time reductions via high heating rate processes, it is necessary to use a tooling material with high thermal conductivity and low thermal mass. Ideally, the optimum process applies conductive heating from all sides of the laminate to maximise the rate of transfer of energy across the

tooling/bagging interface, thus reducing thermal overshoot. However, the study also highlights some physical limitations that must be overcome through material development and tooling design. As can be observed in Figure 6.26, there are currently no tooling material with sufficiently high thermal conductivity ($> 10 \text{ W/mK}$) and low thermal mass for a given volume ($< 600 \text{ J}$). Precious metals and stones have the ideal thermal properties, with diamond being the only material (in the study) having the ideal coefficient of thermal expansion. However, such materials are (currently) neither cost effective nor feasible for tooling applications. Also, as shown in Chapter 1, current novel tooling solutions embed heating elements within a ceramic matrix, composite tooling or carbon foam; materials which the study indicates is not optimum for high heating rate applications due to the efficacy of removing heating released by the laminate. Nevertheless, such materials have been chosen for their secondary characteristics, such as ease of machining/fabrication and relative low cost. Whilst ceramic tooling with the thermal conductivity of Invar (Tooling M) does not exist, the thermal conductivity of ceramic tooling can certainly be enhanced through fibre or particulate reinforcement.

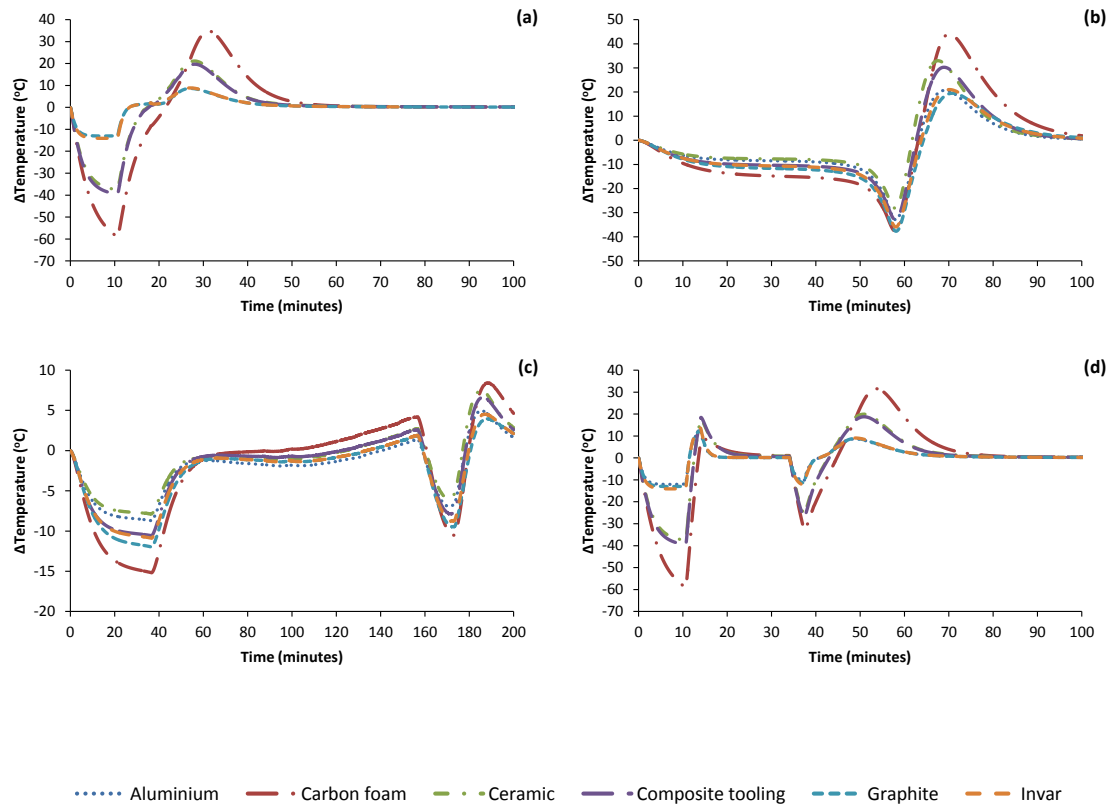


Figure 6.29: Effect of tooling material and cure cycle on the core temperature of a 15mm thick laminate. Figure 6.13 presents the prescribed cure cycles that correspond with the alphabet.

Up to this stage the study has addressed the limitations of tooling material and process ancillaries on reducing cure cycle time. However, there is an additional factor which dominates the maximum achievable reduction in cure cycle time – Laminate thickness. As shown in Figure 6.29 and Figure 6.30, increasing the laminate thickness to 15mm can result in up to 35°C thermal overshoot in the core, leading to thermal degradation of the matrix. Using a temperature profile with a low initial dwell temperature followed by a post cure (Cycle T3) can result in reduced laminate core temperature. However, as seen in Figure 6.29 (c), the poor through thickness thermal conductivity results in temperature creep towards the end of the low temperature dwell. It should be noted that Cycle T3 used convective heating along the mesh boundaries. Using conductive heating along with an increase in ramp rate (from 3°C/min to 15°C/min) can lead to reduced cure cycle time whilst maintaining (if not exceeding) similar levels of thermal overshoot (Figure 6.31). The magnitude of thermal overshoot observed can be reduced by using a tooling with high thermal

conductivity and low thermal mass, like material M, or by increasing through thickness thermal conductivity of the laminate.

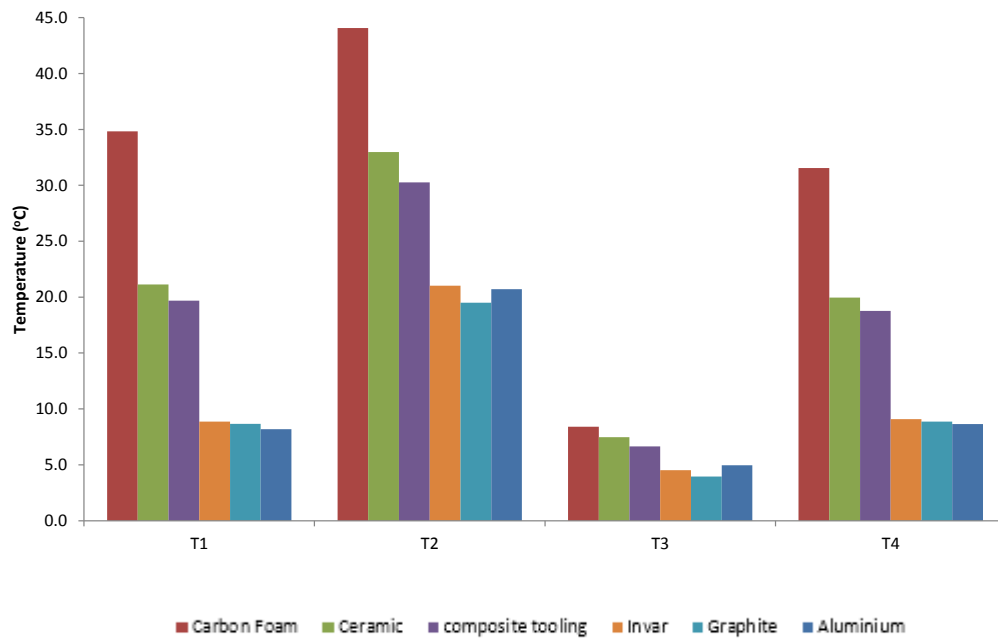


Figure 6.30: Magnitude of thermal overshoot in the core of a 15mm thick laminate. T1 – T4 corresponds to (1) – (d) in Figure 6.29. Note the increase in temperature in comparison to the study on a 5mm thick laminate (Figure 6.24).

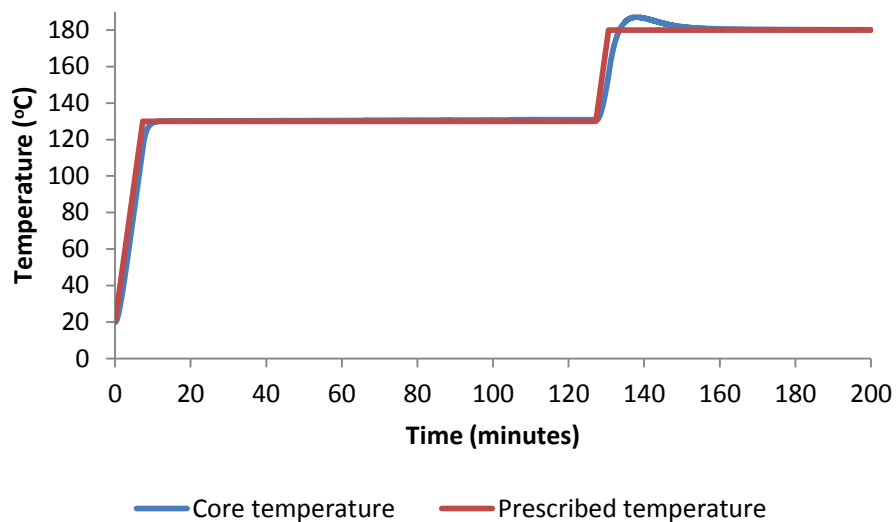


Figure 6.31: Effect of using Cycle 3 with 15°C/min heating rate conduction heating (compared to 3°C/min convection heating) with aluminium tooling.

6.4. Conclusion

The present chapter explored the parameters that hinder reductions in cure cycle time. The kinematic and rheological characteristics of the conditioned MTM44-1

resin system was compared against standard OoA, autoclave and RTM resin systems. The comparative study was used to define the key characteristics of a hypothetical resin system optimised for high heating rate processes. However, owing to the proprietary nature of commercial resin systems, the feasibility of creating such a resin system is unknown. Limitations such as compatibility of the reactive species in the resin, conflicting requirements and cost of the raw materials can hinder the development of such a resin system.

A study on the effect of tooling materials and process ancillaries has been performed. The low thermal conductivity of processing materials has been shown to be detrimental to laminate core temperature, irrespective of heating rate or heating method (conductive or convective heating). Also, the configuration of vacuum bagging and the arrangement of the breather material during lay-up can lead to up to 5°C increase in thermal overshoot and up to 20°C thermal lag. The large thermal lag necessitates low ramp rates and increased recirculation of the heat transfer medium (in convective heating methods). In particular, the low heating rate can lead to increases in cure cycle time. The study identified the characteristics of the most optimum tooling material for reducing cure cycle time. The most optimum tooling material has high thermal conductivity ($>10 \text{ W/mK}$), low thermal mass and a low coefficient of thermal expansion $< 5 \mu\text{m/m}^\circ\text{C}$. However, current commonly used tooling materials do not meet the required characteristics; signalling the need for further development in tooling materials.

6.5. Recommendations

Based on the findings of this study the following tooling recommendations are provided:

- Aluminium tooling is optimum for high heating rate processes owing to the high thermal conductivity and moderate heat capacity. However, owing to the high thermal expansion, Aluminium tooling is only suitable for low part size $< 1\text{m}^2$

- Materials with a combination of high thermal mass/low thermal conductivity (syntactic foam) and low thermal mass/low thermal conductivity (ceramic) necessitate slow heating rate ($< 3^{\circ}\text{C}/\text{min}$) to minimise thermal lag.
- Poor thermal characteristics of processing ancillaries increase thermal lag and thermal overshoot at the laminate core. Omitting processing ancillaries all process ancillaries is not viable for processing prepregs using dynamic cure cycles. Isothermal compression moulding of prepregs can eliminate the need for process ancillaries, but by sacrificing the application of hydrostatic consolidation pressure.
- Further work is needed in developing a resin system optimised for high heating rate cure cycles.
- Irrespective of tooling material, processing thick laminates (15mm) with high heating rate can lead to warpage due to the through thickness temperature distribution. This can potentially be alleviated with nano-particle reinforcement such as Graphene.

7. Conclusion

Owing to increasing pressure to reduce greenhouse gas emissions, the transport sector is investing in processing low density, high performance composites; particularly the aerospace industry. However, current method of choice for processing high performance structural components (autoclave cure of prepregs) is not cost effective, due to large part size ($> 5\text{m}^2$) and low production volume ($< 1,000$ units per annum). Out-of-Autoclave (OoA) processing of prepregs that are specially optimised for low consolidation pressure (1 Bar) has been advocated as a viable alternative. However, studies have reported laminate porosity levels ranging from $< 1\%$ up to 12% ; with the added disadvantages of low margin for error and long cure cycle time. In parallel developments, novel high heating rate OoA processes with low consolidation pressure (~ 1.1 Bar) have been shown to achieve substantial reduction in cure cycle times (50% and greater than that of autoclave) whilst achieving mechanical properties comparable to or even greater than autoclaved laminates. However, studies have reported high void content (up to 12.9%); albeit when using prepregs not optimised for low consolidation pressure processing. Studies on high heating rate processes are currently limited; and the mechanisms of void mitigation in such processes are not well understood.

A novel take on void growth mitigation has been proposed and verified, leading to a better understanding of how void growth is mitigated in high heating rate processes. A novel high heating rate, low consolidation pressure process has been developed and shown to yield $< 1\%$ laminate porosity. In addition, the work defined fundamental limits to cycle time reductions that can be achieved with current tooling, process ancillaries and resin systems.

The present chapter summarises the outcome of the thesis and relates it to the main objectives and hypothesis laid out in Chapter 1. The following sections break down the key findings from each chapter of the thesis.

7.1. Void growth mitigation strategy

Based on the critical review presented in Chapter 2 the primary cause of voids in prepreg processing has been identified – Dissolved moisture and air entrapped air. Due to the low in-plane and through thickness air permeability presence of residual

entrapped air is inevitable, even after extensive de-bulks. This is exacerbated due to long part size and insufficient de-bulk time. As epoxy resin is hygroscopic, the resin absorbs moisture from ambient during long lay-ups. The dissolved moisture can diffuse into existing entrapped air voids, preventing collapse during cure, forming voids.

Contrary to previous suggestions, voids formed during cure cannot be physically drawn out of the laminate. This is due to: (1) large part size combined with low permeability (2) zero bleed prepreg systems used in current generation OoA prepregs (3) small window for resin flow when compared to infusion processes such as RTM. A review of the literature indicated that there is a window within the cure cycle – between the void growth initiation point and resin gelation – during which void growth can be mitigated. This thesis hypothesised that void growth mitigation in high heating rate processes was achieved primarily due to the reduction in time to gelation. As the required pressure is dependent on the cure temperature, the present study proposed that increasing the heating rate and optimising the temperature profile could achieve low laminate porosity with low consolidation pressure.

7.2. Predicting and evaluating laminate porosity

The review established that existing models that predict the pressure required to prevent the growth of a pure water-vapour void can be used to prevent the growth of mixture voids (void composition of entrapped air and water vapour). The study recognised that the pressure exerted by the expanding water-vapour is more dominant than that by entrapped air.

The governing equations of the void growth model were used to predict void growth in hygrothermally conditioned MTM44-1 Out-of-Autoclave prepregs. The prepregs were conditioned so as to simulate the effects of long lay-up times. Furthermore, during lay-up steps were taken to increase the amount of residual entrapped air in the laminate. This is to simulate residual entrapped air after de-bulk of large parts. The prepregs were processed using cure cycles based on manufacturer recommendations and experimental high heating rate cure cycles. High heating rate

cycles included the 'spike' cure, which has been shown to be the most optimum cure cycle to achieve high mechanical properties, low porosity and reduced cure cycle time. A novel tooling system (Pressure Tool) was developed to process laminates using up to 15°C/min heating rate. Furthermore, the Pressure Tool is capable of applying up to 7 Bar hydrostatic pressure.

Good agreement was observed between the experimental data and the model output. The reduction in time to gelation achieved by the high heating rate resulted in reduced void volume fraction, confirming the thesis hypothesis. Furthermore, the study highlighted a principal limitation of the high heating rate 'spike' cure cycle – low margin for error. A 12°C thermal overshoot and a subsequent thermal lag (1.5 minutes) in cooling down to the low dwell temperature shifted the point of gelation. Unlike in earlier studies using the 'spike' cure, resin gelation occurred during the low intermediate dwell, yielding porosity levels comparable to that of autoclaved laminates (0.53%). Whilst the shift in the point of gelation was favourable in the present study, it was concluded that poor temperature control could lead to resin gelation taking place during the temperature 'spike' phase; preventing the dissolution of formed voids and resulting in extensive porosity. However, 2 Bar consolidation pressure was required to obtain autoclave-level porosity.

7.3. Combined effect of high heating rate and consolidation pressure on the physical and mechanical properties of laminates

The mechanical properties of laminates processed using high heating rate combined with up to 3 Bar hydrostatic pressure were comparable (if not greater) to that of laminates processed using standard cure cycles. This is contradictory to earlier studies which showed that high heating rate cure cycles – particularly the 'spike' cure – can yield mechanical properties greater than that of autoclaved laminates. The study was inconclusive on the cause behind the lack of additional gain in mechanical properties. It was speculated that location of voids within the laminate could have had an impact on the failure of the laminates, in-line with suggestions in published literature. Resin rich bands running the entire length of the laminate were observed, with micro voids (< 7µm void diameter) detected predominantly in the

resin rich bands. It was speculated that the voids acted as points of crack initiation and the bands provided a pathway for crack propagation.

Conditioned laminates processed using high heating rate and less than 2 Bar consolidation pressure achieved fibre volume fraction comparable to that of autoclave cured laminates. Whilst conditioned laminates processed using slow heating rates resulted in poor consolidation and low fibre volume fraction. However, autoclave-level fibre volume fraction was also achieved using unconditioned laminates. Plasticisation has been shown to reduce the duration of resin flow and the minimum viscosity that can be achieved. Potentially, the low minimum resin viscosity achieved using high heating rate ensured sufficient wet-out. This indicates that a prepreg system with a high initial viscosity can be used with high heating rate processes and achieve good fibre volume fraction and laminate consolidation.

The implications of this finding are as follows: (1) improve air permeability of the fibre bed resulting in increase in de-bulk efficacy. (2) Potentially longer shelf-life for preregs (3) increase margin for error. Furthermore, the study showed that greater than 95% of the mechanical properties of an autoclaved laminate can be obtained with just 2 Bar consolidation pressure when using high heating rate cure cycles, whilst achieving up to 39% reduction in cure cycle time.

7.4. Effect of resin chemistry

In addition to the build in air evacuation channels, OoA resin systems are optimised for low initial temperatures (~80°C – 130°C). This ensures that during VBO processing the applied pressure is sufficient to prevent the dissolution/diffusion of moisture. However, the study found that the window for resin flow is smaller than that of autoclave resin systems. Furthermore, OoA resin systems have been found to have a higher minimum viscosity than autoclave resin systems. This is potentially a design feature to prevent the premature filling of air evacuation channels. However, the present study found that this can lead to an increased propensity for voids due to insufficient resin flow, especially when processing prepreg near the maximum shelf-life.

A limitation of the low initial processing temperature is the high resin reactivity. The findings of this study show that processing thick laminates (> 5mm) using relatively slow heating rates (3°C/min) can result in a thermal overshoot of the laminate core. Furthermore, the low initial cure temperature necessitates a post-cure to achieve full mechanical properties, increasing cycle time. Also, a 'hot de-bulk', de-bulking at elevated temperature (60°C), can facilitate the removal of dissolved moisture from the resin without advancing cure or affecting resin flow characteristics. This can result in achieving low laminate porosity with 1 Bar consolidation pressure, but at the expense of increasing overall processing time.

It was concluded that a hypothetical resin system optimised for high heating rate processes would have characteristics of both: current generation OoA resin system and autoclave resin systems. Namely: increased window for flow than current OoA resin systems (2) Low minimum viscosity akin to autoclave resin systems (3) Reactivity at low temperature to reduce processing temperature to less than the threshold temperature for void growth in VBO processes, but less than that of current OoA systems (5) Snap gelation to further reduce the window for void growth. (6) Increased resin thermal conductivity to aid in dissipation of the heat released during the exothermic reaction. However, the feasibility creating such a resin system is currently unknown due to the proprietary nature of commercial resin systems.

7.5. Effect of process ancillaries

As highlighted in Section 7.3, poor control over the laminate temperature can lead to extensive porosity and scrappage of the component. The low thermal conductivity of currently used process ancillaries has been shown to limit the maximum reductions in cure cycle times that can be achieved. Furthermore, the lay-up configuration of the process ancillaries has been shown to increase the laminate core temperature by up to 4.4°C. For instance, although release films and vacuum bagging materials are less than 60µm thick, envelope bagging has been shown to induce a 5.3°C thermal lag and up to 1.2°C thermal overshoot at the laminate core, an order of magnitude higher than single sided bagging. This effect is more prominent when used in conjunction with tooling material with high thermal conductivity (such as

aluminium). Furthermore, wrapping a layer breather felt around the laminate-tooling assembly, as possessed to single sided configuration, can lead to up to 30°C lag in temperature and 4.4°C thermal overshoot at the laminate core.

Due to the low thermal conductivity of the foam core, foam cored-sandwich panels cannot be processed on single-sided tooling with on-board heating systems. To achieve a uniform cure of the laminates on both sides of the foam core, a matched tooling system is needed, which limits design flexibility and increases cost. Also, the study has shown that the low thermal conductivity of pressure intensifiers can lead to a localised thermal overshoot (up to 3.4°C) in the laminate directly below the intensifier. This can lead to the build-up of residual stresses and ultimately part warpage.

7.6. Effect of tooling material and laminate thickness

The efficacy of transfer of energy to/from the laminate core is limited by: (1) the heating method (2) thermal conductivity and thermal mass to the tooling material (3) and thermal conductivity of the resin system. Achievable reductions in cure cycle time using convective heating are limited by the convective heat transfer coefficient and the thermal mass of the tooling material. The study highlighted that thermal lag due to convective heating can be up to two times greater than that of conductive heating, when using tooling material with high thermal mass. Thermal conductivity of the tooling material and the matrix of the laminate have been found to have a greater impact on the thermal shoot during cure than thermal mass. Processing 5mm thick on materials with low thermal conductivity ($<0.5 \text{ W/mK}$) can result in up to 10°C thermal overshoot in the laminate core. However, processing 15mm thick laminates can result in up to 30°C thermal overshoot, when processed using high heating rate and high dwell temperature. To minimise thermal lag and thermal overshoot whilst processing large ($> 1\text{m}^2$) composite components, a slow heating rate ($<3^\circ\text{C}/\text{min}$) and low cure temperature is needed, increasing cycle time. Cycle time reductions can be achieved by processing laminates on an optimum tooling material. Such a material would have high thermal conductivity ($> 10\text{W/mK}$), low coefficient of thermal expansion ($< 5\mu\text{m}/\text{m}^\circ\text{C}$) and low thermal mass. However, currently available tooling materials have either a combination of high thermal mass-

high thermal conductivity or low-thermal mass-low thermal conductivity. Materials with high thermal conductivity, low thermal mass and low coefficient of thermal expansion are currently limited to precious stones; which is not feasible for tooling applications.

7.7. Recommendations for future studies

The following have been identified as potential areas for future study

- **Study on the feasibility of metal reinforced (particulate or fibre) ceramic tooling material to increase thermal conductivity.**

Ceramic and composite tooling materials have low thermal mass by low thermal conductivity. The thermal conductivity can be improved through the addition of materials (in particulate or fibrous form) with high thermal conductivity; particularly in the through thickness direction.

- **Development of an optimised resin system for high heating rate processes, with improved resin thermal conductivity and resin characteristics**

Increasing thermal conductivity through the addition of nano-particle reinforcement with high thermal conductivity (such as Graphene) can potentially improve through thickness thermal conductivity of the composite. However, additional processing limitations such as a particle agglomeration and dispersion must be overcome.

- **Technical cost model to study the viability of a pressurised tooling system with on-board heating for processing structural composite components in low volume**

The current study presented a conceptual tooling system which can potentially reduce bottle-necks in composite processing. However, further studies are needed to assess the economic viability of such a system.

- **Process model development to predict the build-up of residual stresses and spring back in composites**

The current work incorporated process models as user-defined functions into a commercial FEA package. Potentially, a similar methodology can be used to create a

portable, sub-routine that can be incorporated into FEA packages to predict the build-up of residual stresses and spring back.

- **Study on the efficacy of ‘hot de-bulks’ on removing dissolved moisture from OoA prepreg system.**

A combination of partial vacuum in the air evacuation channels and elevated temperature (40 – 60°C) facilitate the dissolution and transport of dissolved moisture (and other volatiles) from the prepreg, without the advancement of degree of cure or affecting resin flow characteristics. This can potentially yield low laminate porosity with low consolidation pressure. However, further studies are needed to assess the increased risk in channel collapse and the effect on overall processing time and cost.

7.8. Processing recommendations

When processing laminates using a high heating rate the following are recommended to achieve high laminate quality:

- Use tooling material with a thermal conductivity $> 10\text{W/mK}$
- Limit laminate thickness to 5mm to minimise the build-up of thermal gradient and thermal overshoot at the laminate core
- Use a low initial dwell temperature (100 – 130°C) when applying VBO consolidation pressure. The achievable minimum dwell temperature is dependent on resin chemistry.
- Minimise breather thickness to minimise thermal lag. Also, avoid wrapping the breather around the lay-up assembly.

8. Appendix

8.1. Appendix A

The following section outlines the analytical process undertaken to define the minimum heater power density and the number of strip heaters required for the Pressure Tool.

The Pressure Tool was simplified as a block of Aluminium with dimensions specified so as to process up to 5mm thick 160mm² panels using vacuum bagging. The length and width of the tool was set as 350mm by 400mm to provide sufficient space for lay-up and to machine grooves for the O-Ring – so as to pressurise the lay-up cavity. As a preliminary design, the thickness of the block was set as 60mm. As the volume of the tool and the material property is known (summarised in Table A-A. 1), the energy required to raise the temperature from ambient temperature (25°C) to 180°C is calculated as follows:

$$Q = mC\Delta T \quad \text{Equation A-A. 1}$$

$$Q = 3.08 \times 10^6 \text{ J}$$

The required ramp rate is 15°C/min implies that power density of the heater bank must be such that, ignoring convective and radiation losses, 3.08 x 10⁶ J must be applied to the Pressure Tool in 10.3 minutes – which requires a heater bank with a power density to **4.97kW**. Naturally, the finally design of the Pressure Tool will have reduced mass, thus requiring less energy to heat the tool. However, overestimating the required heater bank power density will reduce the impact of the inevitable convective and radiation losses on the maximum achievable heating rate.

Aluminium – 6061	
Density (kg/m^3)	2719
Mass (m) (Kg)	22.84
Heat capacity (C) (J/KgK)	871
Thermal conductivity (W/mK)	202.4

Table A-A. 1 – Material properties of the Pressure Tool

When optimising the design of the Pressure Tool using Ansys Fluent, an internal heat generation function is used to simulate the working of the heaters. The above calculations is used in Ansys Fluent to verify the working of the internal heat generation function – result of the verification study is summarised in Figure A-A. 1 and Figure A-A. 2.

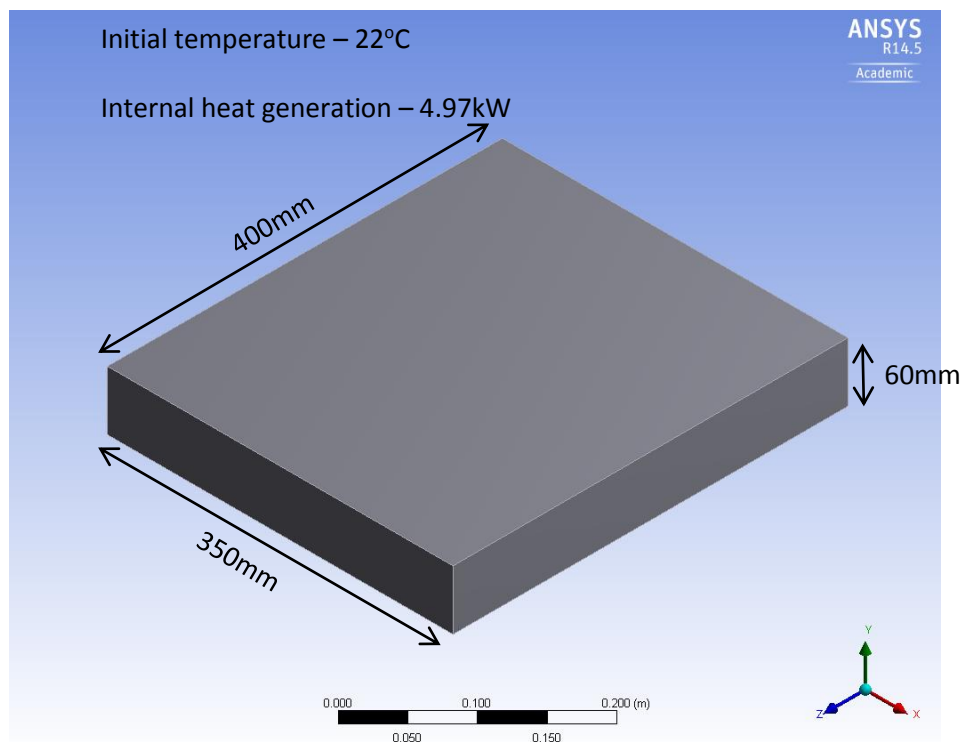


Figure A-A. 1 – Dimensions and initial conditions for the verification of the internal heat generation function

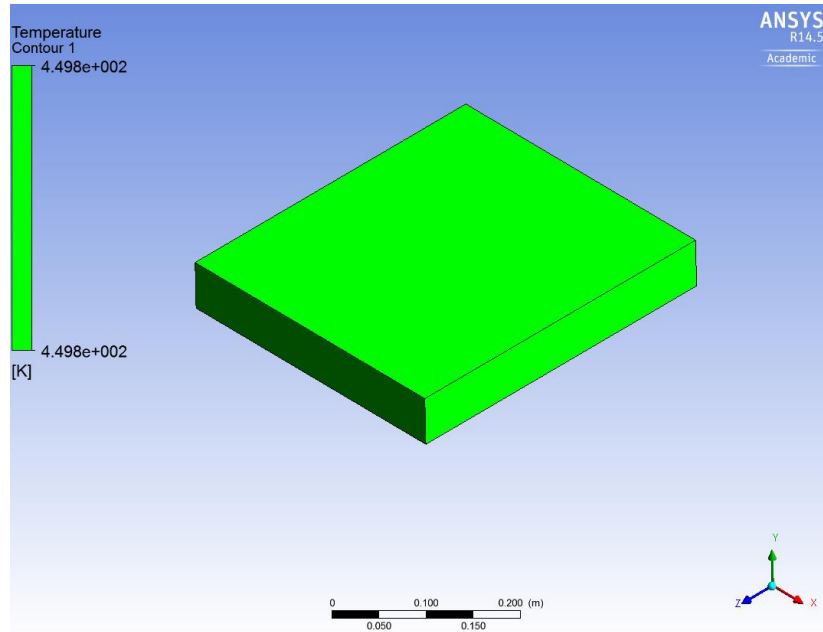


Figure A-A. 2 – Temperature of the block after 10.3 minutes – 155°C increase in temperature

Appendix B: Empirical derivation of optimum burn-off temperature for analysing fibre volume fraction

This section presents the study on the optimum temperature for the burn-off test used to obtain the specimen fibre volume fraction. Preliminary tests were performed to determine the optimum temperature and test duration to minimise oxidation of the fibres. Three off-cut specimens from the autoclave cured plaque were processed in the ashing furnace at the temperature and duration shown in Table A-B.1. The mass (obtained using a mass balance) and visual characteristics of the post burn-off fibres were recorded.

Temperature (°C)	480	500	515	530
Duration (hrs.)	1.5	0.75	0.5	0.5

Table A-B.1: Summary of burn-off test temperature and duration

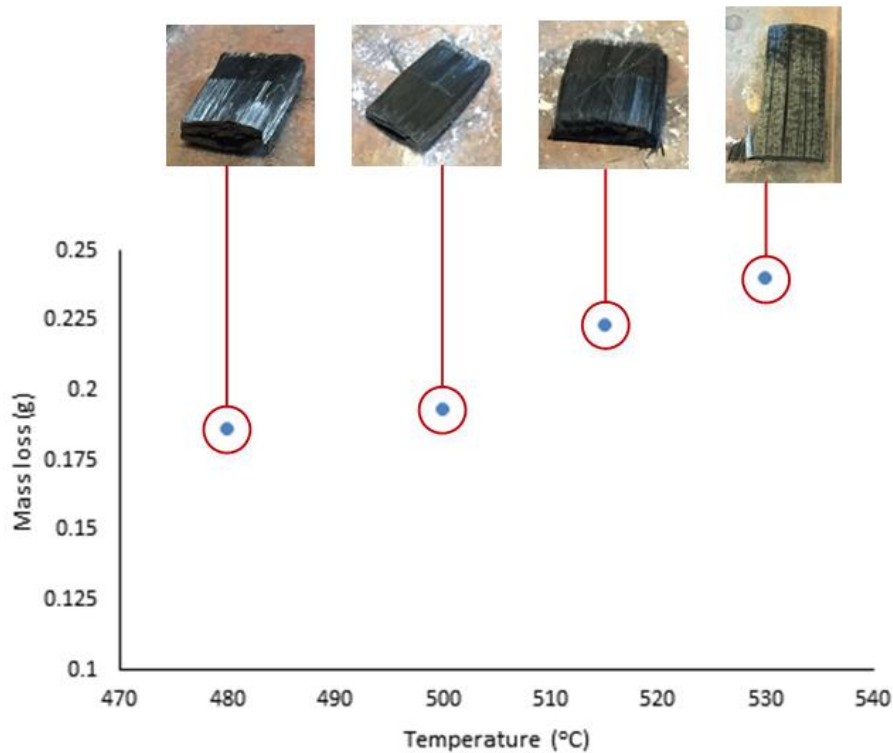


Figure A-B.1: Effect of burn-off temperature on mass loss. Note the increase in fibre oxidation and reduction in specimen rigidity with temperature.

As shown in Figure A-B.1, fibres of specimens processed 540°C and beyond exhibited signs of oxidation; due to which the test temperature was limited to 520°C. Processing at temperatures of less than 500°C resulted in insufficient resin burn-off. In addition, no appreciable loss in mass was observed when processing the specimens beyond 1 hour at 520°C. Specimen weight recorded before and after the test was used to determine the fibre mass fraction and - using fibre and resin density data (from [94, 165]) - volume fraction.

Appendix C: Effect of contact agent on measured thermal conductivity

A contact agent – Distilled water or Wakefield Type 120 heat transfer paste – was applied to improve contact between the sensor of the C-THERM thermal conductivity analyser and the sample. The heat transfer paste was used when analysing the property of materials that can either react with or absorb moisture; such as epoxy resin. A correction factor to account for the impact of the contact agent on the recorded thermal properties was coded into the control PC. Calibration

of the sensor was verified by measuring the average thermal conductivity of the calibration material (Pyrex) provided by the manufacturer of the analyser.

Calibration verification data for both contact agents is summarised in Table A-C:1.

Contact agent	Thermal conductivity (W/m ² K)	Pyrex
Distilled water	1.145 ± ^{0.055} _{0.06}	Expected
	1.154 ± ^{0.011} _{0.004}	Measured
Wakefield Type 120 heat transfer	1.145 ± ^{0.055} _{0.06}	Expected
	1.135 ± ^{0.013} _{0.008}	Measured

Table A-C 1: Summary of the thermal conductivity validation test. Note: The tolerance band represents the range of measured values.

Although the measured thermal conductivity varies depending on the contact material, the range of measured thermal conductivity is within the expected values.

Appendix D: Rheometer calibration

To verify the calibration of the system, the rheometer was used to determine the crossover point – the point where the storage modulus (G') is equal to the loss modulus (G'') – of a material with known rheological characteristics – Wacker Silicone Fluid AK 100000. As per the manufacturer specification, the crossover point occurs at an oscillatory frequency of 125 rad/s when tested at 25°C. An oscillatory frequency sweep was performed with a minimum frequency of 0.1 rad/s and a maximum frequency of 200 rad/s. Two repeats were performed to verify repeatability. As evident from Figure 3.26, the crossover point matches the manufacturer supplied specification, confirming that the setup was within the calibration.

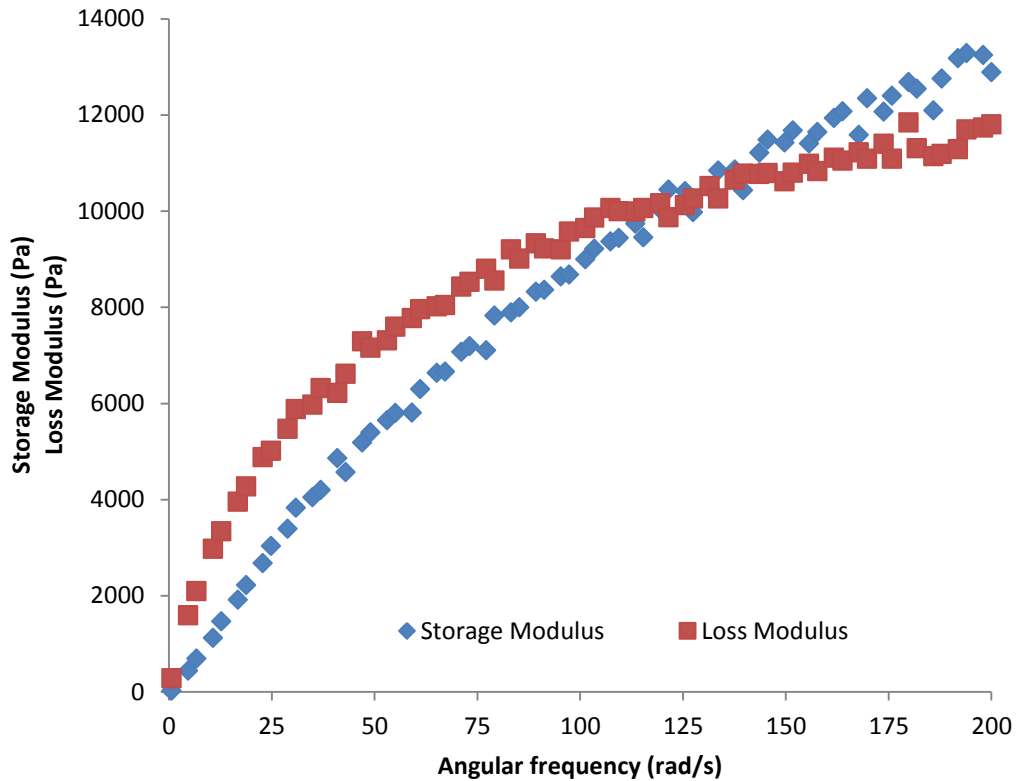


Figure 3.26: Verification of the calibration of the rheometer using Wacker Silicone Fluid. The cross-over point of the storage modulus occurs at 125 rad/s when tested at 25°C, in-line with manufacturer specification

As the MTM44-1 is a thermoset resin system, irreversible bonding of the parallel plates after the resin undergoes gelation is inevitable. However, after each set of experiments, the parallel plates were re-used by burning off the resin using an ashing furnace - set at 400°C for 1 hour – following which the plates were polished using the DAP-7 using the polishing routine specified in Table 3.3, Chapter 3.3.5. Before each run, the parallelism of the plates was verified and the calibration of the rheometer checked. The plates were disposed of if they were found to be warped or they failed the calibration test.

Appendix E: Effect of varying the resin kinematic parameter (D) for conditioned MTM44-1 resin

As stated in chapter 3.4.2.2, the model parameters were optimised for processing temperatures between 130°C and 180°C, the recommended cure temperature for the resin system. While the model parameters (A, m, n and D) can be changed to improve model accuracy at higher temperatures (for instance, 200°C), as shown in Figure A-D.1 this decreases model accuracy at lower temperatures (160°C).

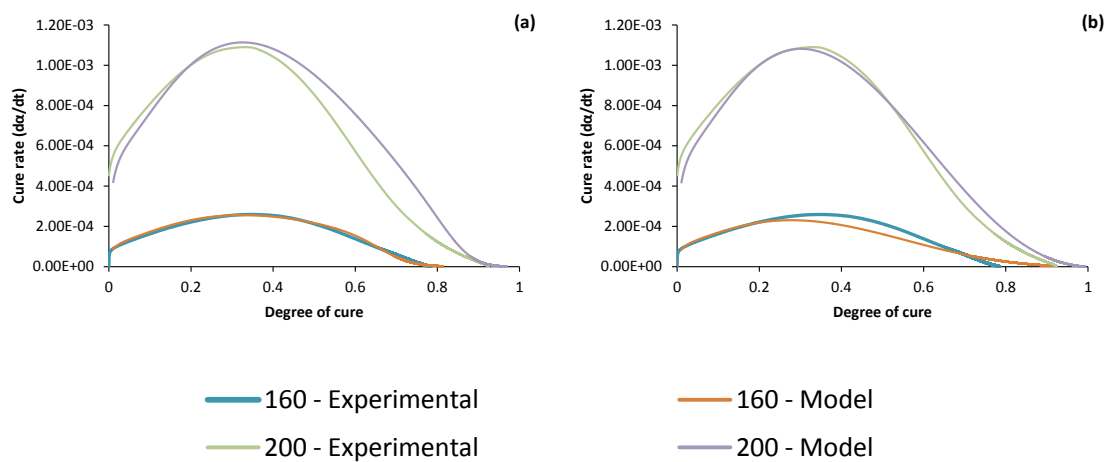


Figure A-D.1: Effect of altering model parameter "D" on degree of cure. Optimising parameter D for cure temperature is at the expense of low temperature accuracy

Similar to other studies [51, 137], model accuracy can only be maximised within a temperature band of approximately 50°C when using fixed model parameters. For instance, parameter D from Table 3.5, Chapter 3.4.2.2 controls the transition to the diffusion controlled cure mechanism. Changing the parameter from 25 (the current value) to 5 improves model accuracy at higher cure temperatures, but by sacrificing accuracy at lower temperatures. Furthermore, at high temperatures (>180°C) secondary reactions take place which current process models cannot fully capture. The secondary reactions at high temperature have been suggested to be due to thermal degradation of the matrix material. Accounting for the secondary reactions will almost certainly improve model accuracy at the thermal overshoot "peak". However, as process models have primarily been designed to predict resin cure well below the point of thermal degradation of the matrix, studies on modelling resin degradation are limited.

Appendix F: Mesh sensitivity analysis

Similar to earlier studies [130, 132], the governing equations of the thermo-kinematic model were solved using a commercial FEA package. As the equations were incorporated into the solver of a commercial Computation Fluid Dynamics package (in this study, Ansys Fluent V14.5) using user-defined functions (UDF). The output from the solver was verified using data available in the literature to ensure model fidelity. The three dimensional thermo-kinematic model developed by Costa et al for the Hercules 3501 resin system was used for the verification study [130]. A 305x254x66mm hexahedral meshed domain was created using Ansys Workbench to represent the laminate domain, with the following mesh sizes: 5, 10 and 15 mm³. The temperature profile was applied along the external walls of the mesh domain. Temperature data from specific points within the meshed domain was recorded by assigning “probes”.

Figure A-E. 1 illustrates the location of the probes within the mesh domain. Probe 1 (P1) records the laminate core temperature and Probe 2 (P2) records the laminate surface temperature. Data from the literature was extrapolated using a license-free image analysis Matlab script [166].

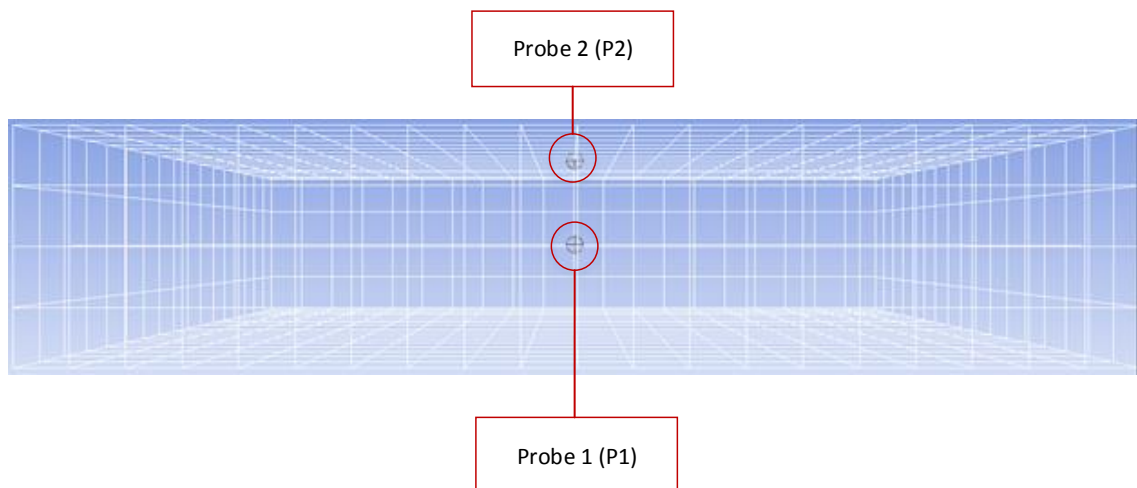


Figure A-E. 1: Location of probes within the mesh domain to record temperature and degree of cure

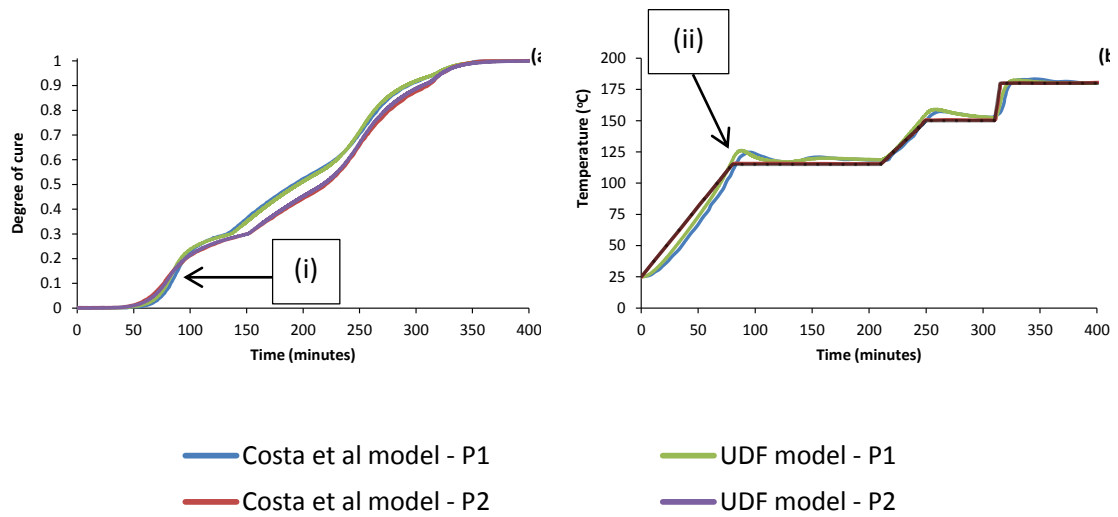


Figure A-E.2: (a) Comparison of the degree of cure output between the UDF model and the published data. (b) Comparison of the temperature output between the UDF model and the published data. (i) and (ii) presents the locations where model data deviates from the published results.

Figure A-E.2 (a) and (b) compares the output from the model against the results published by Costa et al. Although there is some inconsistency between the UDF model and published data, this is to be expected. The UDF model attempts to approximate laminate consolidation by incorporating a correction factor to capture the change in resin volume fraction within each cell in the laminate domain. On the other hand, Costa et al incorporated a Darcy flow model to better capture the change in fibre volume fraction due to resin bleed. Nevertheless, the maximum variation in laminate temperature and degree of cure between the two models is less than 2°C and 2.1% respectively; indicating good agreement between the two models.

To isolate the effect of mesh size on the model outcome, a mesh sensitivity analysis was performed. Figure A-E.3 presents the effect of mesh size on model outcome. As evident, the model output is insensitive to the changes in mesh size. Therefore, a relatively large mesh size can be safely used in the following studies without sacrificing model accuracy, whilst reducing computational cost.

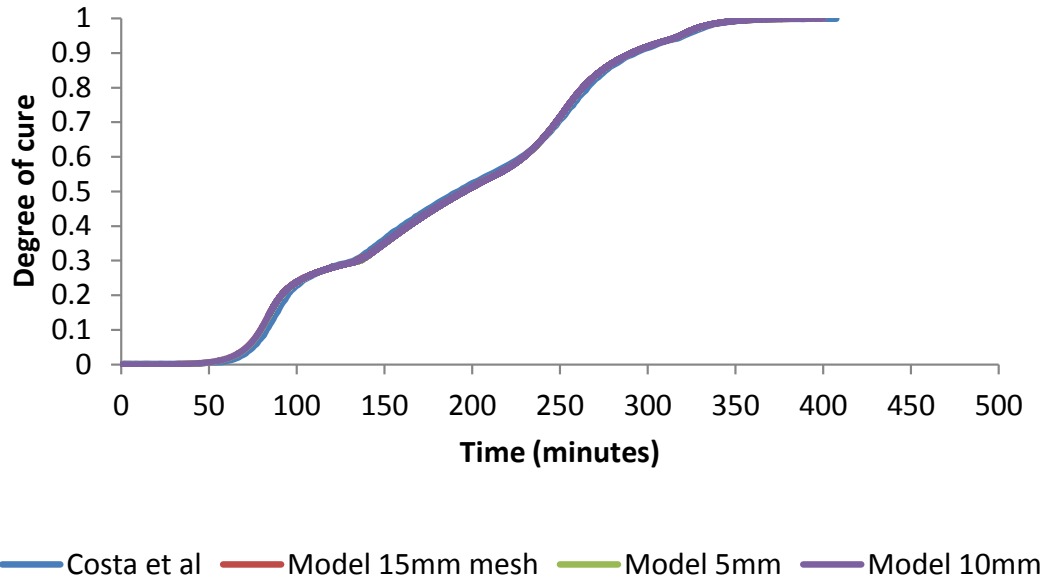


Figure A-E.3: Effect of mesh size on model output.

Appendix G – Model verification

This section presents the results of the thermo-kinematic model verification. Whilst process models for various resin systems are available in the literature, experimental verification using prepregs is few and far apart [51]. In this study the model verification is performed by curing a thick prepreg laminate (23mm) and monitoring the changes in core temperature.

The 23mm thick conditioned MTM44-1 laminate was cured in a down-stroke platen press. Whilst standard lay-up and vacuum bagging procedures was followed, the edges of the laminate are insulated with multiple layers of breather to minimise heat loss. K-Type thermocouples and a National Instruments data logger were used to monitor and record temperature. Thermocouples have been embedded within the laminate in a stepped pattern so as to record both in-plane and through-thickness temperature across the laminate. A schematic of the thermocouple location is shown in Figure A-F.1 and Figure A-F.2. Additional thermocouples have been attached to the top and bottom platens, near the laminate edges to monitor the platen temperatures. Both platens are set to ramp at 3°C up to 180°C.

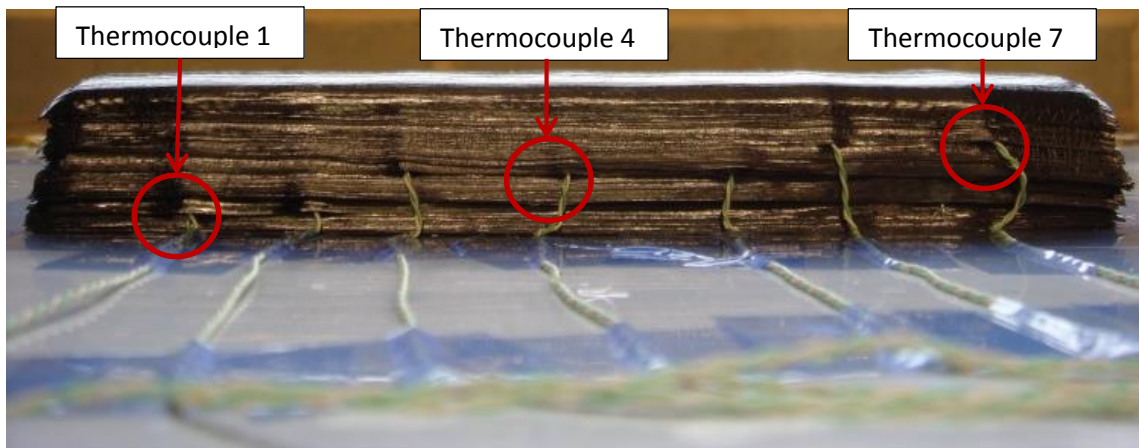


Figure A-F.1: Thermocouples embedded in a 23mm thick laminate to verify the cure kinematic model by monitoring changes in temperature due to exotherm

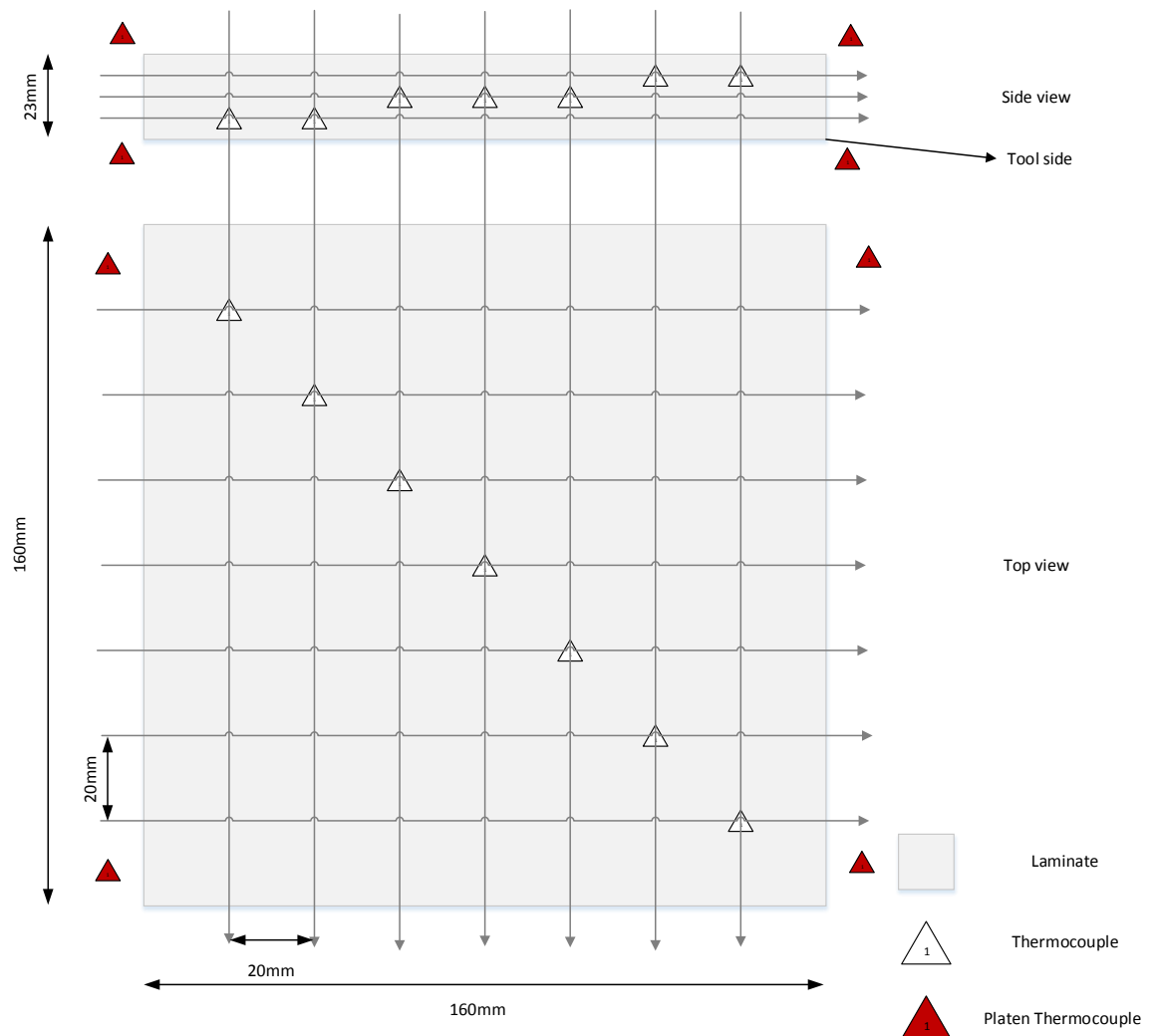


Figure A-F.2: Schematic showing the location of thermocouples for stage two of the design of experiment

Figure A-F.3 and Figure A-F.4 present the temperatures of the top and bottom platens were measured using K-Type thermocouples. In addition to the cyclic

fluctuations, average temperature varies by up to 24°C across the bottom platen surface. This has been found to be due to a failed heater bank within the platen. Attempts were made to minimise the effect of the temperature gradient and the cyclic fluctuations; the experimental setup was positioned away from the failed heater. A median of the lower platen temperature was interpolated (Figure A-F.3) to form the lower platen boundary condition in the model. Figure A-F.4 presents the temperature recorded by the thermocouples on the top platen and the representative temperature profile used as the upper platen temperature in the model.

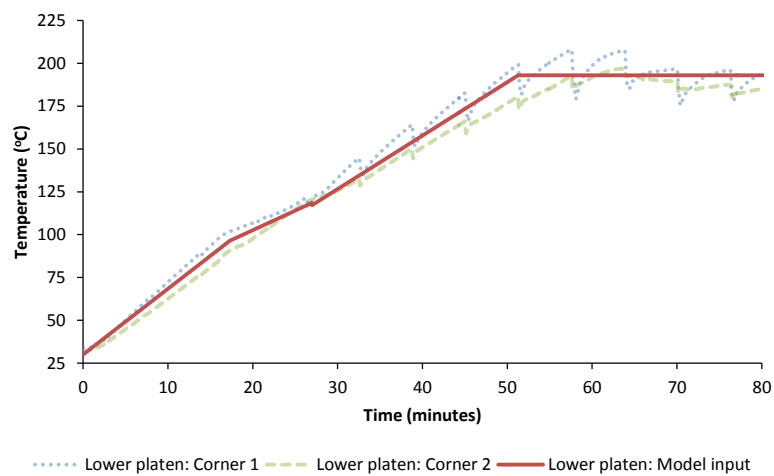


Figure A-F.3: Lower platen temperature and model input

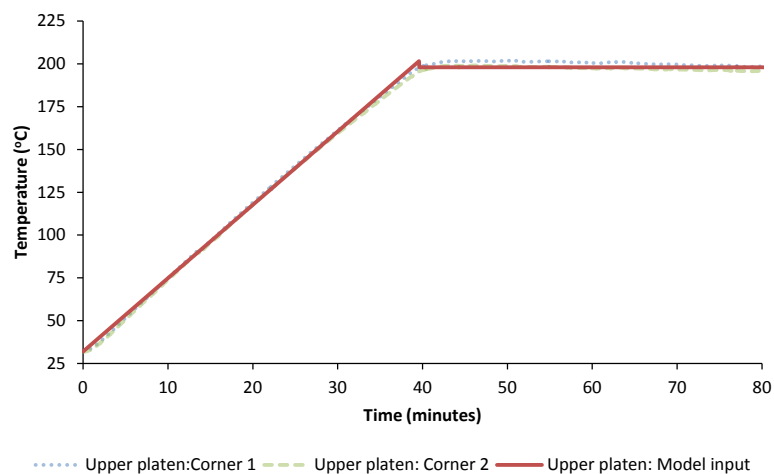


Figure A-F.4: Upper platen temperature and model input

Figure A-F.5 summarises the boundary conditions used in the model. The top and bottom platen temperatures were applied as conductive heating. Figure A-F.6

presents a comparison between the recorded laminate core temperature (Thermocouple 4, figure 3.4) and the model output from the equivalent position in the mesh domain. Also, Figure A-F.6 highlights the effect of laminate thermal conductivity on laminate core temperature.

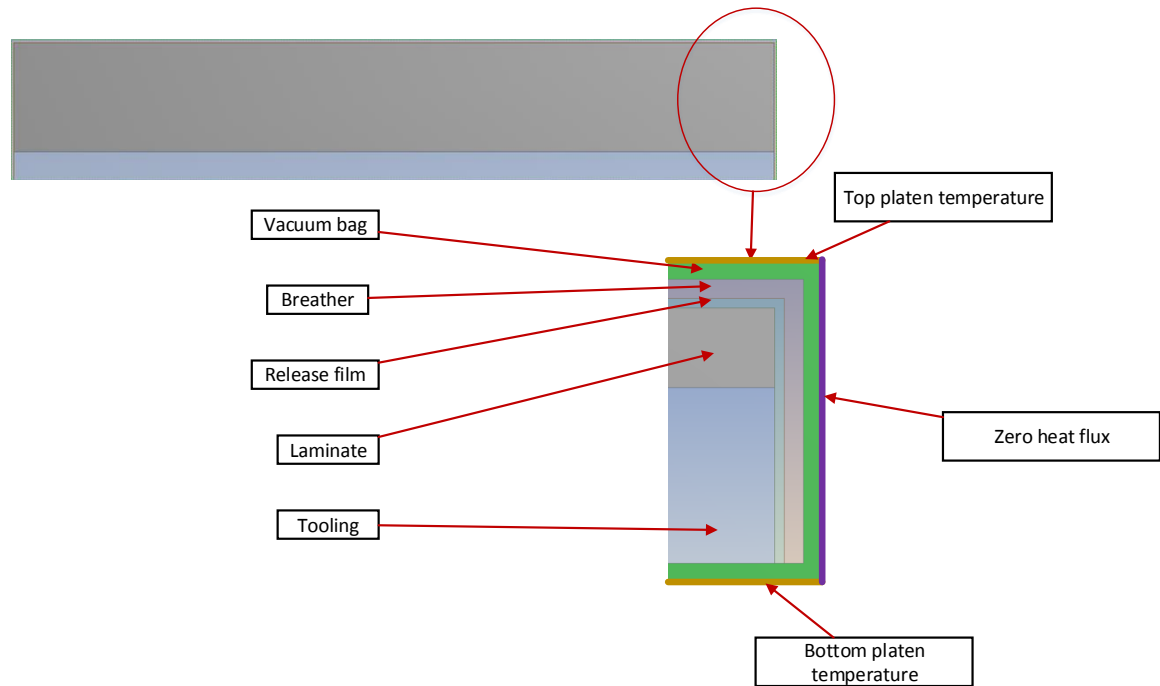


Figure A-F.5: Representative cross-section of geometry used in the kinematic model verification study. Note: section is not to scale. Dimensions have been changed to improve clarity.

In scenario “T/C – 1” a constant laminate thermal conductivity was used and in “T/C – 2” a variable resin thermal conductivity was used. Table A-F.1 summarises the uncured and cured laminate thermal conductivities in the in-plane and out-of-plane (both transverse and through thickness) direction. Figure A-F.7 presents a comparison between the laminate temperature recorded by thermocouples positioned near the periphery of the laminate (Thermocouple 1 and Thermocouple 7) and the model results. In general, there is good agreement between the model and the experimental data. However, the model data deviates from the experimental results in two key points: during the temperature ramp and on either side of the thermal overshoot “peak” (highlighted in Figure A-F.6).

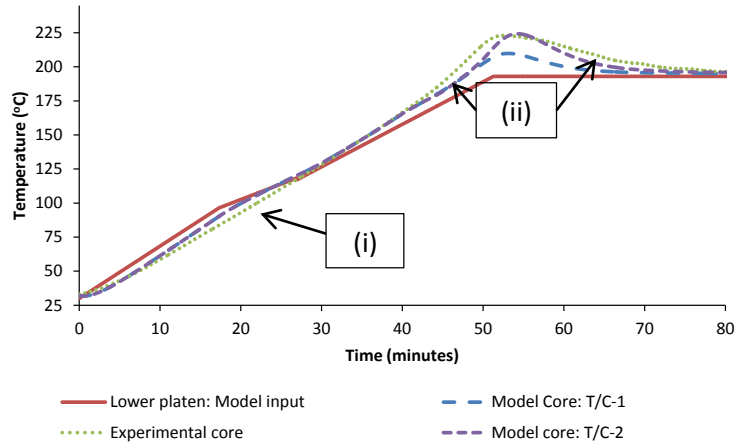


Figure A-F.6: Comparison between the experimentally obtained laminate core temperature (Thermocouple 4) and the model outcomes.

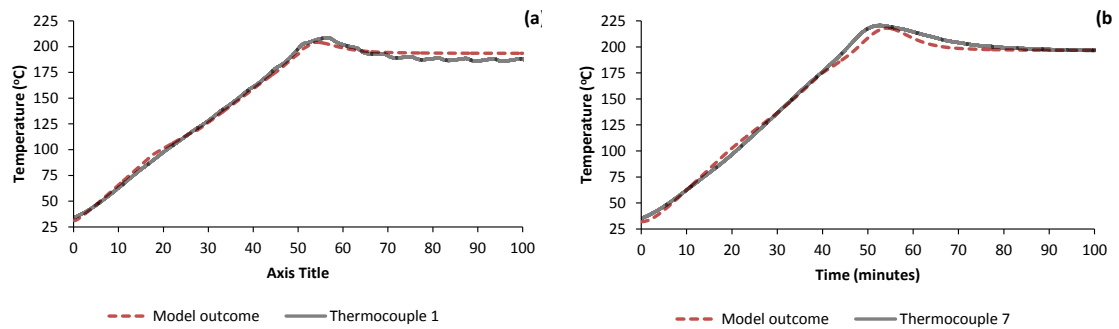


Figure A-F.7: (a) Comparison between experimentally obtained laminate temperature (from Thermocouple 1) and model result (variable thermal conductivity). (b) Comparison between experimentally obtained laminate temperature (from Thermocouple 7) and model result (variable thermal conductivity).

Thermal conductivity	K_x (W/mK)	K_y, K_z (W/mK)
Uncured prepreg (T/C-1)	15.56	1.40
Cured prepreg (T/C-2)	3.34	0.53

Table A-F.1: Difference in thermal conductivity between cured and uncured laminate

The deviations are due to variations between the recorded lower platen temperature and the applied boundary condition (i), changes in thermal conductivity of the resin system due to advancement of cure (ii) and exceeding the applicable temperature range of the model (ii). Nevertheless, the trend observed in scenario “T/C – 1” is in-line with the findings by Kratz et al [51]. Kratz et al observed similar deviation between the experimental core temperature and the model outcome at the “peak” in laminate core temperature. The authors attributed the variation to the

constant laminate thermal conductivity used in the model and the absence of a resin consolidation model to account for changes in resin volume fraction. As shown in Figure A-F.6, the model grossly underestimated the laminate core temperature when using a constant thermal conductivity. Thermal conductivity was found to decrease with cure. However, owing to the limitation of the measuring technique employed, changes in thermal conductivity with respect to degree of cure could not be measured; especially near gelation. As the initial and final laminate thermal conductivity were known, a sub-routine was created in the UDF to approximate thermal conductivity in relation to degree of cure (Table A-F.2). Further gains in model accuracy could potentially be achieved through the use of a phenomenological thermal conductivity sub-model. The limiting factor to model accuracy at the “peak” is due to the limited applicable temperature range of the model (Discussed in Appendix D).

Condition	K_x (W/mK)	K_y, K_z (W/mK)
$\alpha < 0.15$	15.6	1.4
$0.15 \leq \alpha < 0.3$	11	1.07
$0.3 \leq \alpha < 0.4$	6.405	0.75
$0.4 \leq \alpha < 0.5$	3.34	0.53
$\alpha > 0.5$	3.34	0.53

Table A-F.2: Points of change in thermal conductivity. A sub-routine was incorporated into the UDF to change thermal conductivity at set degree of cures.

Appendix H: References

1. IATA FACT SHEET: Industry statistics. December 2014. 04/02/2015]; Available from: https://www.iata.org/pressroom/facts_figures/fact_sheets/Documents/industry-facts.pdf.
2. The Boeing Company - Current Market Outlook 2014 - 2033. 27/04/2015]; Available from: <http://www.boeing.com/commercial/market/>.
3. Airbus - Global Market Forecast "Flying on Demand" 2014 - 2033. 27/04/2015]; Available from: <http://www.airbus.com/company/market/forecast/>.
4. Bombardier Commercial Aircraft - Market Forecast 2014 - 2033. 27/04/2015]; Available from: www.bombardier.com.
5. Scelsi, L., et al., *Potential emissions savings of lightweight composite aircraft components evaluated through life cycle assessment*. Express Polymer Letters, 2011. **5**(3): p. 209-217.
6. IATA. *Technology Roadmap*. June 2013. 04/02/2015]; 4th Edition:[Available from: <http://www.iata.org/whatwedo/environment/Documents/technology-roadmap-2013.pdf>.
7. IATA FACT SHEET: Fuel. December 2014. 04/02/2015]; Available from: https://www.iata.org/pressroom/facts_figures/fact_sheets/Documents/fuel-fact-sheet.pdf.
8. ICAO. *Environment - 2013 Environmental Report*. 04/02/2015]; Available from: <http://cfapp.icao.int/Environmental-Report-2013/>.
9. ACARE. *Strategic Research Agenda*. October 2002. 04/02/2015]; Volume 2.: [Available from: <http://www.acare4europe.org/sites/acare4europe.org/files/document/volume2-01-preface-intro.pdf>.
10. Taib, R.M., *Cellulose Fiber-Reinforced Thermoplastic Composites: Processing and Product Characteristics*. 1998, Virginia Polytechnic Institute and State University.
11. Roberts, T., *Rapid growth forecast for carbon fibre market*. Reinforced Plastics, 2007. **51**(2): p. 10-13.
12. Fielding, J., P. Stocking, and H. Smith. *COMPARISON OF FUEL BURN AND NOISE CHARACTERISTICS OF NOVEL AIRCRAFT CONFIGURATIONS*. in *27th International Congress of the Aeronautical Sciences, ICAS, Nice, France*. 2010.
13. Dirk, H.-J.L., C. Ward, and K.D. Potter, *The engineering aspects of automated prepreg layup: History, present and future*. Composites Part B: Engineering, 2012. **43**(3): p. 997-1009.
14. Mills, A., *Automation of carbon fibre preform manufacture for affordable aerospace applications*. Composites Part A: Applied science and manufacturing, 2001. **32**(7): p. 955-962.
15. Hou, J.W., *Optimal cure cycle design for autoclave processing of thick composites laminates: A feasibility study*. 1985.
16. Olivier, P., J.P. Cottu, and B. Ferret, *Effects of cure cycle pressure and voids on some mechanical properties of carbon/epoxy laminates*. Composites, 1995. **26**(7): p. 509-515.
17. Tang, J.-M., W.I. Lee, and G.S. Springer, *Effects of cure pressure on resin flow, voids, and mechanical properties*. Journal of composite materials, 1987. **21**(5): p. 421-440.
18. Liu, L., et al., *Effects of cure pressure induced voids on the mechanical strength of carbon/epoxy laminates*. Journal of Materials Science & Technology, 2005. **21**(1): p. 87-91.
19. Liu, L., et al., *Effects of cure cycles on void content and mechanical properties of composite laminates*. Composite structures, 2006. **73**(3): p. 303-309.

20. Koushyar, H., et al., *Effects of variation in autoclave pressure, temperature, and vacuum-application time on porosity and mechanical properties of a carbon fiber/epoxy composite*. Journal of Composite Materials, 2012. **46**(16): p. 1985-2004.
21. Boey, F.Y.C. and S.W. Lye, *Void Reduction in Autoclave Processing of Thermoset Composites .1. High-Pressure Effects on Void Reduction*. Composites, 1992. **23**(4): p. 261-265.
22. Costa, M.L., S.F.M. de Almeida, and M.C. Rezende, *The influence of porosity on the interlaminar shear strength of carbon/epoxy and carbon/bismaleimide fabric laminates*. Composites Science and Technology, 2001. **61**(14): p. 2101-2108.
23. Brosius, D., *Curing of complex composites*. 2011 01/11/2011]; Available from: http://www.quickstep.com.au/files/document/238_Quickstep_Advantages_in_more_detail.pdf.
24. *The Boeing Company, Boeing Rolls Out First 787 Dreamliner at Increased Production Rate*. 29/04/2015]; Available from: <http://boeing.mediaroom.com/2014-01-24-Boeing-Rolls-Out-First-787-Dreamliner-at-Increased-Production-Rate>.
25. *Airbus, Delivering on commitments and preparing for the future (2015)*. 29/04/2015]; Available from: <http://www.airbus.com/company/history/the-narrative/delivering-on-commitments-and-preparing-for-the-future-2015/>
26. *Reuters - Boeing Celebrates Groundbreaking for 777x Composite Wing Center*. 25/03/2015]; Available from: <http://uk.reuters.com/article/2014/10/21/wa-boeing-777x-idUSn4jNZxp+8c+PRN20141021>.
27. Advani, S.G. and E.M. Sozer, *Process modeling in composites manufacturing*. 2012: CRC Press.
28. Goel, A., *Economics of Composite Material Manufacturing Equipment*. 2000, Massachusetts Institute of Technology.
29. Hinkle, D. and C. Toomey, *Applying case-based reasoning to manufacturing*. AI magazine, 1995. **16**(1): p. 65.
30. Dumont, F., W. Fröhlingsdorf, and C. Weimer, *Virtual autoclave implementation for improved composite part quality and productivity*. CEAS Aeronautical Journal, 2013. **4**(3): p. 277-289.
31. Carvalho, S., *Boeing plans to develop new airplane to replace 737 MAX by 2030*. 29/04/2015]; Available from: <http://www.reuters.com/article/2014/11/05/us-boeing-ceo-idUSKBN0IP27320141105>.
32. Davies, L., et al., *Effect of cure cycle heat transfer rates on the physical and mechanical properties of an epoxy matrix composite*. Composites Science and Technology, 2007. **67**(9): p. 1892-1899.
33. Khan, L.A., A. Nesbitt, and R.J. Day. *Double Vacuum Bagging (Dvb) Process Coupled With Quickstep Process*. in ICCM-17. 2009. Edinburgh, Scotland.
34. Alam Khan, L., et al., *Effect of double vacuum bagging (DVB) in quickstep processing on the properties of 977-2A carbon/epoxy composites*. Polymer Composites, 2013. **34**(6): p. 942-952.
35. Shao, R.L. and D.M. Kaschak, *Carbon foam tooling with durable skin*. 2010, Google Patents.
36. Miller, D.J., I.C. Lewis, and R.A. Mercuri, *High strength monolithic carbon foam*. 2013, Google Patents.
37. Marsh, G., *Tooling up for large wind turbine blades*. Reinforced Plastics, 2007. **51**(9): p. 38-43.
38. Matthew W Arney, S.M.G., Iosif Progoulakis, and D.S. Tim J Searle, Julian Spooner and John Summerscales. *Integrally-Heated Tooling for the Manufacture of Fibre-Reinforced Composites*. in *Composites Processing 2004*. 2004. Bromsgrove: Composites Processing Association.

39. Progoulakis, L., *Heated tooling for aerospace composites manufacture*. 2004, University of Plymouth.
40. Ó Brádaigh, C.M., et al. *Electrically-Heated Ceramic Composite Tooling for Out-of-Autoclave Manufacturing of Large Composite Structures*. in *SAMPE 2011*. 2011. Long Beach, CA.
41. Ó Brádaigh, C.M., A. Doyle, and P.J. Feerick. *Electrically-Heated Ceramic Composite Tooling for Out-of-Autoclave MANufacturing of LARGE Thermoset and THERMoplastic Composite Structures*. in *SAMPE SEICO'13*. 2013. Paris, France.
42. Payette, S., et al., *Out-of-Autoclave Manufacturing: Benchmarking of an Integrally Heated Tool-plate*. *SAMPE JOURNAL*, 2015. **51**(1): p. 27-35.
43. Sharpe, A.J. *An evaluation of high performance self-heated, freestanding carbon composite tooling with advanced thermal control (PtFS)*. in *SEICO '13*. 2013. Paris, France.
44. *Quickstep*. 29/03/2015]; Available from: <http://www.quickstep.com.au/>.
45. Agius, S.L., K.J.C. Magniez, and B.L. Fox, *Cure behaviour and void development within rapidly cured out-of-autoclave composites*. *Composites Part B: Engineering*, 2013. **47**: p. 230-237.
46. Coenen, V., et al. *A feasibility study of Quickstep processing of an aerospace composite material*. in *Proceedings of twenty-sixth SAMPE Europe International Conference and Forums. Paris*. 2005.
47. Khan, L.A., R. Day, and U.o.M.S.o. Materials, *Cure Optimization of 977-2A Carbon/epoxy Composites for Quick Step Processing*. 2010: University of Manchester.
48. Haro, A., et al., *Rapid Out-of-Autoclave Composite Manufacturing for Aerospace-Grade Prepregs*. *SAMPE JOURNAL*, 2015. **51**(2): p. 7-14.
49. Golfman, Y., *Hybrid Anisotropic Materials for Wind Power Turbine Blades*. 2012: CRC Press.
50. Hernandez, S., et al., *Effect of curing cycle on void distribution and interlaminar shear strength in polymer-matrix composites*. *Composites Science and Technology*, 2011. **71**(10): p. 1331-1341.
51. Kratz, J., et al., *Thermal models for MTM45-1 and Cycom 5320 out-of-autoclave prepreg resins*. *Journal of Composite Materials*, 2012. **47**(3): p. 341-352.
52. Walczyk, D., et al., *Consolidating and curing of thermoset composite parts by pressing between a heated rigid mold and customized rubber-faced mold*. 2013, Google Patents.
53. Khan, L.A., A. Nesbitt, and R.J. Day, *Hygrothermal degradation of 977-2A carbon/epoxy composite laminates cured in autoclave and Quickstep*. *Composites Part A: Applied Science and Manufacturing*, 2010. **41**(8): p. 942-953.
54. Ahn, H., et al., *Development of carbon composite bike fork using finite element analysis and a new pressure molding process*. *Fibers and Polymers*, 2014. **15**(7): p. 1517-1522.
55. Feraboli, P., A. Masini, and A. Bonfatti, *Advanced composites for the body and chassis of a production high performance car*. *International journal of vehicle design*, 2007. **44**(3): p. 233-246.
56. Malnati, P., *Faster cycle, better surface: Out of the autoclave*. 2013 23/02/2015]; Available from: <http://www.compositesworld.com/articles/faster-cycle-better-surface-out-of-the-autoclave>.
57. Walczyk, D., J. Koppers, and C. Hoffman, *Curing and Consolidation of Advanced Thermoset Composite Laminate Parts by Pressing Between a Heated Mold and Customized Rubber-Faced Mold*. *Journal of Manufacturing Science and Engineering*, 2011. **133**(1): p. 011002.

58. Walczyk, D. and J. Koppers, *Thermal press curing of advanced thermoset composite laminate parts*. Composites Part A: Applied Science and Manufacturing, 2012. **43**(4): p. 635-646.
59. Koppers, J. and D. Walczyk, *Refinement of the Thermal Press Curing Process for Advanced Composites*. Journal of Manufacturing Science and Engineering, 2014. **136**(2): p. 021014.
60. LeGault, M., *Tooling Update: New dimensions in tooling*. 2008 01/02/2015]; Available from: <http://www.compositesworld.com/articles/tooling-update-new-dimensions-in-tooling>.
61. Lowndsale, G.R. and R.W. Murch, *Method and system for forming composite articles*. 2012, Google Patents.
62. LU Xin, S.Z., LI Chao, GU Yizhuo, LI Min, XIN Chaobo, ZHANG Zuoguang, *Resin pressure variation in prepreg stack during thermal expansion process with silicone rubber*. AMCS, 2011. **28**(3): p. 50-55.
63. Xin, C., et al., *STUDY ON THERMAL EXPANSION PRESSURE AND RESIN PRESSURE VARIATION DURING THERMAL EXPANSION MOLDING PROCESS*, in *18th International Conference on Composite Materials*. 2011: Jeju Island, Korea.
64. Witik, R.A., et al., *Economic and environmental assessment of alternative production methods for composite aircraft components*. Journal of Cleaner Production, 2012. **29-30**: p. 91-102.
65. Tong, R., *Cost Analysis on L-shape Composite Component Manufacturing*. 2012, Concordia University Montreal, Quebec, Canada.
66. Sutter, J.K., et al. *Comparison Of Autoclave And Out-of-autoclave Composites*. in *42nd ISTC*. 2010. Salt Lake City, UT.
67. Centea, T., L. Grunenfelder, and S. Nutt, *A review of out-of-autoclave prepregs—Material properties, process phenomena, and manufacturing considerations*. Composites Part A: Applied Science and Manufacturing, 2015. **70**: p. 132-154.
68. Grunenfelder, L.K. and S.R. Nutt, *Void formation in composite prepregs - Effect of dissolved moisture*. Composites Science and Technology, 2010. **70**(16): p. 2304-2309.
69. Kay, J. and G. Fernlund, *Processing conditions and voids in out of autoclave prepregs*, in *SAMPE 2012*. 2012: Baltimore, USA.
70. Berejka, A.J., et al., *X-ray curing of composite materials*. Nuclear Instruments and Methods in Physics Research Section B: Beam Interactions with Materials and Atoms, 2005. **241**(1): p. 847-849.
71. Boey, F.Y.C. and S.W. Lye, *Void Reduction in Autoclave Processing of Thermoset Composites .2. Void Reduction in a Microwave Curing Process*. Composites, 1992. **23**(4): p. 266-270.
72. Thostenson, E.T. and T.W. Chou, *Microwave and conventional curing of thick-section thermoset composite laminates: Experiment and simulation*. Polymer Composites, 2001. **22**(2): p. 197-212.
73. Thostenson, E. and T.-W. Chou, *Microwave processing: fundamentals and applications*. Composites Part A: Applied Science and Manufacturing, 1999. **30**(9): p. 1055-1071.
74. Abliz, D., et al., *Low-energy electron beam cured tape placement for out-of-autoclave fabrication of advanced polymer composites*. Composites Part A: Applied Science and Manufacturing, 2014. **65**: p. 73-82.
75. Endruweit, A., M. Johnson, and A. Long, *Curing of composite components by ultraviolet radiation: a review*. Polymer composites, 2006. **27**(2): p. 119-128.
76. Nightingale, C. and R.J. Day, *Flexural and interlaminar shear strength properties of carbon fibre/epoxy composites cured thermally and with microwave radiation*. Composites Part A: Applied Science and Manufacturing, 2002. **33**(7): p. 1021-1030.

77. Papargyris, D.A., et al., *Comparison of the mechanical and physical properties of a carbon fibre epoxy composite manufactured by resin transfer moulding using conventional and microwave heating*. Composites Science and Technology, 2008. **68**(7-8): p. 1854-1861.
78. Drzal, L., K. Hook, and R. Agrawal. *Enhanced chemical bonding at the fiber-matrix interphase in microwave processed composites*. in *MRS Proceedings*. 1990. Cambridge Univ Press.
79. Lopata, V.J., et al., *Electron-beam-curable epoxy resins for the manufacture of high-performance composites*. Radiation Physics and Chemistry, 1999. **56**(4): p. 405-415.
80. Janke, C., K. Yarborough, and L. Drzal. *Fiber-matrix interface studies on electron beam cured composites*. in *International SAMPE symposium and exhibition*. 1999. Long Beach, CA: SAMPE.
81. Zhang, Z., et al., *The effect of carbon-fiber surface properties on the electron-beam curing of epoxy-resin composites*. Composites Science and Technology, 2002. **62**(3): p. 331-337.
82. Tavares, S.S., V. Michaud, and J.A.E. Manson, *Through thickness air permeability of prepregs during cure*. Composites Part a-Applied Science and Manufacturing, 2009. **40**(10): p. 1587-1596.
83. Shim, S.B. and J.C. Seferis, *Thermal and air permeation properties of a carbon fiber/toughened epoxy based prepreg system*. Journal of applied polymer science, 1997. **65**(1): p. 5-16.
84. Kardos, J., M. Duduković, and R. Dave, *Void growth and resin transport during processing of thermosetting—matrix composites*, in *Epoxy Resins and Composites IV*. 1986, Springer. p. 101-123.
85. Louis, B.M., *Gas transport in out-of-autoclave prepreg laminates*. 2010.
86. Ridgard, C., *Out of autoclave composite technology for aerospace, defence and space structures*. SAMPE '09 spring symposium conference, 2009.
87. Thorfinnson, B. and T. Biermann. *Production of void free composite parts without debulking*. in *31st International SAMPE Symposium*. 1986.
88. Thorfinnson, B. and T. Biermann, *Degree of Impregnation of Prepregs--Effects on Porosity*. Advanced Materials Technology'87, 1987: p. 1500-1509.
89. Nam, J.D., et al., *Gas permeation and viscoelastic deformation of prepregs in composite manufacturing processes*. Polymer composites, 1995. **16**(5): p. 370-377.
90. Hsiao, K., *Gas Transport And Water Vapourization In Out-Of-Autoclave Prepreg Laminates*. The Faculty of Graduate Studies (Materials Engineering), 2012. **Master of Applied Science - MAsc**.
91. Grunenfelder, L. and S. Nutt. *Air Removal in VBO Prepreg Laminates: Effects of Breathe-out Distance and Direction*. in *Proceedings of the SAMPE Tech 2011 Conference and Exhibition: Developing Scalable Materials and Processes for Our Future*. 2011.
92. Arafath A.R, *Gas Transport in Prepregs: Model and Permeability Experiments*. ICCM-17, 2009.
93. Repecka, L. and J. Boyd, *Vacuum-bag-only-curable prepregs that produce void-free parts*. 47th International Sampe Symposium and Exhibition, Vol 47, Books 1 and 2: Affordable Materials Technology-Platform to Global Value and Performance, ed. B.M. Rasmussen, L.A. Pilato, and H.S. Kliger. 2002, Covina: Soc Advancement Material & Process Engineering. 1862-1874.
94. *MTM44-1 Material Datasheet*. 22/09/2014]; Available from: <https://www.cytec.com/sites/default/files/datasheets/MTM44-1.pdf>.
95. Kay, J., et al. *Effect of process conditions on porosity in out-of-autoclave prepreg laminates*. in *ICCM 18*. 2011.

96. Zhang, D., A. Levy, and J. Gillespie, *On the Void Consolidation Mechanisms of Continuous Fiber Reinforced Thermoplastic Composites*. SAMPE 2012-Baltimore, MD, 2012: p. 16.
97. Ridgard, C. *Next generation out of autoclave systems*. in *SAMPE 2010 Conference and Exhibition" New Materials and Processes for a New Economy"*, May 17, 2010-May 20. 2010.
98. Cauberghs, J., *Out-of-Autoclave Manufacturing of Aerospace Representative Parts*. 2012.
99. Brilliant, M., *Out-of-Autoclave Manufacturing of complex shape composite laminates*. Department of Mechanical Engineering, 2011. **Master of Engineering**.
100. Hughes, S.M. *Out-of-autoclave Prepreg Processing: Effect of Integrated Geometric Features on Part Quality*. in *SAMPE Tech Wichita*. 2013.
101. Tyberg, C., et al., *Tough, void-free, flame retardant phenolic matrix materials*. *Construction and Building Materials*, 1999. **13**(6): p. 343-353.
102. Wu, H.D., et al., *Pultruded fiber-reinforced polyurethane-toughened phenolic resin. II. Mechanical properties, thermal properties, and flame resistance*. *Journal of applied polymer science*, 1996. **62**(1): p. 227-234.
103. Anderson, J. and M. Altan, *Formation of voids in composite laminates: Coupled effect of moisture content and processing pressure*. *Polymer Composites*, 2014.
104. Brand, R.A., G.G. Brown, and E.L. McKague, *Processing science of epoxy resin composites, Tenth Quarterly Report*. 1983(Contract No. F33615-80-C-5021).
105. Scriven, L.E., *On the dynamics of phase growth*. *Chemical Engineering Science*, 1959. **10**(1-2): p. 1-13.
106. Jones, S.F., G.M. Evans, and K.P. Galvin, *Bubble nucleation from gas cavities — a review*. *Advances in Colloid and Interface Science*, 1999. **80**(1): p. 27-50.
107. Epstein, P. and M. Plesset, *On the Stability of Gas Bubbles in Liquid-Gas Solutions*. *Journal of Chemical Physics*, 1950. **18**: p. 1505-1509.
108. Subramanian, R. and M. Weinberg, *Asymptotic expansions for the description of gas bubble dissolution and growth*. *AIChE Journal*, 1981. **27**(5): p. 739-748.
109. Kim, K.Y., S.L. Kang, and H.Y. Kwak, *Bubble nucleation and growth in polymer solutions*. *Polymer Engineering & Science*, 2004. **44**(10): p. 1890-1899.
110. Ledru, Y., et al., *Coupled visco-mechanical and diffusion void growth modelling during composite curing*. *Composites Science and Technology*, 2010. **70**(15): p. 2139-2145.
111. Amon, M. and C.D. Denson, *A study of the dynamics of foam growth: Analysis of the growth of closely spaced spherical bubbles*. *Polymer Engineering & Science*, 1984. **24**(13): p. 1026-1034.
112. Wood, J.R. and M.G. Bader, *Void control for polymer-matrix composites (1): theoretical and experimental methods for determining the growth and collapse of gas bubbles*. *Composites Manufacturing*, 1994. **5**(3): p. 139-147.
113. Gu, Y., et al., *Void Formation Model and Measuring Method of Void Formation Condition During Hot Pressing Process*. *Polymer Composites*, 2010. **31**(9): p. 1562-1571.
114. Campbell, F.C., *Structural Composite Materials*. 2010, Materials Park, OH, USA: ASM International.
115. Xin, C., et al., *Online monitoring and analysis of resin pressure inside composite laminate during zero-bleeding autoclave process*. *Polymer Composites*, 2011. **32**(2): p. 314-323.
116. Hubert, P., et al., *Cure kinetics and viscosity models for Hexcel 8552 epoxy resin, in 2001: A Materials and Processes Odyssey, Books 1 and 2*, L. Repecka and F.F. Saremi, Editors. 2001. p. 2341-2354.

117. Dykeman, D., *Minimizing uncertainty in cure modeling for composites manufacturing*. 2008, UNIVERSITY OF BRITISH COLUMBIA (Vancouver.
118. Watlow, *Mineral Insulated (MI) Strip Heaters*. 05/03/2015]; Available from: <http://www.watlow.co.uk/downloads/en/specsheets/stlmis0413.pdf>.
119. Vonroll.
120. Cui, W., M. Wisnom, and M. Jones, *Failure mechanisms in three and four point short beam bending tests of unidirectional glass/epoxy*. The Journal of Strain Analysis for Engineering Design, 1992. **27**(4): p. 235-243.
121. Little, J.E., X. Yuan, and M.I. Jones, *Characterisation of voids in fibre reinforced composite materials*. NDT & E International, 2012. **46**: p. 122-127.
122. Turner, T.A., *The effects of processing variables on the energy absorption of composite crash structures*. 2004, University of Nottingham.
123. Little, J., X. Yuan, and M. Jones. *VOIDS CHARACTERISATION IN CARBON FIBRE/EPOXY COMPOSITE LAMINATES*. in *18TH INTERNATIONAL CONFERENCE ON COMPOSITE MATERIALS*.
124. C-Therm, 06/05/2015]; Available from: <http://www.ctherm.com/>.
125. Yousefi, A., P. Lafleur, and R. Gauvin, *Kinetic studies of thermoset cure reactions: a review*. Polymer Composites, 1997. **18**(2): p. 157-168.
126. Lee, W.I., A.C. Loos, and G.S. Springer, *Heat of reaction, degree of cure, and viscosity of Hercules 3501-6 resin*. Journal of Composite Materials, 1982. **16**(6): p. 510-520.
127. Bogetti, T.A. and J.W. Gillespie, *Two-dimensional cure simulation of thick thermosetting composites*. Journal of Composite Materials, 1991. **25**(3): p. 239-273.
128. Young, W.B., *Compacting Pressure and Cure Cycle for Processing of Thick Composite Laminates*. Composites Science and Technology, 1995. **54**(3): p. 299-306.
129. Hubert, P. and A. Poursartip, *A review of flow and compaction modelling relevant to thermoset matrix laminate processing*. Journal of Reinforced Plastics and Composites, 1998. **17**(4): p. 286-318.
130. Costa, V.A.F. and A.C.M. Sousa, *Modeling of flow and thermo-kinetics during the cure of thick laminated composites*. International Journal of Thermal Sciences, 2003. **42**(1): p. 15-22.
131. Dimopoulos, A., *Effect of carbon nanoparticle addition on epoxy cure*. 2007, Cranfield University.
132. Ganapathi, A.S., S.C. Joshi, and Z. Chen, *Simulation of bleeder flow and curing of thick composites with pressure and temperature dependent properties*. Simulation Modelling Practice and Theory, 2013. **32**: p. 64-82.
133. Sourour, S. and M. Kamal, *Differential scanning calorimetry of epoxy cure: isothermal cure kinetics*. Thermochimica Acta, 1976. **14**(1): p. 41-59.
134. Joshi, S.C., X.L. Liu, and Y.C. Lam, *A numerical approach to the modeling of polymer curing in fibre-reinforced composites*. Composites Science and Technology, 1999. **59**(7): p. 1003-1013.
135. Cole, K., J. Hechler, and D. Noel, *A new approach to modeling the cure kinetics of epoxy/amine thermosetting resins. 2. Application to a typical system based on bis [4-(diglycidylamino) phenyl] methane and bis (4-aminophenyl) sulfone*. Macromolecules, 1991. **24**(11): p. 3098-3110.
136. Khanna, U. and M. Chanda, *Kinetics of anhydride curing of isophthalic diglycidyl ester using differential scanning calorimetry*. Journal of applied polymer science, 1993. **49**(2): p. 319-329.
137. Khoun, L., T. Centea, and P. Hubert, *Characterization Methodology of Thermoset Resins for the Processing of Composite Materials -- Case Study: CYCOM 890RTM Epoxy Resin*. Journal of Composite Materials, 2009. **44**(11): p. 1397-1415.

138. Martinez, G.M., *Fast cures for thick laminated organic matrix composites*. Chemical engineering science, 1991. **46**(2): p. 439-450.
139. Loos, A.C. and G.S. Springer, *CURING OF EPOXY MATRIX COMPOSITES*. Journal of Composite Materials, 1983. **17**(2): p. 135-169.
140. Bogetti, T.A. and J.W. Gillespie Jr, *Cure Simulation of Thick Thermosetting Composites*. 1990, DTIC Document.
141. Tredoux, L. and J. Van der Westhuizen, *Development of a numerical code that simulates combined heat transfer, resin flow and compaction during composites processing*. Composites Manufacturing, 1995. **6**(2): p. 85-92.
142. Telikicherla, M., M. Altan, and F. Lai, *Autoclave curing of thermosetting composites: process modeling for the cure assembly*. International communications in heat and mass transfer, 1994. **21**(6): p. 785-797.
143. Yi, S., H.H. Hilton, and M.F. Ahmad, *A finite element approach for cure simulation of thermosetting matrix composites*. Computers & structures, 1997. **64**(1): p. 383-388.
144. Weber, M.J., *Handbook of Optical Materials*. 2002: Taylor & Francis.
145. *JB TB 650 Epoxy Tooling Board - Datasheet*. 26/05/2015]; Available from: <http://www.johnburn.co.uk/docs/datasheets/JB%20TB%20650.pdf>.
146. Anghelescu, M.S. and M.K. Alam. *Carbon Foam Tooling For Aerospace Composites*. in *39th ISTC*. 2007. Cincinnati, Ohio.
147. Engle, G.B., *Properties of unirradiated HTGR core support and permanent side reflector graphites: PGX, HLM, 2020, and H-440N*. 1977. p. Medium: ED; Size: Pages: v.
148. *Styrofoam solutions - LB-X Datasheet*. 26/05/2015]; Available from: http://msdssearch.dow.com/PublishedLiteratureDOWCOM/dh_0158/0901b80380158e56.pdf?filepath=styrofoam/pdfs/noreg/802-00251.pdf&fromPage=GetDoc.
149. Pierson, H.O., *Handbook of Refractory Carbides and Nitrides*. William Andrew Publishing/Noyes.
150. Potter, K.D., et al., *The generation of geometrical deformations due to tool/part interaction in the manufacture of composite components*. Composites Part A: Applied Science and Manufacturing, 2005. **36**(2): p. 301-308.
151. Wisnom, M.R., et al., *Mechanisms generating residual stresses and distortion during manufacture of polymer–matrix composite structures*. Composites Part A: Applied Science and Manufacturing, 2006. **37**(4): p. 522-529.
152. Hatton, P., *Back of a cigarette packet approach to composite property prediction and structural design [Seminar]*. 2013 10/10/2014]; Available from: http://www.sampe.org.uk/assets/pdfs/MasterClass2013/CTAerocomp_F00_2013_140%20issue1%20Hatton.pdf.
153. Monaghan, P.F., M.T. Brogan, and P.H. Oosthuizen, *Flow Processes in Composite Materials '91 Heat transfer in an autoclave for processing thermoplastic composites*. Composites Manufacturing, 1991. **2**(3): p. 233-242.
154. Slesinger, N., et al., *Heat transfer coefficient distribution inside an autoclave*. ICCM-17; Edinburgh (UK): International Committee of Composite Materials, 2009.
155. Hernández, S., et al., *Optimization of curing cycle in carbon fiber-reinforced laminates: Void distribution and mechanical properties*. Composites Science and Technology, 2013. **85**: p. 73-82.
156. Hsu, D.K. and A. Minachi, *Defect characterization in thick composites by ultrasound*, in *Review of Progress in Quantitative Nondestructive Evaluation*. 1990, Springer. p. 1481-1488.
157. Centea, T. and P. Hubert, *Measuring the impregnation of an out-of-autoclave prepreg by micro-CT*. Composites Science and Technology, 2011. **71**(5): p. 593-599.

158. Wells, J., et al., *Surface and bulk porosity in Out-of-Autoclave prepregs*, in *20th International Conference on Composite Materials*. 2015: Copenhagen, Denmark.
159. *Cytec Materials, LTM-10 series Datasheet*. 30/04/2015]; Available from: <http://cytec.com/sites/default/files/datasheets/LTM101216.pdf>.
160. *Hexcel M56 datasheet*. [17/06/2015]; Available from: http://hexcel.com/Resources/DataSheets/Prepreg-Data-Sheets/M56_eu.pdf.
161. Bowles, K.J. and S. Frimpong, *Void effects on the interlaminar shear strength of unidirectional graphite-fiber-reinforced composites*. *Journal of Composite Materials*, 1992. **26**(10): p. 1487-1509.
162. Huang, H. and R. Talreja, *Effects of void geometry on elastic properties of unidirectional fiber reinforced composites*. *Composites Science and Technology*, 2005. **65**(13): p. 1964-1981.
163. Shahkarami, A. and D.V. Ee, *Material Characterization for Processing: ACG MTM45-1*. 2009 [09/12/2013]; Available from: http://www.niar.wichita.edu/coe/ncamp_documents/ACG%20MTM45-1/ACGMTM45-1-ProcessingCharacterizationV1-0.pdf.
164. Shahkarami, A. and D.V. Ee, *Material Characterization for Processing: Hexcel 8552*. 2009 [15/04/2014]; Available from: http://www.niar.wichita.edu/coe/ncamp_documents/Hexcel%208552/Hexcel8552MaterialCharacterizationBinderV0-9.pdf
165. Torayca, *T300 Datasheet*. [04/05/2015]; Available from: <http://www.toraycfa.com/pdfs/T300DataSheet.pdf>.
166. Doke, J., *Grabit*. 2007 [01/08/2015]; 1.0:[Available from: <http://uk.mathworks.com/matlabcentral/fileexchange/7173-grabit>